The scandium content of beryllium-bearing minerals and micas from Tørdal pegmatites and its genetic and economic implications

Markus Nytun Wilhelmsen

Master Thesis in Geosciences

Study programme: Mineralogy, Petrology and Geochemistry
60 credits

Department of Geosciences
Faculty of Mathematics and Natural Sciences
And
Natural History Museum

University of Oslo

15 June, 2020

Supervisor: Prof. Axel Müller (Natural History Museum, University of Oslo)
Co-supervisor: Associate Prof. Henrik Friis (Natural History Museum, University of Oslo)

This work is published digitally through DUO – Digitale Utgivelser ved UiO
http://www.duo.uio.no
It is also catalogued in BIBSYS (http://www.bibsys.no/english)

Glossary

AB – Alkali Basalts

BABB – Back-Arc Basin Basalts

BSE – Backscattered Electrons

CAB – Calc-Alkaline Basalts

EPMA – Electron Micro Probe Anlayzer

GPS – Global Positioning System

HREEs – Heavy Rare Earth Elements (Gd – Lu)

IAT – Island-Arc Tholeiites

ICP-OES – Inductively Coupled Plasma – Optical Emission Spectrometry)

LA-ICP-MS – Laser Ablation Inductively Coupled Plasma Mass Spectrometry

LCT – Lithium-Caesium-Tantalum

LOD – Limit of Detection

LREEs – Light Rare Earth Elements (La – Eu)

MDL – Mean Detection Limit

MORB – Mid Ocean Ridge Basalt

NYF – Niobium-Yttrium-Fluorine

OIB – Ocean-Island Basalts

PGNAA – Prompt Gamma Neutro Activation Analysis

PPL – Plane Polarized Light

ppm – parts per million

REEs – Rare Earth Elements (Y + Lanthanides: La-Lu)

SOFC – Solid Oxide Fuel Cells

UCC – Upper Continental Crust

XPL – Cross Polarized Light

Acknowledgements

First of all, I want to give my highest gratitude and thanks to my main supervisor Axel Müller and co-supervisor Henrik Friis. I sincerely thank them for their help, advices, time, motivational words, guidance, patience, friendship, and support throughout the master thesis project. Their help was important for this project, especially in this hard time during the Covid-19 pandemic, which I really appreciate.

I would like to thank peoples at Natural History Museum of Oslo (NHM) for their help and support, especially Nanna-Rosing Schow, Emil Gulbransen, Øyvind Sunde, Nélia Castro, and Fabrice Dal Bo. I also want to thank Lars Tveit for letting us in to the Høydalen area and other pegmatite areas of the Tørdal pegmatite field for investigation and geological mapping.

Many thanks to Muriel Marie Laure Erambert and Magnus Kristoffersen for their help, introduction and assistance during electron probe micro analysis (EPMA) and laser ablation inductively coupled plasma mass spectrometry (LA-ICP-MS) analysis of my samples. I would also like to thank Salahalldin Akhavan for preparing some of my samples into thick sections, and Øyvind Sunde again for sending my host rock samples to Actlabs (Activation Laboratories Ltd), Ontario, Canada, for chemical whole rock analysis.

Thanks to Actlabs (Activation Laboratories Ltd), Ontario, Canada, for preforming chemical whole rock analysis of my host rock samples.

Last, I would like to thank my family and friends, especially my mom, sister and brother-in-law, for their help, motivational words and for supporting me, not only during my master thesis project, but for five years as a student at the University of Oslo.

Abstract

The granitic pegmatites of Tørdal pegmatite field, which are situated in the Vestfold and Telemark county in South Norway, have gained lot of mineralogical and economic interest the last hundred years mainly because of their enrichments of the rare elements Sc, Be, Li and Mo. In this study, Sc- and Be-bearing minerals, comprising mica, beryl, gadolinite-(Y) and bazzite, have been studied from 17 Tørdal pegmatites in order to better understand the distribution of Sc and Be within pegmatite bodies as well as across the entire pegmatite field. The mineral chemistries were determined with EPMA and LA-ICP-MS. In addition, whole rock chemistries of pegmatites and their host rocks, amphibolites of the Nissedal Outlier and the Tørdal granite, were evaluated in order to discuss possible sources of Sc and Be. Detailed geological mapping of the Høydalen area was performed to reveal the spatial distribution, size and shape of pegmatite bodies.

The chemical data of investigated micas illustrate a variation of average Sc concentration from 38 to 1576 ppm. At pegmatite scale, micas from the border and wall zones (margin of the pegmatite body) contain higher average Sc concentrations compared to micas from the intermediate and albite replacement zones (inner zones of the pegmatite body). In the Svåheii 2b pegmatite, for example, average Sc compositions range from 1125 ppm in wall zone micas to 38 ppm in albite zone micas. This indicates that the Sc concentration in micas continuously decreases from pegmatite margin towards the core of individual pegmatite bodies, which is accompanied by decreasing K/Rb ratios. Comparison of micas and coexisting garnets from same pegmatite bodies revealed a distribution coefficient of Sc-in-mica : Sc-in-garnet of 0.85 : 1, indicating that slightly more Sc is incorporated in garnet than in co-existing mica. Mapping of Be-minerals shows that gadolinite-(Y) occurs only in the wall zones of pegmatites, while beryl is found in the intermediate and albite replacement zones. The Na, Li, and Cs content of the beryl increases continuously whereas Fe decreases from early crystallized green beryl to late crystalized pink beryl (variety morganite).

At regional scale, the distribution of Sc and Be across Tørdal pegmatites shows a general increase of these elements from the SW (Mjeltedalen 2a-Kleppe-Buvatnet area) to the NE (Heftetjern-Høydalen-Skardsfjell area) documented by mica and garnet chemistries and Be-mineral abundance.

Whole rock analysis of amphibolitic host rocks (bulk mean 35 ppm Sc; this study) and Tørdal pegmatites (Heftetjern = bulk mean 53 ppm Sc; Rosing-Schow et al., 2020) define both rocks as Sc-enriched compared to the Sc-poor Tørdal granite (bulk mean 2 ppm Sc; Steffensen, 2018).

In addition, Li, Ta, Sn, and W are enriched in both amphibolitic host rocks and Tørdal pegmatites compared to average crustal compositions and to the Tørdal granite. These findings supports the most recent model that Tørdal pegmatite melts were formed by partial melting of their amphibolitic host rocks. Traditionally it was suggest that the pegmatite melts are residual melts originating from the adjacent Tørdal granite pluton occurring immediately south of the pegmatite field. The finding that the Sc content in pegmatite melts decreases with fractionation degree and the field relationships observed at the Kleppe quarry indicate that the anatectic melts migrated only about 10 to 500 m to their final location of emplacement and crystallization. Previously it was assumed that the Sc enrichment in the Heftetjern-Høydalen-Skardsfjell area is related to the fractionation when the melts moved for 4 to 5 km the from SW to the NE of pegmatite field. The relative low K_2O content of the Sc-rich Heftetjern pegmatite (4.1 wt.% K_2O; Rosing-Schow et al., 2020) compared to the high K_2O content of the Sc-poor Kleppe quarry (7.4.wt% K_2O; Rosing-Schow et al., 2020) indicate that the Heftetjern pegmatite melt was formed by a higher degree of partial melting (about 10 to 15%) compared to the Kleppe quarry (<5%) (Kushiro et al., 1996). This suggests that the Sc enrichment in Tørdal pegmatite melts is related to low but not very low degree of partial melting of Sc-rich amphibolites and not to the fractionation degree. Analysis of these amphibolitic host rocks indicates a high Sc and Be content in amphiboles (bulk mean 56 ppm Sc and 6 ppm Be) compared to biotites (bulk mean 3 ppm Sc and <2 ppm Be). Both minerals are relative rich in F (1.2 wt.% F in biotite and 0.5 wt.% F in amphibole) causing the lowering of the melting temperature of the amphibolites. During partial melting, F formed Sc-F and Be-F complexes enabling transported of Sc and Be by the anatectic pegmatite melt to their place of crystallization, where these elements become incorporated in gadolinite-(Y), mica, garnet, beryl and bazzite during final crystallization. Economic implications of this study are that mica and garnet are the major carriers of Sc, while gadolinite-(Y) and beryl are major carrier of Be, minerals which are abundant in the NE of Tørdal pegmatite field. Scandium is most enriched in garnets and micas from the pegmatite margin and the Sc content of these minerals decreases towards the core of the pegmatites. However, the Sc-enriched pegmatites of the Heftetjern-Høydalen-Skardsfjell area are small in size (500 – 10,000 m^3) and bulk pegmatite Sc concentrations are about 50 ppm, which is below of the current cut-off grade of about 300 ppm of active Sc mines, making them economically not profitable.

Table of contents

1. Introduction

Granitic pegmatites, which are defined as very coarse-grained igneous rocks with crystal sizes >3 cm, are one major source for the industrial minerals feldspar, quartz, and mica, and can be economically enriched in the rare elements Sc, Be, Li, Y, Sn, Nb, Ta, Cs, REE and Mo (Černý, 1991b; Simmons et al., 2003; Glover et al., 2012). Because of the elevated abundances of these rare elements, granitic pegmatites can contain a great variety of rare minerals such as beryl, bazzite, thortveitite, lepidolite, gadolinite-(Y), euxenite-(Y), molybdenite, etc (Mindat, 2020g). These commodities are the raw materials for a wide range of products such as glass, ceramics, silicon metal used for solar panels, super magnets for wind turbines, Li carbonate for batteries, micro capacitators, etc., and are, thus, crucial for the production and storage of renewable green energy.

In south Norway, granitic pegmatite have been mined mainly for feldspars, quartz and mica since the end of the 19th century. Scandium, Be, REE, U and Mo have been served as by-products, because some of the south Norwegian pegmatites are enriched in these rare elements. In the Tørdal area in SE of Telemark, a few granitic pegmatites were mined for mica and Mo in historical times (Segalstad and Raade, 2003).

In 1903, the first Sc mineral was discovered by Per Schei in granitic pegmatites of the Evje-Iveland pegmatite field, situated 80 km SW of Tørdal, and described scientifically by Schetelig (1911, 1922) as the first Sc-silicate ($Sc_2Si_2O_7$). This Sc mineral was named thortveitite. Except the thortveitite from the Evje-Iveland pegmatites, no other occurrences of Sc minerals have been recorded in Southern Norway until the late 1980`s.

Bergstøl and Juve (1988) and Juve and Bergstøl (1990) discovered the first Sc-bearing minerals in the Tørdal pegmatite field. They described the minerals bazzite, scandian ixiolite, and pyrochlore from the Heftetjern pegmatite. This indicated that some granitic pegmatites of the Tørdal pegmatite field, in particular the pegmatites of the Heftetjern area, are unusually enriched in Sc beside Be.

Mainly for that reason, the Tørdal pegmatite field has been in the past subjected to several exploration campaigns, most recently by the Canadian company Scandium International Mining Corporation (Scandium International Mining Corp., 2020b). This company reported that the highest measured Sc concentrations in Tørdal pegmatites was about 1600 ppm from XRF bulk rock analysis. In the Tørdal pegmatites, Sc is mainly bounded and incorporated into garnets and micas as trace amounts but also occurs in rare Sc minerals as major constituents (Rosing-Schow et al., 2018; Steffensen, 2018).

The aims of this study are (1) to determine the Sc concentrations in mica of some Tørdal pegmatites and to compare the concentrations with those of co-genetic garnets. The Sc concentrations of co-genetic garnets were previously investigated by Steffensen et al. (2018); (2) to identify Be minerals, such as beryl, gadolinite group minerals, and bazzite, and their Be concentrations in order to establish if there are local and regional associations between Sc and Be distribution in the Tørdal pegmatites; and (3) to investigate Sc and Be concentrations in pegmatite host rocks, in order to establish if Sc and Be enrichments of Tørdal pegmatites are related to Sc and Be concentrations of the host rocks. The results are discussed in terms to get a better understanding of the origin of Sc and Be in the Tørdal pegmatites and the possible sources of the melts of the Tørdal pegmatites.

In order to achieve the aims of this study, analysis were performed with state-of-the-art mineral-characterizing and analytical methods. These methods included optical microscopy, electron microprobe analysis (EPMA), laser ablation inductively coupled plasma mass spectrometry (LA-ICP-MS) and scanning electron microscopy (SEM). Whole rock analyses were carried out externally by Actlabs Laboratories, Ontario, Canada. The analyses were performed on specimen from the collection of the Natural History Museum of Oslo and on samples collected during a one-week field campaign in Tørdal. In addition, detailed geological field mapping was carried out in the Høydalen area, where some of the most Sc- and Be-enriched granitic pegmatites of the Trødal field occur.

1.1 Granitic pegmatites

1.1.1 What is a granitic pegmatite?

When describing very coarse-sized crystal textures in intrusive rocks, the term “pegmatite” is widely applied (Simmons et al., 2003). This very coarse-grained texture of pegmatites, with crystal sizes > 3 cm, is not the only but most important characteristics, which defines an igneous rock as pegmatite. London (2008) suggested a range of additional attributes, beside the very coarse-grained texture, to define pegmatites, such as very variable grain sizes, sharply bounded spatial zonation, skeletal crystal habits and graphic intergrowths of feldspar and quartz. In terms of pegmatite chemistry, Simmons et al. (2003) stated that: “Pegmatites can be any intrusive igneous rock type, which may vary from ultramafic, granitic and syenitic compositions, where pegmatites of granitic composition is the most used form”. Granitic pegmatites, such as pegmatites of the studied Tørdal pegmatite field, comprise worldwide the most common chemical group of pegmatites (Segalstad and Eggleston, 1993). Therefore, in the following, it is focused mainly on pegmatites with granitic composition. Due to their granitic composition

they comprise mainly feldspars, quartz and mica (Simmons et al., 2003; London, 2008). They may also be relative enriched in rare elements, which leads to exotic assemblages of rare minerals. The formation of different rare minerals are, however, dependent on the rare elements, which are enriched in the granitic pegmatites (Simmons et al., 2003; London, 2008). The main reason why granitic pegmatites are of great economic interest is that they concentrate the industrial minerals feldspars, quartz and micas, are enriched in rare metals, and are the major source of gemstones (Černý, 1991b; Glover et al., 2012; Linnen et al., 2012). The unique and diverse textures of granitic pegmatites and their specific mineralogy have attracted scientists more than 150 years, which resulted in countless mineralogical publications. Despite the wide range of mineralogical studies, the processes of pegmatite formation are still hardly debated. Therefore, their mineralogy, internal structure, origin, classification and economic importance are in the following discussed in more detail.

1.1.2 Mineralogy of granitic pegmatites with emphasis on Sc- and Be-minerals

Because of their name, granitic pegmatites consists of the major minerals feldspars, quartz and micas. Feldspars usually comprise K-feldspar (mostly microcline) and plagioclase with oligoclase to albite composition (e.g. Simmons et al., 2003). The platy variety of albitic plagioclase, commonly referred as "cleavealandite", is often observed in the chemically most evolved granitic pegmatites, such as Høydalen and Skardsfjell pegmatites of the Tørdal field (Raade and Kristiansen, 2000; Simmons et al., 2003). Quartz forms often a massive core of the pegmatite (Simmons et al., 2003; London, 2008). Quartz together with feldspars commonly form characteristic graphic intergrowth textures in granitic pegmatites, known as graphic granite because its texture may look like Egyptian hieroglyphs (Simmons et al., 2003; London, 2008). This graphic intergrowth texture is by some authors considered as a characteristic feature of granitic pegmatites (e.g. London, 2008). Micas are the third most common mineral in granitic pegmatites (Rosing-Schow et al., 2018). However, in some granitic pegmatites mica can be very rare and is in these cases considered as accessory mineral. Micas occur either as dioctahedral, white and K enriched micas (i.e. muscovite) or trioctahedral, dark and Fe-Mg enriched micas (i.e. biotite) (Simmons et al., 2003; London, 2008). The granitic pegmatites can be divided into two families based on their enrichments of rare elements according to Černý (1990, 1991a): NYF (niobium-yttrium-fluroine) and LCT (lithium-caesium-tantalum). In the most chemical evolved and complex zoned granitic pegmatites of the Li enriched LCT or F enriched NYF families, K enriched micas mainly dominates over Fe-Mg enriched micas. This is due to the progressive evolution in granitic pegmatites, where micas becomes Fe-poor and Mn-rich and relatively enriched in K. In the most fractionated pegmatites they become

“lepidolite”, which is a Li enriched mica type (London, 2008; Rosing-Schow et al., 2018). The chemical variation of micas in pegmatite NYF families, such as granitic pegmatites of Tørdal pegmatite field, may range from magnesian siderophyllite, which are highly Mg and Fe enriched, to Fe poor and Li rich polylithionite within one pegmatite body (e.g. Rosing-Schow et al., 2018).

Beside the major mineralogy of granitic pegmatites, they may also contain a wide range of accessory minerals. The diversity of accessory minerals depends on the enrichments of rare elements in the pegmatite (Simmons et al., 2003; London, 2008). Characteristic accessory minerals of granitic pegmatites, which are also used for pegmatite classifications, include beryl, spodumene, petalite, lepidolite, tourmaline, amblygonite, columbite group minerals, hambergite, cassiterite, microlite, and topaz for the LCT family, while allanite, euxenite, gadolinite, monazite, zircon, rutile, fluorite, ilmenite, fergusonite, and zinnwaldite are typical for the NYF family (Černý and Ercit, 2005). The concentrations and enrichments of rare elements are mainly dependent on the source rock and fractionation degree of granitic pegmatite melts. Scandium and Be concentrations in granitic pegmatite melts and the sources and processes of their enrichment are of major interest in this study. If granitic pegmatite melts contain high enough concentrations of Sc and Be they may form rare Sc and Be minerals, such as beryl, gadolinite-(Y), and bazzite. In Table 1.1 the most common Sc and Be minerals found in granitic pegmatites are listed (Simmons et al., 2003; Mindat, 2020g).

Table 1.1. Common Be- and Sc-minerals found in granitic pegmatites

Sc minerals		**Be minerals**	
Mineral name:	**Formula:**	**Mineral name:**	**Formula:**
Bazzite	$Be_3(Sc,Fe^{3+},Mg)_2Si_6O_{18} \cdot Na_{0.32} \cdot nH_2O$	Agakhanovite-(Y)	$YCa\square_2KBe_3Si_{12}O_{30}$
Cascandite	$Ca(Sc, Fe^{3+})(HSi_3O_9)$	Barylite	$BaBe_2Si_2O_7$
Heftetjernite	$ScTaO_4$	Bavenite	$Ca_4Be_{2+x}Al_{2-x}Si_9O_{26-x}(OH)_{2+x}$ (x = 0 to 1)
Kristiansenite	$Ca_2ScSn(Si_2O_7)(Si_2O_6OH)$	Bazzite	$Be_3(Sc,Fe^{3+},Mg)_2Si_6O_{18} \cdot Na_{0.32} \cdot nH_2O$
Oftedalite	$K(Sc,Ca,Mn^{2+})_2\square_2[(Be,Al)_3Si_{12}O_{30}]$	Behoite	$Be(OH)_2$
Scandiobabingtonite	$Ca_2(Fe^{2+},Mn)ScSi_5O_{14}(OH)$	Bertrandite	$Be_4Si_2O_7(OH)_2$
Thortveitite	$Sc_2Si_2O_7$	Beryl	$Be_3Al_2Si_6O_{18}$
		Beryllite	$Be_3(SiO_4)(OH)_2*H_2O$
		Bityite	$CaLiAl_2(Si_2BeAl)O_{10}(OH)_2$
		Boheseite	$Ca_4Be_{3+x}Al_{1-x}Si_9O_{25-x}(OH)_{3+x}$, (x = 0 to 1)
		Bromelite	BeO
		Chkalovite	$Na_2BeSi_2O_6$
		Chrysoberyl	$BeAl_2O_4$
		Danalite	$Be_3Fe^{2+}{}_4(SiO_4)_3S$
		Epididymite	$Na_2Be_2Si_6O_{15}*H_2O$
		Eudidymite	$Na_2Be_2Si_6O_{15}*H_2O$
		Euclase	$BeAlSiO_4(OH)$
		`Gadolinite-Group`	$A_2MQ_2T_2O_8\varphi_2$ *A* = Ca, REE, (Y and lanthanoids) *M* = Fe, □ (vacancy), Al *Q* = B, Be, Li *T* = Si φ = O, OH
		Genthelvite	$Be_3Zn_4(SiO_4)_3S$
		Helvine	$Be_3Mn^{2+}{}_4(SiO_4)_3S$
		Milarite	$KCa_2(Be_2AlSi_{12})O_{30} \cdot H_2O$
		Oftedalite	$K(Sc,Ca,Mn^{2+})_2\square_2[(Be,Al)_3Si_{12}O_{30}]$
		Phenakite	$Be_2(SiO_4)$

Among the Be minerals, beryl, $Be_3Al_2Si_6O_{18}$, is most common in granitic pegmatites (Simmons et al., 2003; London, 2008). Beryl is relative common in such environments, despite the fact that Be has a low abundance in the Earth`s continental crust, in average 3 ppm (Mason and Moore, 1982; London, 2008). In granitic pegmatite bodies, beryl may occur in any zones or places. The beryl crystallization depends on the Be saturation (>35 ppm Be) of the granitic pegmatite melt (London and Evensen, 2002; London, 2015). Beryl comes in many different colours. The green colour is the most common one. These colour variants include mainly aquamarine (blue), helidore (yellow), emerald (dark green), morganite (pink) and goshenite (colorless) (London, 2008; London, 2015).

The Sc analogue for beryl is bazzite, $Be_3Sc_2Si_6O_{18}$, which occurs mainly in granitic pegmatites with NYF affinity (Juve and Bergstøl, 1990; Simmons et al., 2003). Bazzite forms a solid solution with beryl, where main differences between these two minerals are different occupations in their octahedral site *(o)*. Scandium mainly dominates, together with Fe^{3+}, the octahedral site *(o)* of bazzite, while Al dominates the octahedral site *(o)* of beryl (Armbruster, 1995; Simmons et al., 2003). Bazzite is a rare accessory mineral, which was discovered in the studied Heftetjern pegmatite of Tørdal pegmatite field by Bergstøl and Juve (1988) and Juve and Bergstøl (1990). Beside Heftetjern, bazzite was later also discovered in the nearby Høydalen pegmatites (Mindat, 2020b; Mindat, 2020c).

Gadolinite-(Y), $Y_2FeBe_2Si_2O_{10}$, is also a common Be mineral in granitic pegmatites such as beryl, and typical for pegmatites of the NYF family (Simmons et al., 2003; Černý and Ercit, 2005). Beside Be, the mineral is relatively enriched in REE, such as Y and REE. Due to its Th and U content the mineral is often metamict and, thus, becomes easily altered by hydrothermal fluids during the latest stages of pegmatite formation and it may alter into hingganite-(Y) (Pezzotta et al., 1999).

1.1.3 Internal structure of granitic pegmatites

The internal structure of granitic pegmatites depends mainly on the fractionation degree of pegmatite melts. Pegmatite melts which are relative unfractionated have generally a homogenous composition with no or little signs of internal zoning of the pegmatite body. Highly fractionated pegmatite melts form granitic pegmatites with heterogenous compositions, which exhibit characteristic zoning throughout the pegmatite bodies (Simmons et al., 2003). Based on these observations, internal structures of granitic pegmatites are classified as unzoned, simple or complex zoned (Cameron et al., 1949; Simmons et al., 2003). Unzoned granitic pegmatites are those with primitive characteristics, homogenous compositions and no distinct zoning (Simmons et al., 2003; London, 2008). Simple zoned granitic pegmatites are moderate evolved compared to unzoned pegmatites. They show a simple, often concentric zoning in terms of texture (i.e. grain size and shape), mineralogy and chemistry (Simmons et al., 2003; London, 2008). These zones are named (from the contact to the core of the pegmatite body) border zone, wall zone, intermediate zone and core (Cameron et al., 1949). The zoning reflects the inward crystallisation and fractionation of the granitic pegmatite body (Cameron et al., 1949). The border zones were the first to crystallize, while wall zones and intermediate zone crystallized later. The last to crystallize was the massive pegmatite core (Cameron et al., 1949; Simmons et al., 2003). During this fractional crystallization process, grain sizes gradually increases from the border zones towards the pegmatite core (Fig. 1.1). Border and intermediate zones are not

necessarily developed in each simple zoned pegmatite. The pegmatite core, which is the last to crystallize, is often formed by massive quartz (Simmons et al., 2003; London, 2008). Complex zoned granitic pegmatites are the most chemical evolved ones and have a primarily similar internal structure as simple zoned granitic pegmatites. In addition to their normal internal zonation, discordant units commonly named as replacement units or discordant albite zones are present in complex zoned granitic pegmatites (Simmons et al., 2003; Müller at al., 2018a). Formation of these replacement units are related to late stages of the pegmatite formation (Cameron et al., 1949; Müller et al., 2018a). The replacement units are commonly known as alkali-rich albite zones, where the albite variant "cleavelandite" is a typical mineral in these units. Since these replacement units may comprise high amounts of exotic mineralogy, they have gained lots of economically interest (Müller at al., 2018a). Figure 1.1 shows a schematic illustration shows of the internal structure of a chemical evolved and complex zoned granitic pegmatite body with late stage replacement units. In this case, the replacement units are developed at the intermediate-wall zone boundary, but replacement units may occur in any part of the granitic pegmatite body.

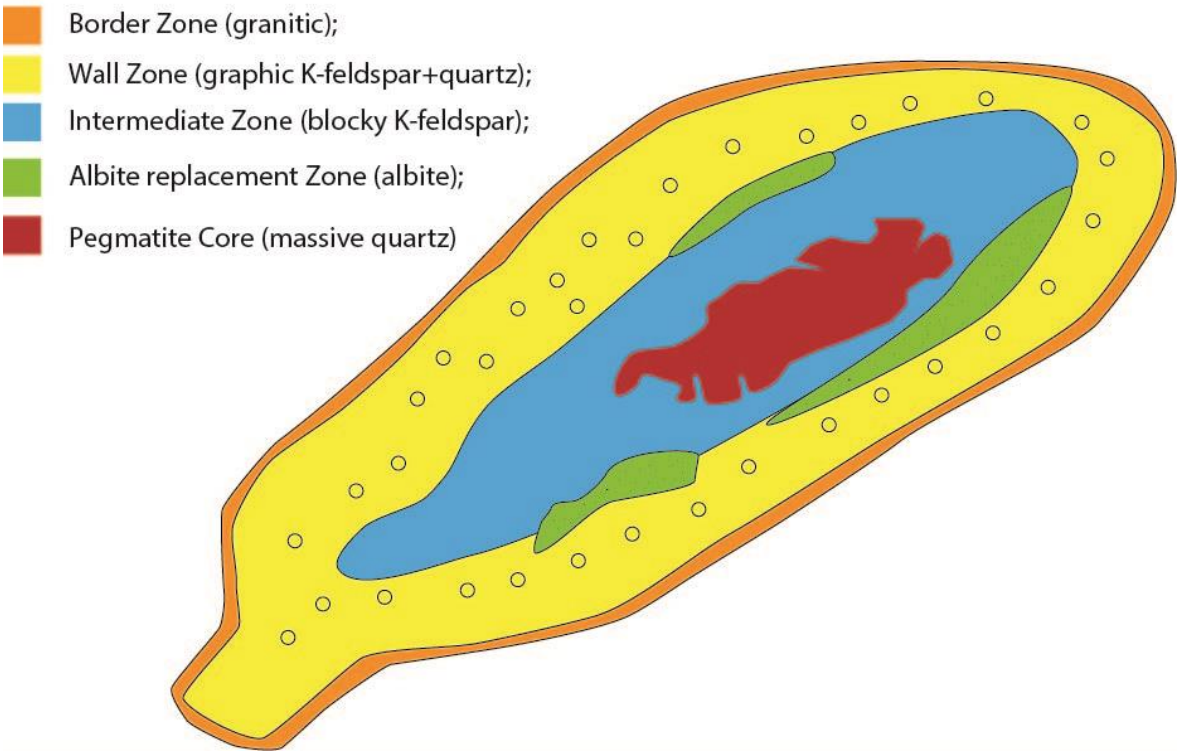

Fig. 1.1. Schematic illustration of a complex zoned granitic pegmatite with primary concentric zones and late-stage replacement units. Initial stages of crystallization starts in the outer zones of the pegmatite from where it gradually moves inward. The pegmatite crystallizes relative fine-grained grain sizes in the initial stages of

crystallization (border zone), where the grain sizes gradually increases towards the core of the pegmatite. In the intermediate zone, the grain texture is commonly very large where blocky K-feldspars up to several meters in size may crystallize. From Simmons et al. (2003) who modified it from Cameron et al. (1949).

1.1.4 Origin of granitic pegmatites

Based on today`s research, geoscientists agree that granitic pegmatites are igneous (magmatic) in origin (London, 2008). In contrast to the majority of granitic pegmatite melts, concentrations of volatiles (i.e. OH, F) and incompatible elements play an important role in these pegmatite melts. Simmons et al. (2003) stated that volatiles in granitic pegmatites melts reduce the viscosity and solidification temperatures. Incompatible elements become strongly enriched in pegmatite melts because they are excluded by rock-forming minerals during progressing crystallization. Today there are two contrasting theories which control the crystallization of pegmatite melts, first, the supercritical melt theory by Thomas et al. (2000) and, second, boundary layer theory by London (2008, 2009).

The supercritical melt theory bases on observations of coexisting melt and fluid inclusions in pegmatite minerals. When the temperature of an initial supercritical pegmatite melt decreases, two types of the melt (inclusions) form (melt/melt immiscibility): a Si-rich and H_2O-poor melt portion and a Si-poor and H_2O-rich melt portion (Thomas et al., 2000; Thomas and Davidson (2012, 2016)). Si-poor and H_2O-rich melt is enriched in Na and able to dissolved high concentrations of compatible elements. This melt has also a much lower crystallization temperature, which probably represent the incompatible-element-enriched albite replacement zones (Müller et al., 2018a).

The second theory, developed by London (2008, 2009), emphasizes on the boundary layer process which developed in front of growing crystals at the contact with the pegmatite melt. During fractional crystallization of the pegmatite melt, pegmatite-forming minerals, the pegmatite melt is gradually depleted in compatible elements in order to form these minerals. During this fractional crystallization process, the boundary melt layer in front of the crystal becomes more and more enriched in incompatible elements, such as Li, Rb, Cs, Be and Ta. After some time, the incompatible elements becomes saturated in the boundary layer melt, where they may form their own rare minerals, such as beryl and lepidolite.

Pegmatite melts themselves are either created by partial melting of metamorphic rocks (anataxis) or the represent restitic, fractionated melts of a large-volume granitic pluton. In the latter case, these restitic melts are enriched in volatiles and incompatible elements, due to their enrichment through long-term fractionation and crystallization of a large volume of granitic

magma. These granite-pluton-derived pegmatite melts may emplace within parental pluton or move out into metamorphic host rocks and crystallize in the vicinity or far away from the granitic pluton forming a pegmatite field (Simmons et al., 2003; Simmons and Webber, 2008). Pegmatite melts may originate directly from partial melting of the metamorphic rocks in high temperature (-pressure) environments, a process which is referred as anataxis (Simmons and Webber, 2008). Indications of anatectic origin of pegmatite melts are given, when there is no any relationship in age or chemical characteristics to the nearby granitic pluton or that there is no granitic pluton in the vicinity of the granitic pegmatites (Simmons and Webber, 2008). Simmons et al. (1995, 1996), for example, proposed that partial melting around plutons in orogenic environments could form pegmatite melts, where pegmatite melts are formed by anataxis, and are not a product of a crystallizing pluton.

In the studied Tørdal pegmatite field, until most recently, the Tørdal granite have been thought to be the source of granitic pegmatites in the area (Juve and Bergstøl, 1997). However, new age by Rosing-Schow et al. (2019) showed that the Tørdal pegmatites are about 40 Ma younger than the Tørdal granite. The enrichment of rare elements in the pegmatite host rocks, as in the Tørdal pegmatites, are significantly higher compared to the Tørdal granite (Bergstøl and Juve, 1988). It is, therefore, believed that the granitic pegmatites of the studied Tørdal pegmatite field may have originated by partial melting of their amphibolitic host rocks (Müller et al., 2015). Similar observations have been made in other Sveconorwegian pegmatites fields, such as Froland and Evje-Iveland (Müller et al., 2015; Müller et al., 2017). Investigations by Andersen (1997) showed that the nearby Herefoss granite is 120 Ma younger than the adjacent pegmatites of the Froland pegmatite field, while Snook (2014) and Müller et al. (2015) explored that the adjacent Høvringsvatnet granite is about c. 50 Ma years older than the nearby pegmatites of the Evje-Iveland field. It is suggested that most of the Sveconorwegian pegmatites may have originated by partial melting of their host rocks instead of being a fractionation product of adjacent granite plutons (Müller et al., 2015).

1.1.5 Classification of granitic pegmatites

Numerous attempts have been made to classify granitic pegmatites, but this has been proven difficult because of their mineralogical and textural complexity (Müller et al., 2018b). Because of their very coarse crystal textures and heterogeneity of granitic pegmatite bodies it is - in most cases – not possibly to determine the bulk chemistry of granitic pegmatites, which could be used for classification as it has been done for other igneous rocks. Therefore, through the centuries, geoscientists have been using different criteria to classify granitic pegmatites (Černý and Ercit, 2005).

The very first, widely recognized classification of granitic pegmatites was established by the Russian mineralogist Fersman (1930). He classified pegmatites on the basis of their crystallization temperature, based upon paragenetic mineral assemblages. Ginsburg and Rodinov (1960), and particularly Ginsburg et al. (1979) introduced the concept of classifying granitic pegmatites according to their emplacement depths. They distinguished four pegmatite classes. Beside the emplacement depth these pegmatite classes where defined by the metamorphic grade of the pegmatite host rocks and their relationship to the granitic plutons. The four pegmatite classes comprise abyssal (high metamorphic grade, high to low pressure), muscovite (high pressure, lower temperature), rare-element (low temperature and pressure), and miarolitic pegmatites (shallow level). Černý and Ercit (2005) refined and extended this depth-zone classification of Ginsburg et al. (1979). In addition to Ginsburg's et al. (1979) four classes, they introduced a new class, known as muscovite-rare-element class (Černý and Ercit, 2005). Beside the classification of granitic pegmatites into classes, Černý (1990, 1991a) introduced the concept of classifying granitic pegmatites based on three petrogenetic signature. These three petrogenetic families are characterized by their enrichments of specific rare elements, where one family has elevated amounts of Nb, Y and F and is referred as the NYF pegmatite family. These granitic pegmatites are mainly fractionated from A- to I-type granites or inherited this signature by partial melting of such rocks involving depleted crust or mantle contributions. The second family is characterized by their high enrichments of Li, Cs and Ta and is, therefore, named the LCT pegmatite family. Granitic pegmatites with such signatures are commonly derived from S-type granites or metasediments, since they are relative enriched in Li, Cs and Ta. If the melt source comprise both igneous A- and I-type rocks and metasedimentary rocks, the granitic pegmatites may develop a mixed NYF-LCT family, representing the third pegmatite family. In summary, the refined pegmatite class classification by Černý and Ercit (2005) comprising of the five pegmatite classes abyssal, muscovite, muscovite-rare element, rare-element, and miarolitc, and the pegmatite family classification by Černý (1990, 1991a) comprising NYF, LCT and mixed NYF-LCT pegmatites, are today the most widely applied classification schemes used for granitic pegmatites (Fig. 1.2).

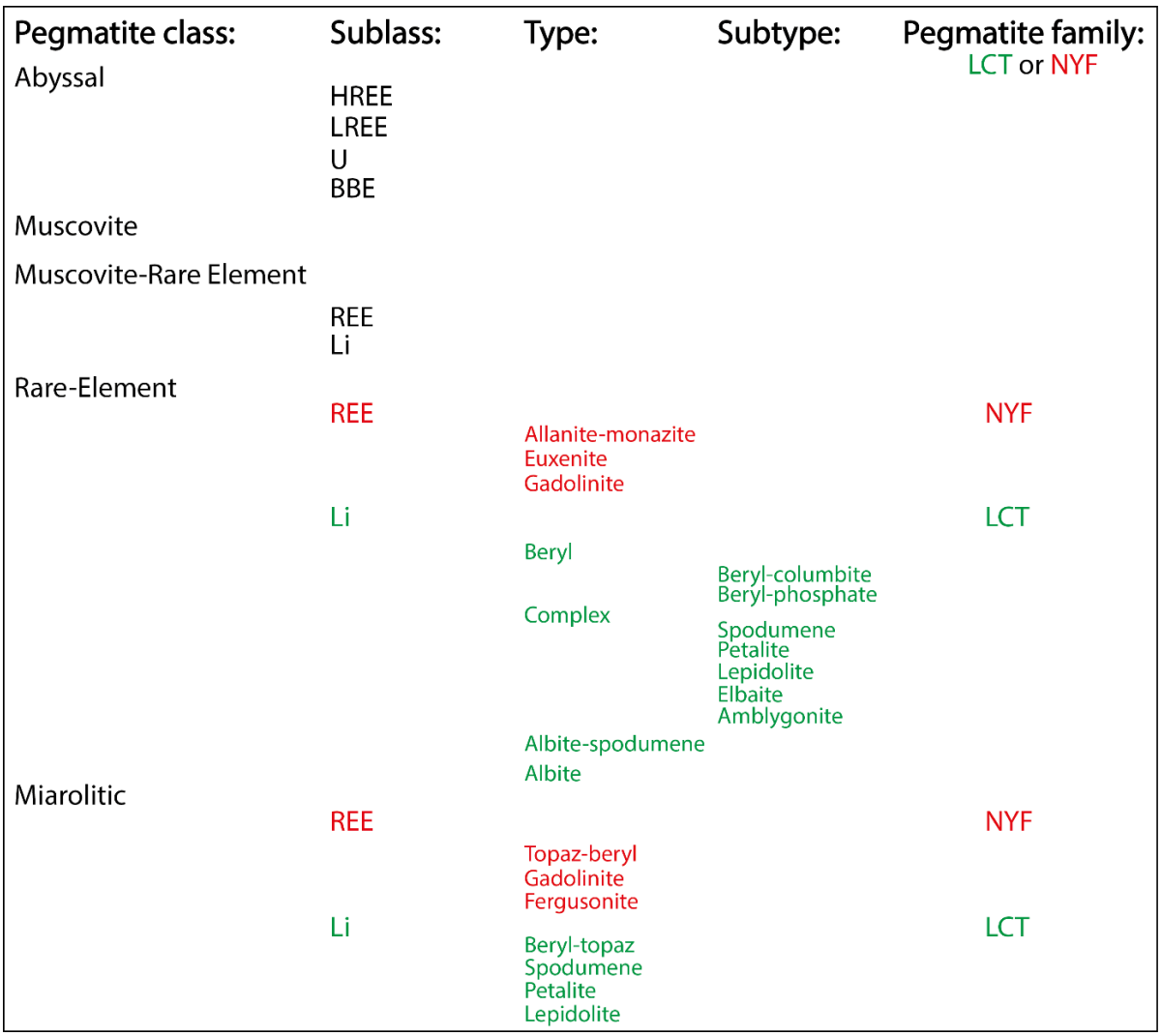

Fig. 1.2. Today`s most used classification scheme for granitic pegmatites according to Černý and Ercit (2005) and Černý (1990, 1991a) based on pegmatite classes and pegmatite families.

1.1.6 Economic importance of granitic pegmatites with special emphasis on scandium and beryllium

Since prehistoric times, granitic pegmatites have been mined for their exotic mineralogy such as gemstones (i.e. beryl, topaz, garnet, etc.) and semi-precious stones (amazonite, smoky and violet quartz) (London, 2008). The economic interest for their major mineralogy, commonly referred as industrial minerals, have extended later on. Of these, quartz and feldspars were mainly used for the manufacture of glass and ceramics, while micas, in form of sheet mica, were mainly mined during Second World War and used in the electrical industries (London, 2008; Glover et al., 2012). Still today, granitic pegmatites are mostly mined for their industrial minerals, because their applications have been extended and changed. Today, quartz is widely used for vitreous silica and other silicate glasses or for the supply for solar-grade silicon metal, while K-feldspar and plagioclase, separately or in combination, are primary ingredients of commercial glass, and significant components of porcelain (London, 2008; Glover et al., 2012).

Micas are widely used as ingredients in paint, make-up and other cosmetic products (London, 2008; Glover et al., 2012). Beside concentrating these industrial minerals, chemical evolved granitic pegmatites may contain exploitable quantities of rare metal minerals (Glover et al., 2012; Linnen et al., 2012).

In this study, major interests emphasizes on the concentrations of the rare elements Sc and Be in granitic pegmatites. Beryllium has a great economic which is predominantly bound by the Be mineral beryl. Primary sources of modern Be production are beryl mined from granitic pegmatites and bertrandite ($Be_4Si_2O_7(OH)_2$) mined from rhyolite (London, 2008; Linnen et al., 2012). Beryl is also a very precious mineral, which may develop gemstone quality, which can be used for jewellery production. Importance of Be in today`s society is its ability to form hard and light Be-Cu alloys, which are stronger and lighter than steel and Al metal (Simmons et al., 2003; London, 2008). These Be-Cu alloys are, used for gears, bearings, electronics and aerospace applications due to its special properties and capabilities (Simmons et al., 2003; London, 2008).

Scandium, which has gained a lot of interests during recent time, is also an economic valuable element. Beside the main deposits of Sc in China and Russia, deposits of Sc in granitic pegmatites, in form of Sc minerals, have some economic potential (William-Jones and Vasyukova, 2018). NYF pegmatites are those, which may contain Sc minerals in considerable amounts, such as the studied Tørdal pegmatite field and also the Evje-Iveland pegmatite field (William-Jones and Vasyukova, 2018). In Evje-Iveland pegmatite field, the major source of Sc is the mineral thortveitite ($Sc_2Si_2O_7$) (William-Jones and Vasyukova, 2018). Scandium, its chemistry, mineralogy and applications are further discussed in the next chapter.

1.2 Scandium

1.2.1 What is scandium (Sc)?

Scandium (Sc) is one of the transition elements and known for its light weight. It has the atomic number 21. Scandium was first discovered through element separation from the REE-bearing minerals gadolinite and euxenite by the Swedish chemist Fredrik Nilson in 1879 (Segalstad and Raade, 2003; Samson and Chassé, 2016; Voncken, 2016; William-Jones and Vasyukova, 2018). Scandium is commonly referred as REE, which comprise of the Lanthanides (La-Lu) and Yttrium (Y) (Voncken, 2016). The reason for its association with the Lanthanides and Y is mainly because Sc has a similar oxidation state and geochemical behavior as these elements (Voncken, 2016). However, Sc is distinguished from them because it has an ionic radii of 75

pm, which is smaller compared to the other REE (103 pm for La to 86 pm for Lu), which makes Sc a more compatible element compared to the more incompatible REE (Voncken, 2016; William-Jones and Vasyukova, 2018). Some of the characteristics of Sc are listed in Table 1.2 (Voncken, 2016).

Table 1.2. Electron configuration, oxidation state and oxide of Sc.

Electron configuration	[Ar] $3d^1 4s^2$
Oxidation state	Sc^{3+}
Oxide	Sc_2O_3

1.2.2 Scandium minerals

In nature, Sc is associated with elements known as high-field strength elements (HFSE), which are commonly enriched in granitic pegmatites, such as studied Tørdal pegmatites (Siegfried et al., 2018; William-Jones and Vasyukova, 2018). In such environments, Sc concentrations in pegmatite melts may be so high that during fractional crystallization they crystallize Sc minerals. However, in most cases, Sc enters major and accessory minerals in granitic pegmatites as traces. This is mainly because Sc substitutes easily for Mg, Fe and Al in ferromagnesian minerals, such as garnet, mica, amphibole, and clinopyroxene, due to their similar ionic radii (Segalstad and Raade, 2003; William-Jones and Vasyukova, 2018). The first Sc mineral was discovered in granitic pegmatites of the Evje-Iveland pegmatite field by Per Schei in 1903. This pegmatite field is situated 80 km SW from the studied Tørdal pegmatite field. This Sc mineral was discovered in the Landsverkbruket also called Landsverk 3 pegmatite (Kristiansen, 2003; William-Jones and Vasyukova, 2018). However, the Sc mineral was not described scientifically until 1911 by Schetelig (1911). He identified the mineral as the Sc-silicate ($Sc_2Si_2O_7$) and named it thortveitite (Schetelig, 1922), according to the name of the owner of the pegmatite mine, Olaus Thortveit (Kristiansen, 2003; William-Jones and Vasyukova, 2018). Concentrations of Sc in this mineral can reach concentrations as much as 32 wt.% Sc_2O_3. Beside in Norway, thortveitite has been discovered in granitic pegmatites in Austria, Brazil, Canada, China, Czecch Republic, Finland, France, Germany, Italy, Japan, Kazakhstan, Madagascar, Poland, Russia, Sweden, and USA (Siegfried et al., 2018; Mindat, 2020e). Thortveitite is one of 18 Sc minerals known today, minerals in which Sc is a major constituent (Table 1.3).

Table 1.3. Known Sc-minerals according to Mindat (2020f).

Minerals:	**Formula:**
Allendeite	$Sc_4Zr_3O_{12}$
Bazzite	$Be_3Sc_2(Si_6O_{18})$
Bonacinaite	$Sc(AsO_4)*2H_2O$
Cascandite	$Ca(Sc, Fe^{3+})(HSi_3O_9)$
Davisite	$CaScAlSiO_6$
Eringaite	$Ca_3Sc_2(SiO_4)_3$
Heftetjernite	$ScTaO_4$
Jervisite	$NaSc^{3+}Si_2O_6$
Juonniite	$CaMgSc(PO_4)_2(OH)*4H_2O$
Kampelite	$Ba_6Mg_3Sc_8(PO_4)_{12}(OH)_6*7H_2O$
Kangite	$(Sc, Ti, Al, Zr, Mg, Ca, \square)_2O_3$
Kolbeckite	$ScPO_4*2H_2O$
Kristiansenite	$Ca_2ScSn(Si_2O_7)(Si_2O_6OH)$
Oftedalite	$K(Sc,Ca,Mn^{2+})_2\ \square_2[(Be,Al)_3Si_{12}O_{30}]$
Pretulite	$Sc(PO_4)$
Scandiobabingtonite	$Ca_2(Fe^{2+},Mn)ScSi_5O_{14}(OH)$
Thortveitite	$Sc_2Si_2O_7$
Warkite	$Ca_2Sc_6Al_6O_{20}$

Beside thortveitite, bazzite ($Be_3Sc_2Si_6O_{18}$) is another Sc mineral associated with NYF granitic pegmatites, which occurs in studied Tørdal pegmatites (Bergstøl and Juve, 1988; William-Jones and Vasyukova, 2018). Bergstøl and Juve (1988) and Juve and Bergstøl (1990) were the very first authors who described this Sc- and Be mineral from the Sc-enriched Heftetjern pegmatite, which lies between the Skardsfjell and Høydalen localities of the Tørdal area (Fig. 1.3). The bazzite from the Heftetjern pegmatite contains as much as 20 wt.% Sc_2O_3 (Bergstøl and Juve, 1988). Beside bazzite and thortveitite, six other Sc minerals have been identified at the Heftetjern pegmatite (Mindat, 2020b; Table 1.4). Bazzite has also been discovered at the Høydalen pegmatites (Mindat, 2020c).

Table 1.4. Known Sc-minerals today of Tørdal pegmatites according to Mindat (2020b, 2020c).

Mineral:	**Formula:**	**Pegmatite locality:**
Bazzite	$Be_3Sc_2(Si_6O_{18})$	Heftetjern and Høydalen
Cascandite	$Ca(Sc, Fe^{3+})(HSi_3O_9)$	Heftetjern
Heftetjernite (TL)	$ScTaO_4$	Heftetjern
Var: Scandian Ixioite	$(Sc,Ta,Nb,Sn,Fe,Ti)_4O_8$	Heftetjern
Kristiansenite (TL)	$Ca_2ScSn(Si_2O_7)(Si_2O_6OH)$	Heftetjern
Oftedalite (TL)	$K(Sc,Ca,Mn^{2+})_2\ \square_2[(Be,Al)_3Si_{12}O_{30}]$	Heftetjern
Scandiobabingtonite	$Ca_2(Fe^{2+},Mn)ScSi_5O_{14}(OH)$	Heftetjern
Thortveitite	$Sc_2Si_2O_7$	Heftetjern

1.2.3 Scandium deposits

According to Rudnick and Gao (2014) the average Sc concentration of Earth`s continental crust (upper, middle and lower) is 21.9 ppm, where the element is more depleted in Earth`s upper crust (average 14 ppm Sc) compared to Earth`s lower crust (average 31 ppm Sc). Scandium is

more enriched in mafic rocks compared to felsic rocks. This is the reason why oceanic crust is more enriched in Sc than continental crust (Samson and Chassé, 2016). Because of the general compatible behavior of Sc, it is relatively evenly distributed in Earth`s crust. Thus, economic enrichments of Sc are very rare and, thus, it is referred as a very expensive commodity (Siegfried et al., 2018). The high Sc demand of the air- and space craft industry has added to the high raw material price in recent times (Siegfried et al., 2018; William-Jones and Vasyukova, 2018). The price of 99.99% Sc concentrate varies from 4,000 to 20,000 US$ per kg during the last decade (Strategic Metal Investments Ltd., 2020). The high variation of the Sc price is mainly because of the limited production and market for Sc and the fluctuating demand (Strategic Metal Investments Ltd., 2020).

Carbonatites are currently the most common source of Sc and the major Sc deposits. The Bayan Obo carbonatite mine in China is currently the Sc largest producer. Clinopyroxene (aegerine) is the major host of Sc in this deposit, where the mineral is formed by fluid alteration of igneous carbonate. However, the primary source of the Sc in the carbonatite remains uncertain (William-Jones and Vasyukova, 2018). Another type of Sc deposits are laterites. Laterites are soils, which form due to intense chemical weathering in tropical climate. Clinopyroxene is the major primary source of Sc in laterites. During tropical weathering, Sc is released from the decaying clinopyroxene and adsorbed by iron oxides, such as goethite (Siegfried et al., 2018). This process is responsible for the formation of the Nyngan deposit in New South Wales, Australia, which is one of the largest laterites Sc deposit. Granitic pegmatites of the NYF type, such as Tørdal and Evje-Iveland pegmatite fields in southern Norway, are known for their Sc enrichments and form the third type of Sc deposits (William-Jones and Vasyukova, 2018). Major hosts of Sc in the Evje-Iveland pegmatites is mainly thortveitite (William-Jones and Vasyukova, 2018), while the major hosts in Tørdal pegmatites is garnet and mica. Since garnet and mica are widely distributed and abundant in these granitic pegmatites, large amounts of them with Sc as traces may have economic potential for Sc extraction.

Today, the main producers of Sc worldwide are China, Russia, Ukraine and the Philippines (Siegfried et al., 2018; William-Jones and Vasyukova, 2018). According to USGS (2019), the global production of Sc varies about 10 to 15 tonnes each year. China produces most Sc dominating and monopolizing the Sc market (Siegfired et al., 2018; William-Jones and Vasyukova, 2018). The Bayan Obo deposit produces almost 90% (15 tonnes) of the worldwide supply of Sc each year (William-Jones and Vasyukova, 2018). This carbonatite deposit mainly produces REE and Fe, but also Sc as a by-product (Duyvesteyn and Putnam, 2014).

1.2.4 Scandium applications

The demand for Sc in today`s industry is continuously increasing. Main use of Sc in today`s society is in solid oxide fuel cells (SOFC). Adding small portions of Sc to SOFC lowers the operating temperature which results in longer cell operation times (Scandium International Mining Corp., 2020a). The ability of Sc to form strong and light alloys with other metals, such as Al, is the major reason for the increasing Sc demand (Kristiansen, 2003). Alloys of Sc-Al are much stronger, lighter, and more heat resistant than conventional Al alloys (Scandium International Mining Corp., 2020a). Due to their special properties, Al-Sc alloys are used in air- and space crafts (Siegfried et al., 2018). The use of these alloys reduces the weight of aircraft, which in turn reduces the fuel consumption and, thus, CO_2 emission (Siegfried et al., 2018). Other applications of these alloys are bicycles, golf clubs and sporting accessories (Kristansen, 2003; Scandium International Mining Corp., 2020a).

1.3 Geological setting of Tørdal pegmatite field

1.3.1 The geology of Tørdal pegmatite field

The Sveconorwegian pegmatite province covering large parts of the Sveconorwegian orogeny in South Norway and southwest Sweden, hosts over 5000 pegmatites and is one of the largest pegmatite provinces in the world (Müller et al., 2015; Müller et al., 2017). The Sveconorwegian orogeny formed as a result of multiple continent-continent collisions between 1.2 to 0.9 Ga (Falkum, 1985; Gower et al., 1990; Bingen et al., 2008; Li et al., 2008; Slagstad et al., 2017). The Sveconorwegian pegmatite province, which covers large areas of the Sveconorwegian orogeny, extends from Hitra Island in SW Norway towards Gothenburg in SW Sweden and is divided into seven pegmatite districts. The Tørdal pegmatite field, the target area of this study, is part of the Nissedal pegmatite district (Müller et al., 2017). The lithology of the Tørdal pegmatite field comprises of three sequences, known as the (1) gneissic basement (<1500 Ma), (2) the volcano-sedimentary sequence of the so-called Nissedal Outlier (1300-1200 Ma), which lies on top of the gneissic basement; and (3) the Tørdal-Treungen granite complex (960-850 Ma), which has intruded the two latter metamorphic sequences (Bergstøl and Juve, 1988; Raade and Kristiansen, 2000). The most common rock types of the Nissedal Outlier are ampihoblite, metagabbro and biotite-hornblende gneiss (Mitchell, 1967; Bergstøl and Juve, 1988; Fig 3.2; Table 3.1). These rocks form the host rocks of the studied Tørdal pegmatites. Historically, it has been suggested that the melts forming the Tørdal pegmatites originated from their nearby Tørdal-Treungen granite (Juve and Bergstøl, 1997). However, Rosing-Schow et al. (2019) determined that the Tørdal-Treungen granitic pluton is approximately 40 Ma older than the

Tørdal pegmatites. This implies that the pegmatite melts of the Tørdal pegmatites do not originate from the Tørdal-Treungen granite, and were probably formed by partial melting of their host rocks of the Nissedal Outlier (Müller et al., 2015; Müller et al., 2017).

1.3.2 Pegmatites of Tørdal pegmatite field

For a long time, the granitic pegmatites of Tørdal have attracted mineral collectors and geoscientists due to its interesting and exotic mineralogy. The rare mineralogy in these granitic pegmatites is mainly because of enrichments of rare elements such as Sc, Be, Li, Sn, Nb and Ta (Bergstøl and Juve, 1988; Juve and Bergstøl, 1997). These enrichments have led to scientific but also economic interest. The first mineralogical descriptions of the pegmatites were published by Oftedal (1941, 1942). He studied the Upper Høydalen, Lower Høydalen and Skardsfjell pegmatites, which he described as relative Li and Sn enriched pegmatites, because of the occurrence of lepidolite and cassiterite. Since the 1980's the Tørdal pegmatites have been intensively studied and described by several authors (Bergstøl and Juve, 1988; Juve and Bergstøl, 1990; Segalstad and Eggleston, 1993; Kristiansen, 1998; Raade and Kristiansen, 2000; Segalstad and Raade, 2003).

The granitic pegmatites of the Tørdal pegmatite field occur mainly as irregular to dyke-like bodies with sizes ranging from few centimeters to several hundred meters in length (Segalstad and Eggleston, 1993; Segalstad and Raade, 2003; Fig. 3.2; Table 3.1). Their compositions and internal structure varies from chemical primitive, homogenous, and unzoned pegmatites to more chemical evolved, heterogenous, and complex zoned pegmatites (Segalstad and Eggleston, 1993; Segalstad and Raade, 2003). Mineralogical most interesting of these Tørdal pegmatites are the chemically evolved, complex zoned pegmatite bodies since they exhibit the greatest diversity of rare accessory minerals and are, therefore, most enriched in rare elements (Table 3.1). These Tørdal pegmatites are mainly situated in the northeast NE of the field according to Segalstad and Eggleston (1993) (Fig. 1.3). These authors introduced the concept of regional zoning of Tørdal pegmatite field, based on the colouring of K-feldspar found in the granitic pegmatites. According to Segalstad and Eggleston (1993), the granitic pegmatite mainly containing pinkish K-feldspar are the most chemical primitive pegmatites, and occur in S of the field (Fig. 1.3). Granitic pegmatites with white K-feldspar are moderate evolved granitic pegmatites and occur slightly N of the pink K-feldspar zone (Fig. 1.3). White K-feldspar zone is followed further towards N by granitic pegmatites with green K-feldspar (amazonite), which represent the most chemical evolved pegmatites of the Tørdal pegmatite field, known as the greenish K-feldspar zone (Fig 1.3).

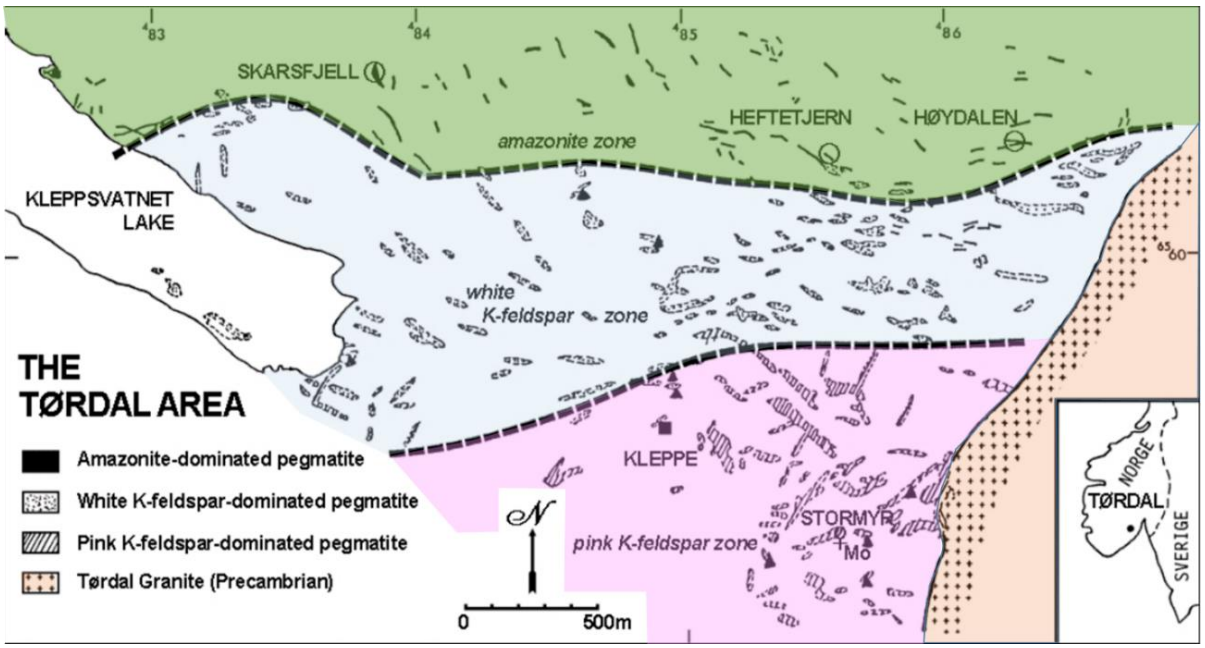

Fig. 1.3. Map of the Tørdal area with indicated granitic pegmatite bodies and the regional zoning of the Tørdal field. The field has been divided into three zones on the base of the colour (white, pink and green) of K-feldspars. Host rocks of pegmatites in the area is the Nissedal Supracrustal Precambrian rocks. Modified from Segalstad and Eggleston (1993).

In the greenish K-feldspar zone, according to Segalstad and Eggleston (1993), the most chemical evolved and complex zoned Høydalen and Heftetjern pegmatites occur (Fig. 1.3). The Heftetjern pegmatites are known for their Sc and Be minerals, such as bazzite, thortveitite and beryl, while the Høydalen pegmatites are known for beryl, gadolinite-(Y), cassiterite, topaz, fluorite and lepidolite due to Be, Y, Sn, Li and F enrichments (Oftedal, 1942; Bergstøl and Juve, 1988; Juve and Bergstøl, 1990; Kristiansen, 1998; Raade and Kristiansen, 2000; Segalstad and Raade, 2003). Since the Tørdal pegmatites are mainly enriched in Nb, Y and F, they are, according to Černý (1992) classified as granitic pegmatites with NYF affinity. Due to the occurrences of late-stage albite zones with Cs-bearing lepidolite and morganite, the Høydalen pegmatites representing highly evolved NYF pegmatites.

As previously mentioned, the most chemical evolved and complex zoned Tørdal pegmatites have the greatest diversity of minerals. Their major and accessory minerals are unevenly distributed within the pegmatites body and commonly found in certain zones. The primary zones of a pegmatite body comprise the border zone, wall zone, intermediate zones and core, and are related to the early magmatic stages of pegmatite formation (Cameron et al., 1949). Discordant albite replacement zones represent the last stage of pegmatite crystallization (Müller et al., 2018a). According to Segalstad and Eggleston (1993) the major minerals of the Tørdal pegmatites comprise mainly of quartz, biotite, muscovite, K-feldspar (pink, white, green),

plagioclase (of oligoclase to albite composition) which occur mainly in the main body, while almost pure albite (var. cleavelandite) is found in the albite replacement zones only. Accessory minerals such as almandine, molybdenite, rutile, zircon, beryl, gadolinite-(Y), allanite-(Ce), fergusonite-(Y), ilmenite, monazite-(Ce), xenotime-(Y), magnetite, titanite, pyrite and chalcopyrite, are typical found in the main body. Typical accessory minerals which occur in the albite replacement zones are, beside cleavelandite, spessartine, topaz, fluorite, lepidolite, microlite group, beryl (var. morganite), schorl, bazzite, and columbite-tantalite group minerals (Müller et al., 2018a; Mindat, 2020b; Mindat, 2020c; Mindat, 2020d; Table 3.1).

2. Sampling and methods

2.1 Field work: mapping and sampling

Sampling and field mapping in Tørdal was carried from 1 to 6 July 2019 and, in addition, at 1 October 2019. The main objectives of the field work were to collect minerals for investigation, including beryl, bazzite, gadolinite and mica from representative pegmatites. The investigated and sampled pegmatite localities were: Heftetjern 2, Bratterud, Grønliheii, Lislegrønlia, Mjeltedalen 2a, Sjauset, Storemyr 1, Storemyr 2, Storemyr 3, Svåheii 2a, Svåheii 2b, Svåheii 3, Kleppe Quarry, Upper Høydalen, and Lower Høydalen. In total 21 micas and seven amphibolitic host rock samples were collected. Beryl, bazzite and gadolinite minerals were not found during the field trip and, therefore, specimens from the mineral collection of the Natural History Museum were used. For the complete list of samples investigated in this study see and Appendix 7.1. Beside the sampling, the area around the Upper and Lower Høydalen pegmatites was mapped to create a detailed geological map. Boundaries of rock unites were recorded with a handhold GPS. However, only a few outcrops occur in the area, which is characterized dense forest, 95% soil cover and strong topography. These conditions made the mapping challenging. The pegmatites, however, form commonly hills and ridges several meters to over hundred meters in length. This is because the pegmatite rock is more resistant to weathering than the host rocks and allow to utilize the morphology as mapping criteria.

2.2 Sample preparation

Beryl, bazzite, gadolinite and mica were casted in Epoxy in 1-inch plastic forms. Amphibolitic host rock samples were crushed and milled for whole rock analyses and prepared as polished thick sections (sample 02071918, 04071903, 04071917, 05071903) for LA-ICP-MS analysis of amphibole and biotite. The thick sections were prepared at the laboratory at the Department of Geosciences of the University of Oslo. The rock powders were sent to Actlabs (Activation Laboratories Ltd) in Canada for whole rock analysis. The manufacture of Epoxy casts was chosen because several minerals can be set into one cast, which makes the analysis by SEM, EPMA and LA-ICP-MS more efficient. For the manufacture of an Epoxy cast, pieces of minerals of interest are arranged in <1-inch cycle on double-sided tape, which is taped on a glass plate. Than a one-inch plastic ring is set around the minerals and Epoxy is filled inside the plastic ring. The Epoxy needs approximately 24 hours to harden. After hardening the cast were removed from the glass plate and the plastic ring and sent to the laboratory at the Department of Geosciences of the University of Oslo for polishing. Six epoxy casts (Cast 31, Cast 32, Cast 33, Cast 34, Cast 35 and Cast 36) were manufactured. In addition, three epoxy

casts (Cast 8, Cast 13 and Cast 14), which have been manufactured from previously, were added to the sample set. These nine Epoxy casts and their mineral contents are listed in Table 2.1

Table 2.1. List of the Epoxy casts, minerals and samples for EPMA and LA-ICP-MS analysis.

Cast	Mineral	Samples
8	beryl and bazzite	OHoy01 July 2017, OHoy02 31542, OHoy03 31511, NHoy01 31541, NHoy02 03071701
13	bazzite	15053
14	beryl and bazzite	15061801, HF441m
31	beryl and bazzite	17320, 31,548, 33376, 33377, 33378, 42326
32	gadolinite	21341a, 21341b, 21345, 23091447
33	mica	02071909b, 02071909m, 02071910, 02071911, 02071912, 02071913b, 02071913m
34	mica	02071914, 02071915, 02071917, 02071919, 04071901, 04071902, 04071905
35	mica	04071907, 04071908, 04071909, 04071910, 04071911
36	mica	04071918, 05071901

2.3 Electron probe micro analysis (EPMA)

Major and minor elements compositions of mineral separates and host rock samples were obtained by Electron Probe Micro Analysis (EPMA). Two EPMA instruments were used, one located at the Department of Geosciences of the University of Oslo and one at the Natural History Museum of London.

2.3.1 Department of Geosciences of the University of Oslo

At the Department of Geosciences major and minor elements compositions of gadolinite group minerals, micas, and beryls in Cast 8 and Cast 32-36 were determined with the assistance by Muriel Marie Laure Erambert. In addition, major and minor elements compostions of amphibole and biotite from the four polished thick sections were analyzed. The EPMA instrument used was a CAMECA SX-100. The Epoxy casts and thick sections were coated with carbon prior to analysis using a Cressington Carbon Coater 208. A series of natural and synthesis standards and X-ray lines were used for calibration. These standards and X-ray lines used for elements during analysis are listed in further tables (see Table 2.2, 2.3, 2.4 and 2.5). The synthetic orthophosphate standards were used from Jarosewich and Boatner (1991). The PAP matrix correction procedure implemented in the CAMECA software were used for all samples analyzed from Pouchou and Pichoir (1984).

Gadolinite group minerals (Epoxy cast 32)

A total of 31 (+ two test point analysis) point analysis were obtained from four gadolinite group minerals (Cast 32) by using the operating parameters: accelerating voltage of 20 kV and a beam current of 20 nA, with a beam size of 5 µm. The counting time on peak were 60 s for Mn, 30 s for Si, Ca, Y, Ce, La, and the rest, Fe^{2+}, Pr, Nd, Sm, Gd, Dy, Er, Yb had 20 s. Weight percent concentrations of oxides (wt.%) from analyzed samples were normalized to 10 oxygen for *apfu* calculation. An estimation of Be and OH, both close to the stoichiometric value of 2 *apfu*, were preformed on the samples. This were necessary since BeO and H_2O can`t be detected from the EPMA instrument. The elements, standards, and detection limits for both elements (ppm) and oxides (wt.%) of investigated gadolinite group minerals are further listed in Table 2.2.

Table 2.2. Elements, X-ray lines, standards and limit of detections (LOD) for elements and oxides of studied gadolinite group minerals measured by EPMA.

Elements and X-ray lines	Standards	LOD* (ppm)	LOD* (wt%)
Si Kα	Wollastonite	160	0.03
Ca Kα	Wollastonite	106	0.01
Mn Kα	Pyrophanite	489	0.06
Fe^{2+} Kα	Fe metal	315	0.04
Y Lα	Synthetic orthophosphate	390	0.05
La Lα	Synthetic orthophosphate	383	0.04
Ce Lα	Synthetic orthophosphate	395	0.05
Pr Lβ	Synthetic orthophosphate	1230	0.14
Nd Lβ	Synthetic orthophosphate	1206	0.14
Sm Lβ	Synthetic orthophosphate	1351	0.16
Gd Lβ	Synthetic orthophosphate	1317	0.15
Dy Lβ	Synthetic orthophosphate	1478	0.17
Er Lβ	Synthetic orthophosphate	1501	0.17
Yb Lα	Synthetic orthophosphate	833	0.09

LOD – limit of detection

Micas (Epoxy casts 33-36)

For the investigated micas (Cast 33-36), a total of 68 point analysis were obtained. Operating parameters used for micas were an accelerating voltage of 15 kV and a beam current of 15 nA with a beam size of 5 µm. The counting time on peak were 20 s for elements Rb, Fe^{2+}, Mn, Mg, and the rest of the elements, Si, Ca, Al, K, Na, and F, had 10 s. A normalization of 24 oxygen were applied instead of 12 oxygen for *apfu* calculation. This were necessary for the classification diagram of micas by Tischendorf et al. (2001). Therefore, an estimation of OH approximately close to the stoichiometric value of 4 *apfu* were applied instead of 2 *apfu*. The elements, standards, and detection limits for both elements (ppm) and oxide (wt.%) of investigated micas are further listed in Table 2.3

Table 2.3. Elements, X-ray lines, standards and limit of detections (LOD) for elements and oxides of studied mica minerals measured by EPMA.

Elements and X-ray lines	Standards	LOD* (ppm)	LOD* (wt%)
Si Kα	Wollastonite	390	0.08
Fe^{2+} Kα	Fe metal	491	0.06
Mn Kα	Pyrophanite	430	0.06
Ca Kα	Wollastonite	517	0.07
K Kα	Orthoclase	291	0.04
Ti Kα	Pyrophanite	311	0.05
Al Kα	Synthetic Al_2O_3	317	0.06
F Kα	Synthetic F-phlogopite	3010	
Na Kα	Albite	321	0.04
Rb Kα	$RbNO_3$	593	0.06
Mg Kα	MgO	236	0.04

LOD – limit of detection

Beryl (Epoxy cast 8)

Beryl samples from Cast 8 were analyzed with 30 analytical points. The analysis were obtained by using an accelerating voltage of 15 kV and a beam current of 15 nA, with a beam size of 5 µm.Counting times on peak were 30 s for Ca, 20 s for Mg, Sc, Cs, Fe^{2+}, Mn, Cr, and 10 s for Si, Al, K, and Na. The *apfu's* were normalized to 18 oxygen atoms. Beryllium was estimated to an approximately stoichiometric value of 3 *apfu*, since BeO cannot be detected by EPMA. The elements, standards, and detection limits for both elements (ppm) and oxide (wt.%) of investigated beryls are further listed in Table 2.4

Table 2.4. Elements, X-ray lines, standards and limit of detections (LOD) for elements and oxides of studied beryl minerals measured by EPMA.

Elements and X-ray lines	Standards	LOD* (ppm)	LOD* (wt%)
Si Kα	Wollastonite	348	0.07
Na Kα	Albite	272	0.04
Fe^{2+} Kα	Fe metal	404	0.05
Mn Kα	Pyrophanite	390	0.05
Cr Kα	Cr_2O_3	365	0.05
Ca Kα	Orthoclase	351	0.05
K Kα	Wollastonite	228	0.03
Al Kα	Synthetic Al_2O_3	267	0.05
Sc Kα	Synthetic orthophosphate	179	0.03
Cs Lα	Pollucite	567	0.06
Mg Kα	MgO	183	0.03

LOD – limit of detection

Biotite and amphibole in host rocks (Thick sections)

A toal of 49 point analysis of biotites (20 grains) and amphiboles (23 grains) were obtained from the four polished thick sections (sample 02071918, 04071903, 04071917, 05071903). The used operating paramters were an accelerating voltage of 15 kV and a beam current of 15 nA, with a focused beam. The beam was focused since it size were, in fact, c. 0.1 µm. The counting time on peak for all elements was 10 s. An estimation of OH close to the approximately stoichiometric value of 2 *apfu* for amphiboles and 4 *apfu* for biotites (24 oxygen normalization) were applied. The elements, standards, and detection limits for both elements (ppm) and oxide (wt%) of investigated biotites and amphiboles are further listed in Table 2.5.

Table 2.5. Elements, X-ray lines, standards and limit of detections (LOD) for elements and oxides of studied pegmatite host rocks containing amphibole and biotite minerals measured by EPMA.

		Amphibole		**Biotite**	
Elements and X-ray lines	**Standards**	**LOD* (ppm)**	**LOD* (wt%)**	**LOD* (ppm)**	**LOD* (wt%)**
Fe_{tot} Kα	Fe metal	721	0.09	721	0.09
Mn Kα	Pyrophanite	626	0.08	622	0.08
K Kα	Orthoclase	250	0.03	288	0.03
Si Kα	Wollastonite	373	0.08	423	0.09
Ca Kα	Wollastonite	294	0.04	264	0.04
Ti Kα	Pyrophanite	314	0.05	315	0.05
Al Kα	Synthetic Al_2O_3	335	0.06	345	0.07
Mg Kα	MgO	435	0.07	424	0.07
Sc Kα	Synthetic orthophosphate	295	0.05	276	0.04
F Kα	Synthetic F-phlogopite	2578		2590	
Na Kα	Albite	377	0.05	343	0.05

LOD – limit of detection

2.3.2 Natural History Museum of London

Beryl and Bazzite (Epoxy cast 13, 14 and 31)

At the Natural History Museum of London, major and minor element analysis of beryls and bazzite on Casts 13, 14 and 31 (Table 2.1) were preformed by John Spratt and main supervisor Axel Müller with a CAMECA SX-100 instrument. A total of 76 analysis point were obtained from latter samples. The instrument beam conditions were 20 kV and 20 nA with a 1 µm spot size. Standards and used for each element and mineral together with their limit of detection are presented in Table 2.6. The formulae were calculated as described above. The bazzite data have a low total, which may relate to water in the structure.

Table 2.6. Elements, standards and limit of detections (LOD) for elements and oxides of studied beryl and bazzite minerals measured by EPMA.

		Beryl		Bazzite	
Elements	**Standards**	**LOD* (ppm)**	**LOD* (wt.%)**	**LOD* (ppm)**	**LOD* (wt.%)**
Na	Jadeite	192	0.03	359	0.05
K	Potassium Bromide	245	0.03	270	0.03
Ca	Wollastonite	214	0.03	230	0.03
Sc	Scandium Phosphate	152	0.03	200	0.03
V	Vanadite	130	0.02	139	0.02
Cr	Chromium Oxide	253	0.05	315	0.06
Si	Fayalite	127	0.03	142	0.03
Al	Corundum	192	0.04	213	0.04
Mg	Forsterite	148	0.02	184	0.03
Ti	Manganese Titanium Oxide	221	0.04	292	0.04
Mn	Manganese Titanium Oxide	204	0.03	240	0.03
Fe^{3+}	Haematite	208	0.03	219	0.03

LOD – limit of detection

2.4 Laser Ablation Coupled Plasma Mass Spectrometry (LA-ICP-MS)

Minor and trace element concentrations of beryl, bazzite and mica minerals (Table 2.1), in addition, to amphibolitic host rocks containing amphiboles and biotites, were obtained by Laser Ablation Inductively Coupled Plasma Mass Spectrometry (LA-ICP-MS) located in the Department of Geosciences at University of Oslo. The analysis was obtained with a Bruker Aurora Elite instrument with attached CETAC LSC213 G2+ Laser, where the performance was assisted by Magnus Kristoffersen. The laser paramters were adjusted to the minerals measured (see below). The average SiO_2 concentration for each mineral sample (determined with EPMA previously), were used as internal standard. The reference materials NIST 610 (Jochum et al., 2011) and BCR 2g from GEOREM preferred value (Jochum, 2009), were used as external standards with values of 69.7007 and 54.400, respectively. The analytical conditions of the reference materials were mainly a laser spot size of 50 µm, a laser energy of 10%, and a laser shot frequency of 10 Hz. The software Glitter was used to process the data. To determine the mean detection limits (MDL) of studied samples, the formula MDL = 2.3*square (2B) where used, where B is total counts in the background according to the Glitter Manual (Achterbergh et al., 2001). The mean detection limit (MDL) for measured elements are listed in Table 2.7. The time of background measurement for all studied samples was 15 seconds and the analysis time of one sample measurement was approximately 55 seconds. The analysis time of one sample measurement were obtained by adding the time of background measurement with the

time of sample measurement. The time of one sample measurement was obtained by dividing the burst count (BC) with the frequency (Hz).

Beryl and bazzite

The used paramters for beryl and bazzite analysis of Casts 8, 13, 14 and 31 (Table 2.1), where a laser spot size of 200 µm, a laser energy of 15-30 %, a laser shot frequency of 20 Hz and a burst count of 800 BC. Lithium (ppm) detected from beryl was converted to Li_2O (wt.%) since it cannot be detected by EPMA and listed in Table 3.3.

Mica

The used paramters for micas (Cast 33-36) were a laser spot size of 50 µm, a laser energy of 5%, a laser shot frequency of 10 Hz and burst count of 400 BC. Lithium (ppm) detected from mica was also converted to Li_2O (wt.%) and listed in Table 3.9.

Amphibole and biotite

The used parameters for analyzing the amphiboles and biotites from thick sections (sample 02071918, 04071903, 04071917, 05071903) were a laser spot size of 50 µm, a laser energy of 50%, a laser shot frequency of 10 Hz and a burst count of 400 BC. Lithium (ppm) and Rb (ppm) detected from biotites was converted to Li_2O (wt.%) and Rb_2O (wt.%) and listed in Table 3.10.

Table 2.7. Elements, isotopes and mean detection limits (MDL) of studied beryl, bazzite and mica minerals from Tørdal pegmatites and amphiboles and biotites from pegmatite host rocks measured by LA-ICP-MS.

Bazzite		**Beryl**		**Mica**		**Amphibole**		**Biotite**	
Element	MDL (ppm)	Element	MDL (ppm)	Element	MDL (ppm)	Element	MDL (ppm)	Element	MDL (ppm)
^{7}Li	7.59	^{7}Li	3.93	^{7}Li	46.75	^{7}Li	25.34	^{7}Li	27.72
^{9}Be	3.04	^{9}Be	4.68	^{9}Be	3.68	^{9}Be	1.64	^{9}Be	1.76
^{11}B	0.84	^{11}B	0.80	^{11}B	4.12	^{11}B	1.51	^{11}B	1.77
^{23}Na	61.90	^{23}Na	59.62	^{23}Na	3066.87	^{29}Si	730.20	^{29}Si	825.90
^{24}Mg	0.34	^{24}Mg	0.37	^{27}Al	125.20	^{45}Sc	0.37	^{45}Sc	0.42
^{27}Al	20.90	^{27}Al	43.47	^{29}Si	1792.80	^{49}Ti	1.47	^{49}Ti	1.70
^{29}Si	52.41	^{29}Si	66.02	^{31}P	9.76	^{51}V	99.99	^{51}V	126.14
^{31}P	0.27	^{31}P	0.31	^{39}K	108.54	^{53}Cr	2.92	^{53}Cr	3.40
^{39}K	1.55	^{39}K	1.14	^{44}Ca	50.11	^{59}Co	0.30	^{59}Co	0.34
^{44}Ca	1.74	^{44}Ca	2.97	^{45}Sc	1.24	^{68}Zn	3.00	^{68}Zn	3.50
^{45}Sc	16.11	^{45}Sc	14.77	^{47}Ti	22.75	^{85}Rb	3.94	^{85}Rb	4.58
^{47}Ti	0.18	^{47}Ti	0.20	^{71}Ga	0.39	^{88}Sr	0.08	^{88}Sr	0.09
^{51}V	0.04	^{51}V	0.06	^{72}Ge	1.30	^{89}Y	0.02	^{89}Y	0.03
^{52}Cr	0.11	^{52}Cr	0.76	^{85}Rb	7.95	^{90}Zr	0.20	^{90}Zr	0.23
^{55}Mn	3.60	^{55}Mn	3.41	^{89}Y	0.43				
^{56}Fe	26.40	^{56}Fe	38.32	^{93}Nb	0.03				
^{69}Ga	0.01	^{69}Ga	0.09	^{115}In	0.05				
^{74}Ge	0.02	^{74}Ge	0.02	^{118}Sn	0.77				
^{85}Rb	0.39	^{85}Rb	0.22	^{133}Cs	5.10				
^{133}Cs	11.01	^{133}Cs	4.48	^{137}Ba	1.04				
				^{181}Ta	0.02				
				^{182}W	0.10				
				^{205}Tl	0.05				

MDL – mean detection limit

2.5 Whole rock analysis

To improve the understanding of the chemistry in Tørdal amphibolitic host rocks, four host rock samples (samples 02071916, 04071903, 04071917, 05071902) was shipped to Actlabs (Activation Laboratories Ltd), Onatiro, Canada, for chemical whole rock analysis. The four analytical packages, which were requested from Actlabs prices are listed further in Table 2.8

Table 2.8. The analytical packes which were used for the chemical whole rock analysis.

1F2	QOP Total (Total Digestion ICPOES)
4F-B(2ppm)	QOP INNA - PGNAA (PGNAA)
4F-F	QOP Fluorine (Fusion Specific Ion Electrode-ISE)
4LITHO(11+)	QOP WRA/ QOP WRA 4B2 (/Major/Trace Elements Fusion ICPOES/ICPMS)

The used analytical methods and limit of detection (LOD) for the measured oxides and elements during the chemical whole rock analysis are further listed in Table 2.9

Table 2.9. Oxides, elements, analytical methods and detection limits of whole rock analyses of amphibolitic host rocks

Oxides of major elements (wt%)	**Analytical methods**	**LOD of oxides (wt%)**
SiO_2	FUS-ICP	0.01
Al_2O_3	FUS-ICP	0.01
Fe_2O_3	FUS-ICP	0.01
MgO	FUS-ICP	0.01
CaO	FUS-ICP	0.01
Na_2O	FUS-ICP	0.01
K_2O	FUS-ICP	0.01
TiO_2	FUS-ICP	0.001
P_2O_5	FUS-ICP	0.01
MnO	FUS-ICP	0.001
Trace elements (ppm)	**Analytical methods**	**LOD of elements (ppm)**
Ag	FUS-MS	0.50
Ba	FUS-ICP	2.00
Be	FUS-ICP	1.00
Bi	TD-ICP	2.00
Cd	TD-ICP	0.30
Co	TD-ICP	1.00
Cr	TD-ICP	1.00
Cu	TD-ICP	1.00
Ga	TD-ICP	1.00
Li	TD-ICP	1.00
Mn	TD-ICP	1.00
Ti	TD-ICP	0.10
Ni	TD-ICP	1.00
Pb	TD-ICP	3.00
Sc	FUS-ICP	1.00
Sr	TD-ICP	2.00
Tl	FUS-MS	0.10
U	FUS-MS	0.10
V	FUS-ICP	5.00
Zn	TD-ICP	1.00
Zr	FUS-ICP	2.00
B	PGNAA	2.00
Ge	FUS-MS	1.00
Rb	FUS-MS	2.00
Nb	FUS-MS	1.00
Sn	FUS-MS	1.00
Cs	FUS-MS	0.50
La	FUS-MS	0.10
Ce	FUS-MS	0.10
Pr	FUS-MS	0.05
Nd	FUS-MS	0.10
Sm	FUS-MS	0.10
Eu	FUS-MS	0.05
Gd	FUS-MS	0.10
Tb	FUS-MS	0.10
Dy	FUS-MS	0.10
Ho	FUS-MS	0.10
Er	FUS-MS	0.10
Tm	FUS-MS	0.05
Yb	FUS-MS	0.10
Lu	FUS-MS	0.01
Hf	FUS-MS	0.20
Ta	FUS-MS	0.10
Th	FUS-MS	0.10
Y	FUS-ICP	1.00
Trace elements (wt%)	**Analytical methods**	**LOD of elements (wt%)**
S	TD-ICP	0.01
F	FUS-ISE	0.01
Ti	TD-ICP	0.01

3. Results

3.1 Results of field work

Field work in the Tørdal pegmatite field was carried out from 1 to 6 July 2019 with an additional mapping day 1 October 2019. During the field work campaign 15 pegmatite localitites were inspected and sampled (Table 3.1). Collected samples included micas from pegmatites and amphibolites, the host rocks of the Tørdal pegmatites. During field work it was also searched for Be minerals, such as beryl, gadolinite, and bazzite, with little success and, thus, specimen of these Be minerals from the Natural History Museum of Oslo were used for analysis. The complete list of sampled and studied Tørdal pegmatites are given in Table 3.1. An area of 350 times 350 m was mapped in order to better understand the distribution of pegmatites and their adjacent host rocks in the Høydalen area (Fig. 3.2). Four of the sampled pegmatites, the Kleppe quarry, Mjeltedalen 2a, Svåheii 2b, and Upper Høydalen, were mapped in more detail. These four pegmatites are representative for different structural types found in the Tørdal pegmatite field, ranging from chemically primitive and unzoned pegmatites (Kleppe quarry, Mjeltedalen 2a) to chemically evolved and complex zoned pegmatites (Svåheii 2b, Upper Høydalen). Investigated Tørdal pegmatites comprise mainly pinkish, whitish and occasionally green "amazonite" K-feldspar, plagioclase (comprising up to 1 m white plagioclase crystals in Upper Høydalen), quartz, biotite and/or muscovite as their major minerals (Table 3.1; Segalstad and Eggleston, 1993). Albite is a major mineral in the Sjauset pegmatite. The Upper and Lower Høydalen, Svåheii 2b, Bratterud, Skardsfjell, and Heftetjern 1 pegmatites contain albite and lepidolite as minor minerals. Representative accessory minerals, which is either from the main body or albite zones within the individual pegmatites, are listed in Table 3.1.

Table 3.1. Mineralogy, size, zoning type and host rocks of sampled Tørdal pegmatites (Müller et al., 2018a; Mindat, 2020b; Mindat, 2020c; Mindat, 2020d; Segalstad and Eggleston, 1993).

Pegmatite locality	**Samples investigated in this study (sample nr.)**	**Main minerals of the pegmatite**	**Representative accessory minerals**	**Pegmatite size**	**Pegmatite zoning**	**Host rock (sample nr.)**
Svåheii 2a	Muscovite from the intermediate zone (02071912), biotite from the wall zone (02071911)	Quartz, plagioclase, white K-feldspar, biotite, muscovite	Almandine, gadolinite	Exploration blast at W end of the E-W-striking 400 m long, up to 50 m wide, boudinaged Svåheii pegmatite dyke.	The complex zoned Svåheii pegmatite contains several zoned domains with cores (5 to 15 m). At Svåheii 2a site an outer biotite-bearing wall zone and a muscovite-bearing intermediate zone can be distinguished. The typical pegmatite core is missing.	Amphibolite (closest sample: 02071901: 32V482708E/ 6556926N)
Svåheii 2b	Bioite from the center of the wall zone (02071909b), muscovite from the center of the wall zone (02071909m), muscovite from the intermediate zone (02071910), green beryl from the intermediate zone (15061801)	Quartz, white K-feldspar, plagioclase, muscovite, biotite	Main body: Almandine, beryl Albite zones: albite (var. cleavelandite), unidentified black minerals	Exploration blast in the central part of the E-W-striking, 400 m long, up to 50 m wide, boudinaged Svåheii pegmatite dyke.	Zoned domains exhibiting border zone, wall zone, intermediate zone and a small pegmatite quartz core. The intermediate zone and pegmatite core are superimposed by albite replacement zones (up to 1 m).	Amphibolite (closest sample: 02071901: 32V482708E/ 6556926N)
Svåheii 3	Biotite from the wall zone (02071913b), muscovite from the wall zone (02071913m), muscovite from the intermediate zone (02071914)	Quartz, plagioclase, pink K-feldspar, biotite, muscovite	Almandine, gadolinite	Exploration blast in a 22 m long, up to 5 m thick, subhorizontal pegmatite sheet.	Simple zoned pegmatite.	Amphibole gneiss.
Grønliheii	Muscovite from near the contact (02071915)	Quartz, white K-feldspar, plagioclase, muscovite	Almandine, gadolinite	C. 500 m long, up to 20 m wide, NW-SE striking, subvertical pegmatite dyke.	Without distinct zoning. However, the pegmatite contains abundant, vein-like batches with aplitic textures.	Fine grained amphibolite (closest sample: 06071704: 32V482611E/ 6557673N)
Lislegrønlia	Biotite (02071917)	Quartz, pink K-feldspar, plagioclase, biotite (rare)		E-W-striking, 40 m long and up to 10 m wide pegmatite sheet.	Chemical primitive, unzoned pegmatite.	Amphibole-biotite gneiss (closest sample: 02071916: 32V483597E/ 6557818N

Mjeltedalen 2a	Biotite near upper contact (02071919)	Quartz, plagioclase, pink K-feldspar, garnet	Almandine, biotite (very rare), pyrite, chalcopyrite	C. 12 m long, up to 1.5 thick, flat northward dipping, boudinaged pegmatite sheet. Extensional cracks (up to 5 cm wide) are filled with massive quartz.	Aplitic, garnet-rich facies (up to 20 cm wide) along the pegmatite margin. Otherwise unzoned pegmatite.	Amphibolite (closest sample: 06071716: 32V484311E/ 6557191N)
Kleppe quarry		Quartz, pink K-feldspar, plagioclase	Garnet, molybdenite	Pegmatites varies mainly from c. 1 mm wide leucocratice granitic veinlets to larger pegmatite sheets, where the largest pegmatite sheet is c. 10 m.	No distinct zoning.	Two types of amphibolites, fine-grained to coarser-grained with gabbroic texture.
Storemyr 1	Biotite from mine dump (04071905)	Quartz, plagioclase, pink K-feldspar, biotite	Almandine, gadolinite	C. 500 m long, E-W striking, up to 40 m wide pegmatite dyke. Mining shaft from World War II (samples site) is at the S contact in central part of the pegmatite dyke.	No visible zoning.	Amphibolite
Storemyr 2	Biotite close to lower contact (04071901), muscovite close to lower contact (04071902)	Quartz, plagioclase, pink K-feldspar, biotite, muscovite	Almandine, molybdenite, gadolinite, magnetite	C. 400 m long, ENE-WSW-striking, up to 25 m wide pegmatite dyke.	No visible zoning.	Amphibolite (closest sample 04071903: 32V485441E/ 6558866N).
Storemyr 3	Muscovite from the centre of the pegmatite (04071907), biotite from the centre of the pegmatite (04071908)	Quartz, plagioclase, pink K-feldspar, muscovite, biotite	Almandine	C. 120 m long, WNW-ESE striking, up to 20 m wide pegmatite dyke.	No visible zoning.	Amphibolite
Sjauset	Muscovite from the centre of the pegmatite (04071918).	Quartz, albite, green K-feldspar (var. amazonite), muscovite	Almandine, beryl	Two subparallel, c. 20 m long, up to 3 m wide pegmatite dykes.	No visible zoning.	Metagabbro (closest samples 05071710: 32V486427E/ 6562148N
Bratterud	Biotite close to the contact (04071909), muscovite close to the	Quartz, plagioclase,	Main body: Almandine, fergusonite (?), altered beryl,	E-W-striking c. 200 m long, up to 4 m wide,	No distinct zoning. Small loose samples of cleavelandite were found	Medium-grained gabbro (closest sample: 04071917:

	contact (04071910), muscovite from the center of the pegmatite (04071911)	white K-feldspar, muscovite, biotite	Albite zones: albite (var. cleavelandite), columbite-tantalite group minerals	subvertical pegmatite dyke.	indicating the existence of albite replacement zones.	32V488812E/ 6562743N).
Heftetjern 2	Biotite close to contact (05071901)	Quartz, white and green K-feldspar (var. amazonite), plagioclase, biotite	Main body: almandine, muscovite(very rare), magnetite, zircon, beryl, allanite-(Ce), gadolinite, monazite-(Ce), molybdenite, rutile, titanite, Albite zones: albite (var. cleavelandite), fluorite, microlite group, bazzite, schorl, spessartine	C. 50 m long, NW-SE-striking, up to 8 m wide pegmatite dyke.	No visible zoning.	Amphibolite (closest sample: 05071902: 32V485239E/ 6560607N
Heftetjern 1	Bazzite in amazonite (33376), bazzite in amazonite (33377), bazzite, with adjacent fluorite, on amazonite and albite replacement zone (33378), bazzite fragments (17320), bazzite (15053), green beryl from intermediate zone (42326)	Quartz, white and green K-feldspar (var. amazonite), plagioclase, muscovite, biotite	Main body: almandine, magnetite, zircon, beryl, allanite-(Ce), gadolinite, monazite-(Ce), molybdenite, rutile, titanite, Albite zones: albite (var. cleavelandite), fluorite, microlite group, bazzite, schorl, spessartine	C. 50 m long, NE-SW-striking up to 4 m wide, subvertical pegmatite dyke.	Complex zoned pegmatite with border zone, wall zone, intermediate zone, quartz core and albite replacement zones.	Metagabbro (closest sample: 20091511: 32V485524E/ 6560371N)
Upper Høydalen	Gadolinite from wall zone (21341a, 21341b, 21345), Green and yellow beryl from intermediate zone (OHoy01, July2017, OHoy03, 31511, pink beryl from albite replacement zone (HF441m, OHoy02 31542)	Quartz, plagioclase, white and green K-feldspar (var. amazonite), biotite, muscovite	Main body: almandine, gadolinite, allanite-(Ce), beryl, ilmenite, monazite-(Ce), xenotime-(Y), zircon Albite zones: albite (var. cleavelandite), lepidolite, spessartine, cassiterite, topaz, fluorite, schorl, beryl (var. morganite), bazzite	C. 50 m long, WNW-ESE-striking, up to 8 m wide, subvertical pegmatite dyke.	Complex zoned pegmatite with border zone, wall zone, intermediate zone, quartz core and albite replacement zones.	Coarse-grained metagabbro (closest samples: 05071903: 32V486274E/ 6560473N and 23091513: 32V486274E/ 6560473N).
Lower Høydalen	Gadolinite from wall zone (23091547), yellow beryl from intermediate zone (NHoy02, 03071701),	Quartz, plagioclase, white and green K-feldspar (var.	Main body: almandine, gadolinite, beryl Albite zones: albite (var. cleavelandite), lepidolite, microlite group, beryl (var. morganite beside green beryl)	C. 25 m long, WNW-ESE-striking, up to 4 m wide, subvertical pegmatite dyke.	Complex zoned pegmatite with border zone, wall zone, intermediate zone, quartz core and albite replacement zones.	Metagabbro (closest sample: 23091548 32V486816E/ 6560188N

	pink beryl from replacement zone (NHoy01, 31541)	amazonite), biotite, muscovite				
Skardsfjell	Green beryl from intermediate zone (31548)	Quartz, plagioclase, green K-feldspar (var. amazonite), biotite, muscovite	Main body: almandine, molybdenite, rutile, zircon, beryl Albite zones: albite (var. cleavelandite), spessartine, topaz, fluorite	Irregular, subhorizontal pegmatite body c. 50 m (N-S) times 40 m (E-W) in size.	Complex zoned pegmatite with border zone, wall zone, intermediate zone, quartz core and albite replacement zones.	Amphibolite (closest samples: 04061615: 32V483772E/ 6560519V; 04061616: 32V484230E/ 6560517N; 04061617: 32V484284E/ 6560384N

3.1.1 Description of Tørdal pegmatites with special emphasis on Høydalen area

Geological mapping of the Høydalen area

The Høydalen area including the Upper and Lower Høydalen pegmatites were mapped in order to better understand the distribution, shape and size of pegmatites, their adjacent host rocks and tectonic settings (Fig. 3.2). The area comprise a total of 19 exposed pegmatites which contain amazonite beside white K-feldspar and, thus, belong to the "amazonite zone" of the Tørdal pegmatite field defined by Segalstad and Eggleston (1993). The sizes of pegmatites vary from as low as c. 5 m in length and c. 2 m in width to as long as c. 95 m in length and c. 12 m in width. Smaller pegmatites was not mapped. The mapped pegmatites occur mainly as irregular to dyke-like or sheet-like bodies (Fig. 3.2). They form commonly ridges and hills because the pegmatites are more resistant to weathering than their host rocks. Pegmatite host rocks of the Høydalen area comprise non-foliated metagabbro, which lies in the centre of the mapped area, foliated mettagabbro sourrounding the un-foliated gabbro body, and biotite-hornblende gneisses in the NE of the mapped area (Fig. 3.2). A small body of dark amphibolite was identified N of the metagabbro body (Fig. 3.2). All rocks belong to the Nissedal Supracrustal Outlier (Mitchell, 1967; Bergstøl and Juve, 1988). Holocene river sediments cover the crystalline rocks in the NE of the mapped area (Fig. 3.2). The un-foliated and foliated metagabbro have similar compositions but distinguishes by the texture (Fig. 3.1 A-F).

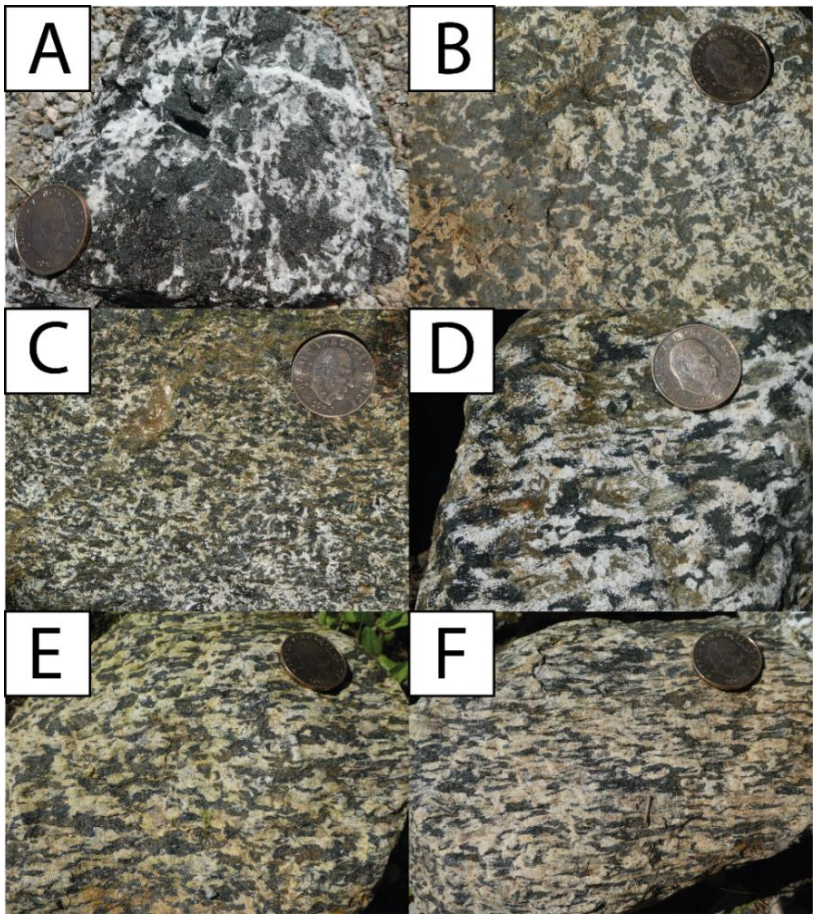

Fig. 3.1. Photograph sequence illustrating the transition from un-foliated metagabbro (A) to foliated metagabbro (F) in July 2019 at Høydalen area. A – Un-foliated and relative coarse-grained metagabbro. B – Un-foliated and more medium-grained metagabbro. C – Sligthly more foliated and even finer-grained metagabbro. D – Foliated metagabbro. E – Even more foliated metagabbro. F – Relative foliated metagabbro.

The un-foliated metagabbro has kept its original coarse-grained, random mineral texture (Fig. 3.1 A) whereas in the foliated metagabbro plagioclase and amphiboles/pyroxene mineral clusters are aligned to different degrees (Fig. 3.1 E-F). There is a gradual textural transition from un-foliated metagabbro to foliated metagabbro. The observation can be explained in that why that the central part of the gabbro intrusions was very rigid, restent to stress and the shear stress moved along the margins of the gabbro intrusion causing that only the outer part of the intrusion became deformed.

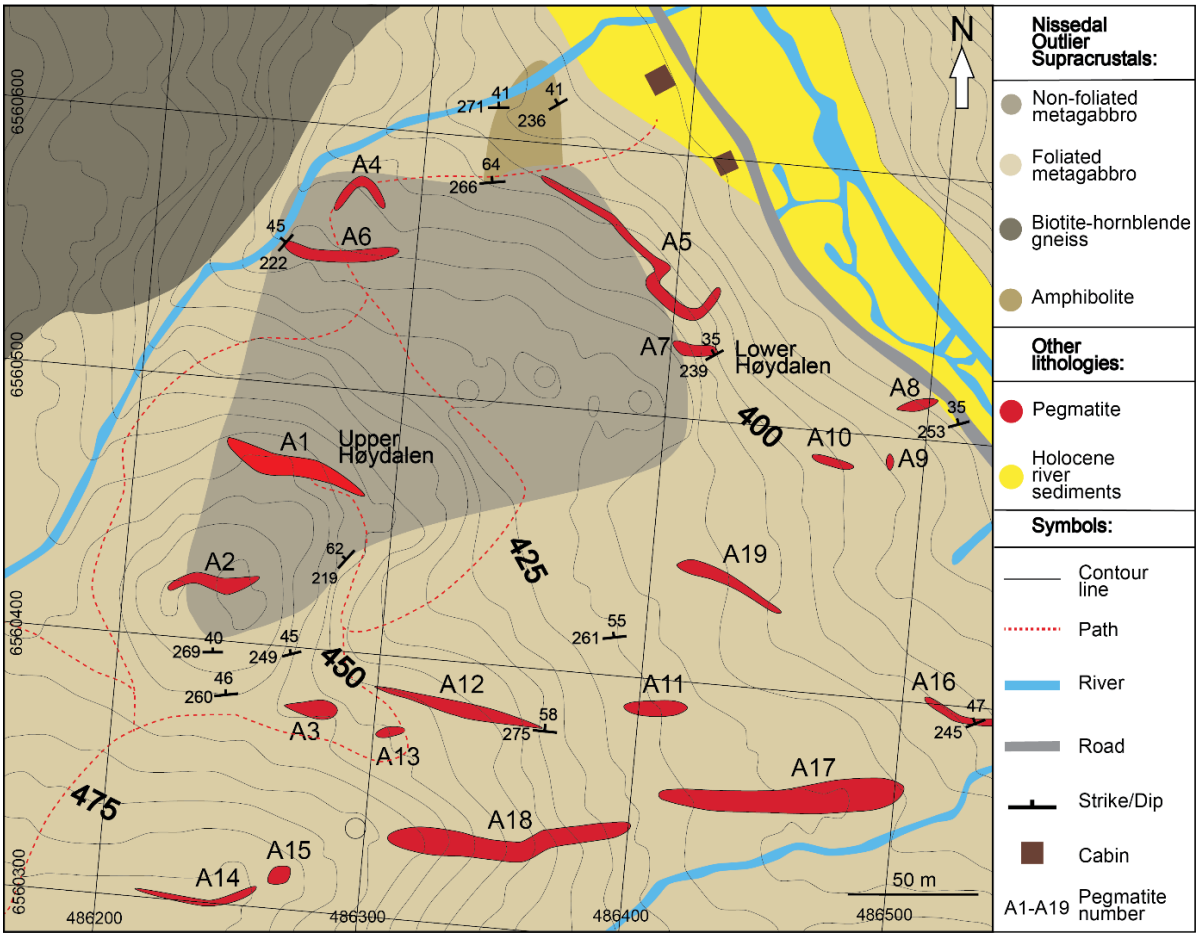

Fig. 3.2. The geological map of the Høydalen area showing the distribution of mapped granitic pegmatites and their host rocks. A total of 19 granitic pegmatites >10 m^3 (named A1 to A19) were mapped in the area. All pegmatites contain amazonite beside white K-feldspar and, thus, belong to the "amazonite zone" according to Segalstad and Eggleston (1993).

Kleppe amphibolite quarry: anatecitc structures and unzoned pegmatites

The unzoned pegmatites exposed at the Kleppe quarry are great examples to explore how the Tørdal pegmatites were formed by partial melting (anataxis) of their amphibolitic host rocks. The host rocks comprise principally two types of amphibolites. The first one is fine-grained and the second one is coarser-grained with medium-grained gabbroic texture (Fig. 3.3 A). Within the fine-grained amphbiolites fine, leucocratice granitic veinlets (leucosomes; about 1 mm in width) are observed which develop into up to 2 m thick pegmatite sheets over a distance of about 10 meters (Fig. 3.3 B). In the areas were the fine veinlets originate, the amphibolites appear much darker due to the depletion of leucocratic minerals (i.e. plagioclase) due to the partial melting. These dark amphibolite domains are considered as melanosomes, paleosomes

or restites due to the removal and depletion of leucogratic minerals by partial melting (Fig. 3.3 C). The pegmatite sheets and dykes exposed in the quarry do not show any distinct zoning. However, large dykes and sheets (> 1 m thickness) contain aplitic dyke-like structures embedded in a more or less homogenous coarse-grained pegmatitc matric (Fig. 3.3 D-E). Major minerals of the pegmatites exposed at the Kleppe quarry are quartz, plagioclase, pink K-feldspar and the accessory minerals garnet and molybdenite (Table 3.1). The pegmatites of the Kleppe quarry locality belong to the "pink K-feldspar zone" according to the zone definition of Tørdal pegmatites by Segalstad and Eggleston (1993), which means they are chemically primitive pegmatites. Sub-horizontal pegmatite veins are boudinaged under ductile conditions indicating that the dykes were deformed, more or less, syngenetically, in an extensional tectonic environment (Fig. 3.3 F).

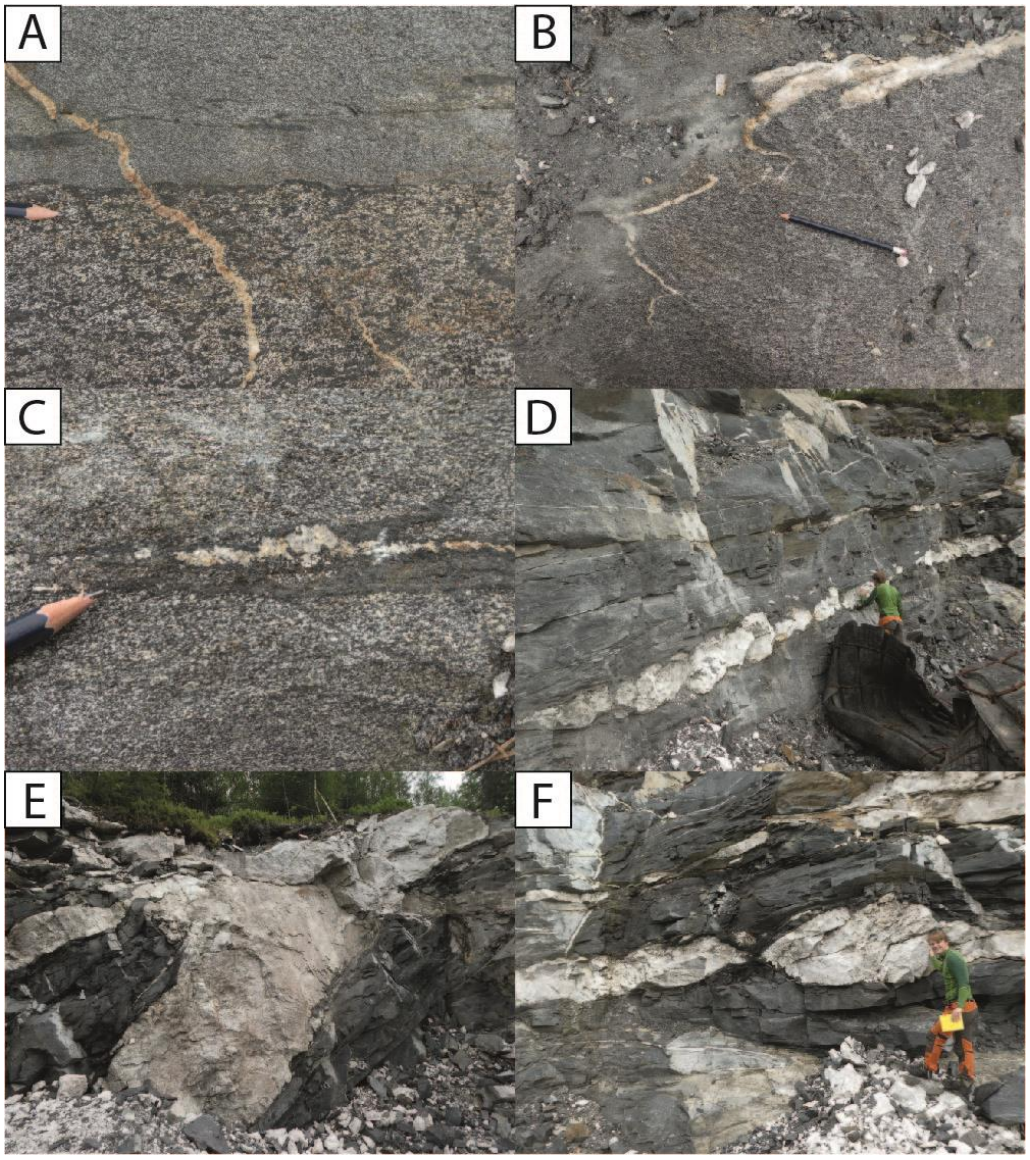

Fig. 3.3. Photographs of rock exposed in the Kleppe quarry in July 2019. A – Contact between fine-grained and medium-grained amphibolites crosscut by a 1 cm wide, granitic/pegmatitic veinlet. B – In the lower left of the

photograph a thin granitic/pegmatitic veinlet appeared in the amphibolite which widens up towards the upper right of the image to a 4 cm wide pegmatite vein. About 10 m away this vein end up in a 2 m thick pegmatite sheet seen in E. C – The formation of amphibolitic melansomes (paleosomes, restites) along the contacts of the leucogratic pegmatite vein (leucosome, neosome). The darker color of the melanosomes is due to the depletion of leucocratic minerals, i.e. plagioclase. D – Sub-horizontal boudinaged pegmatite sheet. E – 2 m wide pegmatite sheet – the largest pegmatite exposed in the Kleppe quarry. F – Characteristic boudinage structures which indicate that pegmatite sheets have been exposed by extensional tectonics.

The unzoned pegmatite at Mjeltedalen 2a

The unzoned pegmatite located at Mjeltedalen 2a is in the following described in detail because it is a well exposed pegmatite of its type being representative for many chemically primitive and unzoned pegmatites from Tørdal pegmatite field. The granitic pegmatite occurs as a flat northward dipping pegmatite sheet, which is at least 12 m long and up to 1.5 m thick and hosted mainly by massive, fine- to medium-grained amphibolite (Fig. 3.4 A-B; Table 3.1). The pegmatite is characterized by large-scale tectonic boudinage, which is similar to the boudinaged pegmatite sheets exposed at Kleppe quarry. During boudinage the competent pegmatite sheet was broken up into lens-shaped boudins due to extensional tectonics in a transitional brittle/ductile environment (Fig. 3.4 C). Beside the boudin formation, the granitic pegmatite is cross-cut by vertical, extensional quartz-filled cracks (Fig. 3.4 D). A garnet-rich aplitic facies surrounds partially the coarser inner parts of the pegmatite (Fig. 3.4 D). The pegmatite contains beside plagioclase and quartz, pink K-feldspar, similar as pegmatites exposed at Kleppe quarry. Accessory minerals are almandine, biotite (very rare), pyrite, and chalcopyrite (Table 3.1). The almandines are abundant in the aplitic marginal facies and have crystal sizes between 0.1 to 1 cm. The abundance of Fe-rich, water-free almandines and the almost absence of micas, indicates that the melt of the Mjeltedalen 2a pegmatite was probably H_2O-poor.

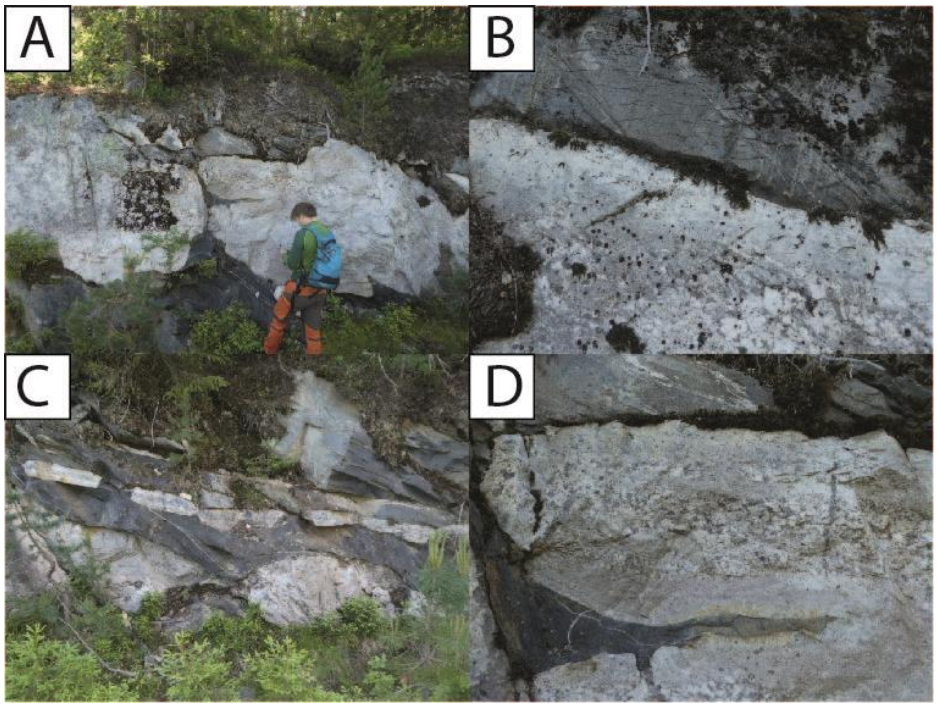

Fig. 3.4. Photographs of rocks exposed at the Mjeltedalen 2a locality in July 2019. A – The Mjeltedalen 2a pegmatite sheet and its amphibolite host rock. B – Sharp contact between pegmatite and the massive, fine-grained amphibolite. C – Boudinaged pegmatite dykes. The structures are very similar to those found at the Kleppe quarry. D – A garnet-rich, fine-grained aplitic facies surrounds the coarser inner part of the Mjeltedalen 2a pegmatite. A vertical quartz-filled crack (appearing darker than the pegmatite) is seen at right part of the image.

The complex zoned pegmatite at Svåheii 2b

The Svåheii 2b site is an exploration blast at the eastern end of the large E-W-striking, boudinaged and complex zoned Svåheii pegmatite dyke. The pegmatite dyke is about 400 m long and up to 50 m wide (Fig. 3.5 A; Table 3.1). The Svåheii 2b site is situated in fine-grained amphibolite being part of the Nissedal Outlier supracrustals. In the 8-m long exposure, the pegmatite shows distinct, concentric zoning. The exposed parts comprising, from outwards to inwards, a wall zone, an intermediate zone with albite replacement zones, and a massive quartz core. This zoned part is embedded in granitic pegmatite which comprise the majority of the pegmatite body (Fig. 3.5 A). The wall zone consists of plagioclase, quartz and micas, with biotite in outer parts and muscovite in inner parts. Formation of biotite in outer parts of the wall zone is due to the initial elevated Fe content of the pegmatite melt. The intermediate zone contains large, blocky and massive white K-feldspar crystals (up to 60 cm in size), quartz and muscovite. The center is formed of massive quartz. Up to 30 cm long, yellow to blue beryl crystals occur in the intermediate zone and pegmatite core (Fig. 3.5 B). Albite replacement zones are up to 1 m in size and occur at the border between intermediate zone and pegmatite core. The albite replacement zone contains the albite variant cleavelandite, which forms masses

of platy crystals. Garnet-bearing, aplitic vein-like domains cross-cut the wall and intermediate zone of the pegmatite (Fig. 3.5 C-D).

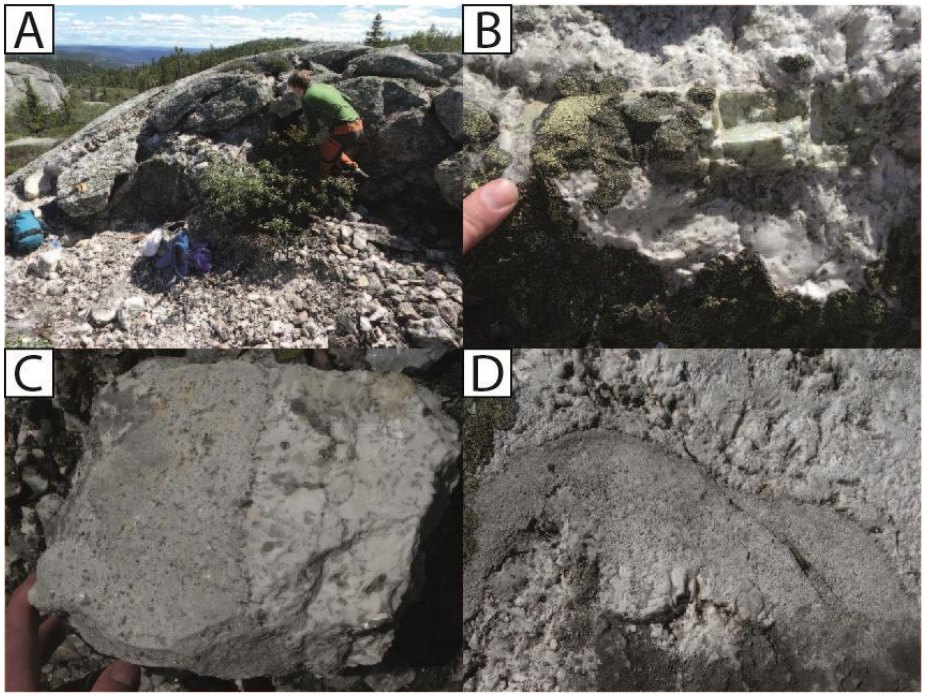

Fig. 3.5. Photographs of rocks exposed at the Svåheii 2b locality in July 2019. A – Overview of the complex pegmatite exposed at the Svåheii 2b site. B – Beryl from the intermediate zone. C and D – Examples of garnet-rich aplititc veins crosscutting the pegmatite.

The complex zone pegmatite at Upper Høydalen pegmatite

The complex zoned Upper Høydalen pegmatite forms a WNW-ESE-striking, sub-vertical pegmatite dyke, which is c. 50 m long and up to 8 m wide (Fig. 3.6 A; Table 3.1). This amazonite-bearing pegmatite is situated in northeast NE of the Tørdal pegmatite field. Because of its complex zoning, the occurrence of amazonite and a great diversity of accessory rare-metal minerals (Table 3.1), the Upper Høydalen pegmatite is referred as one of the chemically most evolved pegmatites of Tørdal pegmatite field (Fig. 3.6 A). The major minerals of the pegmatite are quartz, plagioclase, albite (shape variet cleavelandite), white and green K-feldspar (colour variety amazonite), biotite, and muscovite (Table 3.1). Charactersitic is the occurrence of megacrystic lepidolite related to albite zones in the inner parts of the pegmatite body. The pegmatite is situtated coarse-grained metagabbro belonging to Nissedal Outlier supracrustals. The contact between the pegmatite and coarse-grained metagabbro is very irregular. Up to 30 cm wide and several meter long pegmatite apophyses extend from the main pegmatite body into the metagabbro, while meter-sized metagabbro xenoliths are found in the roof and along the contacts of the pegmatite. The pegmatite shows distinct textural as well as mineralogical and complex zonings, similar as the Svåheii 2b locality. These zonings comprise, from outwards

to inwards, an up to 5 cm wide, biotite-bearing border zone of medium- to coarse-grained granitic texture, a wall zone, an intermediate zone, a massive quartz core, and irregular albite replacement zones. These albite replacement zones occur predominantly in the intermediate zone or along the border between the intermediate zone and core. The wall zone consist of megacrystic plagioclase (up to 20 cm in size) and coarse quartz filling the interstices between plagioclase crystals. In contrast to the border zone, which contains biotite, the wall zone contains muscovite as the only mica. The absence of biotite and the occurrence of muscovite reflects the Fe depletion of the pegmatite melt during fractional crystallization, a similar observation made at Svåheii 2b locality. The intermediate zone has a blocky structure with sub-euhedral amazonite crystals (up to 2 m in size) and roundish plagioclase megacrysts with wavy crystal boundaries (up to 2 m in diameter). Both amazonite and plagioclase are embedded in massive quartz (Fig. 3.6 B). The plagioclase megacrysts shows graphic intergrowths with centimeter-sized quartz, known as graphic granite, where the content of which decreases from the core of the megacrysts towards the margins. The outmost growth zone (up to 20 cm wide) of the plagioclase megacrysts is free of quartz and contains ball-shaped muscovite (up to 5 cm) and a garnet line instead. An up to 50 cm thick layer of platy albite (var. cleavelandite) occurs predominantly along the contact between the intermediate zone and pegmatite core (core-boundary). At the inner side (towards the core) of the cleavelandite layer, up to 30 cm large, lepidolite booklets are developed forming a comp texture. Batches of this cleavelandite zone occur also within the intermediate zone. The pegmatite core consit mainly of massive, greyish quartz. In addition, the core contains some, up to 50 cm large irregular batches of medium- to coarse-grained lepidolite. C. 150 m SE from the Upper Høydalen pegmatite, the Lower Høydalen pegmatite occurs, which exhibits similar zoning and mineralogy (Table 3.1). However, there is no field evidence if these two pegmatites are linked or not (Fig. 3.2).

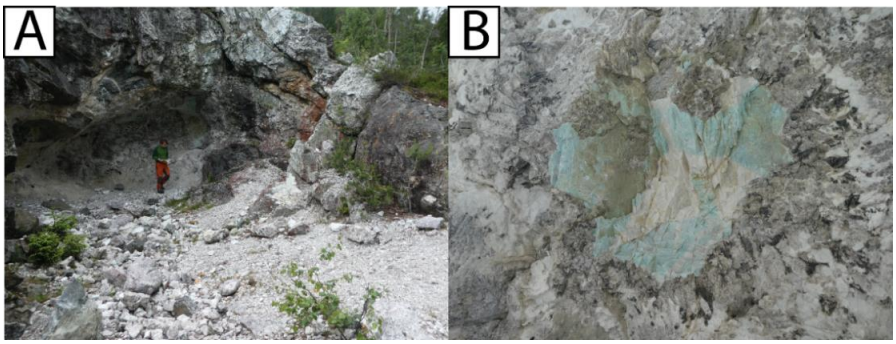

Fig. 3.6. Photographs of rocks exposed at the Upper Høydalen locality in July 2019. A – Overview photograph of the the Upper Høydalen pegmatite mine. B – Example of greenish K-feldspar (amazonite) megacryst (c. 30 cm diameter) exposed in the intermediate zone of the Upper Høydalen pegmatite.

3.2 Beryl

3.2.1 Major and minor elements determined by EPMA

The chemical formula of the beryl group is given as ^{ch}(Na, Cs, Rb, K, H_2O, He, Ar) $^{T(2)}$(Be, Li)$_3$ ^{o}(Al, Fe^{3+}, Sc, Cr, V, Fe^{2+}, Mg, Mn)$_2$ $^{T(1)}$(Si_6O_{18}) according to Franz and Morteani (2002). The group consists mainly of six different members or group members (Table 3.2). These beryl group members are, however, distinguished from each other dependent on which elements that occupy their sites. The sites are known as *(ch)* the channel site, *T(2)* the second tetrahedral site, *(o)* the octahedral site and *T(1)* the first tetrahedral site. The different element occupancies in the sites of the beryl group, which distinguishes the members from each other, are further listed in Table 3.2.

Table 3.2. Occupation in the structural sites of beryl group minerals. The six solid solution endmembers of the beryl mineral group are according to Mindat (2020a).

Mineral	*T(1)*	*T(2)*	*(o)*	*(ch)*	*O*	(O, OH)
Avdeevite	Si_6	Be_2, Li	Al_2	Na, Cs	O_{18}	
Bazzite	Si_6	Be_3	Sc_2		O_{18}	
Beryl	Si_6	Be_3	Al_2		O_{18}	
Johnkoivulaite	Si_6	Be_2, B	Mg_2	Cs	O_{18}	
Pezzottaite	Si_6	Be_2, Li	Al_2	Cs	O_{18}	
Stoppaniite	Si_6	Be_3	$Fe^{(III)}_2$		O_{18}	*H_2O

Two of solid solution endmembers of the beryl group mineral members, beryl and bazzite, have been discovered in Tørdal pegmatites (Bergstøl and Juve, 1988; Juve and Bergstøl, 1990; Segalstad and Eggleston, 1993). Beryl is given the chemical formula $Be_3Al_2Si_6O_{18}$, which means that the mineral is mainly dominated by Al in its octahedral site *(o)* (Fig. 3.7; Table 3.2). Bazzite ($Be_3Sc_2Si_6O_{18}$), on the other hand, is known as the Sc analogue of beryl (Juve and Bergstøl, 1990). Major difference between these two beryl group minerals lies mainly in their octahedral site *(o)*, where bazzite is mainly dominated by Sc instead of Al as in beryl (Table 3.2).

The studied beryl and bazzite samples are further classified in the ternary diagram of "octahedral beryls" with the endmembers beryl (Al), bazzite (Sc) and stoppaniite (Fe^{3+}) (Pezzotta et al., 2005). All studied beryl samples plot in the beryl field and close to the beryl-endmember (Al) and the bazzite samples in the bazzite field as suspected.

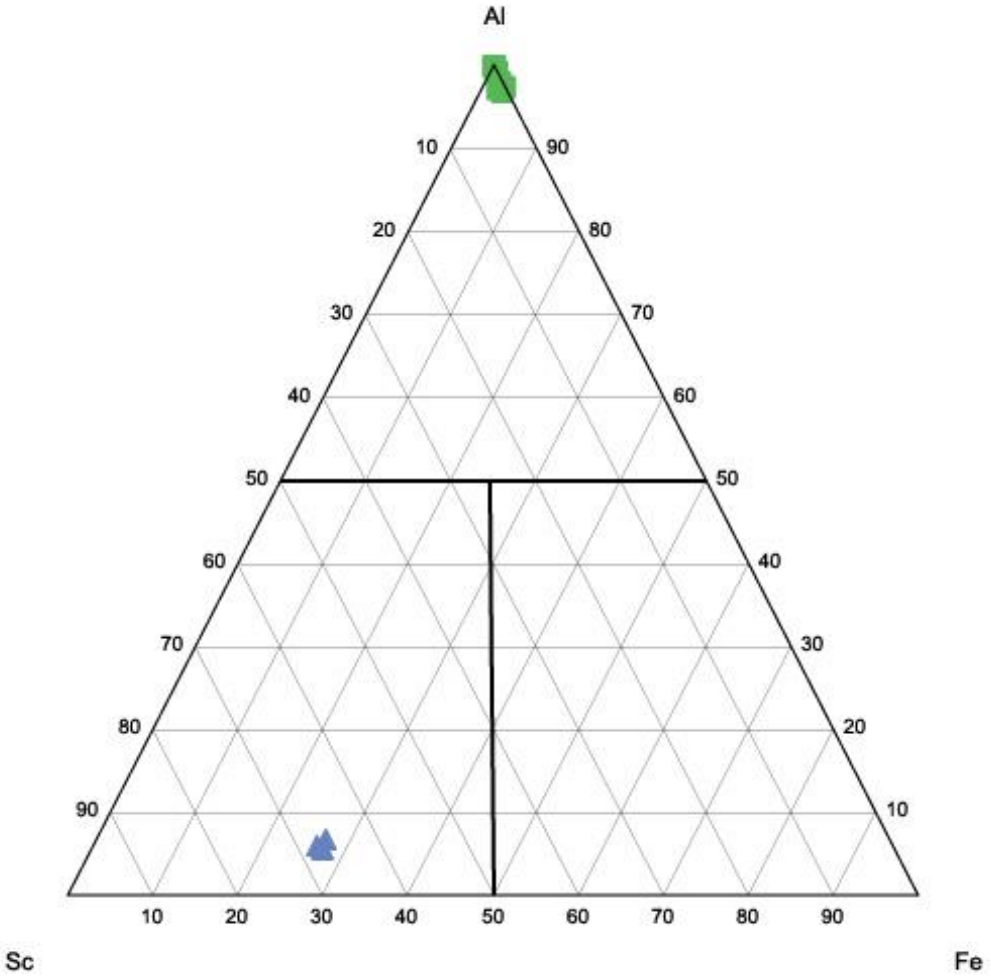

Fig. 3.7. Ternary diagram of the "octahedral beryls" with the three endmembers beryl (Al), bazzite (Sc) and stopaniite (Fe^{3+}) according to Pezzotta et al. (2005). The studied beryl samples (green squares) plot close to the beryl-endmember composition, while the studied bazzite samples (blue triangles) plot in the bazzite field.

67 point EPMA analysis were performed on four green, three pink, and two yellow beryls collected from intermediate and albite replacement zones of studied Tørdal pegmatites. The complete list of results of major and minor element analyses are provided in Appendix 7.5. Average concentrations of beryl crystals are summarized both as weight percents (wt.%) of oxides and apfu (atoms per formula unit) in Table 3.3. In addition, concentrations of Li (ppm) was detected by LA-ICP-MS and, thus, converted to Li_2O wt.% and afterwards Li *apfu*, since Li_2O wt.% can`t be detected through EPMA.

Table 3.3. Average concentrations of electron probe analysis of studied beryl samples. Numbers in parenthesis indicate standard deviation.

Sample	0Hoy01, July 2017	0Hoy02, 31542	0Hoy03, 31511	NHoy02, 03071701	NHoy01,31541	31548	42326	15061801	HF441m
Pegmatite	Upper Høydalen	Upper Høydalen	Upper Høydalen	Lower Høydalen	Lower Høydalen	Skardsfjell	Heftetjern 1	Svåheii 2b	Upper Høydalen
Mineral	Green beryl	Morganite	Yellow beryl	Yellow beryl	Morganite	Green beryl	Green beryl	Green beryl	Morganite
n	*6*	*6*	*6*	*6*	*6*	*7*	*14*	*8*	*8*
MgO (wt.%)	<0.03	<0.03	<0.03	<0.03	<0.03	<0.03	<0.03	0.065	<0.03
Al_2O_3	18.5 (2)	18.4 (1)	18.4 (2)	18.1 (2)	18.4 (4)	18.4 (1)	18.3 (4)	18.3 (2)	18.9 (3)
FeO	0.1 (1)	<0.05	0.2 (1)	0.43 (2)	<0.05	0.67 (3)	0.47 (6)	0.66 (2)	<0.03
Sc_2O_3	<0.03	<0.03	<0.03	0.05 (1)	<0.03	0.15 (1)	0.2 (1)	<0.03	<0.03
Na_2O	0.43 (4)	0.73 (6)	0.4 (1)	0.37 (2)	0.71 (3)	0.36 (3)	0.48 (3)	0.19 (3)	0.67 (5)
Cs_2O	0.066 (6)	0.18 (5)	<0.06	<0.06	0.18 (4)	<0.06	0.20 (4)	<0.06	0.15 (8)
SiO_2	66.5 (7)	65.7 (7)	65.7 (8)	65.9 (7)	66.1 (4)	66.4 (2)	66.9 (3)	66.7 (6)	67.2 (8)
BeO*	13.863	13.736	13.725	13.736	13.796	13.863	13.954	13.877	14.035
Li_2O**	0.162	0.444	0.221	0.111	0.429	0.089	0.222	0.041	0.480
Total	99.809	99.359	98.889	98.936	99.748	99.981	100.905	99.895	101.494
Mg (*apfu*)	0.001	0.001	0.000	0.002	0.000	0.000	0.000	0.009	0.000
Al	1.965	1.980	1.979	1.950	1.966	1.955	1.935	1.946	1.986
Fe^{2+}	0.013	0.001	0.016	0.033	0.000	0.051	0.036	0.050	0.000
Sc	0.000	0.000	0.001	0.005	0.000	0.012	0.019	0.000	0.000
Σ*O*-site	1.980	1.984	1.997	1.992	1.968	2.017	1.989	2.005	1.986
Na	0.077	0.130	0.074	0.066	0.125	0.063	0.084	0.034	0.116
Cs	0.003	0.007	0.002	0.001	0.007	0.000	0.008	0.000	0.006
Σ *CH*-site	0.080	0.139	0.077	0.070	0.135	0.063	0.092	0.034	0.122
Si	5.998	5.978	5.986	5.998	5.990	5.984	5.994	6.002	5.980
Σ *T1*-site	5.998	5.978	5.986	5.998	5.990	5.984	5.994	6.002	5.980
Be	2.941	2.837	2.920	2.959	2.845	2.967	2.920	2.985	2.828
Li	0.059	0.163	0.081	0.041	0.156	0.033	0.080	0.015	0.172
Σ *T2*-site	3.000	3.000	3.001	3.000	3.001	3.000	3.000	3.000	3.000

*BeO: the BeO is esitmated to fully ocupy the *T2*-site with minor Li_2O; **Li_2O: the Li (ppm) detected by LA-ICP-MS was converted to Li_2O (wt.%) to occupy minor amounts of the BeO dominated *T2*-site.

Results of their major and minor element analysis of beryl revealed that Si as their major constituent with a relative consistent concentration varying from 5.978 to 6.002 a*pfu* (66.1 to 67.2 wt.% SiO_2) in the *T(1)* site, which is relative close to the stoichiometric value of 6 (Table 3.3). The octahedral site *(o)* is dominated by the second most abundant constituent Al, which varies from 1.935 to 1.986 *apfu* (18.1 to 18.9 wt.% Al_2O_3) and is close to the stoichiometric value of 2 (Table 3.3). This confirms that *T(1)* and *(o)* of studies beryl samples are approximately fully occupied by Si and Al. The octahedral site *(o)* is where most of the detected trace elements occur together with Al (Table 3.3). These elements are Fe^{2+}, Sc, Mg and their concentrations vary from below the limit of detection to 0.051, 0.019 and 0.009 *apfu*, respectively (Table 3.3). The channel site *(ch)* contains small amounts of Na, which varies from 0.034 to 0.130 *apfu* (0.19 to 0.73 wt.% Na_2O), and traces of Cs (0.008 *apfu*) (Table 3.3). Lithium varies from 0.015 to 0.172 *apfu* (0.041 to 0.480 wt.% Li_2O), where it occupies the *T(2)* site and usually substitutes for Be (Černý et al., 2003; Table 3.3).

In this study, attention is paid to the Sc distribution in beryls, which mainly occupies the octahedral site *(o)*. Concentrations of Sc and its substituion into the octahedral site is illustrated in Figures 3.8 and 3.9, where Al_2O_3 versus Sc_2O_3 and Sc (*apfu*) versus Al (*apfu*) are plotted against each other, respectively. Both diagrams are shown to illustrate the difference between *apfu*-based and wt.%-based plots. The Al_2O_3 versus Sc_2O_3 wt.% plot does not show a distinctive correlation between both oxides. However, the Sc (*apfu*) versus Al (*apfu*) plot reveals a weak negative correlation, where the Sc concentration decreases with the increasing Al concentrations. The negative correlation, which is seen in Figure 3.9, confirms that Sc usually substitues for Al in the octahedral site *(o)*. The green beryl from Heftetjern 1 (sample 42326) has the highest Sc concentrations compared to other studied beryls. The green beryl from Skardsfjell (sample 31548) and the yellow beryl from Lower Høydalen (sample NHoy02 03071701) consist of moderate concentrations of Sc, while the remaining beryls have very low Sc or Sc concentrations below the limit of detection (<0.03 wt.% Sc_2O_3) (Table 3.3). These low-Sc beryls include the pink morganites from Upper Høydalen (sample OHoy03 31511, OHoy01 July 2017, HF441m, OHoy02 31542), Lower Høydalen (sample NHoy01 41541) and the green beryl from Svåheii 2b (sample 15061801).

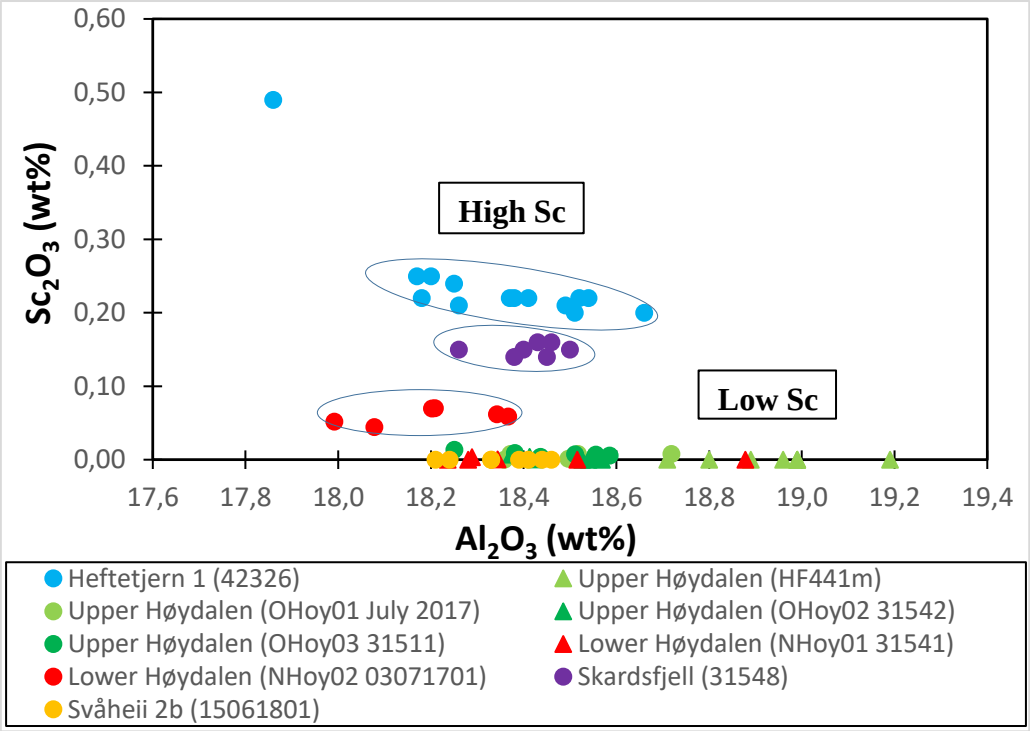

Fig. 3.8. Sc_2O_3 versus Al_2O_3 diagram of investigated beryl samples from Tørdal. The data do not show a correlation between Sc_2O_3 and Al_2O_3. Beryls from Heftetjern 1, Skardsfjell and Lower Høydalen are most enriched in Sc_2O_3, while the beryl and morganite samples from Svåheii 2b, Upper Høydalen and Lower Høydalen are least enriched in Sc_2O_3.

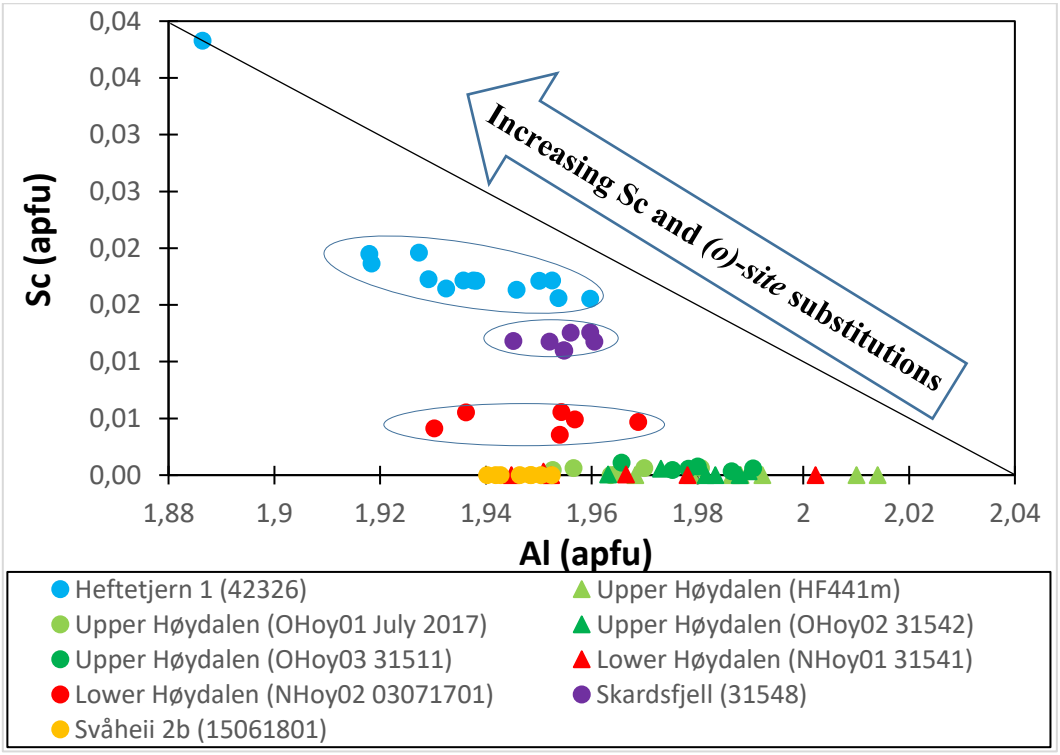

Fig. 3.9. Scandium versus Al plot of investigated beryls from the Tørdal pegmatites. The data show a weak negative correlation between decreasing Sc and increasing Al due to the substitution mechanism in the *(o)* site. This trend is not obvious in the Sc_2O_3 versus Al_2O_3 diagram (see Fig. 3.8).

However, not only Sc substitutes for Al in the octahedral site *(o)* but also other elements, such as Fe^{2+}, Mg and Sc, as illustrated in Figure 3.10, where Al versus Fe^{2+}+Mg+Sc are plotted against each other. The concentrations of Al and Fe^{2+}+Mg+Sc correlate negatively, which confirms the substitution mechanism among the elements in the octahedral site *(o)*. Green beryls from Skardsfjell (sample 31548), Svåheii 2b (sample 15061801), and Heftetjern 1 (sample 42326) have the highest Fe^{2+}+Mg+Sc and lowest Al concentrations, whereas the yellow beryl from Lower Høydalen (sample NHoy02 03071701) consists of moderate Fe^{2+}+Mg+Sc (*apfu*) and Al (*apfu*) concentrations. This is followed by samples from Upper Høydalen (sample OHoy01 July 2017, OHoy03 31511), which have slightly elevated Fe^{2+}+Mg+Sc and moderate Al concentrations and consist of green and yellow beryls, while other samples from Upper Høydalen sample (HF441m, OHoy02 31542) together with samples from Lower Høydalen (sample NHoy01 31541) have the lowest Fe^{2+}+Mg+Sc and the highest Al concentrations, and are considered as morganites (Fig. 3.10).

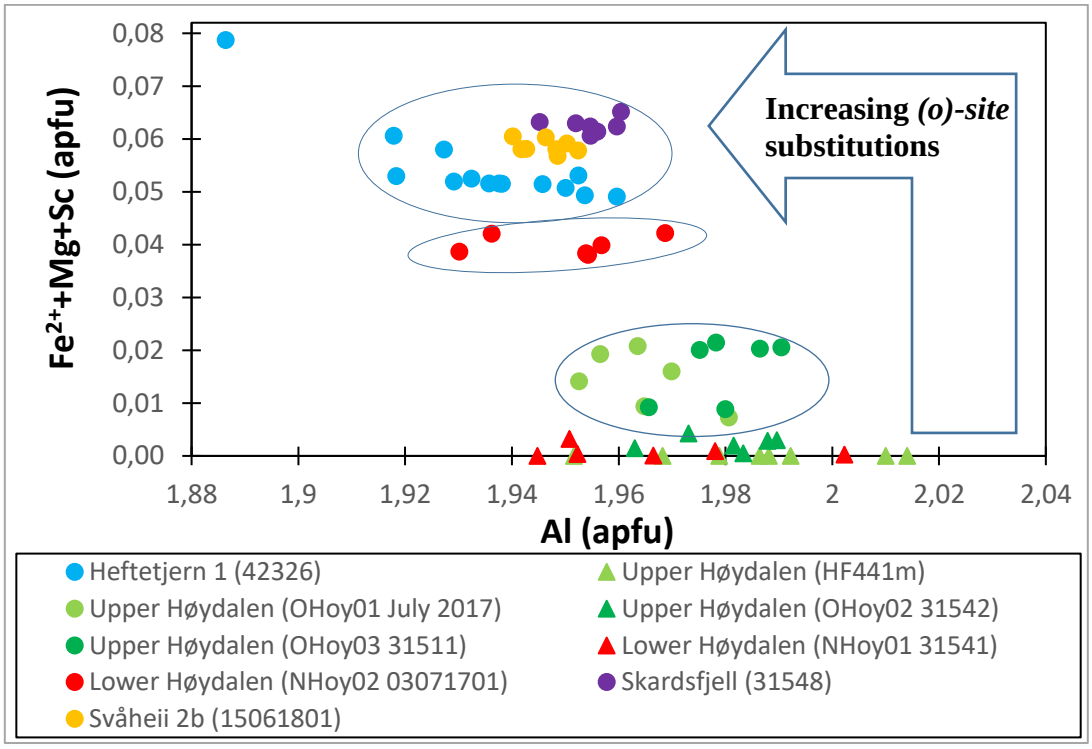

Fig. 3.10. Plot of Fe^{2+}+Mg+Sc against the Al contents of beryl according to Groat et al. (2010). The plot shows that the octahedral site *(o)* of the beryls from Tørdal is dominated by Al and only small amounts of the other elements are substituted for Al. The data reveal a negative correlation whereby Al decreases with increasing Fe^{2+}+Mg+Sc contents.

Another substitiuion mechanism, which occurs between the channel site *(ch)* and octahedral site *(o)* in studied beryls, known as channel-octahedral site substitutions, is illustrayed in Figure 3.11 according to Uher et al. (2010). A negative correlation between Fe^{2+}+Mg and Na confirm

that Na substitutes Fe^{2+} and/or Mg. Low Fe^{2+}+Mg and high Na reflects a high channel-octhaedral substitution, while high Fe^{2+}+Mg and low Na documents a lower channel-octahedral substitution. The highest Fe^{2+}+Mg and lowest Na has the green beryl from Svåheii 2b (sample 15061801) indicating very limited subsituion by Na. Moderate high Na and relative high Fe^{2+}+Mg is found in the green beryl from Skardsfjell (sample 3158). The green and yellow beryls from Heftetjern 1 (sample 42326) and Lower Høydalen (sample NHoy02 03071701) consist of a moderate Fe^{2+}+Mg and Na (especially sample 42326), while the green and yellow beryls from Upper Høydalen (OHoy01 July 2017, OHoy03 31511) contain relative low Fe^{2+}+Mg. The lowest Fe^{2+}+Mg and highest Na are discovered in the pinkish morganite samples from Upper Høydalen (sample OHoy02 31542, HF441m) and Lower Høydalen (sample NHoy01 31541), indicating very high substitution by Na.

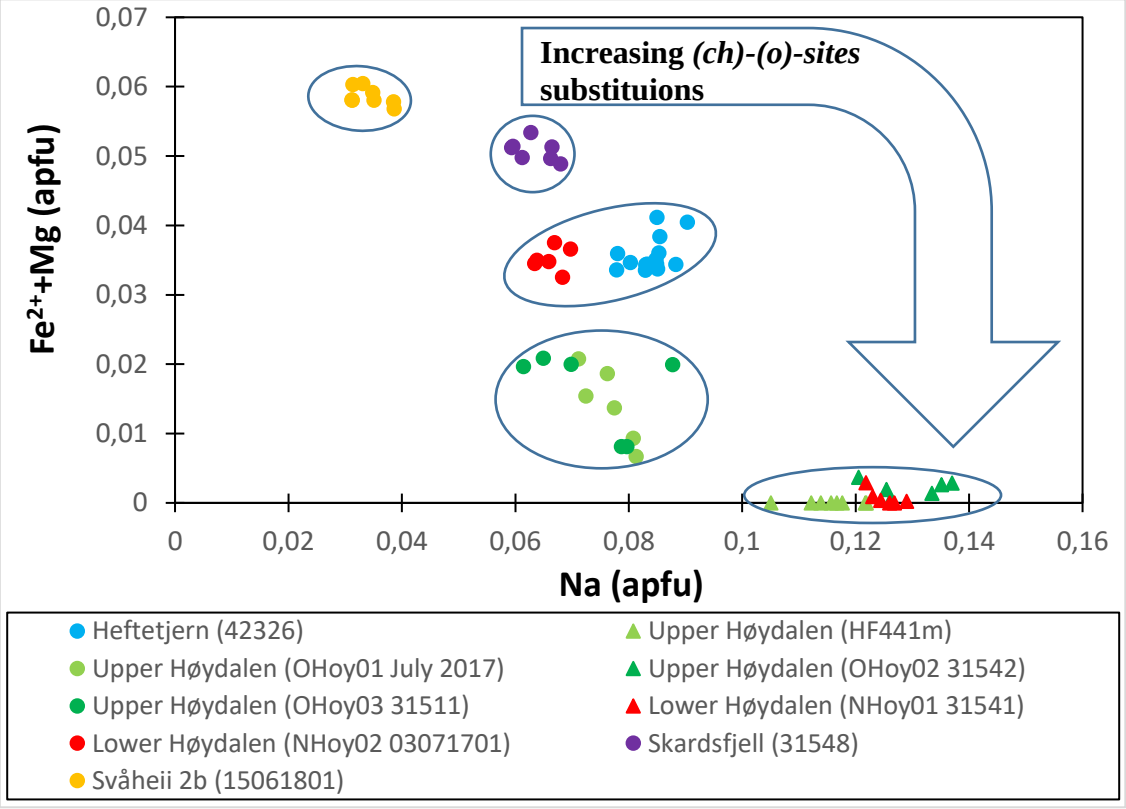

Fig. 3.11. Fe^{2+}+Mg versus Na diagram which illustrated the substitution between channel site *(ch)* and octahedral site *(o)* of studied beryls according to Uher et al. (2010). The plot shows a negative correlation which illustrated the substitution of decreasing Fe^{2+}+M by. increasing Na.

The degree of substitutions is linked to the differenatiation degree of the pegmatite from which the beryl grew. Thus, the beryl chemistry may be used to distinguish chemically primitive beryl from chemically evolved beryls. High Fe^{2+} and Mg together with low Na, Li, and Cs represent the chemically most primitive beryls, while low Fe^{2+} and Mg together with high Na, Li, and Cs

is typical for chemical evolved beryls. Therefore, increasing Na, Li, and Cs accompanied by decreasing Fe^{2+} and Mg in beryls reflect the progressive evolution (Černý et al., 2003; Uher et al., 2010; Sardi and Heimann, 2014). The following plots, Figures. 3.12, 3.13, 3.14, illustrate the concentrations of Na, Li, Cs, Fe^{2+}, and Mg of the investigated beryls.

In Figure 3.12 Al is plotted against Fe^{2+} illustrating the replacement of Al by Fe^{2+} in the octahedral site *(o)*. Chemical primitive beryls have high Fe^{2+} concentrations, while those with evolved characteristics have the low Fe^{2+}. The green beryls from Skardsfjell (sample 31548) and Svåheii 2b (sample 15061801) are most enriched in Fe^{2+} compared to the other studied beryls, which are the most primitive investigated beryls. The green beryl from Heftetjern 1 (sample 42326) and the yellow beryl from Lower Høydalen (sample NHoy01 03071701) contain moderately high Fe^{2+}. Intermediate Fe^{2+} (*apfu*) concentrations were discovered in the green and yellow beryls from Upper Høydalen (sample OHoy01 July 2017, OHoy03 31511), while the morganites from Lower Høydalen (sample NHoy01 31541) and Upper Høydalen (sample OHoy02 31542, HF441m) have the lowest Fe^{2+}contents. The morganites are the chemically most evolved beryls in the Tørdal pegmatites.

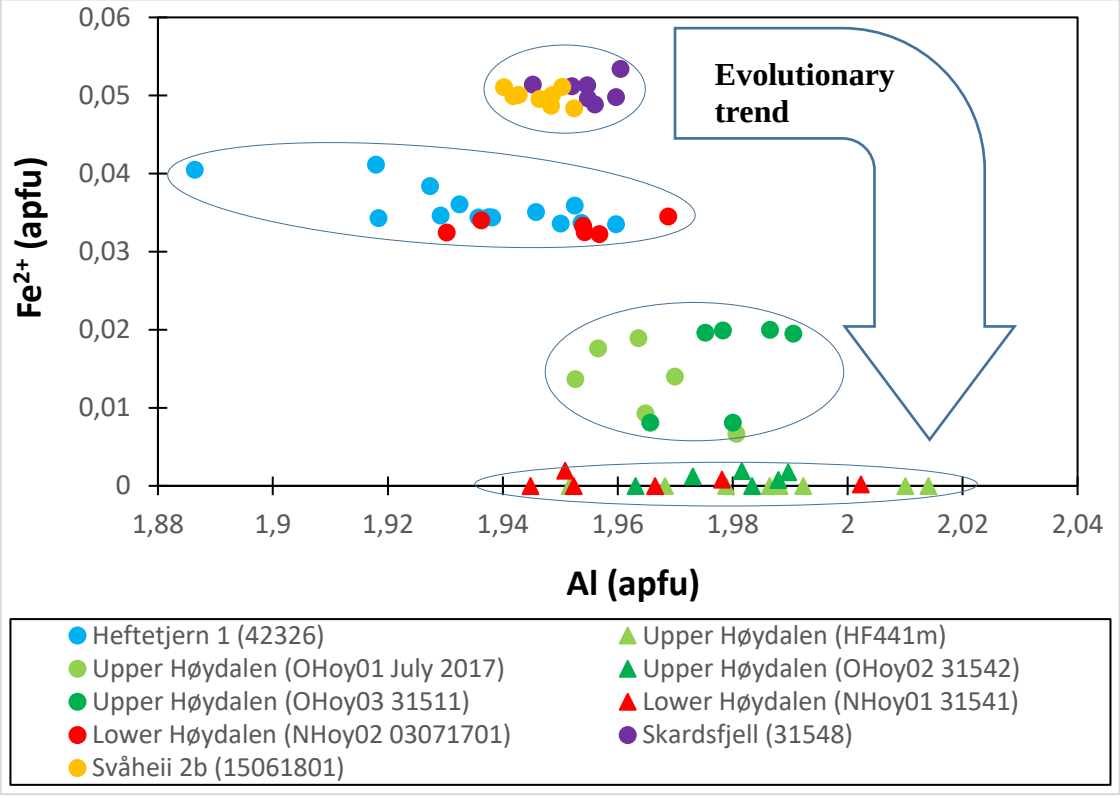

Fig. 3.12. Plot of Al versus Fe^{2+} (*apfu*) in the octahedral site *(o)* of beryls from Tørdal pegmatites. Chemically primitive green beryls from Skardsfjell and Svåheii 2b are most enriched in Fe^{2+}. The chemically most evolved morganites from Upper and Lower Høydalen have lowest Fe^{2+}.

Figure 3.13 illustrates the concentrations of Li and Na in the studied beryls. Similar as Figure 3.12, the plotted concentrations of the alkalis Li and Na help distinguish the chemically primitive beryls from the most evolved beryls. Beryls with highest Li and Na are the chemically most evolved ones, represented by the two morganites from Upper Høydalen (samples OHoy02 31542, HF441m) and Lower Høydalen (sample NHoy01 31541). Lowest Li and Na contents, typical for primitive beryls, are found the beryl from Svåheii 2b (sample 15061801). The most important observation here is, that the morganites have a much higher Na and Li than green and yellow beryls.

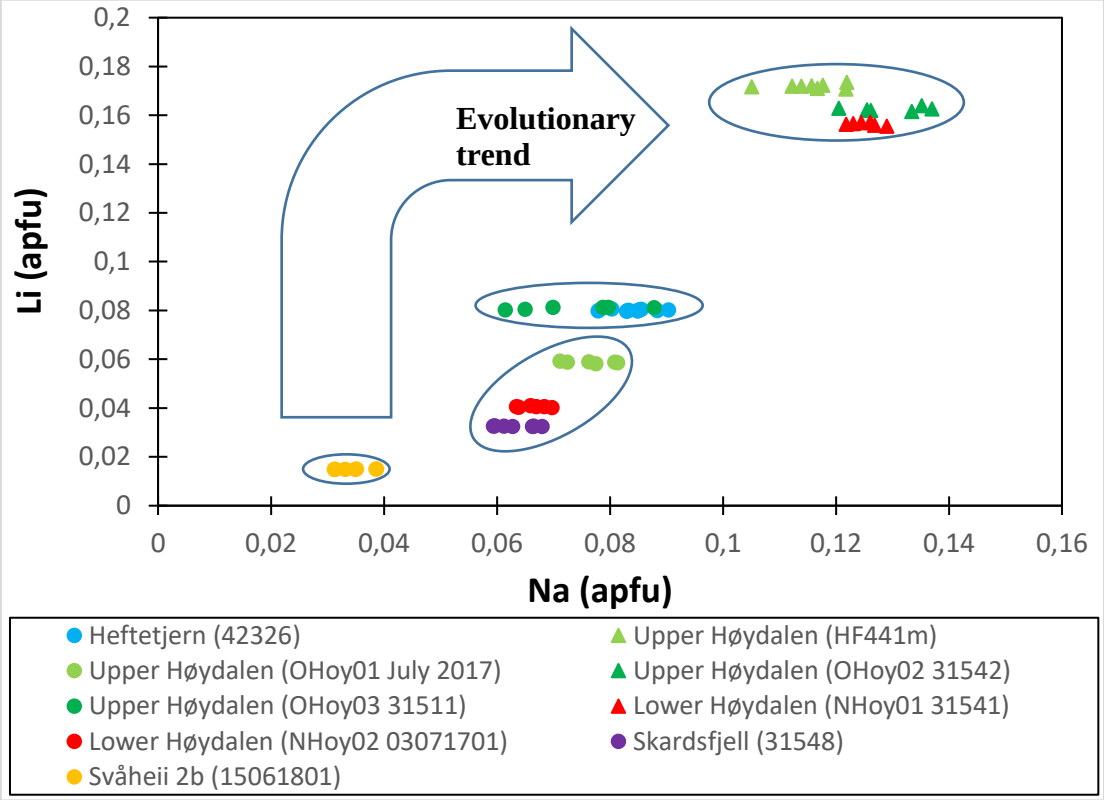

Fig. 3.13. Sodium versus Li plot of beryls from Tørdal pegmatites. The data shows a distinct positive correlation. The morganites have significantly higher Na and Li as the yellow and green beryls, confirmin that the morganites are the most evolved beryls from Tørdal.

The Na+Li+Cs versus Fe^{2+}+Mg plot in Figure 3.14 illustrates the overall trace element trends of the investigated beryls. The increasing Na, Cs and Li together with the decreasing Fe and Mg reflects the increasing fractionation degree of beryls and, thus, of the melt form which the beryls grew (Černý et al., 2003; Uher et al., 2010; Sardi and Heimann, 2014). In overall, the studied beryls mark a clear chemical evolutionary trend from primitive beryls, high Fe^{2+}+Mg and low Na+Li+Cs, to evolved beryls with low Fe^{2+}+Mg and high Na+Li+Cs. The green beryl samples from Svåheii 2b (sample 15061801) and Skardsfjell (sample 31548) contain the highest

contents of Fe^{2+}+Mg and lowest Na+Li+Cs. Moderate high Fe^{2+}+Mg occurs in the yellow and green beryl from Lower Høydalen (sample NHoy02 03071701) and Heftetjern 1 (sample 42326), which are characterized by moderate low Na+Li+Cs. Intermediate Fe^{2+}+Mg and Na+Li+Cs are observed in green and yellow beryl from Upper Høydalen (sample OHoy01 July 2017, OHoy03 31511). The morganites from Upper Høydalen (sample HF441m, OHoy02 31542) and Lower Høydalen (sample NHoy01 31541) have lowest Fe^{2+}+Mg and highest Na+Li+Cs. Thus, the most primitive beryl samples comprise of the green beryls from Svåheii 2b (sample 15061801) and Skardsfjell (sample 31548). The moderate primitive samples are the green and yellow beryls from Heftetjern 1 (sample 42326) and Lower Høydalen (sample NHoy03 03071701). The moderate evolved samples are the green and yellow beryls from Upper Høydalen (OHoy01 July 2017, OHoy03 31511) and the most highly evolved ones are the morganites from Upper Høydalen (sample HF441m, OHoy02 31542) and Lower Høydalen (NHoy01 31541).

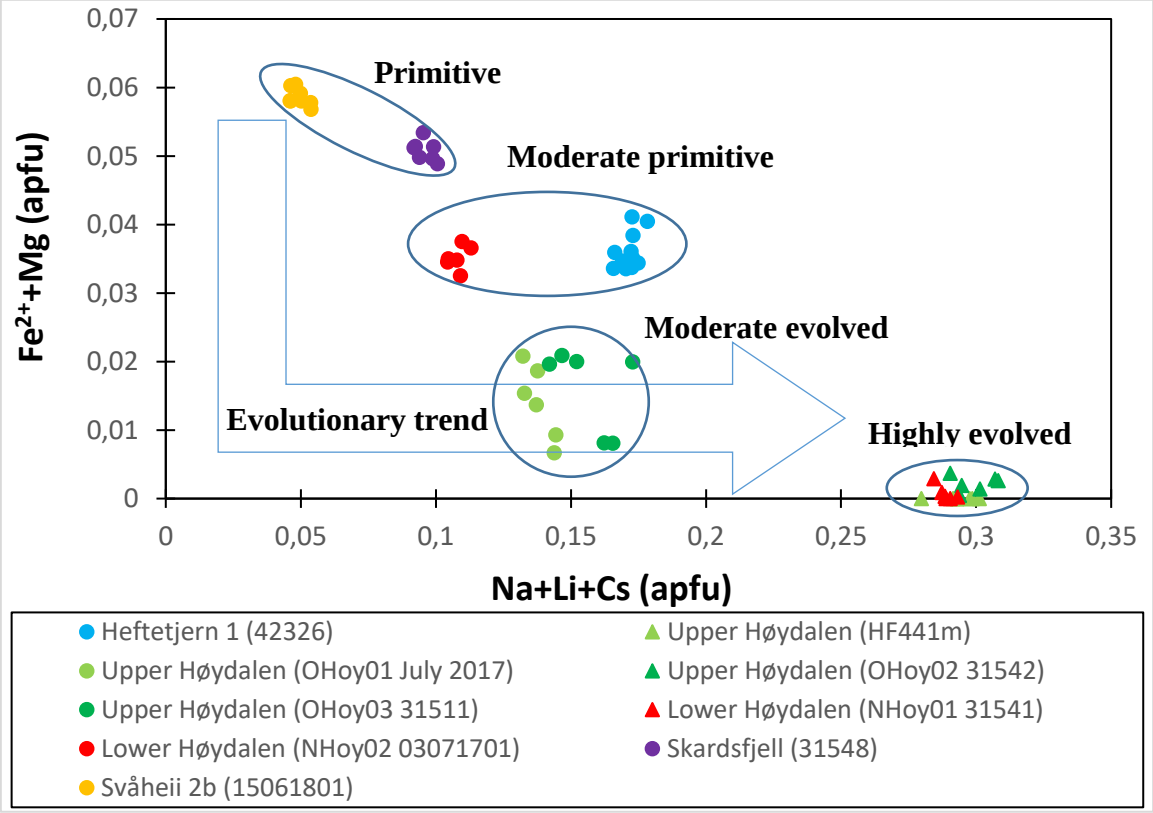

Fig. 3.14. The Na+Li+Cs versus Fe^{2+}+Mg diagram showing the chemical variation of the investigated beryls from Tørdal pegmatites. The samples follow a chemical trend from chemically primitive beryls with high Fe^{2+}+Mg and low Cs+Na to evolved beryls with low Fe^{2+}+Mg and high Cs+Na.

The Na_2O/Li_2O wt.% ratio versus Cs_2O wt.% discrimination diagram for beryls according to Černý (1992) shown in Figure 3.15, is another way to describe the chemical evolutionary trends

of pegmatite melts using beryl chemistry. Chemical primitive pegmatites, barren, are distinguished from more chemical evolved beryl-type pegmatites by the thresfold of c. 018 Cs_2O wt.% in beryl. Cs_2O of studied beryls varies from below the limit of detection (<0.06 wt.%) to approximate 25 wt.%. Among the studied beryls, the green beryl from Heftetjern 1 (sample 42326) and the morganites from Upper Høydalen (sample HF441m, OHoy02 31542) and Lower Høydalen (sample NHoy01 31541) have the highest concentrations of Cs_2O and the lowest Na_2O/Li_2O ratios. This data plot predominantly in the beryl-type pegmatite field according to Černý (1992) indicating that the pegmatite melt was chemically highly evolved. The green and yellow beryl samples from Upper Høydalen (sample OHoy01 July 2017, OHoy03 31511), together with the yellow beryl from Lower Høydalen (sample NHoy02 03071701) have intermediate concentrations of Cs_2O and Na_2O/Li_2O ratios. The green beryl samples from Skardsfjell (sample 31548) and Svåheii 2b (sample 15061801) contain the lowest Cs_2O concentrations but highest Na_2O/Li_2O ratios. The latter 6 beryls plot in the barren-type pegmatite field indicating that the pegmatitic melt was chemically primitive.

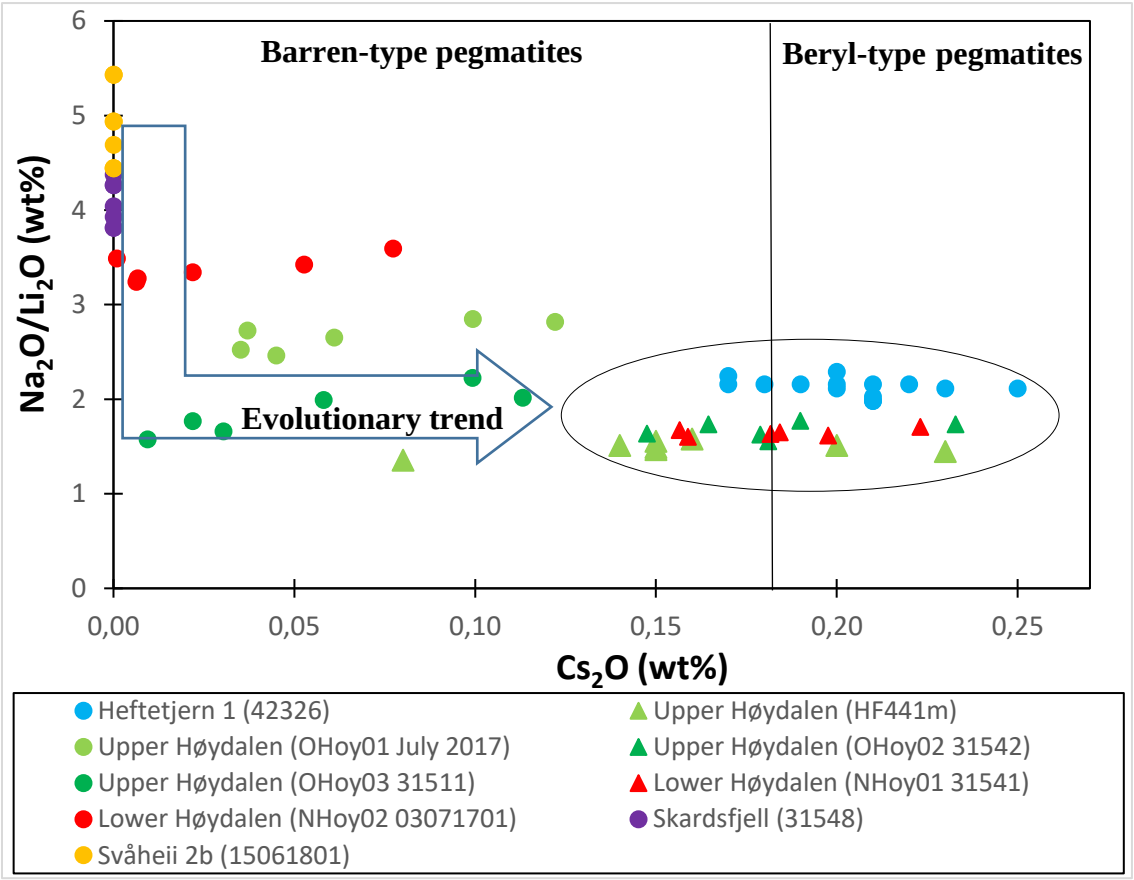

Fig. 3.15. Na_2O/Li_2O ratio versus Cs_2O content according to Černý (1992) with plotted concentrations of the investigated beryl samples. The decreasing Na_2O/Li_2O and increasing Cs_2O of beryls mark the evolutionary trend of the investigated Tørdal pegmatites. Samples plotting in barren-type pegmatites comprise of more primitive pegmatites compared to beryl-type pegmatites represented by beryl with >0.18 wt.% Cs_2O.

3.2.2 Minor and trace elements in beryl determined by LA-ICP-MS

All green, yellow and pinkish beryls, which were measured by EPMA were analyzed also by LA-ICP-MS in order to get addiational information about ther concentrations and distribution of their trace elements, escpecially Sc, Li, Rb, Cs, Fe^{2+} and Mg. The complete list of trace elements detected by LA-ICP-MS of studied beryls are given in Appendix 7.11. Average concentrations are summarized in Table 3.4.

Table 3.4. Average trace element concentrations of beryls from Tørdal determined by LA-ICP-MS. Numbers in parenthesis indicate the standard deviation. n = number of measurements

Sample	42326	31548	15061801	0Hoy01, July 2017	0Hoy03, 31511	HF441m	NHoy02, 03071701	0Hoy02, 31542	NHoy01, 31541
Pegmatite	Heftetjern 1	Skardsfjell	Svåheii 2b	Upper Høydalen	Upper Høydalen	Upper Høydalen	Lower Høydalen	Upper Høydalen	Lower Høydalen
Mineral	Green beryl	Green beryl	Green beryl	Green beryl	Yellow beryl	Morganite	Yellow beryl	Morganite	Morganite
n	*4*	*4*	*4*	*4*	*4*	*3*	*4*	*2*	*3*
Li (ppm)	1034(10)	418(25)	192(40)	754(31)	1028(52)	2232(151)	516(26)	2065(45)	1996(54)
Be	44556(384)	45143(850)	47063(1854)	45589(561)	44784(638)	44539(2207)	50248(618)	40361(197)	41948(2747)
B	15(6)	11 (2)	7(1)	15(2)	19(4)	57(33)	10(1)	34(10)	30(12)
Na	4482(185)	2853(8)	1723(65)	2983(45)	2983(70)	6898(607)	3000(113)	6104(224)	5941(298)
Mg	29(10)	49(9)	388(28)	2.3(8)	1.0(5)	5(5)	98(20)	1.4(6)	1(1)
P	5.1(5)	5.2(1)	6(1)	6.2(8)	6(1)	7.0(1)	6.1(2)	5(1)	5.6(4)
K	208(12)	128(29)	125(11)	52(15)	148(5)	224(16)	99(10)	119(9)	137(82)
Ca	91(5)	87(6)	90(13)	198(15)	200(5)	144(53)	153(14)	189(13)	181(21)
Sc	1114(64)	893(99)	<16.11	46(12)	<16.11	<16.11	442(42)	<16.11	<16.11
Ti	5(1)	4.8(2)	2.4(5)	6(1)	9.4(2)	11(1)	5.8(1)	13(1)	13(1)
V	0.80(9)	1.9(9)	4(2)	<0.04	<0.04	0.7(1)	<0.04	<0.04	<0.04
Cr	2.7(4)	2.7(3)	2.5(1)	4(2)	5(2)	3.4(3)	4(2)	4(1)	4(1)
Mn	198(22)	86(6)	35(16)	65(13)	61(1)	75(8)	83(14)	99(12)	78(5)
Fe	3205(339)	5272(247)	5832(387)	2131(66)	1557(88)	<26.40	6138(710)	<26.40	<26.40
Ga	174(5)	107(1)	75(2)	81(1)	58(1)	109(3)	82(3)	117(2)	119(2)
Ge	2.0(1)	1.170(8)	0.90(5)	0.99(3)	1.40(3)	1.52(7)	0.97(3)	1.6(1)	1.64(2)
Rb	257(12)	167(7)	84(5)	140(5)	168(7)	413(30)	130(4)	423(21)	381(58)
Cs	2307(444)	275(11)	262(26)	205(26)	317(24)	1327(35)	359(30)	1850(1)	1469(411)

To better understand the Sc concentration and its distribution in the studied beryls, the Sc and Li concentrations (ppm) were plotted against each other in Figure 3.16. Similar to EPMA-determined Sc concentrations (Figs. 3.8, 3.9), the green and yellow beryls from Heftetjern 1 (sample 42326), Skardsfjell (sample 31548) and Lower Høydalen (sample NHoy02 03071701) comprise the highest Sc with average concentrations of 1114, 894, and 442 ppm, respectively (Table 3.4). These Sc-rich beryls have low to moderate Li. The green and yellow beryls from Upper Høydalen (sample OHoy01 July 2017, OHoy03 31511) contain low Sc with average concentrations of 46 ppm and below the limit of detection (<16 ppm). In fact, all remaining samples have Sc concentrations below the limit of detection (<16 ppm). The morganites have highest Li but do not contain Sc. The Sc concentrations determined by LA-ICP-MS are similar to those determined by EPMA.

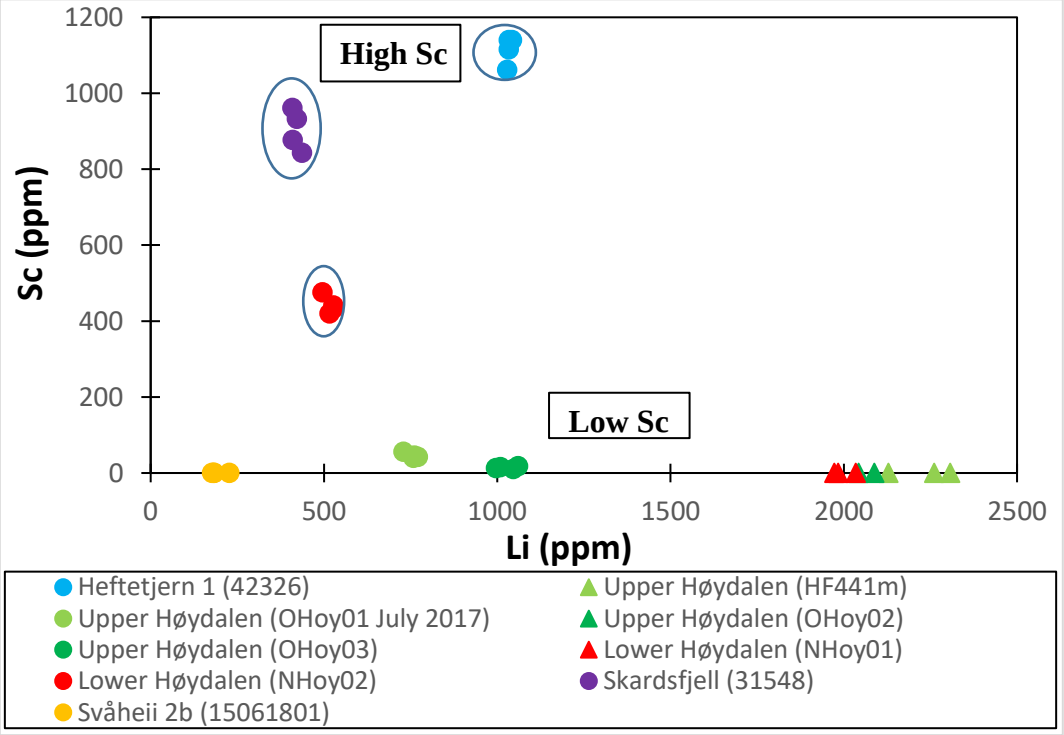

Fig. 3.16. Lithium versus Sc plot showing the distribution of these elements in the investigated beryls from the Tørdal pegmatites. Green and yellow beryls from Heftetjern 1, Skardsfjell and Lower Høydalen are most enriched in Sc, while all other the green beryls and morganites have very low or no detectable Sc.

In the following Figures 3.17, 3.18, and 3.19 illustrate in different ways to distinguish chemically primitive from chemically evolved beryls based on concentrations of Li, Cs, Mg, Fe^{2+}, and Rb. These Figures are similar to Figures 3.12, 3.13, and 3.14 with difference that the concentrations were determined with LA-ICP-MS.

In Figure 3.17 Fe^{2+} versus Li concentrations are plotted. In overall, Fe^{2+} correlates negatively

with Li. High Fe^{2+} and low Li concentrations is characteristic for primitive beryls. Chemically evolved beryls contain low Fe^{2+} and high Li. Chemically primitive yellow and green beryls from Lower Høydalen (sample NHoy02 03071701), Svåheii 2b (sample 15061801) and Skardsfjell (sample 31548) have high average Fe^{2+} contents of 6138, 5832 and 5272 ppm, respectively. By following the chemically evolutionary trend towards higher Li concentrations, the moderate evolved beryls include green and yellow beryls from Heftetjern 1 (sample 42326) and Upper Høydalen (sample OHoy01 July 2017, OHoy03 31511) with average Fe^{2+} concentrations of 3205, 2131 and 1557 ppm, respectively. Their Li concentrations are 1034, 1028 and 754 ppm, respectively. Chemically evolved morganites from Upper Høydalen (sample HF441m, OHoy02 31542) and Lower Høydalen (sample NHoy01 31541) have Fe^{2+} concentrations below the limit of detection (<26.40 ppm). The Li contents of the morganites are very high, being 2232, 2065 and 1996 ppm, respectively. This defineds them as the most evolved beryls.

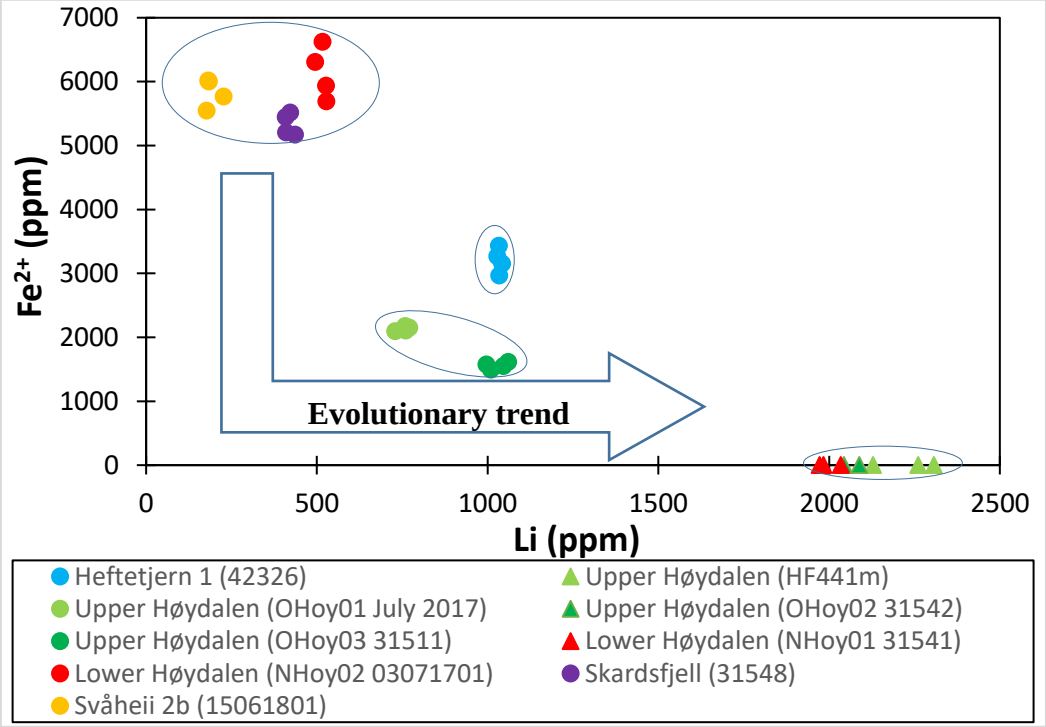

Fig. 3.17. Lithium versus Fe^{2+} plot showing the chemical variation of the investigated Trødal beryls. In overall, the data show a negative correlation from primitive beryls with high Fe^{2+} and low Li (Svåheii 2b, Skardsfjell and Lower Høydalen) towards the more evolved morganites from Upper Høydalen and Lower Høydalen with low Fe^{2+} and high Li.

However, Fe^{2+} concentrations alone does not allow to differentiate between chemically primitive beryls from Svhåheii 2b, Skardsfjell and Lower Høydalen. However, if trace element compositions of Li+Rb versus Cs are plotted against each other (Fig. 3.18), the beryl from

Svåheii 2b is distinctly more primitive (lower Li+Rb) than the beryls from Skardsfjell and Lower Høydalen. In general, Li+Rb and Cs are postiviely correlated with the expection of the Heftetjern sample. High Li+Rb and Cs concentrations correspond to beryls which are chemically most evolved. Green beryl from Heftetjern 1 (sample 42326) and morganites from Upper Høydalen (samples HF441m, OHoy02 31542) and Lower Høydalen (sample NHoy01 31541) comprise the highest Cs concentrations from Tørdal with averages of 2307, 1327, 1850 and 1469 ppm, respectively. Cesium in the remaining beryls is low and varies from 359 to 205 ppm (Table 3.4). The morganites, which have highest Li+Rb contents compared to other green and yellow beryls are the most chemical evolved beryls (Table 3.4). The green beryl from Heftetjern 1 (sample 42326), on the other hand, contains lower Li compared to the morganites but is relatively evolved due to its high Cs concentration. The green and yellow beryls from Upper Høydalen (sample OHoy01 July 2017, OHoy03 31511) have moderate Li+Rb concentrations, reflecting their moderate evolved beryl chemistries. The remaining yellow and green beryls samples from Lower Høydalen (sample NHoy02 03071701), Skardsfjell (sample 31548) and Svåheii 2b (sample 15061801) are relative low in Li+Rb and Cs and comprise a chemically primitive character (Fig. 3.18; Table 3.4).

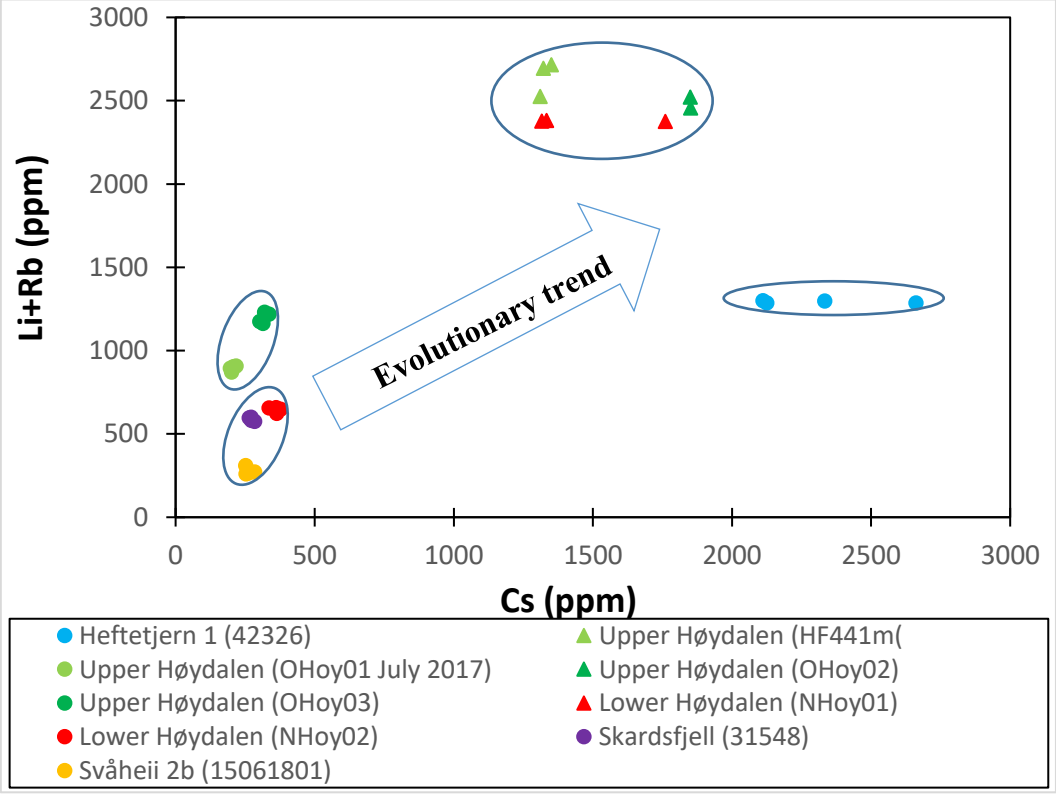

Fig. 3.18. Lithium+Rb versus Cs plot showing the chemical variation of beryls from the Tørdal pegmatites. In overall, the data follow a chemical trend from primitive, low Cs-Rb-Li beryls to evolved high Cs-Rb-Li beryls. The morganites from Upper and Lower Høydalen represent the chemically most evolved beryls of the Tørdal pegmatites.

The studied beryls from Tørdal contain traces of Mg. In Figure 3.19 Mg is plotted against Rb. Beryls containing the lowest Mg and highest Rb are considered as the most evolved, while beryls with highest Mg and lowest Rb are more chemically primitive. Among studied beryls, the sample Svåheii 2b (sample 15061801) has highest average Mg of 388 ppm. Samples from Lower Høydalen (sample NHoy02 03071701), Skardsfjell (sample 31548), and Heftetjern 1 (sample 42326) contain moderate Mg concentrations of 98, 49, and 29 ppm, respectively. Lowest Mg concentrations (<5 ppm) were detected in the green, yellow and morganite beryls from Upper Høydalen (sample HF441m, OHoy01 July 2017, OHoy02 31542, OHoy03 31511) and Lower Høydalen (sample NHoy01 31541). Highest Rb are discovered in the morganites from Upper Høydalen and Lower Høydalen, followed by the green beryl from Heftetjern 1. These beryls contain average Rb of 423, 413, 381 and 25 ppm, respectively (Table 3.4). The green and yellow beryls from Upper Høydalen (sample OHoy03 31511, OHoy01 July 2017), Skardsfjell (sample 31548) and Lower Høydalen (NHoy02 03071701) comprise 168, 150, 167 and 130 ppm Rb, respectively. The lowest Rb was found in the green beryl from Svåheii 2b (sample 15061801) with 84 ppm.

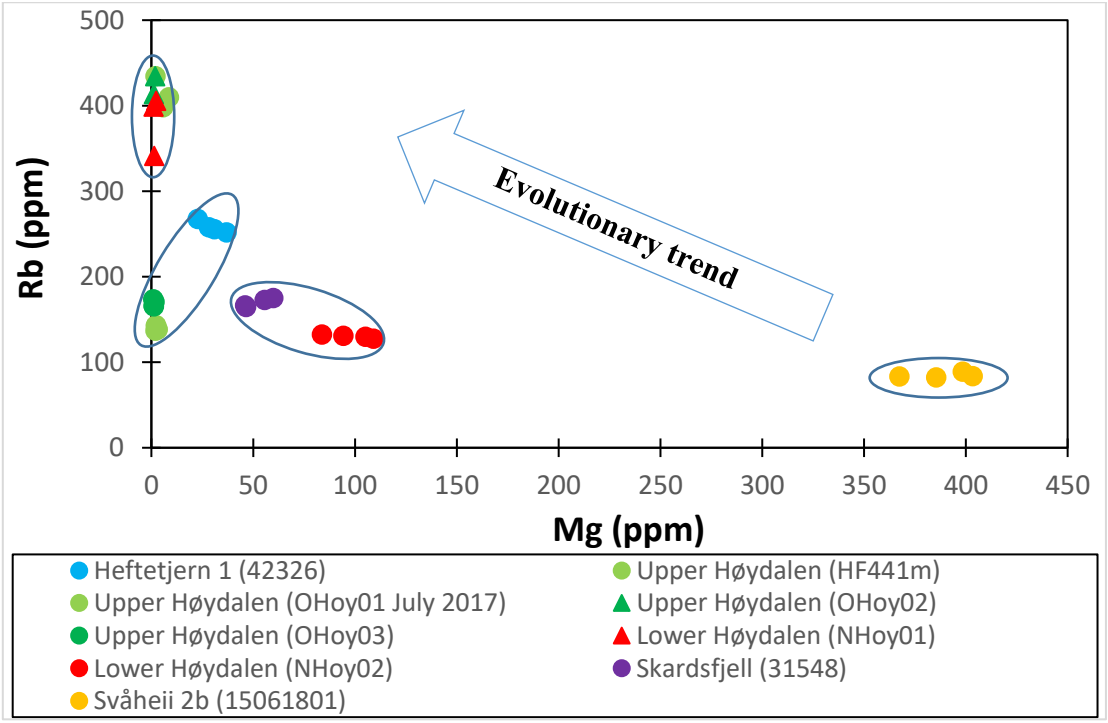

Fig. 3.19. Magnesium versus Rb plot of beryls from the Tørdal pegmatites. The data mark exponential correlation, whereby beryls with high Rb and low Mg represent the chemically most evolved samples. Low Rb and High Mg reflects more chemically primitive beryls.

3.2 Bazzite

3.1 Major and minor elements determined by EPMA

As discussed above, the studied bazzites are clearly classified as bazzites in the ternary diagram of "octahedral beryls" according to Pezzotta et al. (2005) (Fig. 3.7). Th studied bazzites contain a large amount of Fe^{3+} in the *(o)* site and therefore the data plot close to the stoppaniite boundary (Fig. 3.7).

Five bazzite samples, which were collected from albite replacement zones of the Heftetjern 1 pegmatite, were analyzed by EPMA for their major and minor element concentrations. The Heftetjern 1 and Høydalen pegmatite is the only pegmatites in Tørdal were bazzite has been found (Mindat, 2020b; Mindat, 2020c). In total 38 point analyses were carried out. The complete list of analyses is given in Appendix 7.6. Average concentrations are summarized in Table 3.5.

Table 3.5. Average concentrations of major elements of bazzites from the Heftetjern 1 pegmatites. Data were obtained with electron probe micro analysis. Numbers in parenthesis indicate standard deviation. n = number of analyses.

Sample	15053	17320	33376	33377	33378	Average
Pegmatite	Heftetjern 1	Heftetjern 1	Heftetjern 1	Heftetjern 1	Heftetjern 1	Heftetjern 1
Mineral	Bazzite	Bazzite	Bazzite	Bazzite	Bazzite	Bazzite
n	*8*	*6*	*8*	*8*	*8*	
MgO (wt.%)	0.07(1)	0.06(2)	0.09(2)	0.09(1)	<0.03	0.07
MnO	1.57(2)	1.61(5)	1.47(8)	1.48(3)	1.66(4)	1.56
Al_2O_3	0.86(4)	1.04(6)	0.88(2)	0.85(3)	0.92(3)	0.91
Fe_2O_3	6.44(8)	6.4(1)	6.5(1)	6.49(8)	6.26(6)	6.44
Sc_2O_3	13.9(2)	13.8(2)	14.0(2)	13.9(1)	14.0(1)	13.97
Na_2O	1.57(4)	1.54(4)	1.58(5)	1.59(5)	1.49(3)	1.56
K_2O	0.15(1)	0.17(2)	0.14(3)	0.14(2)	0.14(1)	0.15
Cs_2O	3.1(1)	2.97(9)	2.9(4)	3.00(6)	3.24(4)	3.06
SiO_2	57.9(3)	57.3(2)	57.9(8)	57.8(4)	57.5(2)	57.74
BeO*	12.22	12.13	12.2	12.21	12.14	12.19
Total	97.988	97.220	97.799	97.754	97.507	97.654
Mg (apfu)	0.011	0.010	0.015	0.015	<0.03	0.013
Mn	0.137	0.141	0.128	0.129	0.145	0.136
Al	0.105	0.127	0.106	0.103	0.112	0.110
Fe^{3+}	0.496	0.501	0.500	0.500	0.485	0.496
Sc	1.242	1.241	1.251	1.247	1.260	1.248
Σ*O*-site	1.990	2.019	2.000	1.994	2.001	2.001
Na	0.312	0.309	0.314	0.317	0.298	0.310
K	0.020	0.023	0.018	0.019	0.019	0.020
Cs	0.138	0.131	0.127	0.131	0.143	0.134
Σ *CH*-site	0.470	0.462	0.459	0.468	0.460	0.464
Si	5.926	5.908	5.920	5.923	5.920	5.919
Σ *T1*-site	5.926	5.908	5.920	5.923	5.920	5.919
Be	3.002	3.000	3.001	3.002	3.001	3.001
Σ *T2*-site	3.002	3.000	3.001	3.002	3.001	3.001

*BeO: the BeO is esitmated to fully ocupy and dominate the *T2*-site.

The five bazzites have a relative consistent composition of major and minor elements (Table 3.5). Occupancies of detected elements in the sites of studied bazzites are in the following described. In the first tetrahedral site *T(1),* Si is dominating constituent with average concentrations of 5.908 to 5.926 *apfu* (57.3 to 57.9 wt.% SiO_2) which is almost the stoichiometric value of 6. Scandium is the second major constituent and has average concentrations of 1.241 to 1.260 *apfu* (13.8 to 14.0 wt.% Sc_2O_3), while Fe^{3+}, another common constituent, varies from 0.485 to 0.501 *apfu* (6.26 to 6.5 wt.% Fe_2O_3) (Table 3.5). Scandium and Fe^{3+} together dominate the octahedral site *(o)*. In addition, the *(o)* site is occupied by minor concentrations of Mn, Al and Mg. The concentrations of these elements vary from 0.128 to 0.145 *apfu* Mn (1.47 to 1.66 wt.% MnO), 0.103 to 0.127 *apfu* Al (0.85 to 1.04 wt.% Al_2O_3), and 0 to 0.015 *apfu* Mg (<0.03 to 0.09 wt.% MgO). The channel site *(ch)* is mainly dominated by Na and Cs which vary from 0.298 to 0.317 *apfu* Na (1.49 to 1.58 wt.% Na_2O) and 0.127 to 0.143 *apfu* Cs (2.97 to 3.24 wt.% Cs_2O). Small amounts of K occur in this site as traces with concentrations of 0.018 to 0.023 *apfu* K (0.14 to 0.17 wt.% K_2O). Based in these results, an average chemical formula of the five studied bazzite samples from Heftetjern 1 locality is given as: $Be_{3.001}$ ($Sc_{1.248}$, $Fe^{3+}_{0.496}$, $Mn_{0.136}$, $Al_{0.110}$, $Mg_{0.013}$)$_{\Sigma=2.001}$ $Si_{5.919}O_{18}$ [$Na_{0.310}$, $Cs_{0.134}$, $K_{0.020}$] $_{\Sigma=0.464}$. Juve and Bergstøl (1990) described a Cs bazzite from the same Heftetjern pegmatite, where they estimated the chemical formula of the described bazzite to be: $Be_{3.1}$ ($Sc_{1.24}$, $Fe_{0.42}$, $Mn_{0.12}$, $Al_{0.10}$, $Mg_{0.02}$)$_{1.9}$ ($Na_{0.30}$, $Cs_{0.12}$, $Li_{0.05}$, $Rb_{0.02}$, K)$_{0.5}$ ($Si_{5.7}$, $Be_{0.3}$)$_6$ O_{18} *0.36 H_2O. The formula of Juve and Bergstøl (1990) is very similar to the formula calculated from the results of this study. According to Juve and Bergstøl (1990) the relative high concentrations of Cs_2O (up to 3.0 wt.% Cs_2O) in their described bazzite, makes it a Cs bazzite. This applies also for the studied bazzites, because the same amount Cs (3.0 wt.%) was detected (Table 3.5).

In the Figure 3.20 Sc, which dominates the octahedral site *(o)*, is plotted against Fe^{3+}+Al, which also enter the (o) site. This plot provides information about their *(o)* site substituions (Groat et al., 2010) similar to Figure 3.10. The degree of substitution in the *(o)* site of bazzite is also linked to the differentiation of the bazzite chemistry, similar to beryls (Pezzotta et al., 2005). High Sc and low Fe^{3+}+Al contents reflect a lower substituiotn degree and more chemically evolved bazzite, while low Sc and high Fe^{3+}+Al contents suggest a higher substitution degree and chemically primitive bazzite. The plot reveals a weak negative correlation between Sc and Fe^{3+}+Al contents confirming the substitiuion of Sc by Fe^{3+} and Al in the *(o)* site. Due to their homogenous compositions a very small variation is observed. Sample 17320 has highest

Fe^{3+}+Al and lowest Sc contents, which indicate that the bazzite is more primitive with more substituions of Sc by Fe^{3+} and Al in the *(o)* site compared to the other samples 33376, 33377, 15053, and 33378. The most chemically evolved bazzite is sample 33378 since it contains the highest Sc and lowest contetns of Fe^{3+}+Al.

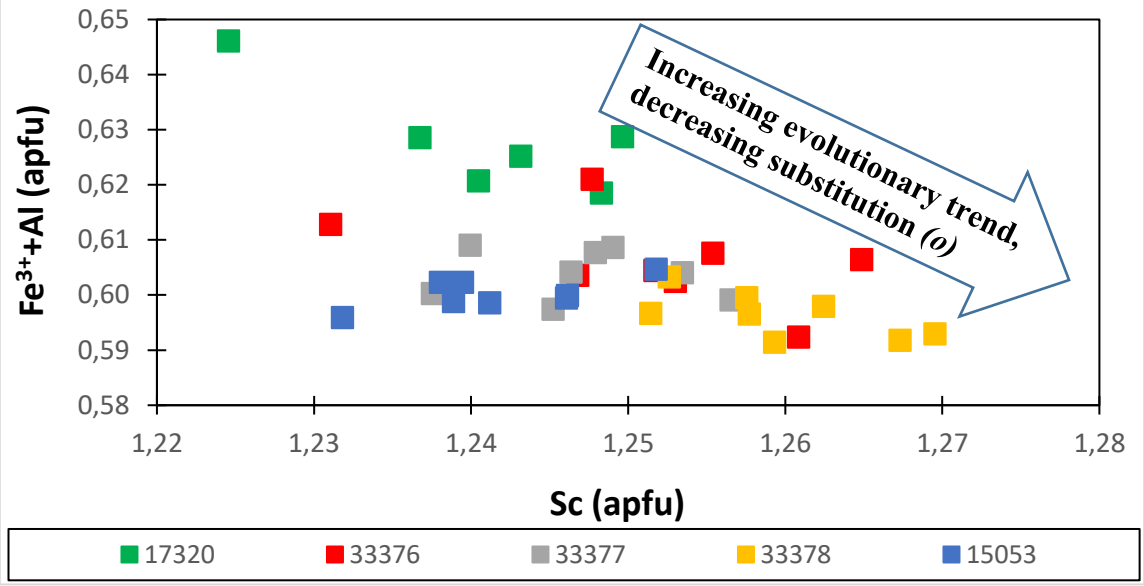

Fig. 3.20. Major element concentrations of Sc, Al and Fe^{3+} are plotted against each other which shows the variation of chemically primitive and evolved bazzite samples as a function of the substitution of Sc by Fe^{3+} and Al in the octahedral site *(o)*. The most evolved bazzite contains with fewer substitutions of Sc by Fe^{3+} and Al, while primitive bazzite has more substitutions of Sc by Fe^{3+} and Al.

To better understand the differences of major and minor element concentrations between chemically primitive and evolved bazzites, element concentrations of Mn, Cs, Na, and K in the *(o)* and *(ch)* sites are plotted in the Figures 3.21 and 3.22. The Mn versus Cs plot is provided in Figure 3.21. The data show a clear positive correlation of increasing Mn in the *(o)* site with increasing concentration of Cs in the *(ch)* site. Sample 33378 contains the highest Mn and Cs contents indicating that thess bazzites are chemically most evovled. Moderate Mn and Cs contents are observed in samples 15053, 33376 and 17320, while sample 33376 has lowest Mn and Cs. The most evolved Tørdal bazzites would contain the highest Mn and Cs.

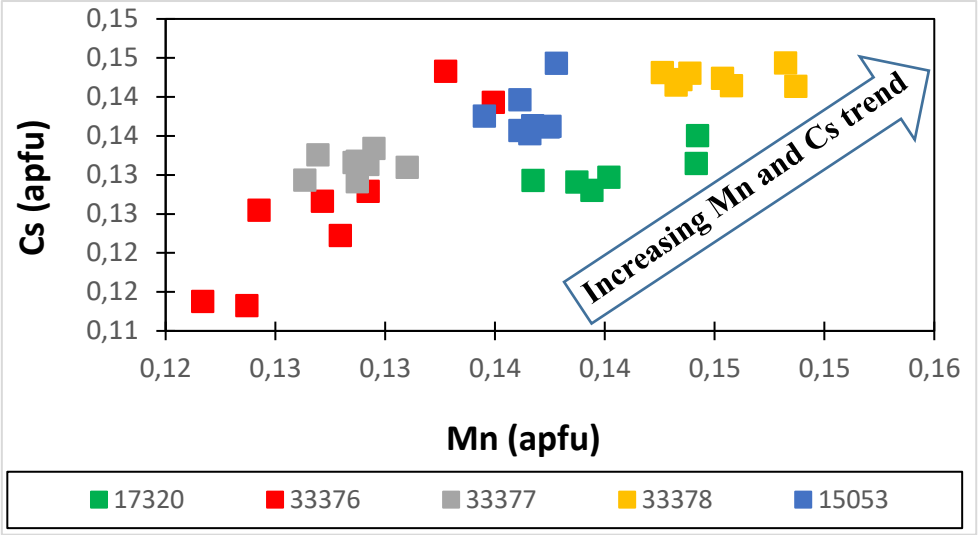

Fig. 3.21. Plot of Mn versus Cs concentrations (apfu) of studied bazzite samples, revealing a positive correlation. Highest Mn and Cs are detected in sample 33378, which represents the most evolved bazzite investigated in this study.

The Fe^{3+} and Al conentrations in octahedral site *(o)* and Na and K concentrations in the channel site *(ch)* are plotted against each other in Figure 3.22. In general, the diagram reveals a weak positive correlation between Fe^{3+}+Al and Na+K. The high average Na+K contents are detected in most bazzites, except sample 33378, which contains significantly lower Na+K. The observed trand may indicate that during progressing evolution of Tørdal bazzites the contents of Na and K slightly decreases.

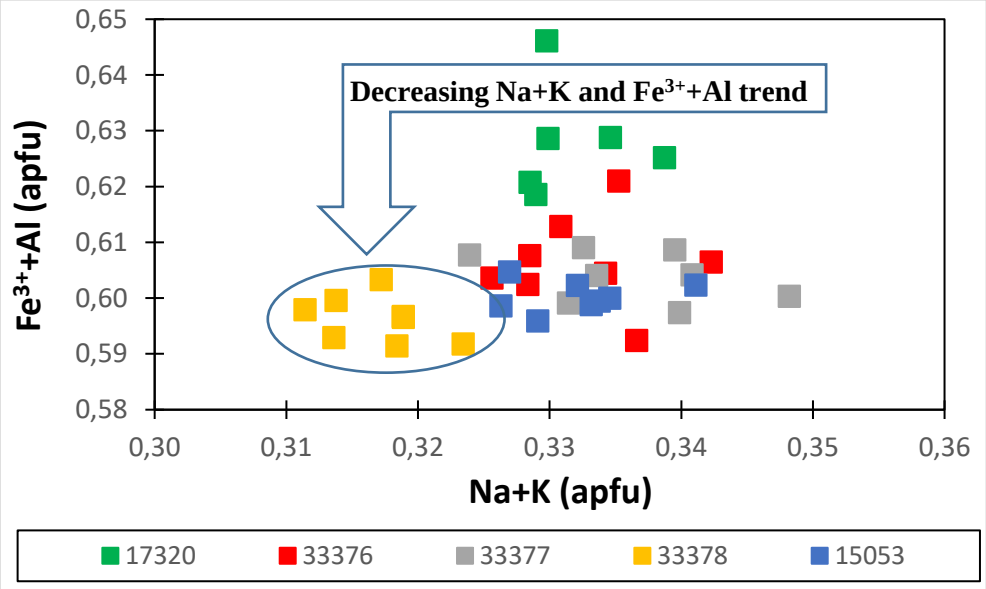

Fig. 3.22. Plot of the Fe^{3+}+Al versus Na+K variation of studied bazzite samples. The data shows a weak positive correlation.

Summarizing, the bazzite sample 33378 is classified as more evolved since it contains the highest Sc, Cs and Mn content and lowest concentrations of Fe^{3+}, Al, Na and K of studied bazzites. The most primitive bazzite is sample 17320, which contains the high Na and K, moderate Mn, and intermediate Cs. Therefore, it is suggested that with progressing evolution of Tørdal bazzites, concentrations of Cs and Mn increase, while those of Na and K decrease.

3.3.2 Minor and trace elements of bazzite determined by LA-ICP-MS

The five bazzite samples, which were analyzed by EPMA for major and minor elements, where in addition analyzed for their minor and trace elements by LA-ICP-MS. The complete list of results are provided in Appendix 7.12. Average concentrations are summarized in Table 3.6. Similar to the major and minor element compositions, the trace elements show little variation.

Table 3.6. Average concentrations of minor and trace elements of bazzites from the Heftetjern 1 pegmatite in Tørdal. Concentrations were determined with LA-ICP-MS. Numbers in parenthesis indicate standard deviation. n = number of analyses.

Sample	33377	33378	17320	33376	15053
Pegmatite	Heftetjern 1	Heftetjern 1	Heftetjern 1	Heftetjern 1	Heftetjern 1
Mineral	Bazzite	Bazzite	Bazzite	Bazzite	Bazzite
n	*4*	*5*	*4*	*5*	*6*
Li (ppm)	507(26)	538(35)	486(26)	530(27)	501(20)
B	50(2)	46(9)	42(7)	51(9)	51(12)
Mg	546(29)	304(5)	408(28)	506(45)	405(8)
Al	4826(133)	5013(119)	5163(733)	4990(49)	4882(200)
P	5(2)	5(1)	4(1)	5(1)	4(1)
K	1461(102)	1334(106)	1526(91)	1384(86)	1447(29)
Ca	308(85)	222(13)	248(15)	269(18)	276(10)
Ti	12(2)	13.4(2)	14(1)	12(2)	11.7(3)
V	2(1)	1.8(2)	2(1)	2.2(7)	12(1)
Cr	4(1)	3(1)	3(1)	4(3)	3(1)
Ga	15(1)	16(2)	16(3)	15(2)	14(1)
Ge	3(1)	4(1)	4(1)	4(1)	4(1)
Rb	1714(117)	1596(27)	1670(54)	1653(56)	1676(13)

To better understand the behevious of the trace elements Li, Rb, and Ca, they are plotted against each other in Figures 3.23 and 3.24. In Figure 3.23 the concentrations of Li and Rb are plotted. The data reveal a weak negative correlation between Li and Rb. The slightly evolved sample 33378 together with sample 33376 contain highest average Li of 538 ppm and 530 ppm, respectively (Table 3.6). Average Li concentrations in sample 33377 and sample 15053 are 507 ppm and 501 ppm, respectively, while the lowest Li was detected in the primitive sample 17320 with 486 ppm Li. Thus, Rb in bazzite decreases with progressive evolution, whereas Li increases.

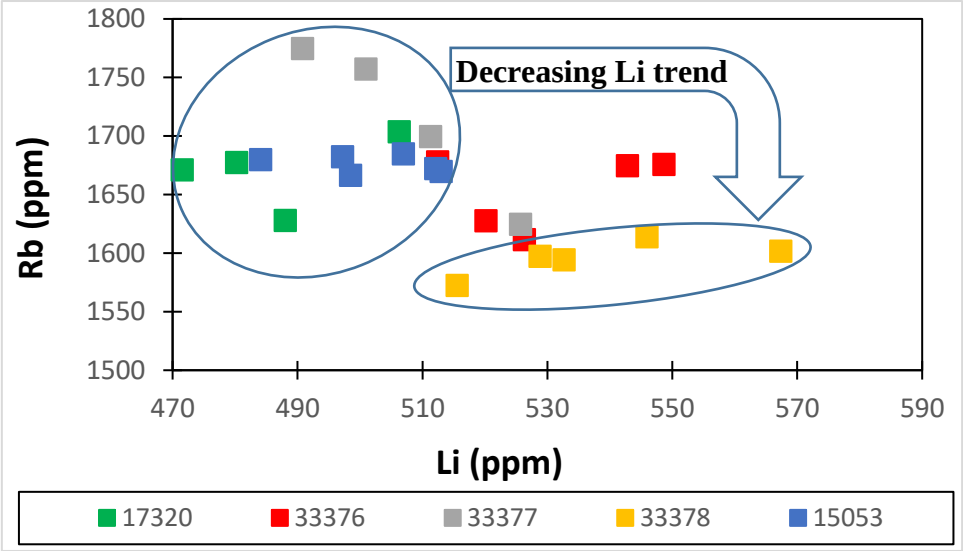

Fig. 3.23. Plot of the Li versus Rb variation of the investigated bazzites. The data show a weak negative correlation.

Concentrations of Rb versus Ca are plotted in Figure 3.24. The data reveal a psotive correltaiton between both elements. Sample 33377 contains the highest Ca (mean 308 ppm), followed by sample 15053 (mean 276 ppm Ca), sample 33376 (mean 269 ppm), and sample 17320 (mean 248 ppm). The lowest Ca was detected in the most evolved sample 33378 (mean 222 ppm). The data indicate that evolved bazzites have low Ca and Rb, while primitive bazzite contain higher Ca and Rb.

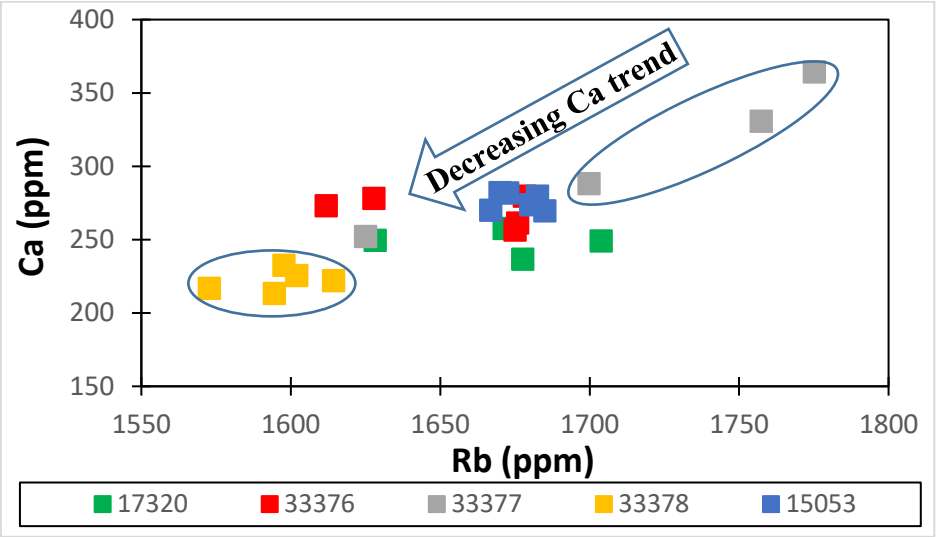

Fig. 3.24. Plot of the Ca versus Rb concentration of the investigated bazzites. Ca is positively correlated to Rb. Lowest Ca contents is discovered in the evoled sample 33378, while the highest are discovered in sample 33377.

Summarzizing, the most evolved bazzite sample 33378 contains the highest Li and lowest K, Rb and Ca, whereas the most primitive bazzite is the sample 33377with high Rb, Ca and K and low Li.

3.4 Gadolinite

3.4.1 Major and minor elements determined by EPMA

The chemical formula for the gadolinite-datolite mineral group is given as: $W_2XZ_2T_2O_8V_2$ according to Bačík et al. (2014), where the *W*-site is mainly occupied by Ca, REE and Y, the *X*-site by Fe^{2+}, Mg, Mn, Zn, Cu, Al and Fe^{3+}, the *Z*-site by B, Be and Li. The *T*-site can be occupied by Si, B, Be, S and P, and the *V*-site by O, OH, F. The group are divided into two main groups: datolite group and gadolinite group. These two groups comprises of nine different members or group minerals (Table 3.7). The two groups are distinguished from each other by the dominant occupant in the *Z-site*, which is either B or Be (Table 3.7). When the Z-site is dominated by Be the mineral belongs to the gadolinite group. When B dominates the Z-site the mineral is classified a datolite group mineral (Table 3.7).

Table 3.7. Occupations in the structural sites of the gadolite-datolite group minerals according to Bačík et al. (2014).

Mineral	*W*	*X*	*Z*	*T*	*O*
Datolite Subgroup					
Datolite	Ca_2		B_2	Si_2	$O_8(OH)_2$
Homilite	Ca_2	Fe^{2+}	B_2	Si_2	O_{10}
Bakerite	Ca_4		B_4	Si_3B	$O_{12}(OH)_3*(H_2O)$
Gadolinite Subgroup					
Gadolinite-(Ce)	Ce_2	Fe^{2+}	Be_2	Si_2	O_{10}
Gadolinite-(Y)	Y_2	Fe^{2+}	Be_2	Si_2	O_{10}
Hingganite-(Ce)	Ce_2		Be_2	Si_2	$O_8(OH)_2$
Hingganite-(Y)	Y_2		Be_2	Si_2	$O_8(OH)_2$
Hingganite-(Yb)	Yb_2		Be_2	Si_2	$O_8(OH)_2$
Minasgeraisite-(Y)	Y_2	Ca	Be_2	Si_2	O_{10}

According to Pezzotta et al. (1999), low Ca contents (below 0.50 *apfu* Ca) leads to increased Be incorporation in the Z-site, instead of B, which results in the formation of gadolinite group minerals instead of datolite group minerals (Table 3.8).

In the following, the studied gadolinite group minerals are further classified based on the subgroup classification diagram introduced by Pezzotta et al. (1999). The diagram utilizes the Fe^{2+} and Ca contents of gadolinite group minerals for the subgroup classification (Figure 3.25). Based on this, the samples are either classified as hingganite (low Fe^{2+} and Ca), datolite (low Fe_{2+} and high Ca), gadolinite (high Fe^{2+} and low Ca) or homilite (high Fe^{2+} and Ca). Samples from Upper Høydalen (sample 21341a, 21341b, 21345) plot in the gadolinite field, very close to the endmember-gadolinite composition with average Fe^{2+} contents close to 0.92 *apfu* and average Ca contents close to 0.01 *apfu* (Table 3.8). However, crystal domains with relative low Fe^{2+} contents, which plot closer to the hingganite field (sample 23091547) compared to other

samples, are interpreted as slightly altered gadolinite. The strongly altered domains in sample 21341b from Upper Høydalen plot in the hingganite field due to their very low Fe^{2+} contents (below 0.50 Fe *apfu*; Table 3.8). Summarizing, all four studied minerals are classified as gadolinite due to their relative high Fe^{2+} contents. However, strongly altered domains in sample 21341b from Upper Høydalen have hingganite composition due to lower Fe^{2+} contents (Fig. 3.25; Table 3.8).

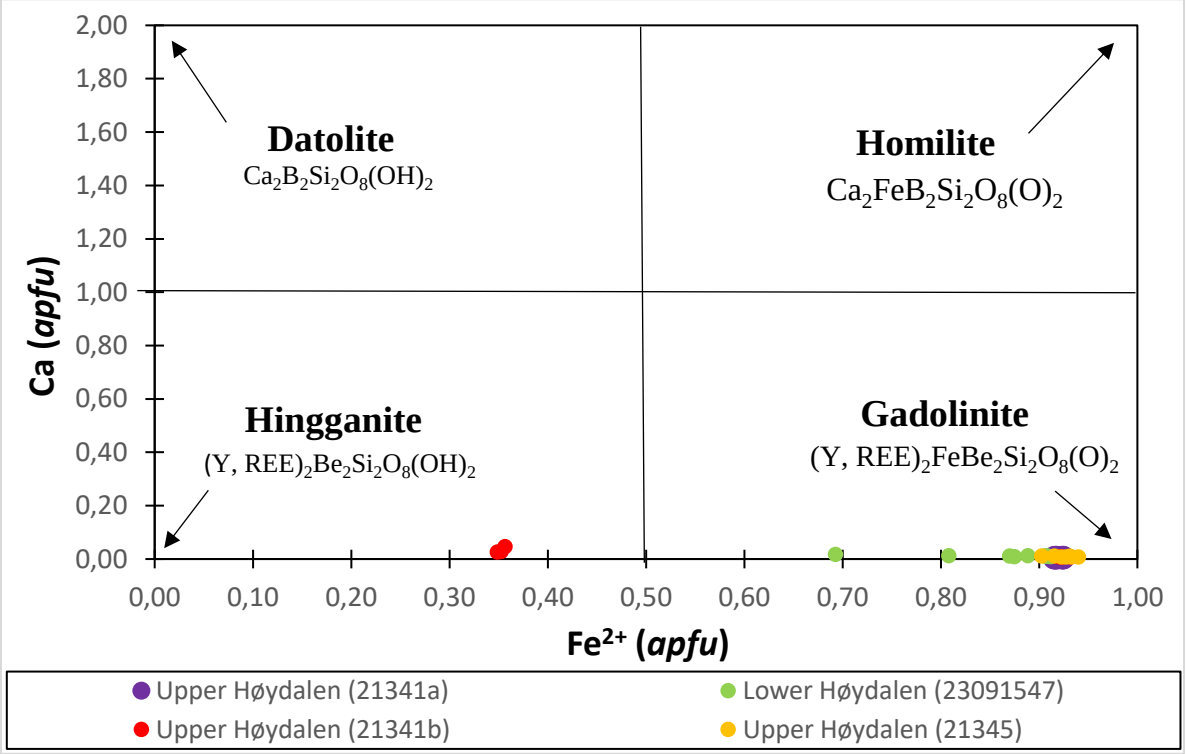

Fig. 3.25. Classification diagram of gadolinite-datolite group minerals according to Pezzotta et al. (1999). All Tørdal mineral samples plot in the gadolinite field, except the strongly altered domains in sample 21341b which plot in the hingganite field. Weakly altered crystal domains in sample 23091547 plot in the gadolinite field but close to hingganite-gadolinite boundary.

The investigated samples are further classified based on the dominant element concentration in their *W*-site according to Nickel and Grice (1998). Concentrations of the rare earth elements (REE), such as Y and Lanthanides (Ce, Pr, Nd, Sm, Gd, Dy, Er, and Yb), dominate *W*-site. Gadolinites from Upper Høydalen (samples 21341a, 21341b, 21345) have average Y contents close to 1.62 *apfu*, and Lanthanides contents close to 0.40 (Table 3.8). The hingganite domains in sample 21341b contain average Y concentrations of 1.537 *apfu* and Lanthanides of 0.367 *apfu* (Table 3.8). The gadolinite from Lower Høydalen (sample 23091547) has 1.557 *apfu* Y and 0.473 *apfu* Lanthanides. The results confirm that studied gadolinite samples are classified as gadolinite-(Y) since their *W*-site is mainly dominated by Y > Lanthanides. This applies also

for the altered hingganite domains in sample 21341b which classify as hingganite-(Y) (Table 3.8). This means that the inveatigated samples are strongly Y enriched.

A total of 33 point analysis were obtained by EPMA analysis from four gadolinite group minerals collected from the wall zones of the Upper and Lower Høydalen pegmatites in Tørdal pegmatite field. The complete list of analytical results is given in Appendix 7.7 and average concentrations are summarized in Table 3.8.

Table 3.8. Average concentrations of major and minor elements of studied gadolinite group minerals from Tørdal. The compositions were determined with EPMA. Number in parenthesis indicate standard deviation. n = number of analysis.

Sample	21341b		21341a	21345	23091547
Pegmatite	Upper Høydalen		Upper Høydalen	Upper Høydalen	Lower Høydalen
Mineral	Gadolinite-(Y)	Hingganite-(Y)	Gadolinite-(Y)	Gadolinite-(Y)	Gadolinite-(Y)
n	*5*	*3*	*7*	*8*	*10*
SiO_2 (wt.%)	23.9(2)	25.59(7)	24.0(2)	23.9(3)	23.8(2)
CaO	0.09(2)	0.3(1)	0.065(9)	0.10(3)	0.13(5)
MnO	0.27(4)	0.05(3)	0.30(3)	0.26(5)	0.28(6)
FeO	13.15(7)	4.96(8)	13.1(1)	13.1(3)	12(1)
Y_2O_3	36.3(6)	38.8(3)	36.46(9)	36.2(7)	34.4(4)
La_2O_3	0.30(4)	0.27(3)	0.42(3)	0.24(3)	0.45(2)
Ce_2O_3	1.6(1)	1.6(1)	2.54(5)	1.4(1)	2.50(6)
Pr_2O_3	0.31(7)	0.291(9)	0.48(6)	0.30(9)	0.49(8)
Nd_2O_3	2.01(9)	2.07(7)	2.35(8)	1.7(2)	2.7(1)
Sm_2O_3	0.9(1)	1.03(8)	0.73(9)	0.9(1)	1.09(9)
Gd_2O_3	2.2(2)	2.31(5)	1.3(1)	2.4(3)	2.1(1)
Dy_2O_3	2.7(1)	2.8(1)	1.7(1)	3.0(2)	2.5(1)
Er_2O_3	1.9(1)	2.09(5)	1.7(1)	2.0(1)	2.0(1)
Yb_2O_3	2.13(4)	2.24(5)	2.7(1)	2.0(2)	2.49(8)
BeO*	9.910	11.200	9.951	9.891	9.799
H_2O**	0	4.037	0	0	0
Total	97.990	99.969	98.158	97.756	97.198
La (apfu)	0.009	0.007	0.013	0.008	0.014
Ce	0.051	0.045	0.078	0.044	0.078
Pr	0.010	0.008	0.015	0.009	0.015
Nd	0.060	0.055	0.070	0.053	0.084
Sm	0.027	0.026	0.021	0.028	0.032
Gd	0.062	0.057	0.039	0.068	0.061
Dy	0.074	0.069	0.048	0.082	0.070
Er	0.051	0.049	0.045	0.053	0.054
Yb	0.055	0.051	0.069	0.052	0.065
Y	1.622	1.537	1.622	1.621	1.557
Ca	0.008	0.029	0.006	0.010	0.012
Σ *W*-site	2.030	1.934	2.026	2.027	2.041
Fe	0.923	0.309	0.920	0.925	0.867
Mn	0.019	0.004	0.022	0.019	0.020
Σ *X*-site	0.943	0.312	0.941	0.944	0.888
Si	2.010	1.901	2.012	2.011	2.027
Σ *T*-site	2.010	1.901	2.012	2.011	2.027
Be	1.997	1.999	1.998	1.998	2.001
Σ *Z*-site	1.997	1.999	1.998	1.998	2.001
Lanthanides (La-Lu)	0.400	0.367	0.398	0.397	0.473

*BeO: the BeO is estimated to fully occupy and dominate the *Z*-site; **H_2O: the H_2O is estimated to fully occupy and dominate the *V*-site.

Average Si contents vary from 2.010 to 2.027 *apfu* (23.8 to 24.0 wt.% SiO_2) in the gadolinite-(Y). The altered hingganite-(Y) domains have lower average Si (1.901 *apfu* Si; 25.59 wt.% SiO_2) (Table 3.8). The second most abundant constituent is Y which dominates over the Lanthanides and Ca in the *W*-site with average contents of 1.537 to 1.622 *apfu* (34.4 to 38.3 wt.% Y_2O_3) (Table 3.8). The average contents of Y is relative similar in the gadolinites-(Y) from Upper Høydalen (sample 21341a, 21345, 21341b) varying from 1.621 to 1.622 *apfu*, while the gadolinite-(Y) from Lower Høydalen (sample 23091547) have a slightly lower average Y of 1.557 *apfu* (Table 3.8). Lowest Y was detected in the altered hingganite-(Y) domains in sample 21341b with an average Y content of 1.537 *apfu*. The Lanthanides comprise the elements La, Ce, Pr, Nd, Sm Gd, Dy, Er and Yb (Table 3.8). The highest sum of Lanthanides was discovered in the gadolinite-(Y) from Lower Høydalen (sample 23091547) with an average content of 0.473 *apfu*. The other gadolinite-(Y) samples from Upper Høydalen (sample 2341b, 21341a and 21345) contain 0.400, 0.398 and 0.397 *apfu* Lanthanides, respectively. Whilst the lowest average contents of Lanthanides was found in the altered hingganite-(Y) domains with average concentrations of 0.367 *apfu*. Minor contents of Ca occupy also the *W*-site with relative small average content of 0.006 to 0.012 *apfu* Ca (0.09 to 0.065 wt.% CaO) in all gadolinites-(Y) samples. However, the highest average Ca content was detected in the altered hingganite-(Y) domains in sample 21341b from Upper Høydalen (0.029 *apfu* Ca; 0.3 wt.% CaO) (Table 3.8). The *X*-site in gadolinite-(Y) samples are mainly dominated by Fe^{2+} where minor contents of Mn are present (Table 3.8). Highest average Fe^{2+} concentrations are detected in Upper Høydalen samples (sample 21345, 21341b, 21341a) which varies from 0.920 to 0.925 *apfu* Fe^{2+} (13.1 to 13.15 wt.% FeO). The gadolinite-(Y) from Lower Høydalen (sample 23091547) has slightly higher average contents of 0.867 *apfu* Fe^{2+} (12.0 wt% FeO). The Fe^{2+} concentrations are significantly lower in hingganite-(Y) domains in sample 21341b compared to the gadolinites-(Y) as discussed above. Small concentrations of Mn is present in the *X*-site, which vary from 0.019-0.022 *apfu* Mn (0.26 to 0.30 wt.% MnO) in all gadolinite-(Y) samples. However, it is a bit lower in the altered hingganite-(Y) domains in 21341b (0.004 *apfu* Mn; 0.05 wt.% MnO).

3.5 Mica

3.5.1 Major and minor elements of micas determined by EPMA

According to Rieder et al. (1998) the given chemical formula for the mica group is given as: $XY_{2-3}Z_4O_{10}T_2$, where the elements which mainly occupies the different sites are:

Cs, K, Na, NH_4, Rb, Ba, and Ca for the *X*-site,

Li, Fe^{2+} or Fe^{3+}, Mg, Mn^{2+} or Mn^{3+}, Zn, Al, Cr, V, and Ti for the *Y*-site,

Be, Al, B, Fe^{3+}, and Si for the *Z*-site,

Cl, F, OH, O, and S for the *T*-site.

Micas of this study comprise mainly of Al-rich muscovites, named dioctahedral micas, and Fe-Mg rich biotites, named trioctahedral micas. These two mica subgroups are distinguished from each other based on their maximum occupancy in their *Y*-site. The maximum occupancy for dioctahedral micas is Y= ∑2.00, while the trioctahedral micas contain a *Y*-site with a maximum occupancy of Y= ∑3.00.

In Figure 3.26. studied micas from Tørdal pegmatites and their adjacent host rocks are plotted in the chemistry-based classification diagram according to Tischendorf et al. (2001). The x-axis comprises of "mgli" which stands for Mg - Li and the y-axis "feal" which stands for Fe_{tot} + Mn + Ti – Al^{4+}. The Al-rich dioctahedral micas from Tørdal pegmatites are classified as muscovites (Ms) and ferroan muscovites (Fe-Ms), except the mica from Sjauset (sample 04071918) which is classified as lithian ferroan muscovite (Li-Fe-Ms) (Fig. 3.26; Table 3.9). The Fe-Mg-rich triocahedral micas from Tørdal pegmatites are classified as siderophyllites (Sid) and magnesian siderophyllites (Mg-Sid), except the sample from Heftetjern 2 (sample 05071901) which is a lithian siderophyllite (Li-Sid) (Fig. 3.26; Table 3.9). The Fe-Mg-rich trioctahedral micas from pegmatite host rocks of Tørdal pegmatites are classified as ferroan phlogopites (Fe-Phl). These ferroan phlogopites are rich in Fe and especially Mg (highest average: 3.28 *apfu* Mg; 14.6 MgO wt.%) compared to trioctahedral micas from the Tørdal pegmatites (Fig. 3.26; Table 3.10).

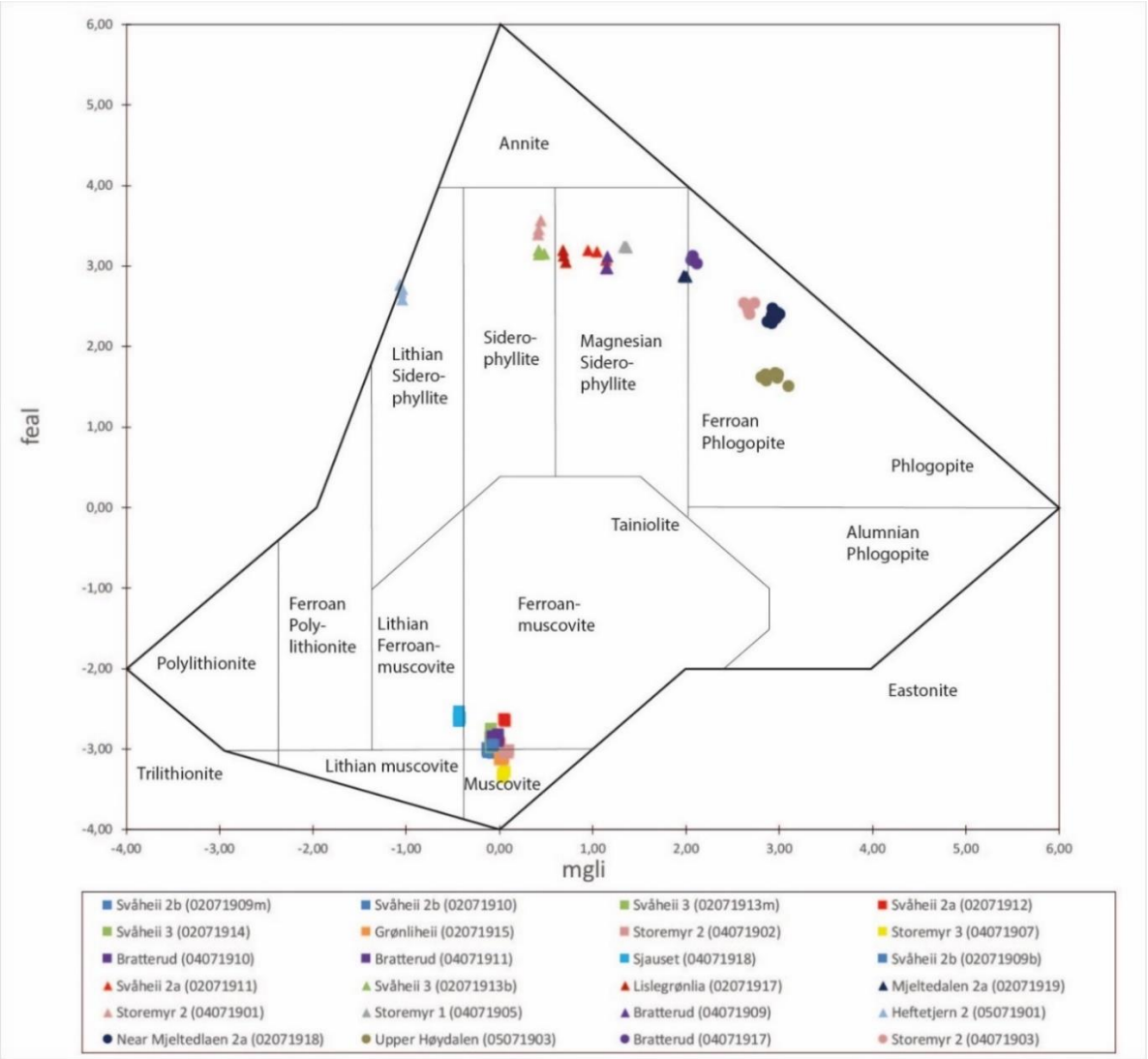

Fig. 3.26. Classification diagram of micas according to Tischendorf et al. (2001). Micas from Tørdal pegmatites plot in muscovite (Ms), ferroan muscovite (Fe-Ms), lithian ferroan muscovite (Li-Fe-Ms), siderophyllite (Sid), magnesian siderophyllite (Mg-Sid) and lithian siderophyllite (Li-Sid) fields. Micas from amphibolitic host rocks of Tørdal pegmatites plot in the ferroan phlogopites (Fe-Phl) field. Squares are dioctahedral micas, while triangles are triocthedral micas from Tørdal pegmatites. Trioctahedral micas from amphibolitic host rocks are shown as circles. The legend applies also for the following diagrams.

A total of 63 point analysis were obtained from 11 dioctahedral and 9 trioctahedral micas collected from Tørdal pegmatites. The micas were collected from wall zone, intermediate zone, and albite replacement zones of the studied Tørdal pegmatites. The complete list of analytical results are given in Appendix 7.8. Average concentrations of major and minor elements are summarized in Table 3.9. In addition, 23 point analyses were obtained from 20 biotites in amphibolites, the host rocks of the Tørdal pegmatites (sample 02071918, 04071903, 04071917, 05071903). The complete list of analytical results of biotites is provided in Appendix 7.9. Average concentrations of major and minor elements in biotite are summarized in Table 3.10.

Table 3.9. Average major and minor element compositions of studied mica samples. Data were obtained with electron probe micro analysis. Numbers in parenthesis indicate the standard deviation. n = number of analysis.

Sample	02071909m	02071910	02071913m	02071912	02071914	02071915	04071902	04071907	04071910	04071911
Pegmatite	Svåheii 2b	Svåheii 2b	Svåheii 3	Svåheii 2a	Svåheii 3	Grønliheii	Storemyr 2	Storemyr 3	Bratterud	Bratterud
Mineral	Ms	Ms	Fe-Ms	Fe-Ms	Fe-Ms	Ms	Ms	Ms	Fe-Ms	Fe-Ms
n	*3*	*3*	*3*	*3*	*3*	*3*	*3*	*3*	*3*	*3*
SiO_2 (wt.%)	44.9(5)	45.1(4)	44.7(5)	45.1(2)	44.6(2)	44.7(7)	45.3(1)	44.5(4)	44.7(3)	44.3(6)
Al_2O_3	33.0(5)	33.26(9)	32.8(1)	31(1)	32.4(5)	33.54(5)	32.8(6)	35.2(4)	32.3(3)	32.3(3)
FeO	3.1(2)	3.9(2)	3.4(2)	4(1)	4.6(4)	3.6(1)	3.58(9)	2.9(2)	4.7(4)	4.72(8)
MgO	0.59(2)	0.43(3)	0.65(2)	0.9(2)	0.56(3)	0.45(6)	0.8(1)	0.3(1)	0.30(1)	0.28(1)
Na_2O	0.52(6)	0.60(6)	0.55(6)	0.40(6)	0.3(1)	0.343(3)	0.31(5)	0.36(8)	0.41(5)	0.3(1)
K_2O	10.5(3)	10.2(1)	10.3(1)	10.5(3)	10.6(2)	10.4(2)	10.4(3)	10.6(1)	10.3(2)	10.2(4)
TiO2	0.75(1)	0.24(2)	0.65(1)	0.4(1)	0.34(7)	0.30(3)	0.34(3)	0.22(2)	0.36(3)	0.31(5)
MnO	0.07(1)	0.06(3)	0.07(2)	0.08(3)	0.15(4)	<0.06	<0.06	<0.06	0.06(3)	0.28(1)
Rb_2O	0.29(5)	0.596(6)	0.38(4)	0.3(1)	0.58(6)	0.59(5)	0.6(3)	0.067(4)	0.63(6)	0.5(1)
F	0.7(3)	0.8(1)	1.1(4)	0.9(1)	0.9(1)	0.55(7)	0.3(2)	0.12(7)	0.4(2)	0.4(1)
Li_2O*	0.165	0.188	0.201	0.1479	0.1857	0.0654	0.0759	0.0269	0.0666	0.1095
H_2O**	4.01	3.98	3.8	3.92	3.91	4.11	4.2	4.37	4.11	4.11
O=F	0.332	0.373	0.505	0.379	0.392	0.233	0.167	0.051	0.207	0.181
Total	98.525	99.210	98.420	98.411	98.895	98.564	98.986	99.061	98.567	97.798
Si (apfu)	6.14	6.15	6.13	6.22	6.14	6.14	6.20	6.05	6.18	6.17
Al	1.86	1.85	1.87	1.78	1.86	1.86	1.80	1.95	1.82	1.83
Σ Z-site	8.00	8.00	8.00	8.00	8.00	8.00	8.00	8.00	8.00	8.00
Al	3.47	3.49	3.44	3.31	3.39	3.56	3.49	3.68	3.45	3.46
Fe^{2+}	0.36	0.45	0.40	0.52	0.53	0.42	0.41	0.34	0.55	0.55
Li	0.18	0.21	0.22	0.16	0.21	0.07	0.08	0.03	0.07	0.12
Mn	0.01	0.01	0.01	0.01	0.02	0.00	0.00	0.00	0.01	0.01
Ti	0.08	0.02	0.07	0.05	0.04	0.03	0.03	0.02	0.04	0.03
Mg	0.12	0.09	0.13	0.20	0.12	0.09	0.17	0.08	0.06	0.06
Σ Y-site	4.21	4.26	4.27	4.26	4.30	4.17	4.19	4.15	4.19	4.23
K	1.83	1.79	1.80	1.86	1.86	1.83	1.81	1.85	1.82	1.83
Na	0.14	0.16	0.15	0.11	0.08	0.09	0.08	0.10	0.11	0.08
Rb	0.03	0.05	0.03	0.03	0.05	0.05	0.06	0.01	0.06	0.05
Σ X-site	2.00	2.00	1.98	2.00	2.00	1.97	1.96	1.95	1.99	1.96
mgli	-0.06	-0.12	-0.09	0.04	-0.09	0.02	0.09	0.05	-0.01	-0.06
feal	-3.02	-3.01	-2.96	-2.74	-2.81	-3.11	-3.04	-3.32	-2.85	-2.86

Ms = Mucovite, Fe-Ms = Ferroan muscovite, Li-Fe-Ms = Lithian ferroan muscovite, Sid = Siderophyllite, Mg-Sid = Magnesian Siderophyllite, Li-Sid = Lithian siderophyllite. *Li_2O: the Li (ppm) detected by LA-ICP-MS was converted to Li_2O (wt.%) to occupy minor contets in the *Y*-site; **H_2O: the H_2O is estimated to fully occupy the *T*-site with F.

Table 3.9. Continued

Sample	04071918	02071909b	02071911	02071913b	02071917	02071919	04071901	04071905	04071909	05071901
Pegmatite	Sjauset	Svåheii 2b	Svåheii 2a	Svåheii 3	Lislegrønlia	Mjeltedalen 2a	Storemyr 2	Storemyr 1	Bratterud	Heftetjern 2
Mineral	Li-Fe-Ms	Fe-Ms	Mg-Sid	Sid	Mg-Sid	Mg-Sid	Sid	Mg-Sid	Mg-Sid	Li-Sid
n	*6*	*2*	*3*	*3*	*3*	*3*	*3*	*3*	*3*	*4*
SiO_2 (wt.%)	44.7(5)	44.6(2)	34.4(5)	34.7(1)	34.6(7)	35.3(2)	34.5(4)	35.1(1)	35.1(8)	35.3(4)
Al_2O_3	31.0(6)	32.65(9)	16.4(3)	17.1(1)	17.4(2)	15.6(3)	16.5(6)	15.7(1)	16.1(2)	18.5(2)
FeO	5.4(2)	3.53(3)	25.8(3)	25.8(5)	25.1(4)	21.34(2)	26.6(1)	23.5(2)	23.4(3)	23.2(5)
MgO	<0.04	0.65(2)	5.8(6)	3.5(2)	4.1(1)	9.1(1)	3.78(7)	6.9(1)	6.67(6)	1.87(5)
Na_2O	<0.04	0.33(5)	0.08(2)	0.06(1)	0.05(3)	0.09(1)	0.03(3)	0.08(2)	0.11(3)	0.05(3)
K_2O	10.2(1)	10.9(2)	9.17(2)	9.34(3)	9.5(1)	9.66(8)	9.4(1)	9.56(9)	9.40(6)	9.0(1)
TiO_2	0.18(4)	0.58(8)	1.1(5)	2.51(9)	2.99(6)	2.91(6)	2.85(3)	3.0(1)	2.7(2)	3.08(5)
MnO	0.40(7)	0.05(2)	0.96(1)	1.04(7)	1.04(6)	0.83(3)	1.1(1)	1.43(4)	0.70(1)	1.20(9)
Rb_2O	1.1(2)	0.36(3)	0.8(1)	0.84(4)	0.50(6)	0.27(7)	0.48(3)	0.34(2)	0.48(2)	1.40(4)
F	1.4(2)	0.57(5)	0.7(2)	0.60(9)	0.7(1)	0.5(1)	0.9(3)	1.37(8)	1.68(6)	1.5(4)
Li_2O*	0.384	0.365	0.265	0.320	0,224	0.110	0.366	0.203	0.323	1.198
H_2O**	3.610	4.095	3.410	3.490	3.450	3.620	3.350	3.190	3.020	3.070
O=F	0.608	0.241	0.307	0.253	0.317	0.215	0,.83	0.579	0.708	0.667
Total	98.275	99.065	98.877	99.288	99.660	99.318	99.770	100.018	99.166	99.044
Si (apfu)	6.22	6.14	5.49	5.49	5.45	5.48	5.46	5.49	5.49	5.46
Al	1.78	1.86	2.51	2.51	2.55	2.52	2.54	2.51	2.51	2.54
Σ Z-site	8.00	8.00	8.00	8.00	8.00	8.00	8.00	8.00	8.00	8.00
Al	3.31	3.43	0.57	0.69	0.67	0.35	0.55	0.38	0.46	0.84
Fe	0.63	0.41	3.45	3.42	3.31	2.77	3.52	3.07	3.07	3.00
Li	0.43	0.20	0.34	0.41	0.28	0.14	0.47	0.25	0.41	1.49
Mn	0.05	0.01	0.13	0.14	0.14	0.11	0.16	0.19	0.09	0.16
Ti	0.02	0.06	0.14	0.30	0.35	0.34	0.34	0.36	0.32	0.36
Mg	0.00	0.13	1.38	0.84	0.97	2.12	0.89	1.60	1.56	0.43
Σ Y-site	4.45	4.24	6.01	5.81	5.74	5.83	5.91	5.85	5.92	6.27
K	1.81	1.92	1.86	1.89	1.91	1.91	1.90	1.90	1.88	1.78
Na	0.05	0.09	0.03	0.02	0.02	0.03	0.01	0.03	0.03	0.02
Ca	0.00	0.00	0.00	0.00	0.00	0.00	0.00	0.00	0.00	0.00
Rb	0.11	0.03	0.08	0.09	0.05	0.03	0.05	0.04	0.05	0.14
Σ X-site	1.97	2.04	1.97	1.99	1.97	1.97	1.96	1.96	1.96	1.94
mgli	-0.43	-0.07	1.04	0.44	0.69	1.99	0.42	1.35	1.15	-1.06
feal	-2.61	-2.96	3.15	3.16	3.13	2.87	3.47	3.24	3.02	2.68

Table 3.10. Average major compositions of micas in amphibolitic host rocks of Tørdal pegmatites. Data were determined with electron probe micro analysis. Numbers in parenthesis indicate the standard deviation. n = number of analysis.

Sample	05071903	04071917	04071903	02071918
Pegmatite	Upper Høydalen	Bratterud	Storemyr 2	Near Mjeltedalen 2a
Host rock	Coarse-grained gabbro	Medium-grained gabbro	Massive amphibolite	Amphibole-gneiss
Minerals	Fe-Phl	Fe-Phl	Fe-Phl	Fe-Phl
Crystals	6	3	4	7
n	*7*	*3*	*4*	*8*
FeO (wt%)	14.5 (8)	22.4 (3)	18.9 (3)	17.7 (3)
MnO	0.20 (3)	0.14 (3)	0.17 (1)	0.14 (8)
K_2O	9.2 (2)	8.7 (9)	9.2 (5)	9.5 (4)
SiO_2	38.6 (9)	35.6 (7)	36.7 (3)	37.0 (7)
CaO	<0.04	<0.04	<0.04	<0.04
TiO_2	1.3 (3)	3.0 (3)	2.4 (2)	2.6 (3)
Al_2O_3	14.7 (7)	14.6 (4)	14.4 (2)	14.2 (3)
MgO	14.6 (9)	9.5 (3)	12.1 (4)	13.1 (3)
Sc_2O_3	<0.04	<0.04	<0.04	<0.04
F	2.4 (4)	b.d.l	1.2 (4)	1.1 (1)
Rb_2O*	0.399	0.120	0.334	0.207
Li_2O**	0.564	0.196	0.169	0.059
Na_2O	0.12 (3)	0.05 (3)	0.14 (2)	0.12 (1)
H_2O***	2.816	3.814	3.320	3.390
O=F	1.027	0.021	0.516	0.476
Total	100.86	98.76	100.05	99.93
Si (apfu)	5.80	5.56	5.64	5.65
Al	2.20	2.44	2.36	2.35
Σ Z-site	8.00	8.00	8.00	8.00
Al	0.40	0.24	0.26	0.21
Fe	1.83	2.93	2.43	2.26
Mn	0.03	0.02	0.02	0.02
Ti	0.15	0.36	0.28	0.31
Mg	3.28	2.21	2.78	2.99
Li	0.34	0.12	0.10	0.04
Σ Y-site	6.02	5.89	5.88	5.82
K	1.76	1.74	1.81	1.86
Na	0.04	0.02	0.04	0.04
Ca	0.00	0.04	0.01	0.01
Rb	0.038	0.012	0.033	0.020
Σ X-site	1.84	1.81	1.90	1.93
mgli	1.616	3.074	2.482	2.376
feal	2.936	2.086	2.679	2.948

Fe-Phl = Ferroan phlogopite. *Rb_2O: the Rb (ppm) detected by LA-ICP-MS was converted to Rb_2O (wt.%) to occupy minor contents in the *X*-site; ** Li_2O: the Li (ppm) detetcted by LA-ICP-MS was converted to Li_2O (wt.%) to occupy minor contents in the *Y*-site; ***H_2O: the H_2O is estimated to fully occupy the *T*-site with F. b.d.l = below the limit of detection.

Results from EPMA of studied micas from Tørdal pegmatites and their adjacent host rocks are described in the following based upon how the different elements occupy the sites in the mica formula. Average Si concentrations in micas vary from 5.45 to 6.22 *apfu* (34.4 to 45.3 wt.% SiO_2), and together with Al^{4+} (1.78 to 2.55 *apfu* = 14.2 to 35.2 wt.% Al_2O_3), these two elements fully occupy the *Z-site* of the micas (Tables 3.9, 3.10). The *X*-site is mainly dominated by K. Average concentrations vary from 1.74 to 1.92 *apfu* (8.7 to 10.9 wt.% K_2O). In addition, small

potions of Na (0.0 to 0.16 *apfu* = <0.04 to 0.60 wt% Na_2O) and Rb (0.01 to 0.14 *apfu* = 0.067 to 1.40 wt% Rb_2O) are present in *X*-site site (Tables 3.9, 3.10). The different occupancies of thede elements in the *Y*-site distinguishes the investigated micas from each other. The studied micas comprise relative high concentrations of Al in the *Y*-site, whereas the trioctahedral micas contain lower Al and higher concentrations of Fe and Mg. However, the *Y*-site is mainly occupied by Al (0.21 to 5.63 *apfu* = 14.2 to 35.2 wt.% Al_2O_3) followed by Fe (0.34 to 3.52 *apfu* = 2.9 to 26.6 wt.% FeO) and Mg (0 to 3.28 *apfu* = <0.03 to 14.6 wt.% MgO). Small portions of Li (0.03 to 1.49 *apfu* = 0.0269 to 1.198 wt% Li_2O), Ti (0.02 to 0.36 *apfu* = 0.22 to 3.08 wt% TiO_2) and Mn (0.0 to 0.19 *apfu* = <0.05 to 1.43 wt% MnO) were also detected in the *Y*-site (Tables 3.9, 3.10). Concluding, the studied micas comprise mainly Al-rich and Fe-Mg poor dioctahedral micas, and Al-poor and Fe-Mg rich trioctahedral micas from Tørdal pegmatites and their adjacent host rocks (Tables 3.9, 3.10).

The plot of Rb versus Li concentrations shown in Figure 3.27 allows to distinguish primitive micas from chemically evolved ones. In this plot a weak evolutionary trend for the pegmatite micas is observed defined by increasing concentrations of Rb accompanied by increasing Li. Low concentrations of these elements correspond to a primitive chemical character of mica, while with progressive evolution of the pegmatite melt these elements will increase in mica (Rosing-Show et al., 2018). Micas that have highest Li and Rb concentrations can be divided in two groups, where the lithian siderophyllite from Heftetjern 2 (sample 05071901) has highest average Rb and Li concentrations, followed by the lithian ferroan muscovite, magnesian siderophyllite and ferroan phlogopite from Sjauset (sample 04071918), Svåheii 2a (sample 02071911), Svåheii 3 (sample 02071913b), Storemyr 2 (sample 04071901), Brattured (sample 04071909) and Upper Høydalen (sample 05071903) with moderate average Rb and Li concentrations. The remaining mica samples contain relative low Rb and Li. Lowest Rb and Li concentrations are observed in the muscovite from Storemyr 3 (sample 04071907) (Table 3.9). Interestingly some of the ferroan phlogopites of the amphibolites exhibit a slightly higher Rb and Li content and, thus, higher fractionation degree as the most primitive pegmatite micas. The highest Li and Rb concentrations discovered in ferroan phlogopites from pegmatite host rocks are ferroan phlogopites from Upper Høydalen metagabbro (sample 05071903). The lowest Rb and Li contents were detected in ferroan phlogopites from Bratterud (sample 04071917) and Mjeltedalen 2a (sample 02071918).

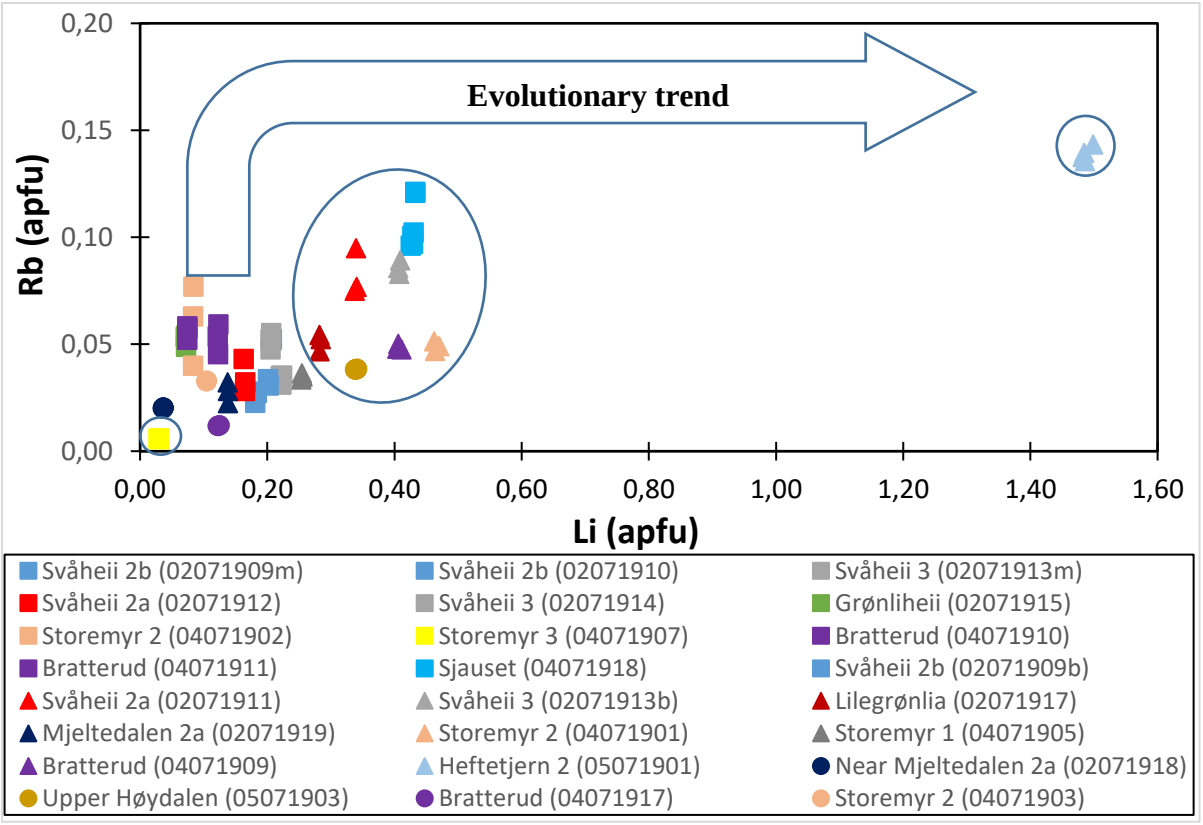

Fig. 3.27. Lithium versus Mn diagram of micas from the Tørdal pegmatites and their amphibolitic host rocks from Rosing-Schow et al. (2018). Increasing Li and Rb corresponds to evolving mica chemistries and, thus, increasing fractionation degree of the pegmatite melt from which the micas crystallized. The most evolved mica is the lithian siderophyllite from Heftetjern 2, while the most primitive mica is the muscovite from Storemyr 3 (see also Fig. 3.28).

In Figure 3.28, variations of the Fe and Mn content in the studied micas are illustrated. Trioctahedral micas from Tørdal pegmatites, which are rich in Fe and Mg, contain significantly higher Mn concentrations than Al-rich dioctahedral micas (Fig. 3.28). Interestingly, trioctahedral micas from the amphibolitic host rocks have similar low Mn concentrations as the dioctahedral micas from Tørdal pegmatites. The highest average Mn concentration is discovered in the magnesian siderophyllite from Storemyr 1 (sample 04071905). Manganese of the other trioctahedral micas from Tørdal pegmatites varies from 0.157 to 0.093 *apfu* (mean values), where the lowest Mn contents of these trioctahedral micas are discovered in the sample from Bratterud (sample 04071909) and Mjeltedalen 2a (sample 02071919). For the dioctahedral micas, the lithian ferroan muscovite from Sjauset (sample 04071918) has outstanding high Mn contents. Remaining dioctahedral micas from pegmatites and trioctahedral micas of the amphibolitic host rocks have low average Mn concentrations. The lowest average Mn contatn has the muscovite from Storemyr 3 (sample 04071907).

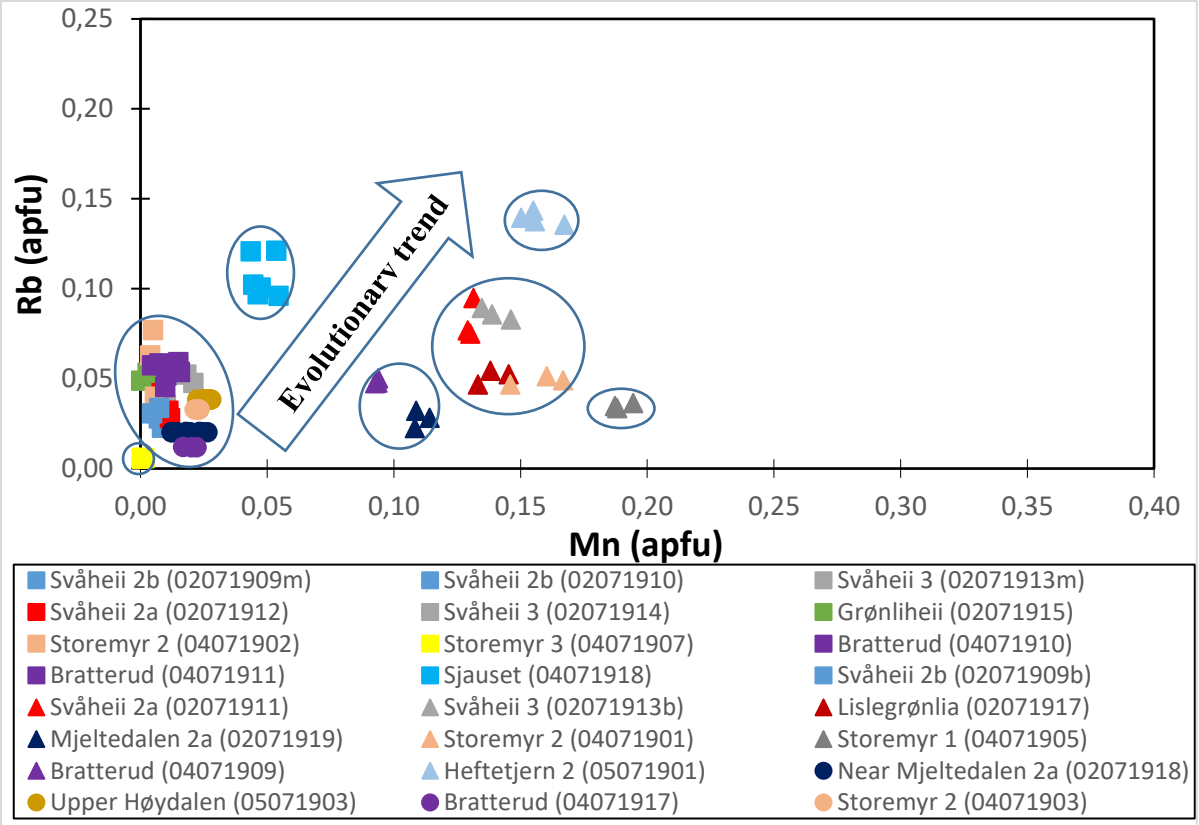

Fig. 3.28. Manganese versus Rb plot of studied micas from the Tørdal pegmatites and their adjacent host rocks from Rosing-Schoe et al. (2018). Trioctahedral (triangles) and dioctahedral (squares) form two separated trends of increasing Mn with increasing Rb. However, trioctahedral (circles) micas from amphibolitic host rocks follows the similar trend as dioctahedral (squares) micas from Tørdal pegmatites. The sample from Heftetjern 2 comprises the most evolved trioctahedral mica and the sample from Sjauset is the most evolved dioctahedral mica.

3.5.2 Minor and trace elements of micas determined by LA-ICP-MS

Micas from Tørdal pegmatites and their adjacent host rocks, which were analysed by EPMA for major and minor elements, were in addition analysed by LA-ICP-MS for some minor and trace elements. LA-ICP-MS data obtained from micas from the Svåheii 2b (sample 02071909b) and Lislegrønlia (sample 02071917) pegmatites were not further considered because these analyses were contaminated by mineral inclusions in the micas. The analyses biotites in the amphibolitic host rocks was quite challenging due to their relative small grain sizes (up to 500 µm). The complete list of results of mica analyses of Tørdal pegmatites and of biotites of the amphibolitic host rocks are provided in Appendices 7.13 and 7.14, respectively. Average concentrations are summarized in Tables 3.11 and 3.12, respectively

Table 3.11. Average concentrations of minor and trace elements of studied micas. Numbers in parenthesis indicate standard deviation. n = number of analysis.

Sample	02071909m	02071910	02071912	02071913m	02071914	02071915	04071902	04071907	04071910
Pegmatite	Svåheii 2b	Svåheii 2b	Svåheii 2a	Svåheii 3	Svåheii 3	Grønliheii	Storemyr 2	Storemyr 3	Bratterud
Mineral	Ms	Ms	Fe-Ms	Fe-Ms	Fe-Ms	Ms	Ms	Ms	Fe-Ms
n	*4*	*4*	*4*	*5*	*5*	*5*	*5*	*3*	*4*
Li (ppm)	762 (43)	874 (88)	701 (140)	935 (95)	862 (54)	304 (37)	352 (81)	112 (36)	300 (37)
Sc	1125 (121)	38 (5)	784 (387)	990(41)	48 (8)	149 (6)	487 (136)	754 (27)	506 (172)
Ti	4037 (239)	1306 (99)	2675 (1624)	3495 (157)	1839 (170)	1672 (136)	1777 (201)	2740 (103)	1961 (290)
Ga	356 (24)	490 (47)	286 (35)	352 (5)	404 (12)	437 (16)	530 (29)	354 (9)	418 (53)
Rb	3590 (167)	5996 (621)	4178 (1103)	4196 (110)	6569 (272)	6494 (450)	7768 (1778)	3565 (78)	6863 (540)
Nb	45 (3)	153 (6)	76 (9)	55 (1)	88 (6)	81 (8)	71 (13)	70 (3)	76 (12)
In	25 (3)	15 (1)	5 (7)	20 (1)	7 (1)	5 (1)	15 (1)	9 (1)	9 (1)
Sn	1412 (129)	1499 (127)	1239 (212)	1422 (48)	1126 (106)	1739 (181)	908 (114)	962 (23)	1537 (99)
Cs	7 (3)	72 (8)	62 (53)	9 (5)	40 (3)	18 (5)	141 (58)	33 (8)	55 (11)
Ta	10 (2)	157 (11)	62 (32)	12 (1)	26 (3)	16 (2)	35(10)	20 (1)	33 (5)
W	9 (1)	15 (1)	27 (17)	12 (1)	15 (1)	10 (1)	6 (1)	15 (1)	15 (1)
Tl	21 (5)	26 (5)	19 (9)	21 (1)	33 (1)	30 (3)	27 (13)	11 (2)	32 (6)

Table 3.11. Continued

Sample	04071911	04071918	02071911	02071913b	02071919	04071901	04071905	04071909	05071901
Pegmatite	Bratterud	Sjauset	Svåheii 2a	Svåheii 3	Mjeltedalen 2a	Storemyr 2	Storemyr 1	Bratterud	Hefttejern 2
Mineral	Fe-Ms	Li-Fe-Ms	Mg-Sid	Sid	Mg-Sid	Sid	Mg-Sid	Mg-Sid	Li-Sid
n	*5*	*5*	*4*	*3*	*5*	*5*	*5*	*4*	*3*
Li (ppm)	508 (41)	1783 (222)	1242 (187)	1883 (357)	512 (22)	1677 (141)	941 (26)	1489 (48)	5570 (277)
Sc	312 (72)	398 (108)	908 (134)	417 (6)	294 (16)	621 (63)	339 (17)	683 (18)	1576 (75)
Ti	1740 (123)	1081 (170)	17387 (893)	16161 (508)	17935 (529)	16705 (464)	18221 (258)	16471 (603)	19531 (644)
Ga	473 (32)	471 (7)	251 (46)	201 (9)	95 (1)	202 (17)	154 (5)	196 (3)	250 (5)
Rb	6669 (441)	14213 (632)	7708 (168)	8585 (206)	2673 (210)	4888 (339)	4362 (537)	4763 (349)	13564 (186)
Nb	101 (10)	98 (15)	102 (4)	95 (1)	128 (6)	57 (1)	87 (2)	87 (18)	184 (13)
In	9 (1)	7 (1)	5 (3)	4 (1)	0.41 (4)	2.1 (1)	2.1 (1)	0.56 (4)	5.71 (4)
Sn	1431 (123)	970 (113)	915 (352)	894 (75)	70 (2)	583 (22)	361 (13)	396 (34)	442 (5)
Cs	57 (8)	167 (26)	82 (9)	114 (21)	208 (17)	176 (37)	58 (16)	111 (36)	173 (14)
Ta	52 (5)	71 (27)	36 (1)	36 (1)	112 (24)	23 (1)	23 (1)	82 (27)	131 (15)
W	15 (2)	11 (4)	1.3 (1)	1.49 (4)	0.7 (1)	0.7 (3)	0.7 (3)	1 (1)	1.7 (2)
Tl	31 (3)	76 (5)	72 (2)	76 (1)	19 (2)	39 (4)	34 (3)	32 (2)	110 (2)

Table 3.12. Average concentrations of minor and trace elements in micas from host rocks of Tørdal pegmatites. Numbers in parenthesis indicate standard deviation. n = number of analysis

Sample	5071903	4071917	4071903	2071918
Pegmatite locality	Upper Høydalen	Bratterud	Storemyr 2	Near Mjeltedalen 2a
Host rock	Coarse-grained gabbro	Medium-grained gabbro	Massive amphibolite	Amphibole-gneiss
Mineral	Fe-Phl	Fe-Phl	Fe-Phl	Fe-Phl
Biotite crystals	5	2	3	3
n	12	6	6	5
Li (ppm)	2615 (217)	928 (1)	782 (124)	265 (49)
Be	<1.76	<1.76	<1.76	<1.76
B	141 (4)	99 (4)	81 (1)	75 (2)
Sc	4 (2)	3.5 (2)	2 (1)	2.5 (5)
Ti	6529 (734)	18308 (48)	12052 (436)	13383 (913)
V	<126.14	1406 (106)	544 (119)	529 (131)
Cr	362 (51)	<3.40	200 (17)	213 (18)
Co	89 (2)	99.6 (4)	94 (3)	92 (2)
Zn	370 (11)	567 (6)	369 (9)	301 (6)
Rb	3607 (309)	1049 (35)	3046 (60)	1813 (105)
Sr	2 (1)	3.7 (8)	1.8 (2)	21 (2)
Y	9 (7)	0.8	4.4 (4.8)	0.3 (3)
Zr	<0.23	<0.23	<0.23	<0.23

In order to better understand the distribution Sc in the studied micas, Sc and Ti were plotted against each other in Figure 3.29. The Sc concentrations detected in trioctahedral micas (ferroan phlogopites) from amphibolitic host rocks (highest average: < 5 ppm Sc) are significantly lower compared to dioctahedral and trioctahedral micas collected from Tørdal pegmatites (highest average 1576 ppm Sc) (Tables 3.11, 3.12). The mica with the highest average Sc concentration is the lithian siderohpyllite from Heftetjern 2 (sample 05071901) with an average Sc content of 1576 ppm. Moderate high average Sc concentrations were discovered in muscovite, ferroan muscovite and magnesian siderophyllite from Svåheii 2b (sample 02071909m), Svåheii 3 (sample 02071913m) and Svåheii 2a (sample 02071911, 02071912) with average Sc concentrations of 1126, 990, 908, and 784 ppm, respectively. Moderate average Sc concentrations (average concentrations of 487 to 754 ppm Sc) were observed in the muscovite, magnesian siderophyllite, ferroan muscovite and siderophyllite samples from Storemyr 3 (sample 04071907), Bratterud (sample 04071909, 04071910) and Storemyr 2 (sample 04071901, 04071902). Relative low average Sc concentrations (294 to 417 ppm Sc) have the siderophyllite, lithian ferroan muscovite, magnesian siderophyllite and ferroan muscovite from Svåheii 3 (sample 02071913b), Sjauset (sample 04071918), Storemyr 1 (sample 04071905), Bratterud (sample 04071911) and Mjeltedalen 2a (sample 02071919). Low average Sc concentrations of 149, 48 and 38 ppm Sc were detected in the muscovite and ferroan muscovite samples from Grønliheii (sample 02071915), Svåheii 3 (sample 02071914) and Svåheii 2b (sample 02071910). Micas from the border or wall

zone have generally higher Sc than micas collected from intermediate zone of the same pegmatite (Table 3.11).

Lowest average Sc concentrations are detected in ferroan phlogopites from the amphibolitic host rocks (Table 3.12). The average Sc concentrations of the phlogopites vary from 2 to 4 ppm. Thus, micas from the Tørdal pegmatites have considerably higher Sc (highest average 1576 ppm Sc from Heftetjern 1; Table 3.11) compared to micas from amphibolitic host rocks (highest average: < 5 ppm Sc; Table 3.12).

The average concentrations of Ti in studied micas are significantly higher in trioctahedral micas compared to dioctahedral micas and, therefore, they can be easily distinguished in the Sc versus Ti plot (Fig. 3.29). The trioctahedral micas from Tørdal pegmatites comprise average Ti concentrations of 16161 to 19532 ppm, whereas trioctahedral micas from amphibolitic host rocks have average Ti concentrations of 6529 to 18308 ppm. Lowest average Ti concentrations of 1081 to 4038 ppm were detected, as mentioned, in the dioctahedral micas.

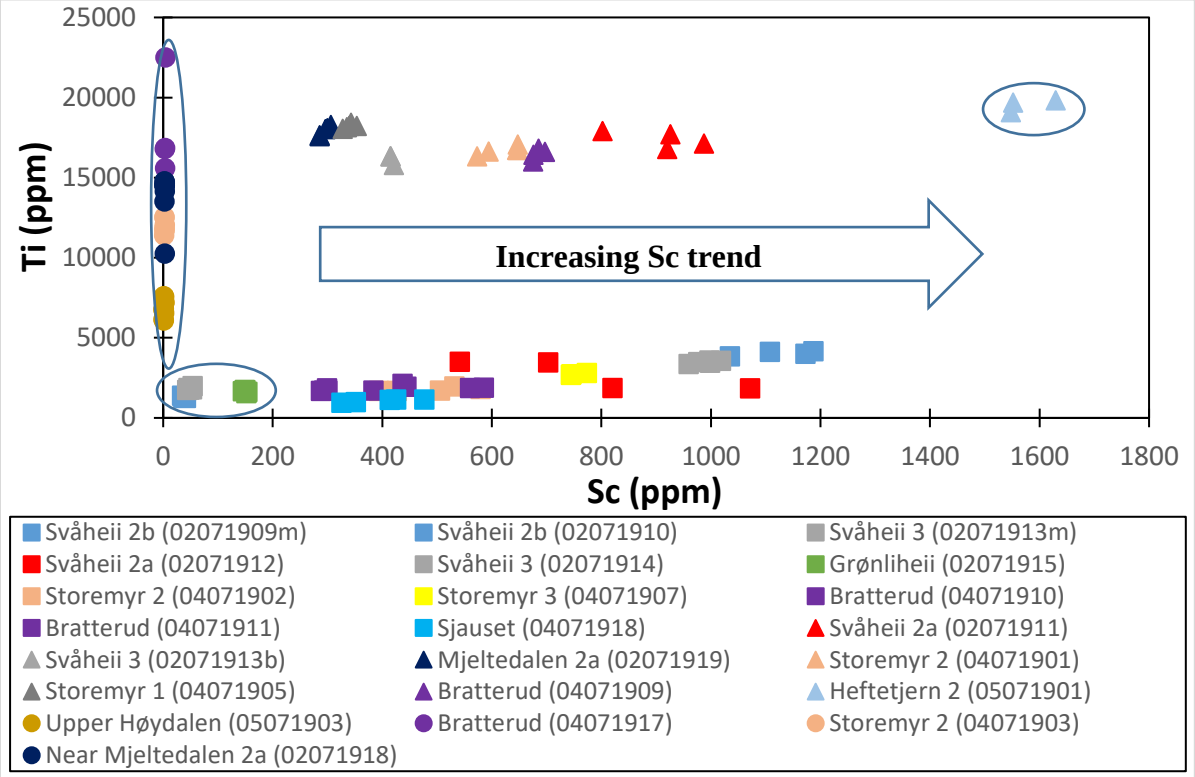

Fig. 3.29. Trace element concentration plot of Sc versus Ti of studied micas from Tørdal pegmatites and their amphiboltic host rocks from Rosing-Schow et al. (2018). Micas from Heftetjern 2, Svåheii 2b, Svåheii 3 and Svåheii 2a are most enriched in Sc (> 800 average ppm Sc). Micas with low Sc are from Svåheii 2b, Svåheii 3 and Grønliheii (< 200 average ppm Sc). Trioctahedral micas from amphibolitic host rocks of Tørdal pegmatites have the lowest Sc

(< 10 ppm average ppm). Triangles and circles are triocthedral micas of the Tørdal pegmatites and their amphibolitic host rocks. Squares are dioctahedral micas from Tørdal pegmatites.

To visualize the chemically evolutionary trend of thhe studied micas, the data are plotted in the Rb versus K/Rb diagram (Fig. 3.30). The trend of increasing Rb with decreasing K/Rb ratio corresponds to the progressive evolution of the mica chemistry in the pegmatites and amphibolitic pegmatite host rocks as well. Highest K/Rb ratio is observed in very primitive ferroan phlogopites from amphibolitic host rocks near the Bratterud pegmatite (sample 04071917) with K/Rb ratio 70.54 to 62.30. This mica is followed by primitive ferroan phlogopites and magnesian siderohylite collected from host rock near Mjeltedalen 2a (sample 02071918) and from the pegmatite itself (sample 02071919). They comprises K/Rb ratio of 42.9 to 40.24 and 42.9 to 37.1. Moderate K/Rb ratios, ranging from 31.9 to 18.8, have the samples from Storemyr 1 (sample 04071905), Storemyr 3 (sample 04071907), Bratterud (sample 04071909), Grønliheii (sample 02071915), Svåheii 2a (sample 02071912), Upper Høydalen (sample 05071903), Storemyr 3 (sample 04071903), Storemyr 2 (sample 04071901), Svåheii 3 (02071913m) and Svåheii 2b (02071909m). Samples from Bratterud (sample 04071911, 04071910), Svåheii 2b (sample 02071910), Svåheii 3 (sample 02071914), Storemyr 2 (sample 04071902), Svåheii 2a (sample 02071911), and Svåheii 3 (sample 02071913b) show intermediate K/Rb ratios varying from 16.4 to 10.3. Lowest K/Rb ratios were detected in the evolved samples from Sjauset (sample 04071918) and Heftetjern 2 (sample 05071901) with ratios varying from 8.1 to 5.6. The lithian ferroan muscovite from Sjauset with an average of 14214 ppm Rb and the lithian siderophyllite from Heftetjern 2 with an average of 13565 ppm Rb have significantly higher Rb concentrations compared to all other micas and are considered as the most chemically evolved. The average Rb concentrations of 8585 to 3046 ppm are considered as moderately to intermediate in concentration and comprises of siderophyllites, magnesian siderophyllites, ferroan muscovites and muscovites. Ferroan phlogopites from amphibolitic host rocks near the Bratterud pegmatite (sample 04071917) and near the Mjeltedalen 2a pegmatite (sample 02071918) have the lowest average Rb concentrations of 1049 and 1813 ppm, respectively, followed by the magnesian siderophyllite from the Mjeteldalen 2a pegmatite (sample 02071918) with an average Rb content of 2674 ppm. These micas have also the highest K/Rb ratio and are considered as relative primitive micas.

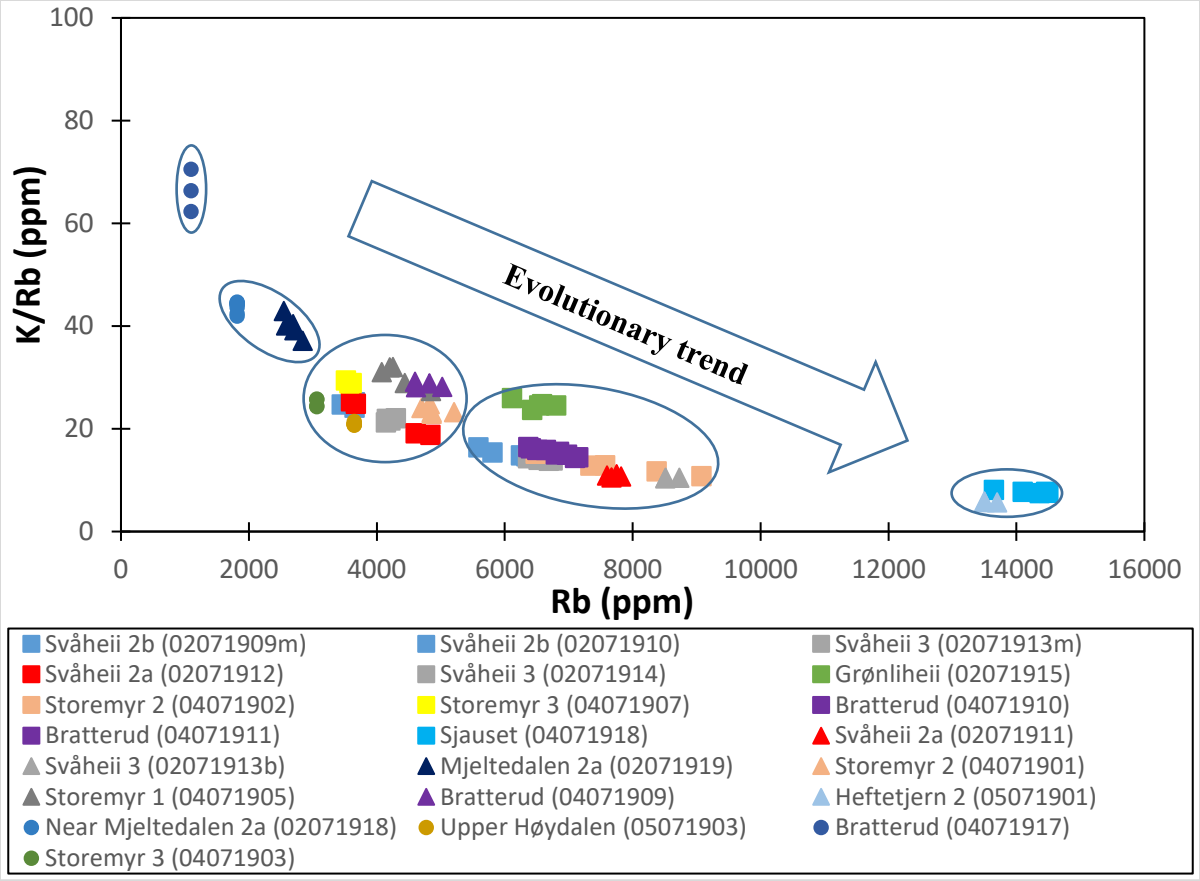

Fig. 3.30. Variation diagram of the K/Rb ratio versus Rb concentration of studied micas from Tørdal pegmatites and their amphibolitic host rocks from Rosing-Schow et al. (2018). The data form an exponential trend reflecting the chemical evolution of the micas. The mica sample from Mjeltedalen 2a pegmatite together with micas from amphibolitic host rocks near the Bratterud and Mjeltedalen 2a pegmatites represent the most primitive micas with the highest K/Rb ratio and lowest Rb content. The most evolved micas are from Sjauset and Heftetjern 2 with very low K/Rb ratio and Rb concentrations >13000 ppm.

3.6 Pegmatite host rocks

3.6.1 Petrographic description of pegmatite host rocks

Four samples of pegmatite host rocks (samples 02071918, 04071903, 04071917, 05071903) collected nearby or adjacent of studied Tørdal pegmatites were investigated by optical microscopy and back-scattered electron (BSE) imaging using polished thick sections (c. 300 µm thick). BSE images was taken together with EPMA analysis at the Blindern facility. Thick sections were used because of the application of LA-ICP-MS for trace element analysis on amphibole and mica (see chapter 2.4). Due to the thickness of section, the describtion of mineral by using optical microscopy

was challenging and, thus, BSE imaging has been applied in addition. The following description focuses, therefore, mostly on BSE images, describing pegmatite host rocks from fine-grained to coarser-grained.

Amphibolites in the vicinity of the Storemyr 2 and Mjeltedalen 2a pegmatites

In optical microscopy, a fine-grained texture is observed in the massive amphibolite and amphibole gneiss collected close to the Storemyr 2 (sample 04071903) and nearby Mjeltedalen 2a (sample 02071918) pegmatites. Due to their relative similar texture, the two samples are described together. Both samples are dominated by amphibole, which comprises approximately 60 vol.% of the rock. The second most abundant constituent is plagioclase (c. 30 vol.%). Other observed minerals include biotite (10 vol.%) and opaque minerals (c. 5 vol.%). Amphibole and biotite crystals are aligned forming a distinct foliation, especially in the amphibole-gneiss from Mjeltedalen 2a (sample 02071918). In optical microscopy the amphiboles appear mainly black because of the light could not pass through the minerals. However, in the margins of the amphiboles are green. The intensity of the green varies due to strong pleochroism. No distinct 120 degree cleaveage was observed in the amphiboles. Plagioclase crystals exhibited a distinct twinning. The light bronze-brown micas have elongated, lath-like shapes. They show a distinct pleochroism from light-brown to more darker-brown. Numerous isometric opaque minerals were observed. In BSE imaging, the amphiboles have subhedral to euhedral hexagonal shapes, which reminds of hornblende, with crystal sizes ranging from 100 to 400 µm (Fig. 3.31 A-B). Plagioclase is anhedral to subhedral, lath-shaped with grain sizes ranging from 50 to 250 µm. The elongated biotites are 200 to 600 µm in length. Opaque minerals form small (<100 µm) anhedral to subhedral grains.

Metagabbro in the vicinity of the Bratterud pegmatite

The amphibolite (sample 04071917) collected close to the Bratterud pegmatite has a less defined foliation and larger average grain sizes than the previous described amphibolites (Fig. 3.31 C). The pre-metamorphic, medium-grained gabbroic texture is partially preserved. Main consitutents of the medium-grained metagabbro are amphibole and plagioclase, both comprising c. 30 vol.% of the rock. Thus, the plagioclase content is higher than in samples 02071918 and 04071903. The content of biotites is about 10 vol.% and the sample also contains a larger amount of opaque minerals (c. 10 vol.%). Crystal sizes of amphiboles range from 200 to 500 µm. The plagioclase

and biotite are up to 500 µm in size and the abundant opaque minerals are 50 to 200 µm in size (Fig. 3.31 C).

Metagabbros in the vicinity of the Upper Høydalen pegmatite

The most coarse-grained studied pegmatite host rock was collected close to the Upper Høydalen pegmatite (sample 05071903). Macroscopically it has the texture of a coarse-grained gabbro. Foliation is not developed. However, using optical microscopy and BSE imaging it turned out that the large appearing (up to c. 2 cm) amphibole and plagioclase crystals are clusters of much smaller minerals (c. 200 to 1000 µm) (Fig. 3.31 D). The major constituent is plagioclase with 60 vol.% and with crystal sizes of up to 1 mm. Amphibole comprises approximately 25 vol.%. Biotite (c. 10 vol.%) and opaque minerals (c. 5 vol.%) are the remaining major minerals. Optical characteristics of minerals in the coarse-grained gabbro are in general similar to the described rocks above. Biotites are up to 500 µm in length and sizes of the opaque minerals range from 50 to 200 µm.

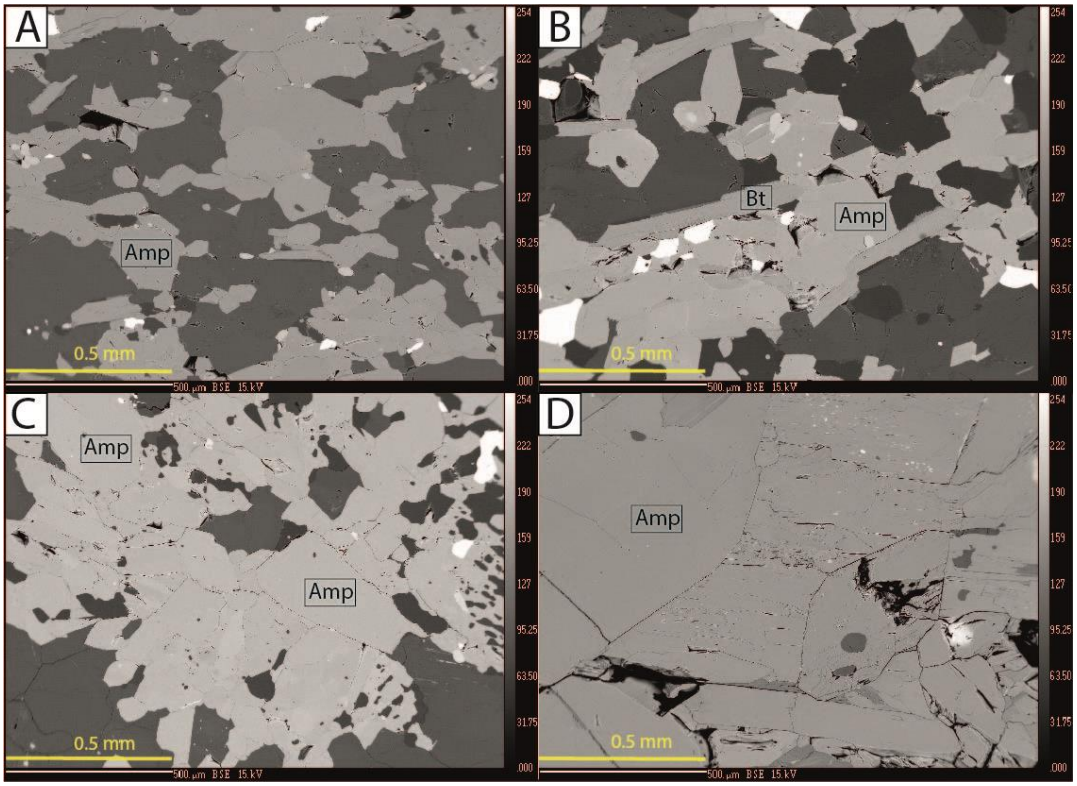

Fig. 3.31. Back-scattered electron (BSE) images of investigated amphibolites from the Tørdal area. A – Fine-grained amphibole gneiss collected close to the Mjetledalen 2a pegmatite. B – Fine-grained amphibolite from the vicinity of the Storemyr 2 pegmatite. C – Medium-grained gabbro occurring close to the Bratterud pegmatite. D – Coarse-grained gabbro collected west of the Upper Høydalen pegmatite. Amp = Amphibole; Bt = Biotite.

3.6.2 Whole rock chemistry of pegmatite host rocks

Four pegmatite host rock samples of fine-to medium-grained amphibolites in the vicinity of the pegmatites Lislegrønlia (sample 02071916), Bratterud (sample 04071917), Heftetjern 2 (sample 05071902), and Storemyr 2 (sample 04071903) were sent to Actlabs (Activation Laboratories Ltd) in Ontario, Canada, for whole rock analysis. The results are provided in Appendix 7.16 and summarized in Table 3.13.

The Ni versus Zr/Ti according to Winchester and Floyd (1984) shown in Figure 3.32 allows to distinguish amphibolites of sedimentary and igneous origin. All samples plot in the field of igneous origin because of their relative low contents of Ni and Zr, and high contents of Ti. Nickel varies from 5 to 55 ppm, while the Zr/Ti ratio varies from 0.015 to 0.027.

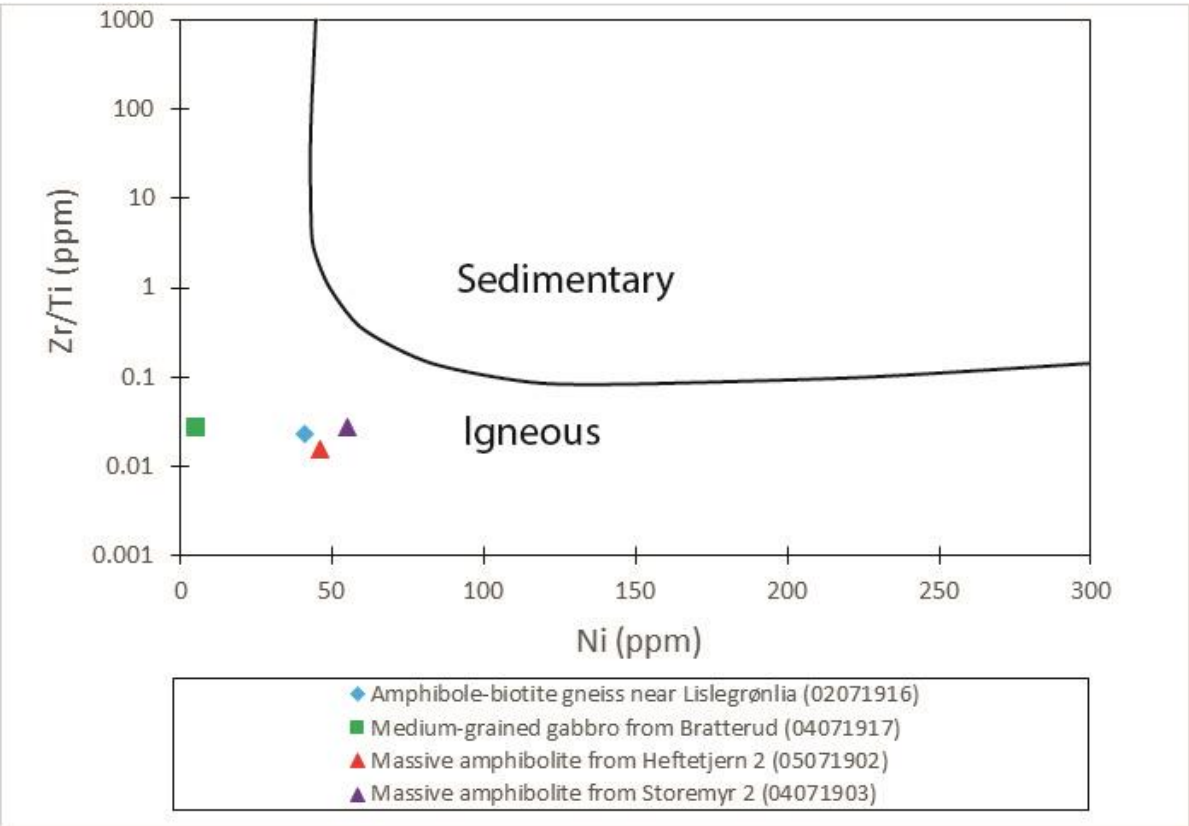

Fig. 3.32. Nickel versus Zr/Ti discrimination diagram of amphibolites according to Winchester and Floyd (1984). The plot allows to distinguishing amphibolites of igneous origin from those of sedimentary origin. All studied rocks plot in the field of igneous origin.

In the next step, the data were plotted in the Ti/1000 versus V diagram according to Shervais (1982) in order to determine which orogrenic setting the igneous amphibolite host rock represent (Fig. 3.33). The igneous amphibolitic host rocks plot in the ocean-island basalt (OIB)/ alkali basalt (AB) field close to the middle ocean ridge basalts (MORB) due to their very high Ti and relative low V (266 to 354 ppm).

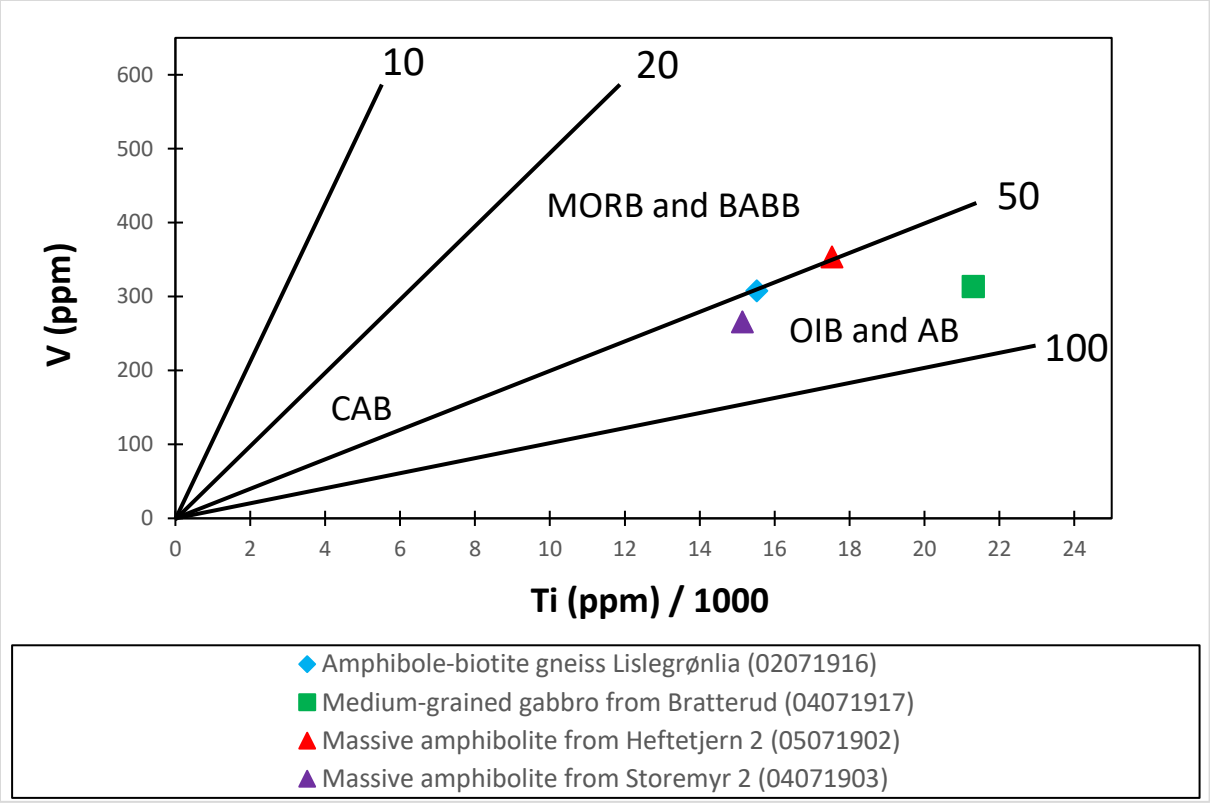

Fig. 3.33. Titanium/1000 versus V discrimination diagram of tholeiitic and alkali rock according to Shervais (1982). IAT – island-arc tholeiites, MORB – mid-ocean ridge basalts, BABB – back-arc basin basalts, CAB – calc-alkaline basalts, OIB – ocean-island basalts and AB alkali basalts. All studied amphibolites of the Tørdal area plot in ocean-island basalt/alkali basalt field (OIB and AB).

These igneous amphibolites which represent the orogenic settings of ocean-island basalt (OIB)/ alkali basalt (AB) are further plotted in the ternary digram of Hf-Th-Ta according to Wood (1980) shown in Figure 3.34. The ternary diagram allows to distinguish which magmatic series the igneous amphibolitic rocks represent. All studied host rocks plot in the primitive arc tholeiite field.

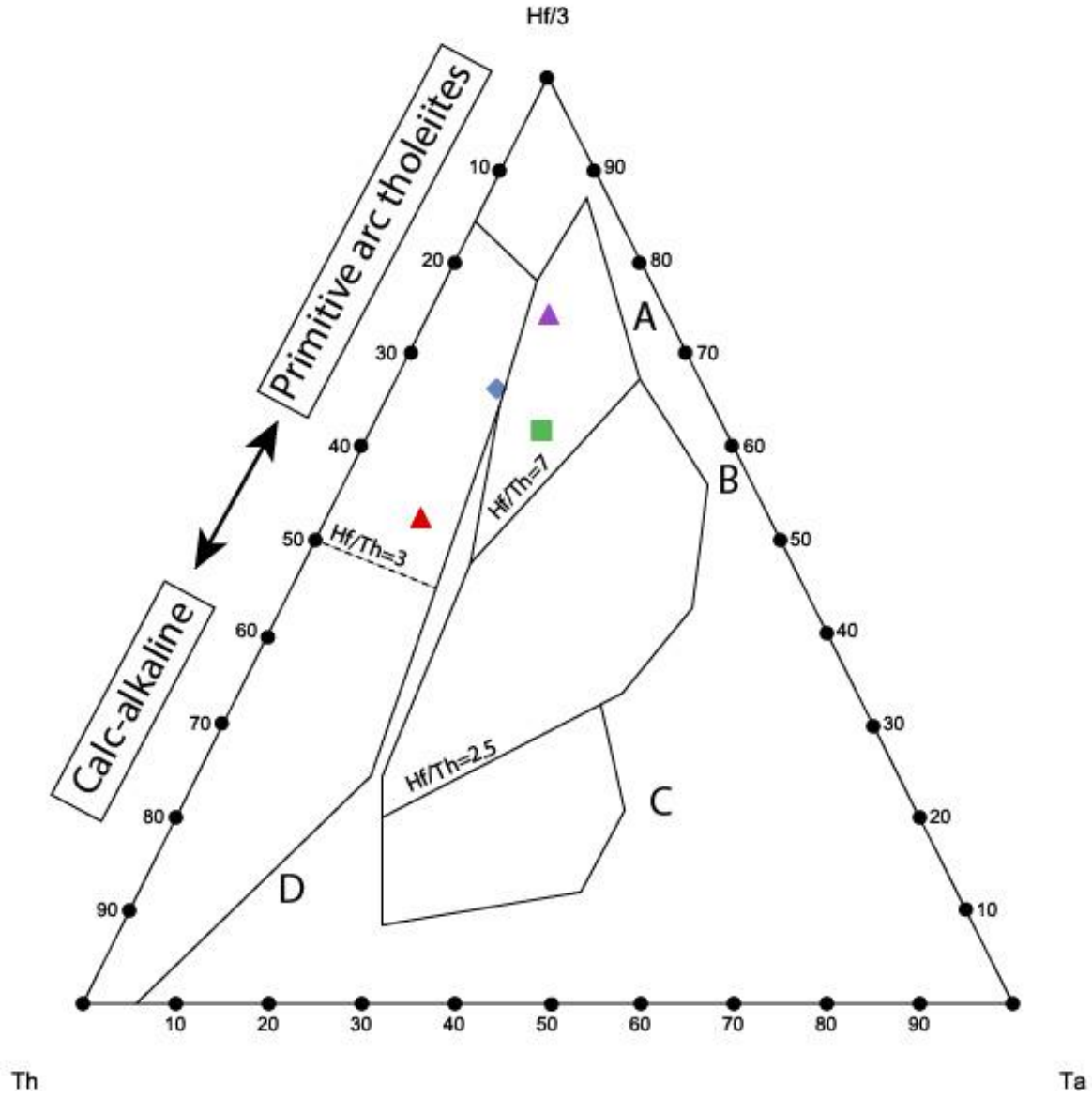

Fig. 3.34. Hf-Th-Ta ternary diagram according to Wood (1980) distinguishes calc-alkaline from tholeiitic magma series in igneous rocks based on their concentrations in Hf, Ta and Th (ppm). All studied amphibolitc host rocks plot in the primitive arc tholeiites field.

The amphibolites and metagabbros contain low SiO_2 (46.7 to 50.7 wt%) and Na_2O (2.8 to 3.3 wt%), relative high Al_2O_3 (13.8 to 14.6 wt%) and high Fe_2O_3 (13.4 to 16.2 wt%), CaO (7.8 to 8.9 wt%), MgO (4.2 to 6.1 wt%), and TiO_2 (2.5 to 3.6 wt%) (Table 3.13). Other oxides have concentrations <1.0 wt% (Table 3.13). Most of the investigated amphibolites are rich in F with concentrations varying from 0.18 to 0.25 wt%. The host rock of the Bratterud pegmatite (sample 04071917) contains significantly lower F of only 0.02 wt.%.

Scandium concentrations in these rocks are of major interest, since the Sc in these rocks could be the source of the Sc found in the Tørdal pegmatites. Figure 3.35 shows Sc versus TiO_2 plot for the amphibolitic host rocks. Scandium concentrations in all four samples are relative consistent and vary from 31 to 38 ppm (Table 3.13). Highest Sc concentrations are detected in the host rock of Heftetjern 2 pegmatite locality (sample 05071902). All samples contain therewith almost twice as much Sc as the upper continental crust (mean 21.9 ppm Sc) according to Rudnick and Gao (2014). Thus, the amphibolitic rocks of the studied Tørdal pegmatites are enriched in Sc.

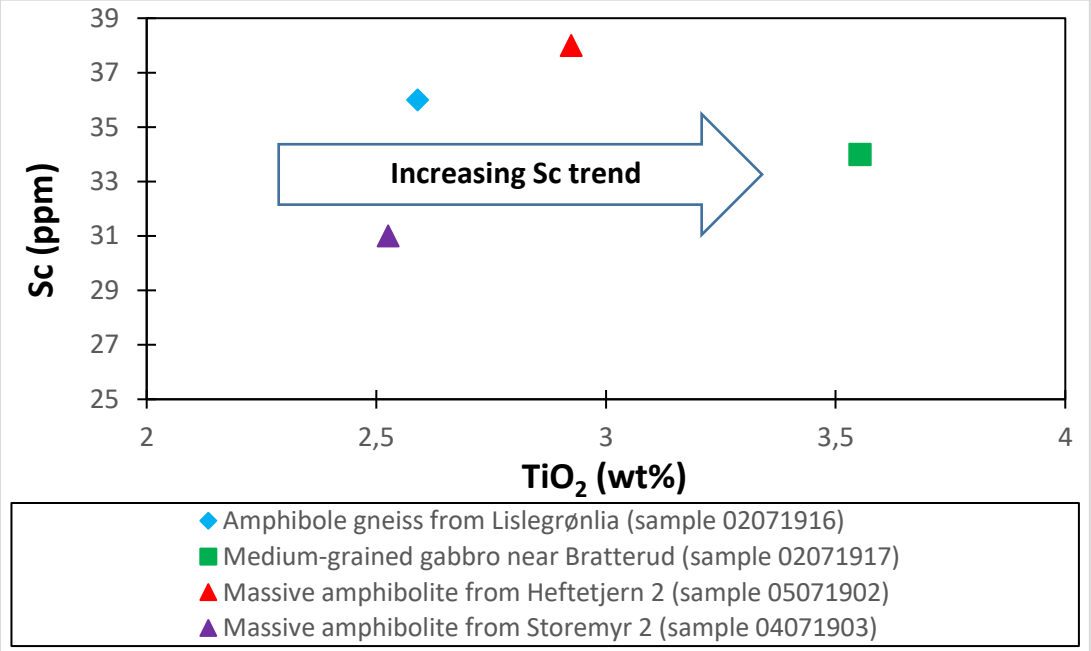

Fig. 3.35. Plot of the TiO_2 (wt.%) versus Sc (ppm) concentration of investigated amphibolitic host rocks. The host rocks have relative consistent Sc contents.

In addition to Sc, the Be content in the host rocks was of major interest for this study. In Figure 3.36. the Be content of amphibolites is plotted against their Y concentrations. In contrast to Sc, Be varies highly from 2 ppm (Bratterud, sample 04071917), over 7 ppm (Storemyr 2, sample 04071903), to up to 17 ppm (Heftetjern 2, sample 05071902) and 18 ppm (Lislegrønlia, sample 02071916).

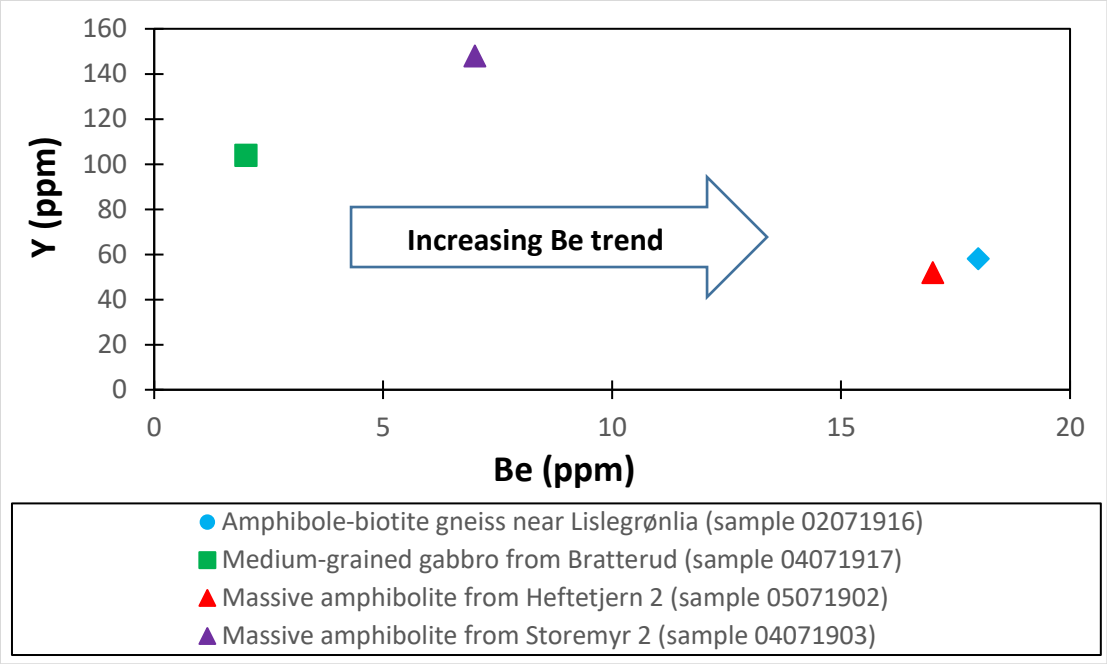

Fig. 3.36. Plot of the Be and Y concentrations in amphibolitic host rocks. Beryllium concentrations differs strongly among the samples.

Table 3.13. Whole rock chemistry of host rocks of the Tørdal area. LOD – Limit of detection

Sample	LOD	Near Lislegrønlia (02071916)	Bratterud (04071917)	Heftetjern 2 (05071902)	Storemyr 2 (04071903)
SiO_2 (wt.%)	0.01	48.44	47.19	46.67	50.71
Al_2O_3	0.01	13.86	13.85	14.61	13.77
Fe_2O_3	0.01	14.33	16.15	15.89	13.41
MgO	0.01	5.31	4.20	6.12	5.40
CaO	0.01	8.91	8.45	8.78	7.81
Na_2O	0.01	3.04	3.26	3.14	2.85
K_2O	0.01	0.86	0.64	1.06	1.32
TiO_2	0.001	2.59	3.55	2.92	2.53
P_2O_5	0.01	0.59	0.92	0.51	0.60
MnO	0.001	0.27	0.23	0.24	0.23
Total		98.20	98.44	99.94	98.63
Ag (ppm)	0.50	1.30	1.80	0.90	1.40
Ba	2.00	264.00	317.00	190.00	154.00
Be	1.00	18.00	2.00	17.00	7.00
Bi	2.00	<2	<2	4.00	8.00
Cd	0.30	0.40	0.50	0.30	<0.3
Co	1.00	36.00	34.00	40.00	41.00
Cr	1.00	57.00	4.00	47.00	77.00
Cu	1.00	25.00	24.00	37.00	12.00
Ga	1.00	26.00	28.00	24.00	24.00
Li	1.00	50.00	63.00	150.00	84.00
Mn	1.00	2010.00	1680.00	1710.00	1700.00
Ti	0.10	15527.27	21300.53	17529.62	15143.58
Ni	1.00	41.00	5.00	46.00	55.00
Pb	3.00	7.00	7.00	5.00	7.00
Sc	1.00	36.00	34.00	38.00	31.00
Sr	2.00	261.00	307.00	274.00	236.00
Tl	0.10	0.60	0.40	1.80	2.50
U	0.10	0.50	0.60	1.10	0.50
V	5.00	308.00	314.00	354.00	266.00
Zn	1.00	208.00	159.00	132.00	135.00
Zr	2.00	348.00	579.00	264.00	407.00
B	2,00	4.00	<2	<2	<2
Ge	1.00	2.00	2.00	2.00	2.00
Rb	2.00	78.00	37.00	198.00	297.00
Nb	1.00	10.00	20.00	7.00	11.00
Li	1.00	50.00	63.00	150.00	84.00
Sn	1.00	7.00	1.00	5.00	14.00
Cs	0.50	11.10	5.20	19,00	12.90
La	0.1	30.80	59.90	26,10	34.20
Ce	0.10	75.4	154.00	45.9	78.8
Pr	0.05	10.70	22.30	8.99	11.90
Nd	0.10	50.30	99.40	40.10	52.40
Sm	0.10	12.60	23.60	9.30	13.50
Eu	0.05	3.45	4.22	2.65	3.01
Gd	0.10	13.80	23.60	9.60	17.00
Tb	0.10	2.20	3.80	1.50	3.10
Dy	0.10	12.90	21.60	8.80	19.80
Ho	0.10	2.50	4.30	1.80	4.50
Er	0.10	6.80	11.60	4.90	13.50
Tm	0.05	0.88	1.51	0.68	1.96
Yb	0.10	5.80	9.80	4.30	12.00
Lu	0.01	0.85	1.46	0.69	1.82
Hf	0.20	8.90	12.20	6.30	10.50
Ta	0.10	0.50	1.20	0.40	0.60
Th	0.10	1.00	1.30	1.50	0.60
Y	1.00	58.00	104.00	52.00	148.00
∑LREE		179.80	359.20	130.39	190.80
∑HREE		49.18	81.89	34.92	76.69
S (wt.%)	0.01	<0.01	0.16	<0.01	0.02
F	0.01	0.18	0.02	0.17	0.25
Ti	0.01	0.20	0.17	0.47	0.64

3.6.3 Major and minor elements in amphiboles determined by EPMA

According to Hawthorne et al. (2012) the amphibole supergroup has the chemical formula $A\ B_2\ C_5\ T_8\ O_{22}\ W_2$ where the elements which mainly occupies the different sites in the formula are:

[], Na, K, Ca, Pb, and Li for the *A*-site,

Na, Ca, Mn^{2+}, Fe^{2+}, Mg, and Li for the *B*-site,

Mg, Fe^{2+}, Mn^{2+}, Al, Fe^{3+}, Mn^{3+}, Cr^{3+}, Ti^{4+}, and Li for the *C*-site,

Si, Al, Ti^{4+}, and Be for the *T*-site,

OH, F, Cl, and O^{2-} for the *W*-site.

Major and minor element concentrations of amphiboles and biotites from amphibolic host rocks of the Tørdal pegmatites were obtained by EPMA. The biotite chemistry is discussed in Chapter 3.5. In this chapter analytical results of amphibole are provided. A total of 27 point analyses were obtained from 23 amphiboles (Table 3.14). The results of major and minor elements analysis are provided in Appendix 7.10 and average concentrations are summarized in Table 3.14.

Table 3.14. Average major and minor element contents of amphiboles from host rocks of Tørdal pegmatites determined by EPMA. Number in parenthesis indicate standard deviation. n= number of measurements.

Sample	05071903	04071917	04071903	02071918
Pegmatite locality	Upper Høydalen	Bratterud	Storemyr 2	Near Mjeltedalen 2a
Host rock	Coarse-grained gabbro	Medium-grained gabbro	Massive amphibolite	Amphibole-gneiss
Mineral	Amphibole	Amphibole	Amphibole	Amphibole
Crystals	5	5	4	9
n	7	5	4	11
FeO (wt.%)	14.9 (3)	20.7 (2)	19.4 (3)	17.2 (3)
MnO	0.36 (6)	0.31 (4)	0.3 (1)	0.36 (5)
K_2O	0.4 (1)	0.70 (5)	0.70 (9)	0.64 (9)
SiO_2	46.7 (9)	43.2 (4)	43 (1)	44.9 (5)
CaO	12.1 (2)	11.6 (1)	11.7 (1)	11.8 (1)
TiO_2	0.5 (1)	0.8 (1)	0.7 (1)	0.83 (8)
Al_2O_3	8.8 (7)	10.0 (3)	10.2 (3)	9.2 (2)
MgO	11.9 (4)	8.5 (3)	9.2 (2)	10.9 (2)
Sc_2O_3	<0.05	<0.05	<0.05	<0.05
F	1.0 (1)	0.06 (3)	0.57 (7)	0.4 (2)
Na_2O	1.4 (2)	1.39 (3)	1.41 (6)	1.42 (9)
H_2O*	1.535	1.926	1.699	1.766
O=F	0.434	0.028	0.241	0.205
Total	99.973	99.459	99.789	99.705
Fe_{tot} (*apfu*)	1.856	2.661	2.474	2.167
Mn	0.046	0.041	0.051	0.047
K	0.078	0.137	0.137	0.124
Si	6.922	6.626	6.624	6.758
Ca	1.934	1.916	1.916	1.909
Ti	0.057	0.096	0.084	0.094
Al	1.551	1.808	1.844	1.635
Mg	2.635	1.950	2.100	2.453
Sc	b.d.l	b.d.l	b.d.l	b.d.l
F	0.483	0.032	0.276	0.232
Na	0.411	0.415	0.418	0.414
OH	1.517	1.969	1.725	1.768

*H_2O: the H_2O is estimated to fully occupy the *W*-site with F.

Results of major and minor element analysis of amphiboles revelas Fe_{tot}, Ca, Mg, and Al as moderately average contents in their compositions ranging from 1.856 to 2.661 apfu Fe_{tot} (14.9 to 20.7 wt.% FeO), from 1.909 to 1.934 apfu Ca (11.6 to 12.1 wt.% CaO), from 1.950 to 2.635 for apfu Mg (8.5 to 11.9 wt.% MgO), and from 1.551 to 1.844 apfu Al (8.8 to 10.2 wt.% Al_2O_3). These elements are considered as main constituents for amphiboles, beside Si which varies from 6.624 to 6.922 apfu Si (43 to 46.7 wt.% SiO_2), and considered as the major constituent in amphiboles (Table. 3.14). Elements Na, K, Ti, and Mn exhibits the minor consituents in the amphibole composition ranging from 0.411 to 0.418 apfu Na (1.39 to 1.42 wt.% Na_2O), from 0.078 to 0.137 apfu K (0.4 to 0.7 wt.% K_2O), from 0.057 to 0.096 apfu Ti (0.5 to 0.83 wt.% TiO_2), and from 0.041 to 0.051 apfu Mn (0.3 to 0.36 wt.% MnO), except Sc which is considered as trace element and

below the limit of detection (< 0.05 wt.% Sc_2O_3). The compostion of amphiboles in the metagabbro from Upper Høydalen (sample 05071903) differs from the compostion of the other samples. The amphiboles from Upper Høydalen exhibit lower contents of Fe_{tot}, K, Ti and Al and are relative enriched in Mg (2.635 *apfu* Mg) and F (1.0 wt.% F) (Table 3.14). In general, there is a relative large variation in the F contents of amphiboles ranging from low F (average 0.06 wt.% F) in the Bratterud sample (04071917) to 1.0 wt.% F in the Upper Høydalen sample (05071903) (Table 3.14). Other amphiboles from Storemyr 2 and Mjeltedalen 2a contain 0.6 wt.% and 0.4 wt.% F, respectively (Table 3.14).

3.6.4 Minor and trace elements in amphiboles determined by LA-ICP-MS

The amphiboles, which were measured by EPMA, were analysed also with LA-ICP-MS to get additional information about the concentrations of Sc and Be in these minerals, since amphiboles in the amphibolitic host rocks may be the source of Sc and Be in Tørdal pegmatites. The complete list of LA-ICP-MS trace element analysis of amphiboles is provided in Appendix 7.15 and average concentrations are summarized in Table 3.15.

Table 3.15. Average trace element concentrations of amphiboles in amphibolites and metagabbros determined by LA-ICP-MS. Number in parenthesis indicate the standard deviation. n = number of measurements.

Sample	05071903	04071917	04071903	02071918
Pegmatite	Upper Høydalen	Bratterud	Storemyr 2	Near Mjeltedalen 2a
Host rock	Coarse-grained gabbro	Medium-grained gabbro	Massive amphibolite	Amphibole-gneiss
Minerals	Amphibole	Amphibole	Amphibole	Amphibole
Crystals	4	3	3	3
n	17	14	8	9
Li (ppm)	103 (43)	49 (34)	<25.34	<25.34
Be	13 (6)	2.1 (2)	8 (1)	2.3 (4)
B	126 (3)	84 (19)	69 (2)	68.0
Sc	44 (3)	64 (16)	63 (2)	54.3 (7)
Ti	2697 (374)	4260 (1512)	3657 (410)	4147 (262)
V	<99.99	1414 (345)	757 (173)	734 (114)
Cr	755 (121)	<2.92	235 (27)	249 (28)
Co	66 (1)	53 (14)	61 (2)	63 (1)
Zn	268 (4)	308 (71)	250 (15)	210 (3)
Rb	6 (2)	<3.94	9 (5)	9 (8)
Sr	14 (2)	16 (3)	21 (2)	24 (13)
Y	16 (3)	100 (40)	83 (13)	51 (20)
Zr	12 (4)	11 (2)	13 (1)	14 (1)

In Figure 3.36 Sc concentrations in amphiboles are plotted against their Y concentrations. The data reveal a weak positive correlation whereby Sc increases with increasing Y contents. Highest average Sc and Y concentrations were detected in amphiboles from Bratterud (sample 04071917) and Storemyr 2 (sample 04071903) with average contents of 64 ppm Sc and 100 ppm Y, and 63 ppm Sc and 83 ppm Y, respectively. The amphibole from Mjeltedalen 2a (sample 02071918) has moderate Sc and Y concentrations of 54.3 ppm and 51 ppm, respectively. Lowest Sc and Y concentrations were found in the coarse-grained gabbro from Upper Høydalen (sample 05071903). The sample comprises average Sc and Y concentrations of 44 ppm and 16 ppm, respectively (Table 3.15).

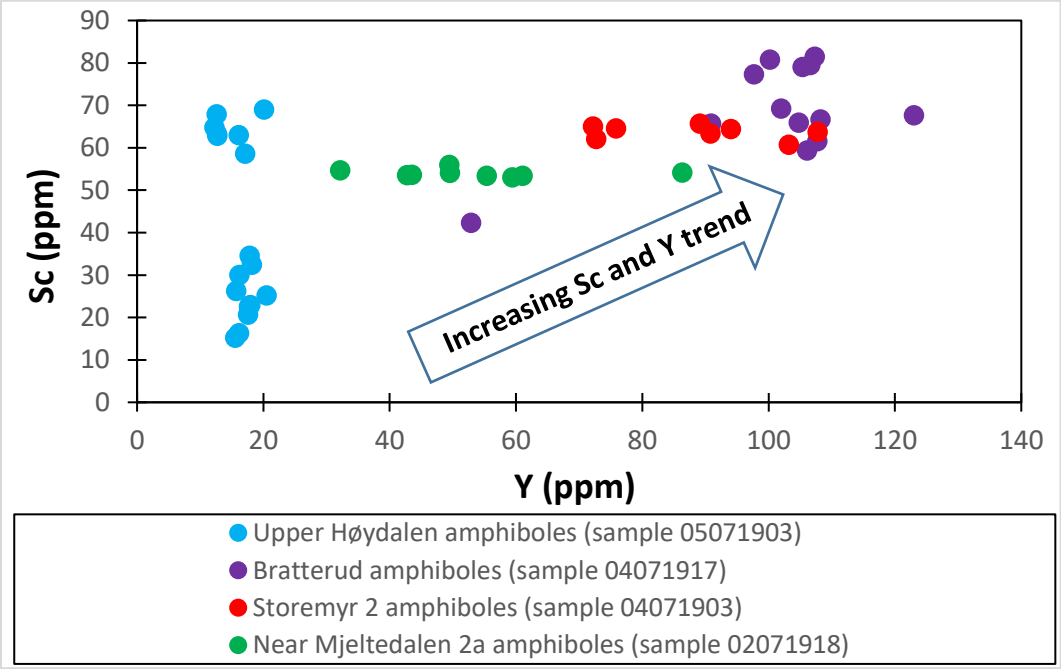

Fig. 3.37. Trace element concentrations of Sc and Y showing their distribution and enrichment in amphiboles from amphibolite host rocks of Tørdal pegmatites. Latter elements shows a weak positive correlated trend due to the increasing concentration of Sc and Y in amphiboles. Highest Sc and Y in amphiboles are found in host rocks of the Bratterud pegmatite while lowest are discovered in host rocks of Upper Høydalen pegmatite.

Beryllium concentrations are low in the investigated amphiboles. The amphiboles from Mjeltedalen 2a (sample 02071918) and Bratterud (sample 04071917) have very low average Be contents of 2.3 and 2.1 ppm, respectively (Table 3.15). Higher average Be contents were found in Storemyr 2 sample (sample 04071903) with average Be contents of 8 ppm, while the highest Be concentrations of 13 ppm were discovered in amphiboles in the metagabbro from the Upper Høydalen pegmatite (sample05071903).

Concluding, the average concentrations of Sc and Be in amphiboles are in general higher compared to biotites (ferroan phlogopites) from the same amphibolitic rocks (Tables. 3.12 and 3.15). Therefore, the amphiboles in the amphibolites are presumably the major source of Sc and Be found in the pegmatites, and not the biotites.

4. Discussion

4.1 Pegmatite-internal distribution of scandium and beryllium within Tørdal pegmatites

4.1.1 Scandium distribution within Tørdal pegmatites

In the following, the distribution of Sc within some Tørdal pegmatite bodies at pegmatite-internal (meter) scale is discussed. Figures 4.1, 4.2, 4.3 and 4.4 show average Sc concentrations of micas collected from different zones (border zone, wall zone, intermediate zone, albite replacement zone) of the Svåheii 3, Svåheii 2b, Svåheii 2a and Bratterud pegmatites to illustrate the Sc distribution within these pegmatites. These pegmatites are located in SW (Svåheii 3, Svåheii 2b, Svåheii 2a) and NE (Bratterud) of the Tørdal pegmatite field (Fig. 4.10).

At the Svåheii 3 locality, ferroan muscovite and siderophyllite from the outer and inner wall zone have average concentrations of 990 ppm Sc and 417 ppm Sc, respectively (Fig. 4.1). The ferroan muscovite from the intermediate zone close to the pegmatite core contains much less Sc (mean 48 ppm Sc). The data indicate a continuously decrease of the Sc concentrations of micas from the pegmatite margin towards the core of the pegmatite. This can be explained by the fact that Sc is compatible in micas and becomes preferentially incorporated in the early crystallized micas. With progressive pegmatite and mica crystallization, Sc becomes therefore gradually depleted in the remaining pegmatite melt and, thus, micas crystallized during later stages contain systematically less Sc.

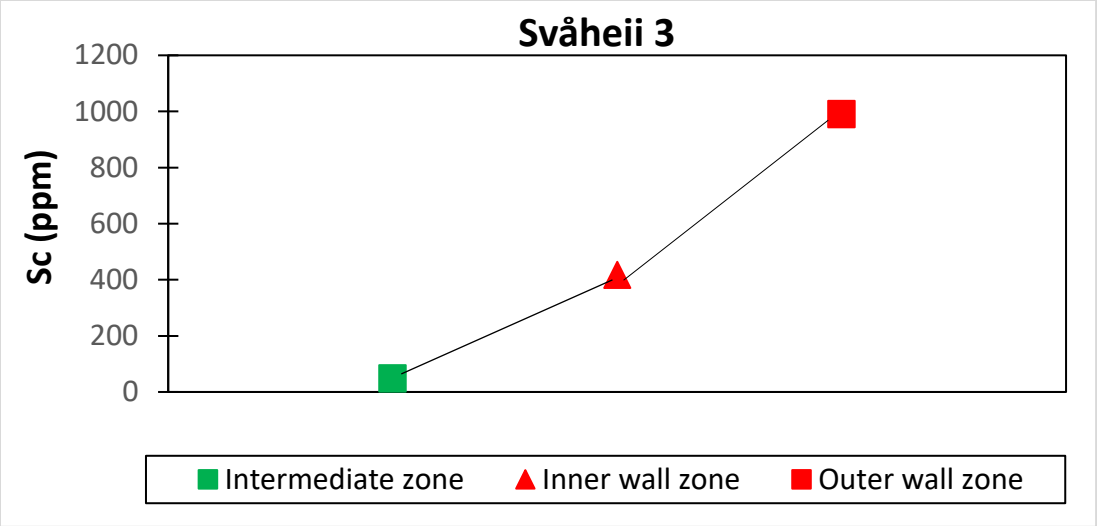

Fig. 4.1. Average Sc concentrations of micas collected from the outer wall zone, inner wall zone and intermediate zone of the Svåheii 3 pegmatite. The Sc decreases continuously from the margin (wall zone) towards the inner part (intermediate zone) of the pegmatite body. Squares are dioctahedral micas, while triangles are trioctahedral micas.

The strong decrease of average Sc concentrations of micas from the pegmatite margin towards the core applies also for the other two investigated Svåheii localities. Muscovites from wall zone (mean 1125 ppm Sc) and from albite replacement zone (mean 38 ppm Sc) of the Svåheii 2b pegmatite show the most drastic decrease of Sc concentrations among the studied Tørdal pegmatites (Fig. 4.2). The Sc decrease is less pronounced in the micas from the Svåheii 2a pegmatite (Fig. 4.3).

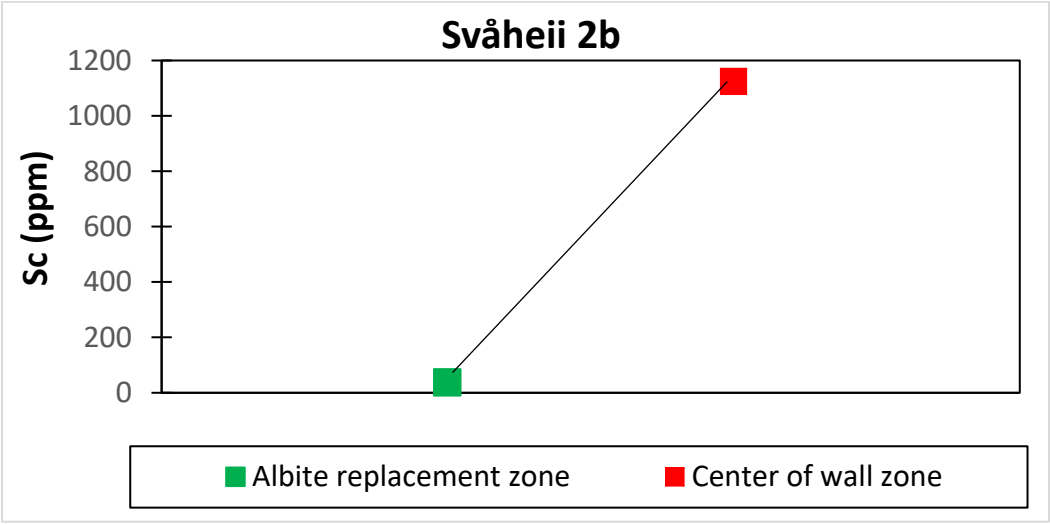

Fig. 4.2. Average Sc concentrations of micas collected from the center of wall zone and albite replacement zone of the Svåheii 2b pegmatite. A significantly decrease of Sc from the center of wall zone towards albite replacement zone is present of the pegmatite. Squares are dioctahedral micas, while triangles are trioctahedral micas.

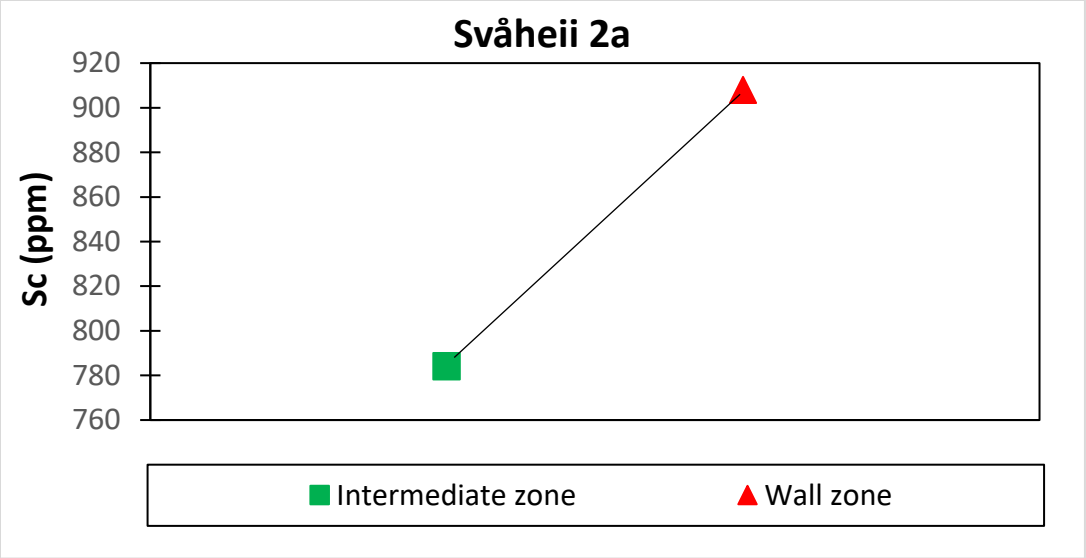

Fig. 4.3. Average Sc concentrations in micas from intermediate zone and wall zone of the Svåheii 2a pegmatite. The Sc decreases continuously from wall zone towards intermediate zone, similar as Figs. 4.1 and 4.2. Squares are dioctahedral micas, while triangles are trioctahedral micas.

The Bratterud pegmatite from the NE of the pegmatite field shows a similar Sc decrease from the margin to the core as the Svåheii pegmatites (Fig. 4.4). Siderophyllite from the border zone of the Bratterud pegmatite comprises highest average Sc concentrations (mean 683 ppm). The ferroan muscovite from the wall zone contains in average 506 ppm Sc and the ferroan muscovite from the intermediate zone 312 ppm.

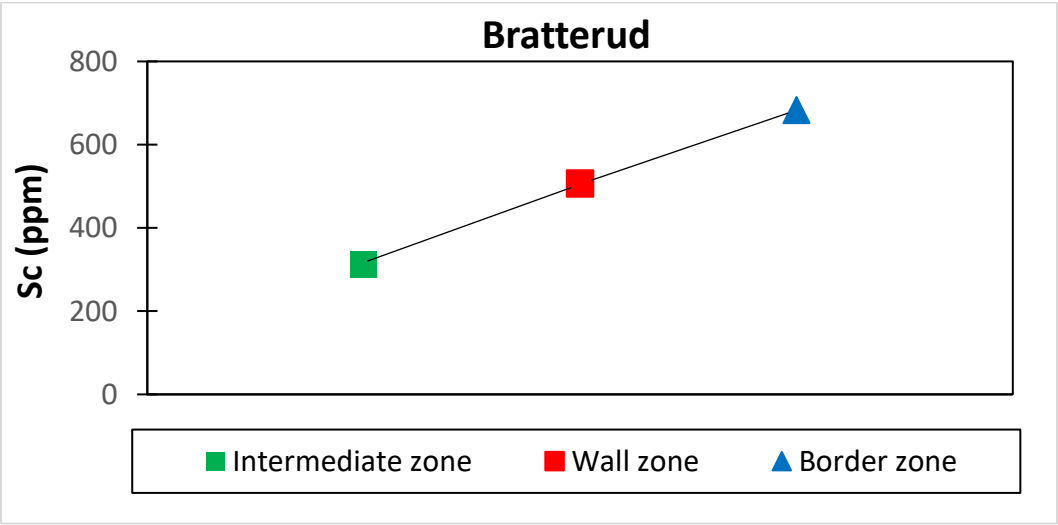

Fig. 4.4. Average Sc concentration in micas from border zone, wall zone and intermediate of the Bratterud pegmatite. Scandium concentrations decreases from the margin towards the center of the Bratterud pegmatite. Squares are dioctahedral micas, while triangles are trioctahedral micas.

The Sc decrease observed within the Tørdal pegmatites applies also for other Sveconorwegian pegmatites as, for example, the Evje-Iveland field as illustrated by Rosing-Schow et al. (2018) for the Solås pegmatite. The Evje-Iveland pegmatite field lies 80 km SW of Tørdal and is similar in age and tectono-metamorphic setting. According to Rosing-Schow et al. (2018), the magnesian siderophyllites from the outer and inner intermediate zone have average Sc concentrations of 146 ppm and 139 ppm, respectively. The ferroan muscovite from the core of the Solås pegmatite contains as low as 13 ppm Sc. Here again, the average Sc concentrations in micas decreases from the margin towards the core of the pegmatite reflecting the decreasing Sc content in the remaining pegmatite melt during progressing pegmatite crystallization. The findings made in this study and by Rosing-Schow et al. (2018) suggest that the decrease of Sc in fractionating pegmatite melts is a common process.

That the Sveconorwegian pegmatites crystallized from the outer margin inwards is supported by the fact that the K/Rb ratio of micas decreases from the edge to the center of the pegmatites. It indicates that the Rb increases in the fractionating pegmatite melt as it does for any fractionating melt of granitic composition (e.g. Chappell and White, 1992). The Svåheii 2b pegmatite, for example, contain wall-zone muscovite with a K/Rb ratio of about 25. The ratio decreases in muscovite from the intermediate zone to about 15. Similar observations have been made for the Evje-Iveland pegmatites (Müller et al., 2015) and for the Froland pegmatites (Rosing-Schow et al., 2018). The Froland field is another Sveconorwegian pegmatite field about 60 km SSW of the Tørdal.

However, in the Svåheii 3 pegmatite, siderophyllite from wall zone contains a lower K/Rb ratio of about 10 than the ferroan muscovite from intermediate zone with ratio of about 14. A similar finding has been made for the Svåheii 2b pegmatite, where the magnesian siderophyllite from wall zone has a K/Rb ratio of 10, and those of the ferroan muscovite from the intermediate zone is about 22. Rosing-Schow`s et al. (2018) made similar observations for micas of the Solås pegmatite in Evje-Iveland: the K/Rb ratio of magnesian siderophyllite from intermediate zone is lower compared to the K/Rb ratio of the ferroan muscovite from the core of the pegmatite. In these cases, the higher K/Rb ratio is probably due to the higher distribution coefficient for Rb in magnesian siderophyllite compared to ferroan muscovite (Joliff et al., 1992) and not a result of reverse pegmatite crystallization.

Steffensen (2018) investigated Sc concentrations of garnets from different zones of Tørdal pegmatites (pegmatite scale) and the Sc distribution within garnet crystals (crystal scale). This study showed that garnets from wall zones of the Heftetjern 1, Heftetjern 2, Upper Høydalen 1 and Svåheii 2a pegmatites have very high average Sc contents of 1568, 1895, 1460, and 987 ppm Sc, respectively. The high average Sc concentration of the wall-zone garnets strongly decreases down to 15 ppm Sc in garnet from late-stage albite replacement zone in the central part of the Upper Høydalen 1 pegmatite, for example. Thus, a higher amount of Sc is incorporated into wall zone garnets during early stages of the pegmatite crystallization, while Sc in garnets that crystallized at later stages is much lower. Steffensen (2018) made also another observation regarding the Sc behavior in pegmatite melts. The highly Sc-rich wall zone garnets of the Heftejtern 1, Heftetjern 2, Upper Høydalen 1 and Svåheii 2a pegmatite contain crystal cores which are richer in Sc than the crystal margins. Thus, higher amounts of Sc were incorporated during initial garnet crystallization (core), while at later stages less Sc was incorporated into the crystal (margin). This indicates that the Sc decrease observed at pegmatite scale is also observed at crystal scale, which documents a shorter period of crystallization, the period of the crystallization of the wall zone.

As discussed above, Sc is compatible in mica and garnet as well and becomes depleted in the remaining pegmatite melt with progressing fractional crystallization. Scandium is a compatible element in micas and garnets with distribution coefficients (K_D) >1. The K_D values depend, however, mainly on the composition of the pegmatite melt (Williams-Jones and Vasyukova, 2018). Bedard (2005, 2007, 2014) illustrated that low MgO contents in the melt lead to higher K_D values for Sc, which is the case for MgO-poor Tørdal pegmatite melts. By assuming the silicic melts are similar in composition to rhyolite melts, the highest K_D values for Sc are as high as 20 for mica (Mahood and Hildreth, 1983; Nash and Crecraft, 1985; Bea et al., 1994), 63 for garnet (Sisson and Bacon, 1992) and as low as 0.01 for plagioclase (Bacon and Druitt, 1988; Druitt and Bacon, 1988). Thus, in these melts, which contain initially high Sc concentrations most of the Sc will be incorporated into micas and garnets, while very low Sc will be incorporated into plagioclase.

In the following, the distribution coefficient of Sc between coexisting micas and garnets originating from the same zone (border zone, wall zone, intermediate zone, albite replacement zone) of some studied Tørdal pegmatites is discussed. For the distribution coefficient determination the average Sc concentrations of micas were compared to the average Sc

concentrations of coexisting garnets (Table 4.1). The Sc values of coexisting garnets were previously determined by Steffensen (2018). In Figure 4.5, average Sc concentrations of coexisting mica and garnet pairs are plotted. The data reveal a relative good correlation with the distribution coefficient of Sc-in-mica : Sc-in-garnet of 0.85 : 1. Thus, slightly more Sc is incorporated into garnet than in coexisting mica. Important to note is, that the distribution coefficient remains constant with progressive pegmatite crystallization: coexisting garnets and micas from late-stage albite replacement zones exhibit a similar distribution coefficient, as coexisting garnets and micas from wall zones, despite much lower average Sc concentrations.

Table 4.1. Average Sc concentrations in coexisting garnets and micas of Tørdal pegmatits their distribution ratios.

	Mica		**Garnet**		
Pegmatite locality	**Zone**	**Average Sc (ppm)**	**Zone**	**Average Sc (ppm)**	**Ratio co-genetic Mica/Garnet**
Svåheii 2a	Wall zone	908	Wall zone	987	0.92
Grønliheii	Close to contact	149	Wall zone	60	2.48
Mjeltedalen 2a	Close to upper contact	294	Wall zone	295	1.00
Storemyr 1	Close to contact	339	Wall zone	338	1.00
Storemyr 2	Close to lower contact	554	Wall zone	529	1.05
Heftetjern 2	Close to contact	1576	Wall zone	1895	0.83
Upper Høydalen 12	Albite zone	3	Albite zone	15	0.20
Bratterud	Close to contact	595	Wall zone	119	5.00

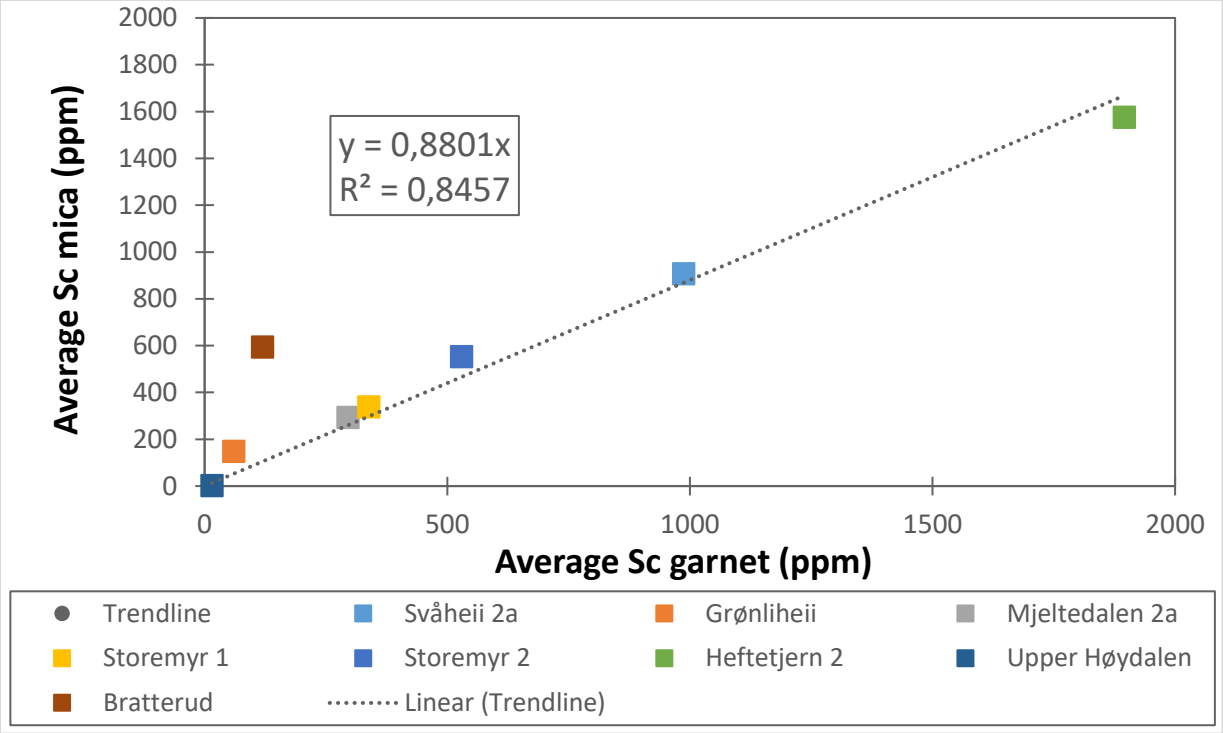

Fig. 4.5. Diagram of the average Sc concentrations of garnets versus the average Sc concentrations in coexisting mica for selected Tørdal pegmatites. The data show positive correlation closely to the 1:1 ratio (0.85:1), which indicate Sc incorporates slightly more in co-existing garnet instead of mica.

Concluding, the observed decrease of average Sc concentrations in micas of Tørdal pegmatites (Svåheii 2a, Svåheii 2b, Svåheii 3, Bratterud) at pegmatite scale (meter) is a result of pegmatite-internal melt fractionation. The Sc decrease is accompanied by a decreasing K/Rb ratio. At the early stage of pegmatite crystallization, wall zone micas incorporate large amounts of Sc. During later stages lower amounts of Sc are incorporated into micas because the remaining pegmatite melt contain less and less Sc. This is because early formed wall zone micas consumed most of the Sc of the melt. The decrease of Sc in the remaining pegmatite melt is not only reflected in mica chemistry but also garnet chemistry. Garnets will incorporate slightly more Sc than coexisting micas, because Sc is slightly more compatible in garnet than in mica. The Sc decrease during pegmatite melt fractionation applies also to other Sveconorwegian pegmatites, such as Evje-Iveland pegmatites, as supported by previous studies by Rosing-Schow et al. (2018).

4.1.2 Beryllium distribution within Tørdal pegmatites

In the following, the Be-minerals beryl and gadolinite-(Y) from different zones (wall zone, intermediate zone, albite replacement zone) of Tørdal pegmatites and the variation of their minor

and trace element concentrations (Na, Li, Cs, and Fe^{2+}) are discussed in order to better understand the pegmatite-internal distribution of Be and other incompatible elements.

Beryl is only present in the chemically evolved pegmatites of Tørdal pegmatite field, which comprise the localities of Upper Høydalen, Lower Høydalen, Heftetjern 1, Heftejtern 2, Skardsfjell, Svåheii 2b, Sjauset and Bratterud (Fig. 4.10; Table 3.1). Beryl usually occurs in the intermediate zone and core of these pegmatites and in the albite replacement zones (Table 3.1). Among these evolved pegmatites, the Upper and Lower Høydalen pegmatites are most abundant in beryl and have also the greatest diversity of beryl in terms of color. Green, yellow and pink beryls are found here (Tables 3.1, 3.3). The greenish beryl represents the first beryl generation, which crystallized in the outer intermediate zone. Yellow beryl crystallized mainly in the inner intermediate zone and pink beryl (var. morganite) in the late-stage albite replacement zone. No beryl occurs in the wall or border zones of the Upper and Lower Høydalen pegmatites. The same observation applies also for the other beryl-bearing Tørdal pegmatites (Heftetjern 1, Heftetjern 2, Skardsfjell, Sjauset and Bratterud) (Fig. 4.10). Pink beryls are typically associated with the latest stage of pegmatite formation, as for example, described from the Bikita pegmatites in Zimbawe (Černý et al., 2003). Sardi and Heimann (2014), for example, showed that yellow beryls crystallized mainly after green beryls from pegmatites in the Pampeana Pegmatite Province of the Velasco district, Argentina.

Beryl crystallization requires a certain concentration of Be in the pegmatite melt (London and Evensen, 2002; London, 2015). Beryllium is an incompatible element, which prefers to stay in the pegmatite melt instead of being incorporated into minerals (London, 2008; London, 2015). In general, concentrations of incompatible elements, such as Be, increase in the melt with progressing fractional crystallization. However, a number of Tørdal pegmatites contain Be-bearing gadolinite-(Y) in the wall zone. Thus, Be was incorporated in this mineral already at an early stage of pegmatite formation consuming parts of Be in the pegmatite melt. This indicates that the gadolinite-(Y)-bearing pegmatites were initially relative rich in Be. According to London and Evensen (2002), Be saturation of pegmatite melts for beryl crystallization is about 35 ppm Be. Because beryl first appears in the outer intermediate zone, it means that already shortly after gadolinite-(Y) stopped to crystallize in the wall zone, there was again or still enough Be (≥35 ppm) in the pegmatite melt to crystallize beryl. Gadolinite-(Y) stopped to crystallize presumably because

there was not enough Y and/or Fe^{2+} in the pegmatite melt. But there was enough Be in the pegmatite melt that beryl could crystallize in the outer intermediate zone and finally as pinkish beryl (var. morganite) in the albite replacement zones of the Upper and Lower Høydalen pegmatites.

Gadolinite-(Y) is also observed in Tørdal pegmatites where no beryl is present. These localities are Svåheii 2a, Svåheii 3, Grønliheii, Storemyr 2, and Storemyr 1 (Fig. 4.10; Table 3.1). Since gadolinite-(Y) is mainly observed in the wall zones, latter mineral started to crystallize during initial stages of pegmatite crystallization, where the pegmatite melt contained enough Be, Y and/or Fe^{2+} to form this mineral. However, during later stages the Be, Y and/or Fe^{2+} concentrations in the pegmatite melt were too low to crystallize gadolinite-(Y). The absences of beryl in these Tørdal pegmatites indicates that there was not enough Be in the pegmatite melt (< 35 ppm Be) to crystallize beryl. Thus, the bulk Be concentrations in these Tørdal pegmatites must have been lower than the Heftetjern (Heftetjern 1, Heftetjern 2) and Høydalen (Upper and Lower Høydalen) pegmatites.

However, a number of beryl-bearing Tørdal pegmatites, such as Skardsfjell, Svåheii 2b, Sjauset, and Bratterud (Fig. 4.10; Table 3.1), contain only beryl and no gadolinite-(Y). These pegmatite melts were probably enriched in Be, but had not enough Y and/or Fe^{2+} to form gadolinite-(Y). Afterwards, with progressing pegmatite crystallization, the Be concentrations in the pegmatite melt increased and reached the limit for beryl crystallization (>35 ppm Be) when the intermediate zone crystallized.

Figures 4.6, 4.7, 4.8 and 4.9 illustrate the distribution of Na+Li+Cs and Fe^{2+} concentrations in green, yellow and pink beryls found in the intermediate and albite replacement zones of the Upper and Lower Høydalen pegmatites. The two pink beryls from albite replacement zones of the Upper Høydalen pegmatite, representing the last crystallization stage of the pegmatite crystallization, contain significantly higher Na+Li+Cs (mean 10457 ppm and 10019 ppm) and very low Fe^{2+} (<26 ppm Fe^{2+}) concentrations compared to green and yellow beryls from the intermediate zone. Similar observations are made for Lower Høydalen samples, where the pinkish beryl from the albite replacement zone contains higher Na+Li+Cs (mean 8318 ppm) and very low Fe^{2+} (<26 ppm Fe^{2+}) concentrations compared to the yellow beryl from the intermediate zone. The data reveal a continuous increase of the Na+Li+Cs and decrease of Fe^{2+} with progressing beryl crystallization.

The decrease of Fe^{2+} concentrations from the pegmatite margin towards the core and, thus, with progressing pegmatite crystallization, is documented, for example, for the Upper Høydalen pegmatite by mica chemistries (Rosing-Schow et al., 2018). Fe-rich micas (i.e. biotite) occur only at the pegmatite margin, while Fe-poor micas (i.e. muscovite, lepidolite) are found in the inner parts of the pegmatite. This indicates that Fe^{2+} concentrations decrease in the melt with progressing pegmatite crystallization, which is reflected in the beryl and mica chemistries.

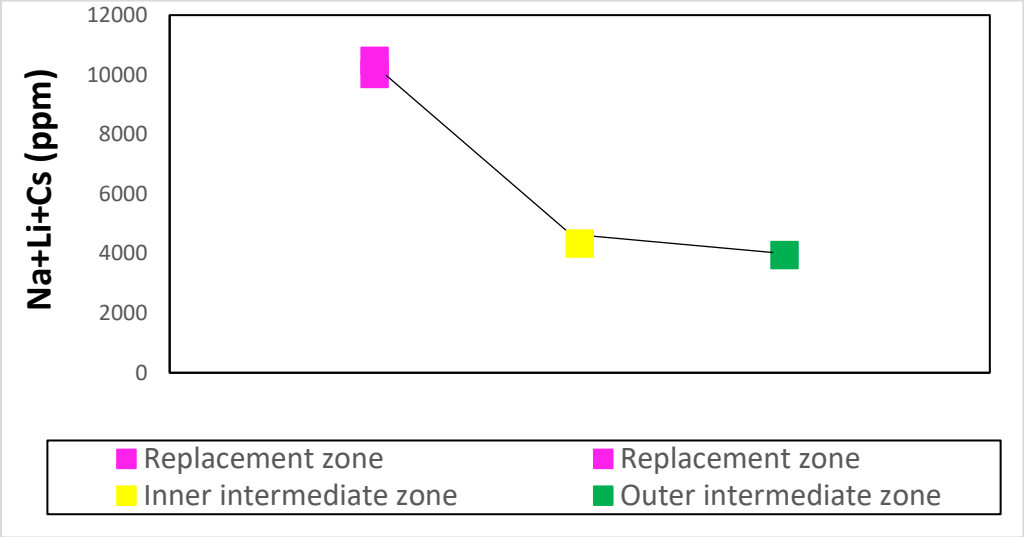

Fig. 4.6. Average Na+Li+Cs concentrations (ppm) of green, yellow and pinkish beryls from the outer intermediate zone, inner intermediate zone and albite replacement zone of the Upper Høydalen pegmatite. The Na, Li and Cs in beryl increases continuously from the outer intermediate zone towards the inner part of the pegmatite body.

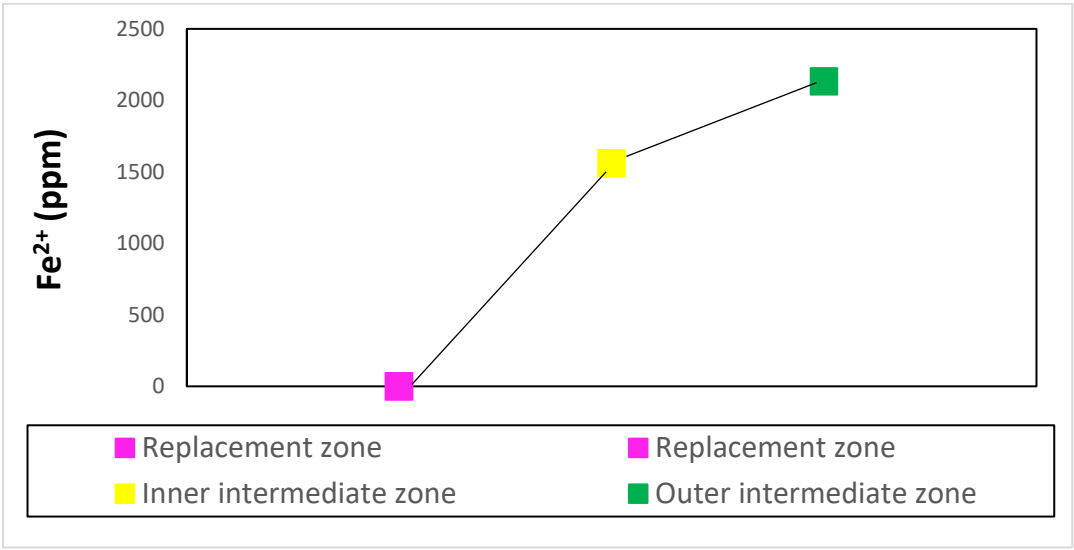

Fig. 4.7. Average Fe^{2+} concentrations (ppm) of green, yellow and pinkish beryls from the outer intermediate zone,

inner intermediate zone and albite replacement zone of the Upper Høydalen pegmatite. The Fe^{2+} decreases continuously from the outer intermediate zone towards the inner part of the pegmatite body.

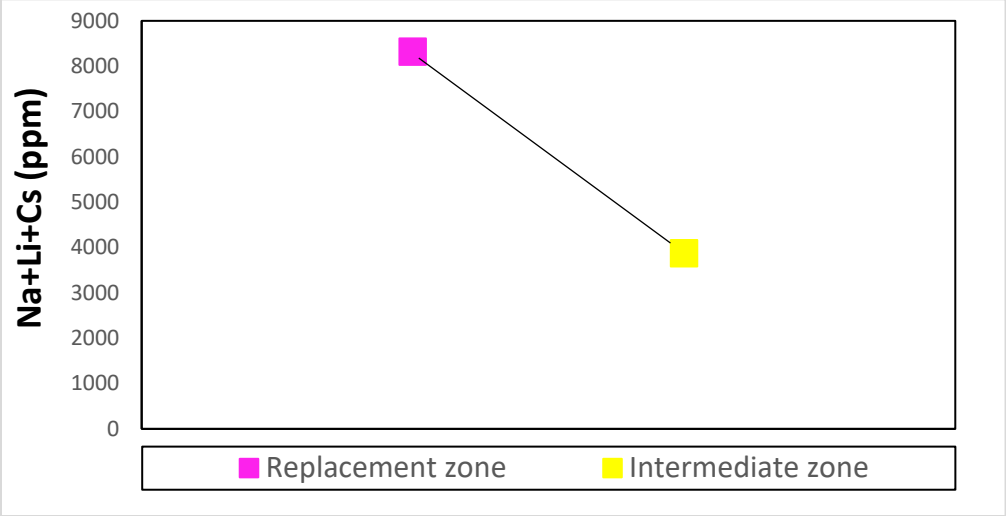

Fig. 4.8. Average Na+Li+Cs concentrations (ppm) of yellowish-green and pinkish beryl from the intermediate zone and replacement zone of the Lower Høydalen pegmatite. The Na, Li and Cs in beryl increases continuously from the intermediate zone towards the inner part of the pegmatite body.

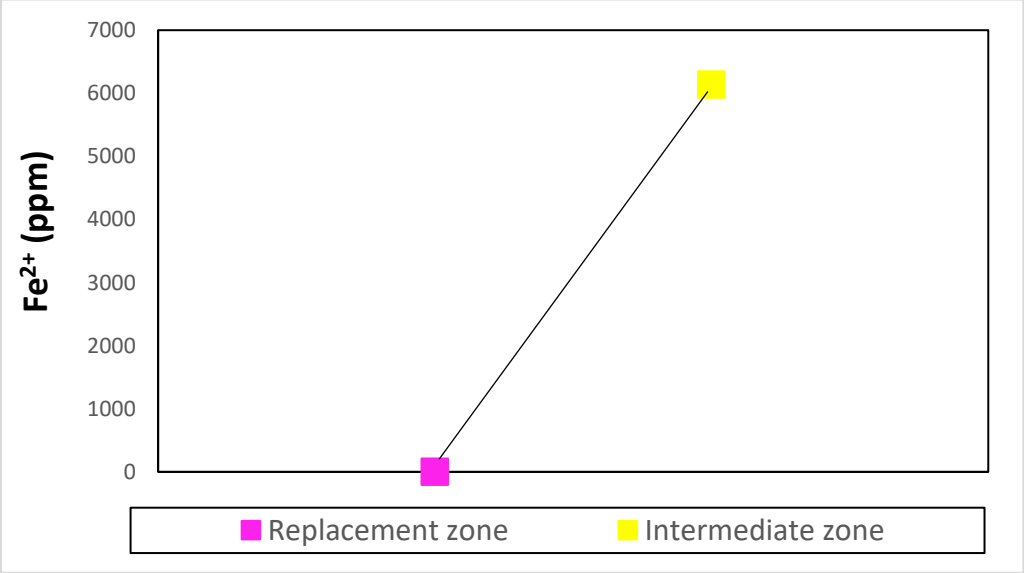

Fig. 4.9. Average Fe^{2+} concentrations (ppm) of yellowish-green and pinkish beryl from the intermediate zone and replacement zone of the Lower Høydalen pegmatite. The Fe^{2+} decreases continuously from the intermediate zone towards the inner part of the pegmatite body.

The observed color variants of the studied beryls reflect the chemical evolution of the pegmatite melts, where the chemically primitive beryls are green, moderate evolved ones are more yellowish, and the most evolved beryls are pink (Figs. 3.12, 3.13, 3.14). The different colors are caused by the variations in Fe^{2+}, Fe^{3+} and Mn^{2+} concentrations and the oxidation state of these elements. According to London (2015), the coloring of the greenish beryls is due to the presence of Fe^{2+} and Fe^{3+}, while yellow coloring is due to Fe^{2+} only. Pinkish beryls have their coloring from trace amounts of Mn^{2+} (London, 2015). The increasing Li and Cs in beryl reflects the increase of these incompatible elements in the pegmatite melt, while the decrease of Fe^{2+} in beryl is due to the consumption of compatible Fe^{2+} by other rock-forming minerals (i.e. mica and garnet). Thus, beryls, which crystallized during later stages, contain significantly higher Na, Li and Cs, and less Fe^{2+}. Similar behavior of Na, Li, and Cs is observed in beryls from the Bikita granite pegmatites, Zimbawe (Černý et al., 2003). These authors showed that Na, Li and Cs concentrations in beryl increase from less evolved exterior zones towards the evolved interior zones of the Bikitia pegmatites. Increasing Na, Li and Cs together with decreasing Fe^{2+} concentrations, which reflects the chemical evolution of beryl and, thus, of the pegmatite melt, were also observed from the Western Carpathians, Slovakia (Uher et al., 2010). Černý et al. (2003) showed that concentrations of Na, Li and Cs in pink beryls increases from the alkali-poor cores towards alkali-rich rims of the crystals. This result shows that the increase of Na, Li and Cs can be observed also at crystal scale. Again, these elements behave incompatible in pegmatite melts, becoming more and more enriched during fractionation.

Concluding, observations of Be-minerals at pegmatite scale document that gadolinite-(Y) occurs only in the wall zones of the Tørdal pegmatites, while beryl is only present in the intermediate zones and/or albite replacement zones. Concentrations of Be increase in the fractionating pegmatite melt which is accompanied by increasing Na, Li, and Cs and decreasing Fe^{2+} documented by the chemistry of beryl from different zones of the same pegmatite. The formation of gadolinite-(Y)-bearing and beryl-bearing Tørdal pegmatites is due to initially high Be contents of the pegmatite melts. Gadolinite-(Y) of wall zone formed already at an early stage of pegmatite crystallization, when enough Be, Y and/or Fe^{2+} was available. During the formation of the intermediate zones in these pegmatites, the melts reached the limit for Be saturation (>35 ppm Be) and crystallized beryl. Based on these observations the Tørdal pegmatites are divided into four types of Be-bearing pegmatites:

- Gadolinite-(Y)- and beryl-bearing pegmatites: Upper Høydalen, Lower Høydalen, Heftetjern 1, and Heftetjern 2.
- Gadolinite-(Y)-bearing pegmatites: Storemyr 1, Storemyr 2, Svåheii 2a, Svåheii 3, and Grønliheii.
- Beryl-bearing pegmatites: Skardsfjell, Sjauset, Svåheii 2b, and Bratterud.
- None Be-bearing pegmatites: Kleppe Quarry, Mjeltedalen 2a, Buvatnet, and Lislegrønlia.

4.2 Regional distribution of Sc and Be across Tørdal pegmatite field

The map of Tørdal pegmatite field shown in Figure 4.10 illustrates the regional distribution of average Sc concentrations in coexisting micas and garnets from the wall zones (where data are available) together with occurrences of beryl, bazzite and gadolinite-(Y). Both micas and garnets were collected mainly from the wall zone or near the contact of the pegmatite to host rock. The provided average Sc concentrations of garnets are from Steffensen (2018). Some Tørdal pegmatites contained only micas or garnets, and for those, average Sc concentrations of one of these minerals could be provided in Figure 4.10. For some pegmatites, such as Heftetjern 1, Upper Høydalen, Storemyr 3 and Sjauset pegmatites, average Sc concentrations of both mica and garnet were determined, but here these minerals were not coexisting because they occur in different mineralogical zones of the pegmatites. Anyway, these data are added to the map to provide a broader set in order to better illustrate the regional Sc distribution across the Tørdal pegmatite field. Detected average Sc concentrations of micas and garnets are classified as low (14 to 183 ppm Sc), intermediate (183 to 621 ppm Sc), moderate (621 to 1137 ppm Sc), high (1137 to 1526 ppm Sc) and very high (1526 to 2806 ppm Sc). Beside the regional distribution of Sc, the map shown in Figure 4.10 also illustrates the regional distribution of Be through the presence of the Be-minerals beryl, gadolinite-(Y), and bazzite (Table 3.1).

Mica and coexisting garnet of the chemically evolved and complex Heftetjern 2 pegmatite have the highest average Sc concentrations (mean 1576 ppm and 1895 ppm, respectively) which classifies the pegmatite as very Sc-rich. This finding confirms previous studies by Bergstøl and Juve (1988) and Juve and Bergstøl (1990) who described the Be-Sc silicate bazzite from this locality. The pegmatite is also home for several other Sc minerals (Table 1.4). Except the Heftetjern pegmatite, the only observed Sc-mineral from other Tørdal pegmatites is bazzite from the chemically evolved and complex Høydalen pegmatites (Upper and Lower Høydalen) (Mindat,

2020b; Mindat, 2020c). The Høydalen pegmatites are only situated c. 750 m slightly E from the Heftetjern pegmatite (Fig. 4.10). The Heftetjern and Høydalen pegmatites are, in fact, the most Be-rich pegmatites of Tørdal pegmatite field, since they are the only Tørdal pegmatites which contain the highest amount and diversity of studied Be-minerals (beryl, gadolinite-(Y), and bazzite) and other Be-bearing minerals, such as betrandite, boseite, milarite, etc, (Mindat, 2020b; Mindat, 2020c). Therefore, the chemically evolved and complex Heftetjern and Høydalen pegmatites are considered as the most Sc- and Be-rich pegmatites of Tørdal pegmatite field.

The Skardsfjell pegmatite, which is situated c. 1500 m W from the Heftetjern pegmatite, is considered as highly Sc- and moderately Be-rich pegmatite since it contains mica with average Sc concentration of 1506 ppm Sc (Rosing-Schow et al., 2018) and beryl (mean 893 ppm Sc; Table 3.4), both collected from the intermediate zone (Fig. 4.10).

Another moderately Be-rich pegmatite, where beryl is present, is the Sjauset pegmatite situated c. 1800 m NE from the Heftetjern and c. 1500 m N from the Høydalen pegmatites (Fig. 4.10). The Sjauset pegmatite is intermediately Sc-rich with mean 398 ppm Sc in mica from the intermediate zone and mean 72 ppm Sc in garnet from the wall zone. Micas from the Sjauset and Heftetjern 2 have the lowest detected K/Rb ratios of c. 8 to 6, which indicate that both are the chemically most evolved pegmatites of the Tørdal field (Fig. 4.10). According to Segalstad and Eggleston (1993) the Sjauset and Heftetjern 2 pegmatites are situated in the green K-feldspar zone and contain significantly high amounts of green K-feldspar (var. amazonite), which further identify them as chemically evolved pegmatites (Table 3.1). This applies also for the Skardsfjell and Høydalen pegmatites, which are as well, situated in the green K-feldspar zone. Thus, the Heftetjern, Høydalen, Skardsfjell and Sjauset pegmatites are considered as the chemically most evolved pegmatites of Tørdal pegmatite field and the most Sc- and Be-rich pegmatites, except the Sjauset pegmatite, which is classified as intermediate Sc-rich.

Northeast of the amazonite-bearing and chemically evolved pegmatites, at the NE edge of Tørdal pegmatite field, the Bratterud pegmatite occurs (c. 2300 m NE from Sjauset pegmatite) which contains white K-feldspar (Fig. 4.10). The pegmatite is considered as chemically evolved pegmatite since boulders of albite (var. cleavelandite) were found, which indicates the presence of albite replacement zones. Such albite replacement zones are also present in the Heftetjern, Høydalen and Skardsfjell pegmatites (Table 3.1). Presence of altered beryl and average Sc

concentrations of 595 ppm in mica and 119 ppm in garnet classify the Bratterud pegmatite as moderately Be- and intermediately Sc-rich pegmatite (Fig. 4.10; Table 3.1). Mica from this pegmatite has a K/Rb ratio of c. 28, which is higher compared to micas from Sjauset and Heftetjern 2. This indicates that the Bratterud pegmatite is less evolved than Sjauset and Heftetjern 2. This might indicate that Sc and Be concentrations, on a regional scale (kilometer), decreases with decreasing fractionation degree of pegmatite melts.

Southwest of the amazonite-bearing pegmatites (c. 1500 m) are the Storemyr pegmatites (localities Storemyr 1, Storemyr 2, and Storemyr 3) which are situated in the pink K-feldspar zone, which is considered as the zone of primitive pegmatites (Segalstad and Eggleston, 1993). Coexisting mineral pairs exhibit average Sc concentrations of 339 ppm for mica and 338 ppm for garnet from the Storemyr 1 locality, and 554 ppm in mica and 529 ppm in garnet from the Storemyr 2 locality. Except the Storemyr 3 locality, which does not contain any Be-minerals, the Storemyr 1 and Storemyr 2 localities exhibit gadolinite-(Y) but no beryl. Thus, the Storemyr pegmatites are classified as intermediately Sc- and Be-rich pegmatites. The K/Rb ratios of micas vary from c. 30 to 20, which indicates a relative low fractionation degree of the melts compared to the amazonite-bearing pegmatites in the NE. Here again, the Sc and Be concentrations decrease with the decreasing fractionation degree of pegmatite melts at regional scale (Fig. 4.10).

Further SW, c. 2-3 km from the Storemyr pegmatites, the Grønliheii and Mjeltedalen 2a are located. The average Sc concentrations (Grønliheii: mean 149 ppm Sc in mica, 60 ppm Sc in garnet; Mjeltedalen 2a: mean 249 ppm Sc in mica, 295 ppm Sc in garnet) are lower than those of the Storemyr pegmatites indicating a continuous decrease from the Heftetjern-Høydalen area towards SW. The Grønliheii and Mjeltedalen 2a pegmatites contain the lowest Sc concentrations detected in coexisting mineral pairs. The Mjeltedalen 2a body is the most primitive pegmatite in Tørdal field since mica from this pegmatite has the highest K/Rb ratio of c. 40. Also garnets from this pegmatite have a primitive character being Fe-rich and Mn-poor (Steffensen, 2018). Except the intermediate Be-rich Grønliheii pegmatite, which contains gadolinite-(Y), the Mjeltedalen 2a is considered as the pegmatite with the lowest Be together with Buvatnet, Kleppe quarry, Lislegrønlia and Storemyr 3 pegmatites since they do not contain Be-minerals (Fig. 4.10). These pegmatites are also considered as low to intermediate Sc-rich pegmatites, except Lislegrønlia, which is moderately Sc-rich (Fig. 4.10). All these pegmatites are situated in the pink K-feldspar

zone, which characterizes them as primitive pegmatites (Segalstad and Eggleston, 1993). Summarizing, the chemically most primitive Tørdal pegmatites contain the lowest Sc and Be concentrations, except the intermediate Be-rich Grønliheii and moderately Sc-rich Lislegrønlia pegmatites.

At the SW edge of Tørdal pegmatite field, c. 1 km SW of the Grønliheii pegmatite, the fractionation degree of pegmatite melts increases together with Sc and Be concentrations manifested by the mineralogy and mineral chemistry of the Svåheii pegmatites (Fig. 4.10). The cleavelandite-bearing, chemically evolved and complex Svåheii 2b pegmatite is considered as moderately Sc- and Be-rich. The reason why is because the Svåheii 2b locality contain beryl, while average Sc concentrations of coexisting mica and garnet of the Svåheii 2a locality are 908 ppm and 987 ppm Sc, respectively (Fig. 4.10). Highest average Sc concentration are discovered in the mica from the Svåheii 2b locality (1125 ppm Sc). Gadolinite-(Y) is present in both the Svåheii 2a and Svåheii 3 localities. The low K/Rb ratio detected in mica from the Svåheii 2a locality, which is about c. 10, identify the pegmatite as relative evolved. Again, this confirms the statement made above, that Sc and Be concentrations is accompanied by the fractionation degree of pegmatite melts (K/Rb ratio) on a regional scale.

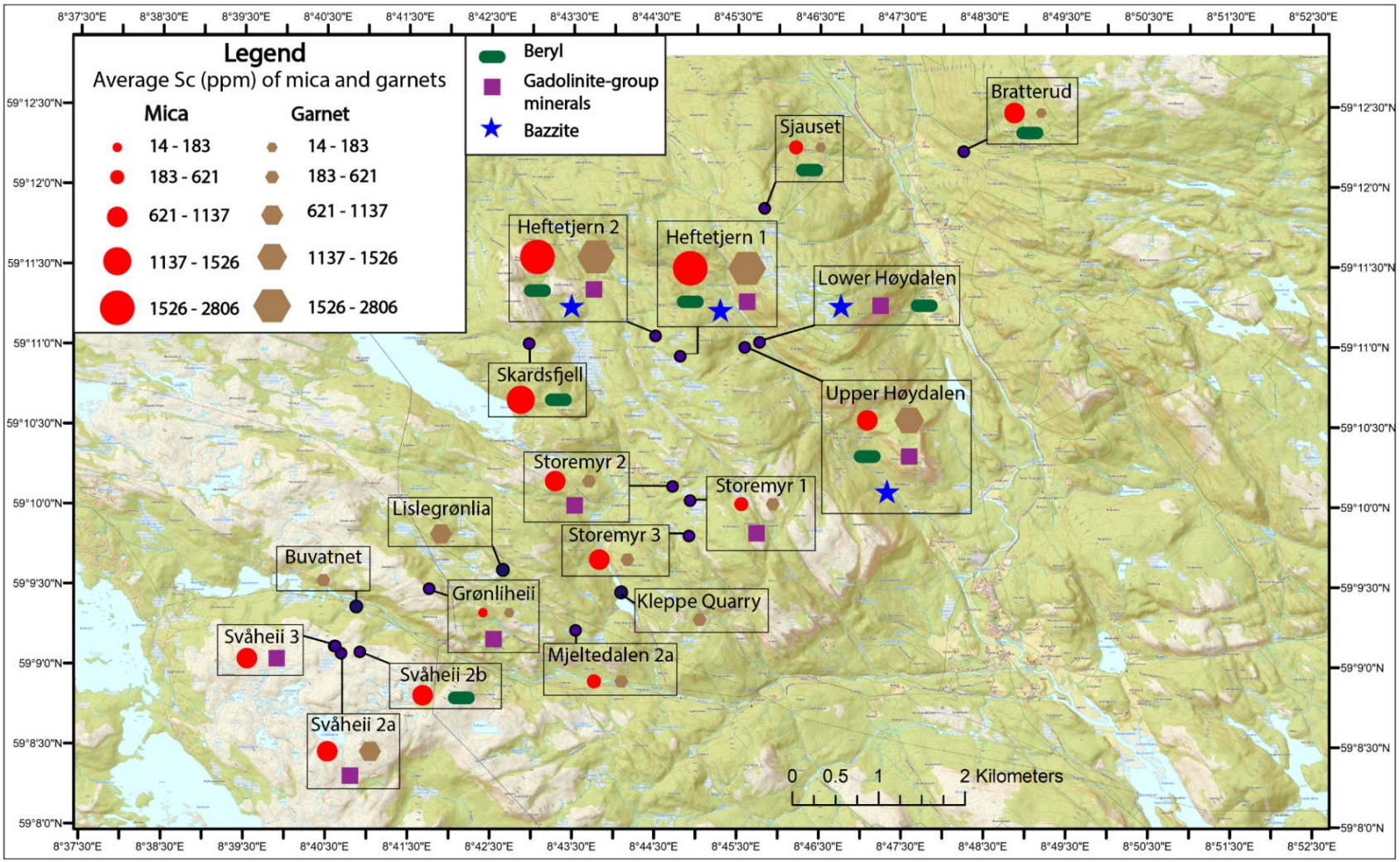

Fig. 4.10. Map of Tørdal pegmatite field illustrating the regional distribution of Sc in studied micas together with their coexisting garnets , and in addition, the regional distribution of Be in studied Be-minerals (beryl, gadolinite-(Y), and bazzite). The highest Sc and Be concentrations are discovered in the Heftetjern (Heftetjern 1, Heftetjern 2) and Høydalen (Upper and Lower Høydalen) pegmatites situated in the greenish K-feldspar zone according to Segalstad and Eggleston (1993), while the lowest is discovered in the Mjeltedalen 2a, Kleppe Quarry and Buvatnet pegmatites situated in the pink K-feldspar zone.

A similar suggestion was made by Steffensen (2018) who focused his study on the Sc concentration in garnets from Tørdal pegmatites. Steffensen (2018) found that the Sc concentration of garnet increases with the increasing fractionation degree of pegmatite melts. The study documents that Sc concentrations of garnets from the wall zone increase with the increasing fractionation degree (reflected by increasing spessartine component of garnets from 20 to 60 mol.%) from chemically primitive pegmatites (Grønliheii and Buvatnet) in the SW towards the chemically evolved pegmatites (Heftetjern and Høydalen) in the NE (Fig. 4.10).

Concluding, the chemically most primitive Tørdal pegmatites in the SW of the field, such as the Mjeltedalen 2a pegmatite, have the lowest Sc and Be concentrations (Fig. 4.10). Towards NE, the fractionation degree of pegmatite melts increases together with the Sc and Be concentrations in more moderate evolved Tørdal pegmatites, such as the Storemyr pegmatites (Fig. 4.10). Highest Sc and Be concentrations are discovered in the chemically most evolved Tørdal pegmatites with the highest fractionation degree of pegmatite melts in the NE of the field, such as the Heftetjern pegmatite (Fig. 4.10). By comparing the findings with the regional zonation of Tørdal pegmatite field suggested by Segalstad and Eggleston (1993), the highest Sc and Be concentrations and highest amounts of "amazonite", are found in the chemically most evolved pegmatites located in the green K-feldspar zone. Lowest Sc and Be concentrations are discovered in the chemically most primitive and unzoned pegmatites, which are situated in the pink K-feldspar zone. Thus, the Sc and Be concentrations across the Tørdal pegmatite field is controlled by the fractionation degree of pegmatite melts.

4.3 The relation and origin of Sc and Be in Tørdal pegmatite melts and their host rocks

Amphibolitic host rocks of the Tørdal pegmatites are classified as igneous primitive arc tholeiites with orogenic settings from oceanic-island/alkaline basalts (OIB/AB) to mid-ocean ridge basalts (MORB), according to classifications by Winchester and Floyd (1984), Shervais (1982), and Wood (1980) (Figs. 3.32, 3.33, 3.34). Whole rock analysis of the host rocks from Heftetjern 2 (mean 38 ppm Sc and 17 ppm Be), Liselgrønlia (mean 36 ppm Sc and 18 ppm Be), Bratterud (mean 34 ppm Sc and 2 ppm Be), and Storemyr 2 (mean 31 ppm Sc and 7 ppm Be) identify them as relative enriched in both Sc and Be (Table 3.13). Scandium and Be concentrations in the amphibolitic host rocks are higher compared to average concentrations of Sc (mean 21.9 ppm Sc) and Be (mean 3 ppm Be) in the continental crust (Rudnick and Gao, 2014; Mason and Moore, 1982). In addition to high Sc and Be, the Tørdal amphibolites are relative rich in the fluxing agent F (Table 3.13).

The amphibolitic host rocks of Tørdal have higher Sc concentrations as the Tørdal granite, which contain 2 ppm Sc (Steffensen, 2018), while a bulk analysis of the Heftetjern pegmatite show a Sc content of 53 ppm Sc (data from Rosing-Schow et al., 2020). Because of the very low Sc concentration of the Tørdal granite, it is unlikely that Tørdal pegmatite melts originated from the Tørdal granite pluton. It is more plausibly that Tørdal pegmatite melts are anatectic melts created by partial melting of their amphibolitic host rocks (anataxis) as suggested by Müller et al. (2015, 2017). The statement is supported by findings of Rosing-Schow et al. (2019), who could show that the Tørdal pegmatites are c. 40 Ma younger than the Tørdal granite. Thus, there is no relationship in age between those two magmatic units. To confirm the anatectic origin of Tørdal pegmatite melts, bulk compositions of amphibolitic host rocks, Tørdal pegmatites (data from Rosing-Schow et al., 2020) and Tørdal granite (data from Steffensen, 2018) are normalized to upper continental compositions according to Rudnick and Gao (2004) and plotted in Figure 4.11. The element distribution patterns of amphibolites and pegmatites show a number of similarities, whereas the pattern of Tørdal granite is very different except Ba, Rb, Y and Yb. Compositions of Li, Ta, Sn, W, and Sc is amphibolites and pegmatites are relative similar, whereas the Tørdal granite is depleted in these elements particularly Sc and Li. Thus, the Tørdal granite has much less geochemical similarities with the Tørdal pegmatites than the amphibolitic host rocks. Concluding, the distribution of incompatible elements and rare metals supports the statement made above that the Tørdal pegmatite melts are most likely a product of partial melting of their amphibolitic host rocks and are not geochemically linked to the Tørdal granite.

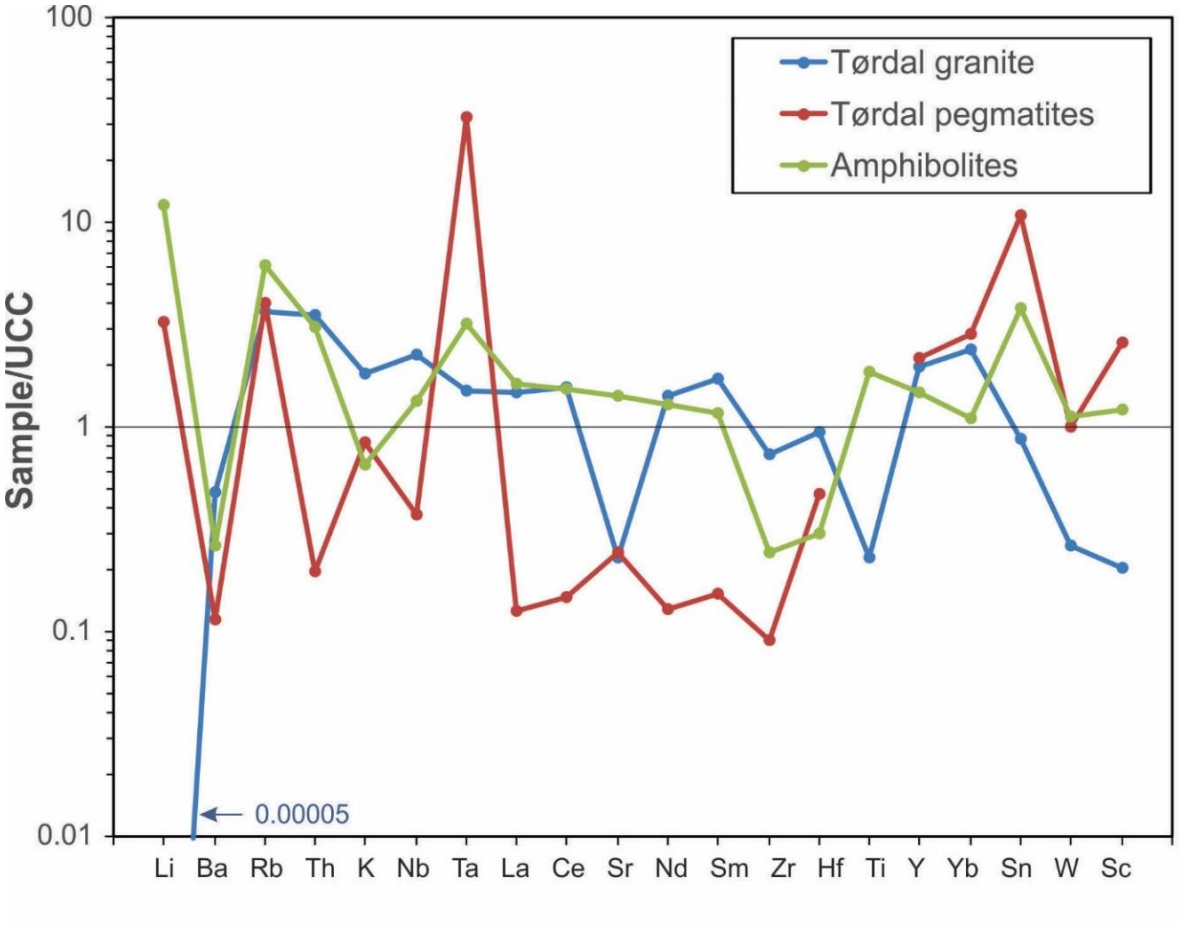

Fig. 4.11. Upper continental crust (UCC)-normalized diagram of selected incompatible elements and rare metals. The used element concentrations of the Tørdal pegmatites, Tørdal granite and amphibolitic host rocks are average values from Rosing-Schow et al. (2020), Steffensen (2018) and this study. UCC values are from Rudnick and Gao (2004). Similar concentrations of Li, Ta, Sn, W, and Sc in amphibolites and pegmatites indicate that the amphibolitic host rocks are the source of Tørdal pegmatite melts.

Steffensen (2018) came also to the conclusion that the Tørdal pegmatite melts are anatectic pegmatite melts created by partial melting of their amphibolitic host rocks. However, according to his theory some of the anatectic pegmatite melts moved over a relative long distance (4-5 km) from SW – the assumed location of the formation of pegmatite melts – to NE of the Tørdal pegmatite field. During their way, the melts became more and more fractionated. Therefore, the most fractionated and Sc-rich pegmatites are found in the NE and the primitive and low-Sc pegmatites are in the SW. The suggestion by Steffensen (2018) seems to be correct in respect to the regional distribution of Be across the Tørdal pegmatite field, since Be – as an incompatible element – continuously increases with the increasing fractionation degree of pegmatite melts, both pegmatite scale and regional scale. However, as discussed in Section 4.1, Sc concentration within a pegmatite body decreases from the margin towards the core, which indicates that the Sc content decreases in the melt with increasing fractionation of the pegmatite

melt. Scandium is a compatible element and it will therefore prefer to enter pegmatite-forming minerals, in particular micas and garnets, instead of staying in the pegmatite melts. Thus, Sc becomes depleted with progressing pegmatite melt fractionation. This implies that Sc would also decrease at large scale formation during melt movement over several kilometers. However, the Sc content across the pegmatite field increases generally together with Be from SW to NE. In contrast to Be, this Sc increase can, therefore, not be explained that the melts moved from SW to NE and become more fractionated (Fig. 4.10). In addition comes that the very most fractionated pegmatite of the Tørdal area at Sjauset has low Sc (mean 398 ppm Sc). For that reason, Steffensen`s (2018) assumption that large proportions of anatectic pegmatite melts travelled far distances from SW towards NE of Tørdal field, accompanied with increasing fractionation degree and increasing Sc concentrations of pegmatite melts, seems unlikely.

Field work observations at the Kleppe Quarry indicate the larger pegmatite bodies (up to 5 m) can be formed by anatectic pegmatite melts which travelled less than 10 m. At Kleppe Quarry small leucocratic pegmatite veinlets (width c. 1 mm), "appear" in the amphibolite and gradually grow in width with increasing distance from the place of "appearance" (Fig. 3.3 B). By following these pegmatite vein for about c. 10 m they turn into a c. 2 m thick pegmatite sheet (Fig. 3.3 E). The field observation contradicts that anatectic Tørdal pegmatite melts travelled over large distances (>1 km). Instead they moved only a few to ten`s of meters, maybe hundred meters, from their place of creation to their place of emplacement.

This study suggests that Sc enrichment observed in pegmatites of the Heftetjern-Høydalen-Skardsfjell area is related to the degree of partial melting of amphibolitic host rocks. The degree of partial melting can be roughly estimated by the approximate K concentration of the anatectic melts (Kushiro et al., 1996). Most K is released from the amphibolites at the beginning of melting causing high K concentrations in the anatectic pegmatite melt formed at low partial melting degrees less <10 % (Kushiro et al., 1996). Because the Tørdal pegmatites are rich in K, these melts were formed generally at low degrees of partial melting. However, the K content of the Tørdal pegmatites is quite variable (data from Rosing-Schow et al., 2020) presumably reflecting different partial melting degrees. The Sc-poor pegmatites at Kleppe Quarry, for example, have high K_2O of 7.4 wt.%, whereas the Sc-rich Heftetjern 2 pegmatite contains 4.1 wt.% K_2O (data from Rosing-Schow et al., 2020). Thus, the partial melting degree at Kleppe Quarry was presumably very low, maybe <5 %, considering the studies of Kushiro et al. (1996). At Heftetjern, the partial melting degree must have been higher, maybe in the range of 10-15 %. Since Sc is a compatible element mostly bound in amphibole of the amphibolitic host rocks

(Table 3.15), it will be released into the anatectic melt when amphibole is melted. At the onset of melting, biotite together with plagioclase of the amphibolites will be melted only. Thus, amphibole starts to melt at somewhat higher melting degrees. Thus, it is suggested that the Sc enrichment in the pegmatites of the Heftetjern-Høydalen-Skardsfjell area, is due to higher partial melting degrees compared to the Sc-poor melts of the other areas.

The mineral analysis of amphiboles and biotites from the Tørdal amphibolitic host rocks by EPMA and LA-ICP-MS revealed that amphiboles are the major host of both Sc and Be (bulk mean of 56 ppm Sc, 6 ppm Be, 0.5 wt.% F), while biotites are major host of F (bulk mean 3 ppm Sc, <2 ppm Be, 1.2 wt.% F) (Tables 3.12, 3.15). Fluorine is a fluxing agent lowering significantly the melting temperature of rocks in addition to water. It is suggested that during partial melting of Tørdal amphibolites, the melts contain moderate amounts of F and water derived from amphibole and biotite melting (Williams-Jones and Vasyukova, 2018). The anatectic pegmatite melts bound Sc and Be in form of stable Sc-F and Be-F ligands or complexes, and transported them to their final place of crystallization (Rupasinghe et al., 1984; Grammaccioli et al., 2000; Segalstad and Raade, 2003).

Concluding, the Sc enrichment in Tørdal pegmatites does not depend on the fractionation degree of pegmatite melts, unlike Be, but mainly on the degree of partial melting. Thus, it is suggested that the pegmatite melt moved over relative short distances (10-500 m) as observed at the Kleppe quarry. Decreasing Sc concentrations with increasing internal fractionation of the pegmatite melt on a pegmatite-internal scale supports this statement. Relative high degrees of partial melting (10-15%) cause high Sc concentrations in the formed anatectic pegmatite melt if the source rock itself is already rich in Sc, as the amphibolites of the Nissedal Outlier. The partial melting of amphibolitic host rocks is enhanced by the elevated F concentrations of these rocks. Fluorine which enter preferentially the newly formed anatectic pegmatite melt will contribute to effectively extract and bound Sc and Be from decaying amphiboles forming Sc-F and Be-F complexes and transport them via pegmatite melts to their final place of crystallization.

5. Conclusion and Outlook

Results of this study can be summarized as follows:

- The study revealed that mica is, together with garnet, the major carrier of Sc in the Sveconorwegian granitic pegmatites of the Tørdal field with average concentrations varying from 38 to 1576 ppm Sc. Highest Sc concentrations in mica were detected in pegmatites of the Skardsfjell-Høydalen-Heftetjern area in the NW part of the field.
- Micas from border zones, wall zones, intermediate zones and late-stage albite replacement zones of individual pegmatite bodies document a continuous decrease of the average Sc concentration from the pegmatite margin towards the core. The continuous Sc decrease is accompanied by decreasing K/Rb, indicating (1) that the pegmatites crystallized from the outer contacts inward and (2) that the compatible Sc decreases in the remaining pegmatite melt with progressive pegmatite crystallization and, thus, with increasing melt fractionation. Thus, micas, which crystallized first and found in the wall zones, incorporated the highest amounts of Sc.
- Comparison of micas and their coexisting garnets of the same pegmatite body revealed a distribution coefficient of Sc-in-mica : Sc-in-garnet of 0.85 : 1. The determined distribution coefficient implies that slightly more Sc is incorporated into garnets. The distribution coefficient remains constant during progressing fractional crystallization.
- The most abundant Be-minerals of the Tørdal pegmatites, gadolinite-(Y) and beryl, show a characteristic distribution within pegmatite bodies. Gadolinite-(Y) is only present in the early-crystallized wall zones, while beryl is found in the intermediate and/or albite replacement zones. This observation indicates that the initial Be-enriched pegmatite melts crystallized first gadolinite-(Y) as long the melt contained enough Y and Fe. Beryl started to crystallize with the intermediate zone if the pegmatite melt became saturated in Be (>35 ppm) and Y and/or Fe had been consumed. Depending on the abundance and availability of Be, Y and Fe, four mineralogical types of Be-bearing pegmatites are distinguished in the Tørdal field: 1) Pegmatites without any Be-bearing minerals: Kleppe Quarry, Mjeltedalen 2a, Buvatnet, Lislegrønlia, Storemyr 3; 2) Gadolinite-(Y)-bearing pegmatites: Storemyr 1, Storemyr 2, Svåheii 2a, Svåheii 3, and Grønliheii; 3) Beryl-bearing pegmatites: Skardsfjell, Sjauset, Svåheii 2b, and Bratterud; and 4) Gadolinite-(Y)- and beryl-bearing pegmatites: Heftetjern 1, Heftetjern 2, Upper Høydalen, and Lower Høydalen. The gadolinite-(Y)- and beryl-bearing pegmatites

occur mainly in the NE area, while gadolinite-(Y)-bearing pegmatites are present in the SW area of Tørdal field.

- Green, yellow and pink beryls of the Høydalen pegmatites, occurring in the outer intermediate, inner intermediate and albite replacement zones respectively, show a continuous increase of Na, Li, Cs accompanied by a decrease of Fe from the pegmatite margin towards the core. This trend, documented by the beryl chemistry, confirms that incompatible elements, such as Na, Li, and Cs, increase in the remaining pegmatite melt with increasing pegmatite-internal melt fractionation.
- On regional scale, the scale of the Tørdal pegmatite field (c. 7.5 km x 5 km; Figure 4.10), the distribution of Sc- and Be-bearing minerals (mica, garnet, beryl, gadolinite-(Y), bazzite) documents a general increase of the Sc and Be concentration from the SW (Mjeltedalen-Kleppe-Buvatnet area) to the NE (Heftetjern-Høydalen-Skardsfjell area) of the field. However, in the far NE end of the pegmatite field (Sjauset-Bratterud area), Sc and Be concentrations decrease again. The general regional increase of the Sc and Be concentration in micas from SW to NE is accompanied by decreasing K/Rb ratio. This implies that the Tørdal pegmatites become more and more fractionated from the SW towards the NE of the field. Lowest Sc and Be contents are observed in primitive pegmatites located in the SW, while highest Sc and Be contents are found in evolved pegmatites in the NE. However, the primitive Lislegrønlia (moderately enriched in Sc) and Grønliheii (moderately enriched in Be) pegmatites in the SW together with the evolved Sjauset pegmatite (moderately enriched in Sc) in NE do not follow the general increasing Sc-Be- and fractionation trend from SW towards NE.
- The amphibolitic host rocks of the Tørdal pegmatites, being part of the supracrustal sequence of the Nissedal Outlier, contain significantly more Sc (mean 35 ppm; Table 3.13) compared to the Sc-poor Tørdal granite (mean 2 ppm; Steffensen, 2018). A bulk analysis of the Heftetjern 2 pegmatite revealed a Sc content of 53 ppm (data from Rosing-Schow et al., 2020). In addition to the similarities in the Sc content, also the Li, Ta, Sn, W, Be compositions of the Tørdal amphibolites are more similar to the Tørdal pegmatites than to those of the Tørdal granite. The amphiboles of the amphibolites are the major source of Sc (mean 56 ppm) and Be (mean 6 ppm Be) while biotite contains only 3 ppm Sc. Based on these findings and on field observations made at the Kleppe quarry, it is suggested that the Tørdal pegmatite melts are anatectic melts formed by partial melting of the amphibolitic host rocks, as previously suggested by Müller et al. (2015, 2017). Both amphiboles and biotites of the amphibolites are relatively rich in F

(0.5 wt.% and 1.2 wt.%, respectively). During partial melting of the amphibolites, F served as flux and lowered the melting temperature. In addition, F formed preferentially complexes with Sc and Be; all three elements released from decaying amphiboles during melting. The statement of the anatectic origin of the Tørdal pegmatite melts is further supported by recent dating results by Rosing-Schow et al. (2019), which showed that the Tørdal granite is about 40 Ma older than the Tørdal pegmatites.

- The associations between migmatitic amphibolite and pegmatites and their structures exposed at the Kleppe quarry indicate that the anatectic pegmatite melts travelled over relative short distances, about 10 to 500 m, from their place of formation to their place of final crystallization. This finding contradicts the statement of Steffensen (2018) who suggested that the Tørdal pegmatite melts moved over long distances of 4 to 5 km from SW to the NE of the field. This suggestion implies that the Sc content in the melt would increase with increasing fractionation during the melt movement. However, in this study it is shown, that Sc, a strongly garnet- and mica-compatible element, decreases in the fractionating pegmatite melt. It is suggested that the initial amount of Sc in the Tørdal pegmatite melts is related to the degree of partial melting of Sc-rich amphibolites instead of being the result of melt fractionation. It is further suggested, that low (c. 10-15%) but not very low (<5%) degrees of partial melting result in the highest Sc content in the formed anatectic melt, as indicated by moderate high bulk K_2O content of 4.1 wt.% in the Sc-enriched pegmatite melt of Heftetjern (K_2O data from Rosing-Schow et al., 2020). According to Kushiro et al. (1996) the K content of anatectic melts reflects the degree of partial melting. Primitive Tørdal pegmatites, formed at very low degrees of partial melting (<5 wt.%) have high K_2O of about 7.4 wt.% and low Sc (Kleppe quarry pegmatites; data from Rosing-Schow et al., 2020). High partial melting degrees of >15% would dilute Sc in the melt resulting in low Sc contents in the melt.
- In economic terms, this study and previous studies by Steffensen (2018) and Rosing-Schow et al. (2018) showed that micas and garnets are the major carriers of Sc in the Tørdal pegmatites. Garnet incorporates slightly more Sc than coexisting mica (Fig. 4.5; Table 4.1). Another important outcome of this study in terms of Sc exploitation is, that micas and garnets of the outer zones of a pegmatite body are most enriched in Sc. Gadolinite-(Y) and beryl are the major carriers of Be. The highest Sc and Be concentrations are found in pegmatites, which are situated in the "amazonite zone", in the NE of the Tørdal field comprising the Heftetjern-Høydalen-Skardsfjell area (Figure 4.10). Therefore, these pegmatites are, in principle, the most interesting ones in terms

of Sc and Be exploitation. However, these pegmatites are small in size (500 – 10,000 m^3) and bulk pegmatite Sc concentrations are about 50 ppm (data from Rosing-Schow et al., 2020) which is below of the current cut-off grade of about 300 ppm of active Sc mines (Williams-Jones and Vasyukova, 2018), making them economically not profitable. However, Sc and Be may serve as by-products in the case the pegmatites will be mined for ceramic feldspar, quartz and/or mica.

The findings of this study rise some new questions, which might be considered in future studies. The determination of the peak metamorphic conditions would contribute to better understand the pressures and temperatures under which the pegmatite melts were formed. The reconstruction of regional tectonics at the time of pegmatite emplacement would improve the knowledge why hundreds of relative small pegmatite bodies were formed instead of a single large-scale granitic intrusion. Additional bulk analyses of pegmatites would reveal to which degree the Sc content of micas and garnets reflect the Sc bulk composition of the host pegmatite and geochemical modelling would provide a better idea about the partial melting degree resulting in the most enriched Sc melts.

6. References

Achterbergh, E.V., Ryan, C.G. and Griffin, W.L. (2001). GLITTER! User`s manual. On-line interactive data reduction for the LA-ICP-MS microprobe. *GEMOC version*

Armbruster, T., Libowitzky, E., Diamond, L., Auernhammer, M., Bauerhansl, P., Hoffmann, C., Irran, E., Kurka, A. and Rosenstingl, H. (1995). Crystalchemistry and optics of bazzite from Furkabasistunnel (Switzerland). *Mineralogy and Petrology*, **52**, pp. 113-126.

Andersen, T. (1997). Radiogenic isotope systematics of the Herefoss Granite, South Norway: an indicator of Swconorwegian (Grenvillian) crustal evolution in the Baltic Shield. *Chemical Geology*, **135**(1-2), pp. 139-158. Doi: https://doi.org/10.1016/S0009-2541(96)00095-2

Bačík, P., Fridrichová, J., Uher, P., Pršek, J. and Ondrejka, M. (2014). The crystal chemistry of gadolinite-datolite group silicates. *The Canadian Mineralogist*, **52**(4), pp. 625-642. Doi: 10.3749/canmin.1400022

Bacon, C.R. and Druitt, T.H. (1988). Compositional evolution of the zoned calc alkaline magma chamber of Mount Mazama, Crater Lake, Oregon. *Contribution to Mineralogy and Petrology*, **98**, pp. 224-256.

Bea, F., Pereira, M.D. and Stroh, A. (1994). Mineral/leucosome trace-element partitioning in a peraluminous migmatite (a laser ablation-ICP-MS study). *Chemical Geology*, **117**(1-4), pp. 291-312. Doi: https://doi.org/10.1016/00009-2541(94)90133-3

Bedard, J.H. (2005). Partitioning coefficients between olivine and silicate melts. *Lithos*, **83**(3-4), pp. 394-419. Doi: 10.1016/j.lithos.2005.03.011

Bedard, J.H. (2007). Trace element partitioning coefficients between silicate melts and orthopyroxene: Parameterizations of D variations. *Chemical Geology*, **244**(1-2), pp. 263-303. Doi: 10.1016/j.chemgeo.2007.06.019

Bedard, J.H. (2014). Parameterizations of calcic clinopyroxene-melt trace element partition coefficients. *Geochemistry Geophysics Geosystems*, **15**(2), pp. 303-336. Doi: 10.1002/2013GC005112

Bergstøl, S. and Juve, G. (1988). Scandian ixiolite, pyrochlore and bazzite in granite pegmatite in Tørdal, Telemark, Norway. *Mineralogy and Petrology*, **38**, pp. 229-243.

Bingen, B., Nordgulen, Ø. and Viola, G. (2008). A four phase model for the Sveconorwegian orogeny, SW Scandinavia. *Norwegian Journal of Geology*, **88**, pp. 43-72.

Cameron, E.N., Jahns, R.H., MnNair, A.H. and Page, L.R. (1949). Internal structure of granitic pegmatites. *Society of Economic Geologists*, **2**, pp. 1-115.

Černý, P. (1990). Distribution, affiliation and derivation of rare-element granitic pegmatites in the Canadian Shield. *Geologische Rundschau*, **79**, pp. 183-226.

Černý, P. (1991a). Fertile granites of Precambrian rare-element pegmatite fields: is geochemistry controlled by tectonic setting or source lithologies? *Precambrian Research*, **51**, pp. 429-468. Doi: https://doi.org/10.1016/0301-9268(91)90111-M

Černý, P. (1991b). Rare-element granitic pegmatites. Part I: Anatomy and internal evolution of pegmatite deposits. Part 2: Regional to global environments and petrogenesis. *Geoscience Canada*, **18**(2), pp. 49-81.

Černý, P. (1992). Geochemical and petrogenic features of mineralization in rare-element granitic pegmatites in the light current research. *Applied Geochemistry*, **7**(5), pp. 393-416. Doi: https://doi.org/10.1016/0883-2927(92)90002-K

Černý, P., Anderson A.J., Tomascak, P.B. and Chapman, R. (2003). Geochemical and morphological features of beryl from the Biktia granitic pegmatite, Zimbawe. *The Canadian Mineralogist*, **41**(4), pp. 1003-1011. Doi: https://doi.org/10.2113/gscanmin.41.4.1003

Černý, P. and Ercit, T. S. (2005). The classification of granitic pemgatites revisited. *The Canadian Mineralogist*, **43**(6), pp. 2005-2026. Doi: https://doi.org/10.2113/gscanmin.43.6.2005

Chappell, B.W. and White, A.J.R. (1992). I- and S-type granites of the Lachlan Fold Belt. *Transactions of the Royal Society of Edinburgh, Earth Sciences,* **83**(1-2), pp. 1-26. Doi: https://doi.org/10.1017/S0263593300007720

Druitt, T.H. and Bacon, C.R. (1988). Petrology of the zoned calcalkaline magma chamber of Mount Mazama, Crater Lake, Oregon. *Contribution to Mineralogy and Petrology*, **101**, pp. 245-259.

Duyvesteyn, W.P.C. and Putnam, G.F. (2014). Scandium, a review of the element, its characteristics, and current and emerging commercial applications. *EMC Metals Corporation The Speciality Metals Company*, pp. 1-12.

Falkum, T. (1985). Geotectonic evoluion of southern Scandinavia in the light of a late-Proterozoic plate collision. In The Deep Proterozoic Crust in the North Atlantic Provinces (A.C. Tobi and J.L.R. Touret, eds.). Springer, Netherlands, pp. 309-322.

Fersman, A. (1930). A geochemical genetic classification of pegmatites. *Monograph Akademia Nauk SSSR* (in Russian).

Franz, G. and Morteani, G. (2002). Be-minerals: synthesis, stability, and occurrence in metamorphic rocks. *Reviews in Mineralogy and Geochemistry*, **50**(1), pp. 551-589. Doi: https://doi.org/10.2138/rmg.2002.50.13

Ginsburg, A.I. and Rodionov, G.G. (1960). On depth of the formation of granitic pegmatites. *Geol. Rudn. Mestorozhd.*, pp. 45-54 (in Russian).

Ginsburg, A.I., Timofeyev, I.N. and Fieldman, L.G. (1979). Principles of Geology of the Granitic Pemgatites. *Nedra, Moscow, USSR* (in Russian).

Glover, A.S., Rogers, W. Z. and Barton, J. E. (2012). Granitic pegmatites: Storehouses of industrial minerals. *Elements*, **8**(4), pp. 269-273. Doi: 10.2113/gselements.8.4.269

Gower, C.F., Ryan, A.B. and Rivers, T. (1990). Mid-Proterozoic Laurentia-Baltica: an overview of its geological evolution and a summary of the contributions made by this volume.

In Mid-Proterozoic Laurenthia-Baltica (C.F. Gower, T. Rivers, and A.B. Ryen, eds.). Geological Association of Canada, Special Paper, **38**, pp. 1-20.

Gramaccioli, C.M., Diella, V. and Demartin, F. (2000). The formation of scandium minerals as an example of the role of complexes in the geochemistry of the rare earths and HFS elements. *European Journal of Mineralogy*, **12**(4), pp. 795-808. Doi: https://doi.org/10.1127/0935-1221/2000/0012-0795

Groat, L. A., Rossman, G.R., Dyar, M.D., Turner, D., Piccoli., P. M.B., Schultz, A.J. and Ottolini, L. (2010). Crystal chemistry of dark blue aquamarine from the true blue showing, Yukon territory, Canada. *The Canadian Mineralogist*, **48**(3), pp. 597-613. Doi: 10.3749/canmin.48.3.597

Hawthorne, F.C., Oberti, R., Harlow, G.E., Maresch, W.V., Martin, R.F., Schumacher, J.C. and Welch, M.D. (2012). IMA report. Nomenclature of the amphibole supergroup. *American Mineralogist*, **97**, pp. 2031-2048. Doi: http://dx.doi.org/10.2138/am.2012.4276

Jarosewich, E. and Boatner, L.A. (1991). Rare-earth element reference samples for electron microprobe analysis. *Geostandards Newsletter*, **15**, pp. 397-399. Doi: https://doi.org/10.1111/j.1751-908X.1991.tb00115.x

Jochum (2009, Acessed 04 June). USGS BCR-2G, GEOREM Preferred Values. From: http://georem.mpch-mainz.gwdg.de/ref_mat_pref_val.asp?refmatid=USGS+BCR-2G

Jochum, K.P., Weis, U., Stoll, B., Kuzmin, D., Yang, Q., Raczek, I., Jacob, D.E., Stracke, A., Birbaum, K., Frick, D.A., Günther, D. and Enzweiler, J. (2011). Determination of Reference Values for NIST SRM 610-617 Glasses Following ISO Guidelines. *Geostandards and Geoanalytical Research*, **35**, pp. 397-429. Doi: 10.1111/j.1751-908X.2011.00120.x

Joliff, B.L., Papike, J.J. and Shearer, C.K. (1992). Petrogenic relationships between pegmatite and granite based on geochemistry of muscovite in pegmatite wall zones, Black Hills, South-Daktoa, USA. *Geochimica et Cosmochimica Acta*, **56**(5), pp. 1915-1939. Doi: https://doi.org/10.1016/0016-7037(92)90320-l

Juve, G. and Bergstøl, S. (1990). Caesian bazzite in granite pegmatite in Tørdal, Telemark, Norway. *Mineralogy and Petrology*, **43**, pp. 131-136.
Juve, G. and Bergstøl, S. (1997). Granitpegmatittene i Tørdal, Telemark, Norway. *Kongsberg Mineralsymposium Norsk Bergvergsmusuem Skrift*, **12**, pp. 56-57.

Kristiansen, R. (1998). Høydalen litium-pegmatitt, Tørdal i Telemark. *Kongsberg Mineralsymposium Norsk Bergverkmuseum Skrift*, **14**, pp. 17-28.

Kristiansen, R. (2003). Scandium-mineraler i Norge. *STEIN*, **30**, pp. 14-23.

Kushiro, I., Basu, A. and Hart, S. (1996). Partial melting of a fertile mantle peridotite at high pressures: An experimental study using aggregates of diamond. *Geophysical Monograph Series*, **95**, pp. 109-122. Doi: https://doi.org/10.1029/GM095p0109

Li, Z.X., Bodanova, S.V., Collins, A.S., Davidson, A., De Waele, B., Ernst, R.E., Fitzsimons, I.C.W., Fuck, R.A., Gladkochub, D.P., Jacobs, J., Karslstrom, K.E., Lu, S., Natapov, L.M., Pease, V., Pisarevsky, S.A., Thrane, K., and Vernikovsky, V. (2008). Assembly, configuration, and break-up history of Rodinia: a synthesis. *Precambrian Research*, **160**(1-2), pp. 179-210. Doi: 10.1016/j.precamres.2007.04.021

Linnen, R.L., Van Lichtervelde, M. and Černý, P. (2012). Granitic pegmatites as sources of strategic metals. *Elements*, **8**(4), pp. 275-280. Doi: 10.2113/gselements.8.4.275

London, D. and Evensen, J.E. (2002). Beryllium in silicic magmas and the origin of beryl-bearing pegmatites. *Reviews in Mineralogy and Geochemistry*, **50**(1), pp. 445-486. In Beryllum: Mineralogy, petrology, and geochemistry, ed. E.S. Grew, 445-86. Mineralogical Society of America reviews in mineralogy and geochemistry 50. Doi: https://doi.org/10.2138/rmg.2002.50.11

London, D. (2008). *Pegmatites* (10th edition). Quebec: Mineralogical Association of Canada.

London, D. (2009). The origin of primary textures in granitic pegmatites. *The Canadian Mineralogist*, **47**(4), pp. 697-724. Doi: 10.3749/canmin.47.4.697

London, D. (2015). Reading Pegmatites: Part 1 – What beryl says. *Rocks and Minerals*, **90**(2), pp. 138-153. Doi: 10.1080/00357529.2014.949173

Mahood, G. and Hildreth, W. (1983). Large partition coefficients for trace elements in high-silica rhyolites. *Geochimica et Cosmochimica Acta*, **47**(1), pp. 11-30. Doi: hhttps://doi.org/10.1016/0016-7037(83)90087-X

Mason, B.H. and Moore, C.B. (1982). *Principles of Geochemistry* (4th edition). New York: John Wiley and Sons

Mindat (2020a, Acessed 27 April). Beryl group. From: https://www.mindat.org/min-40374.html

Mindat (2020b, Acessed 20 April). Heftetjern pegmatite, Tørdal, Drangedal, Telemark, Norway. From: https://www.mindat.org/loc-2517.html

Mindat (2020c, Acessed 20 April). Høydalen, Tørdal, Drangedal, Telemark, Norway. From: https://www.mindat.org/loc-9973.html

Mindat (2020d, Acessed 03 June). Skardfjell pegmatite (Skardsfjell), Tørdal, Drangedal, Telemark, Norway. From: https://www.mindat.org/loc-32662.html

Mindat (2020e, Acessed 03 June). Thortveitite. From: https://www.mindat.org/min-3950.html

Mindat (2020f, Acessed 03 June). The Mineralogy of Scandium. From: https://www.mindat.org/element/Scandium

Mindat (2020g, Acessed 19 March). Tørdal, Drangedal, Telemark, Norway. From: https://www.mindat.org/loc-23233.html

Mitchell, R.H. (1967). The Precambrian rocks of the Telemark area in south central Norway. The Nissedal supracrustal series. *Norsk Geologisk Tidsskrift*, **47**, pp. 295-332.

Müller, A., Ihlen, P.M., Snook, B., Larsen, R., Flem, B., Bingen, B. and Williamson, B.J. (2015) The chemistry of quartz in granitic pegmatites of southern Norway: Petrogenic and

economic implications. *Economic geology and the bulletin of the Society of Economic Geologists*, **110**(7), pp. 1737-1757. Doi: https://doi.org/10.2113/econgeo.110.7.1737

Müller, A., Romer, R. L. and Pedersen, R.-B. (2017). The sveconorwegian pegmatite province – thousands of pegmatites without parental granite. *The Canadian Mineralogist*, **55**(2), pp. 283-315. Doi: 10.3749/canmin.1600075

Müller, A., Spratt, J., Thomas, R., Williamson, B.J. and Seltman, R. (2018a). Alkali-F-rich albite zones in evolved NYF pegmatites: The product of melt-melt immiscibility. *The Canadian Mineralogist*, **56**(4), pp. 657-687. Doi: 10.3749/canmin.1700087

Müller, A., Simmons, W., Beurlen, H., Thomas, R., Ihlen, P.M., Wise, M., Roda-Robles, E., Neiva, A.M.R. and Zagorsky, V. (2018b). A proposed new mineralogical classification system for granitic pegmatites – part 1: History and the need for a new classification. *The Canadian Mineralogist*, **56**, pp. 1-25. Doi: 10.3749/canmin.1700088

Nash, W.P. and Crecraft, H.R. (1985). Partition coefficients for trace elements in silicic magmas. *Geochimica et Cosmochimica Acta*, **49**(11), pp. 2309-2322. Doi: https://doi.org/10.1016/0016-7037(85)90231-5

Nickel, E.H. and Grice, J.D. (1998). The IMA Comission of New minerals and Mineral Names: procedure and guidelines on mineral nomenclature. *Canadian Mineralogist*, **36**, pp. 913-926.

Oftedal, I. (1941). Enrichment of lithium in Norwegian cleavelandite-quartz pegmatites. *Norsk Geologisk Tidsskrift*, **20**, pp. 193-198.

Oftedal, I. (1942). Lepidolit- og tinnstensførende pegmatitt i Tørdal, Telemark. *Norsk Geologisk Tidsskrift*, **22**, pp. 1-14.

Pezzotta, F., Diella, V. and Guastoni, A. (1999). Chemical and paragenetic data on gadolinite-group minerals from Baveno and Cuasso al Monte, Southern Alps, Italy. *American Mineralogist*, **84**(5-6), pp. 782-789. Doi: https://doi.org/10.2138/am-1999-5-613

Pezzotta, F., Diella, V. and Guastoni, A. (2005). Scandium silicates from the Baveno and Cuasso al Monte NYF-granites, Southern Alps (Italy): Mineralogy and genetic inferences. *American Mineralogist*, **90**(8-9), pp. 1442-1452. Doi: https://doi.org/10.2138/am.2005.1478

Pouchou, J.L. and Pichoir, F. (1984). A new model for quantitative X-ray microanalysis I. Application to the analysis of homogenous samples. *Recherche Aérospatiale*, **3**, pp. 13-38.

Raade, G. and Kristiansen, R. (2000). Mineralogy and geochemistry of the Heftetjern granite pegmatite, Tørdal: a progess report. *Kongsberg Mineralsymposium Norsk Bergverksmuseum Skrifter*, **17**, pp. 19-25.

Rieder, M., Gavazzini, G., D`yakonov, Y.S., Frank-Kamenetskii, V.A., Gottardi, G., Guggenheim, S., Koval, P.V., Müller, G., Neiva, A.M.R., Radoslovich, E.W., Robert, J-L., Sassi, F.P., Takeda, H., Weiss, Z. and Wones, D.R. (1998). Nomenclature of the micas. *Clays and Clay Minerals*, **46**(5), pp. 586-595.

Rosing-Show, N., Müller, A. and Friis, H. (2018). A comparison of the mica geochemistry of the pegmatite fields in southern Norway. *The Canadian Mineralogist*, **56**(4), pp. 463-488. Doi: 10.3749/canmin.1700086

Rosing-Schow, N., Müller, A., Romer, R.L. and Friis, H. (2019). New age constraints on the formation of Sveconorwegian pegmatites. *The Canadian Mineralogist*, **57**(5), pp.787-790. Doi: 10.3749/canmin.AB00022

Rosing-Schow, N., Andersen, T. and Müller, A. (2020). *Pb isotopes as a tool for granite pegmatite source modelling – examples from the late Mesoproterozoic Sveconorwegian pegmatite province, Southern Norway*. In review.

Rudnick, R.L., Gao, S. (2004). Composition of the continental crust. In Treatise on Geochemistry; Holland, H.D., Turekian, K.K. (Eds.) Elsevier: Amsterdam, The Netherlands, Volume 3, pp. 1–64.

Rudnick, R.L., and Gao, S. (2014). Composition of the continental crust. In Turekian, K.K., and Holland, H. D. (eds.), Treatise on Geochemistry, 2nd edn. Oxford: Elsevier, Vol. 4, pp. 1-51.

Rupasinghe, M.S., Banerjee, A., Pense, J. and Dissanayke, C.B. (1984). The geochemistry of beryllium and fluorine in the gem field of Sri Lanka. *Mineral. Deposita*, **19**, pp. 86-93.

Sardi, F.G. and Heimann, A. (2014). Pegmatitic beryl as indicator of melt evolution: example from the velasco district, Pampeana pegmatite province, Argentina, and review of worldwide occurrences. *The Canadian Mineralogist*, **52**(5), pp. 809-836. Doi: 10.3749/canmin.1400032

Samson, I.M. and Chassé, M. (2016) Scandium. *Encylopedia of Geochemistry, Springer International Publishing Switzerland*, pp. 1-4. Doi: 10.1007/978-3-319-39193-9_281-1

Scandium International Mining Corp. (2020a, Acessed 19 June). Home Page. From: http://www.scandiummining.com/

Scandium International Mining Corp. (2020b, Acessed 12 June). 2012 Tørdal field exploration. From: https://www.sec.gov/Archives/edgar/data/1408146/000106299316009695/form10q.htm

Schetelig, J. (1911). Ueber Thortveitit, ein neues mineral. Zentralb. *Für Miner*, pp. 721-726.

Schetelig, J. (1922). Thortveitite – a silicate of scandium (Sc, Y)$_2$Si$_2$O$_7$. *Norsk Geologisk Tidskrift*, **6**, pp. 233-244.

Segalstad, T.V. and Eggleston, T.L. (1993) Pegmatittene I Tørdal, Telemark. *STEIN*, **20**, pp. 190-195.

Segalstad, T. V. and Raade, G. (2003). Scandium mineralizations in Southern Norway – geological background for the field trip. *NGF Abstracts and Proceedings*, (2), pp. 57-86.

Shervais, J. W. (1982). Ti-V plots and the petrogenesis of modern and ophiolitic lavas. *Earth and Planetary Science Letters*, **59**, pp. 101-118. Doi: 10.1016/0012-821X(82)90120-0

Siegfried, P., Wall, F. and Moore, K. (2018). In Search of the forgotten rare earth. *Geoscientist*, **28**, pp. 10-15. Doi: https://doi.org/10.1144/geosci2018-021

Simmons, W., Webber, K.L., Falster, A.U. and Nizamoff, J.W. (2003). *Pegmatology: Pegmatite mineralogy, petrology and petrogenesis.* New Orleans: Rubellite Press.

Simmons, W. and Webber, K.L. (2008). Pegmatite genesis: state of the art. *European Journal of Mineralogy*, **20**(4), pp. 421-438. Doi: https://doi.org/10.1127/0935-1221/2008/0020-1833

Simmons, W.B., Foord, E.E., Falster, A.U., King, V.T. (1995). Evidence for an anatectic origin of granitic pegmatites, western Maine, USA. Geol. Soc. Amer. Ann. Mtng., Noew Orelans, LA, Abstr. Prog., A87.

Simmons, W.B., Foord, E.E. and Falster, A.U. (1996). Anatectic origin of granitic pegmatites, Western Maine, USA. GAC-MAC Ann. Mtng., Winnipeg, Abstr. Prog., A87.

Sisson, T.W. and Bacon, C.R. (1992). Garnet/high-silica rhyolite trace element partition coefficients measured by ion microprobe. *Geochimica et Cosmochimica Acta*, **56**(5), pp. 2133-2136. Doi: https://doi.org/10.1016/0016-7037(92)90336-H

Slagstad, T., Roberts, N.M.W. and Kulakov, E. (2017). Linking orogensis across a supercontinent; the Grenvillian and Sveconorwegian margins on Rodinia. *Gondwana Research*, **44**, pp. 109-115. Doi: https://doi.org/10.1016/j.gr.2016.12.007

Snook, B. (2014). Towards exploration tools for high purity quartz: an example from the South Norwagian Evje-Iveland pegmatite belt (Ph.D. Thesis). *University of Exeter, England.*

Steffensen, G. (2018*).* The distribution and enrichment of scandium in garnets from the Tørdal pegmatites, and its economic implications (Master thesis). *Univeristy of Oslo, Norway.*

Strategic Metal Investments Ltd. (2020, Acessed 19 March). Scandium Price. From: http://strategic-metal.com/products/scandium/scandium-price/

Thomas, R., Webster, J.D. and Heinrich, W. (2000). Melt inclusions in pegmatite quartz: complete miscibility between silicate melts and hydrous fluids at low pressure. *Contributions to Mineralogy and Petrology*, **139**, pp. 394-401.

Thomas, R. and Davidson, P. (2012). Water in granite and pegmatite-forming melts. *Ore Geology Reviews*, **46**, pp. 32-46. Doi: 10.1016/j.oregeorev.2012.02.006

Thomas, R. and Davidson, P. (2016). Revisiting complete miscibility between silicate melts and hydrous fluids, and extreme enrichment of some elements in the supercritical state – Consequences for the formation of pegmatites and ore deposits. *Ore Geology Reviews*, **72**(1), pp. 1088-1101. Doi: https://doi.org/10.1016/j.oregeorev.2015.10.004

Tischendorf, G., Förster, H.-J. and Gottesmann, B. (2001). Minor- and trace-element composition of trioctahedral micas: a review. *Mineralogical Magazine*, **65**(2), pp. 249-276.

USGS (2019, Acessed 03 June). Scandium Statistics and Information. From: https://prd-wret.s3-us-west-2.amazonaws.com/assets/palladium/production/atoms/files/mcs-2019-scandi.pdf

Uher, P., Chudik, P., Bačík, P., Vaculovic, T. and Galiova, M. (2010). Beryl composition and evolution trends: an example from granitic pegmatites of the beryl-columbite subtype, Western Carpathians, Slovakia. *Journal of Geosciences*, **55**(1), pp. 69-80. Doi: 10.3190/jgeosci.060

Vonken, J.H.L. (2016). *The Rare Earth Elements, an Introduction*. Dordrecht: SpringerNature. Doi: 10.1007/978-3-319-26809-5.

Williams-Jones, A.E. and Vasyukova, O.V. (2018). The economic geology of scandium, the runt of rare earth element litter. *Economic Geology*, **113**(4), pp. 973-988. Doi: https://doi.org/10.5382/econgeo.2018.4579

Winchester, J. A. and Max, M. D. (1984). Geochemistry and origin of the Annagh Division of the Precambrian Erris complex, NW County, Mayo, Ireland. *Precambrian Research*, **25**(4), pp. 397-414. Doi: https://doi.org/10.1016/0301-9268(84)90011-1

Wood, D.A. (1980). The application of a Th-Hf-Ta diagram to problems of tectonomagmatic classification and to establishing the nature of crustal contamination of basalatic lavas of the British Tertiary volcanic province. *Earth and Planetary Science Letters*, **50**(1), pp. 11-30. Doi: https://doi.org/10.1016/0012-821X(80)90116-8

7. Appendix

7.1 Overview of studied samples from Tørdal pegmatites and their host rocks

Locality	NHM collection nr	Sample preparation	Specimen description	UTM Zone	UTM East	UTM North	Stored	Aquired by	Aquired when
Bratterud	04071909	Epoxy cast	Biotite 4 cm from the contact (Border zone)	32V	0488812	6562743		Axel Müller and Markus Wilhelmsen	04.07-2019
	04071910	Epoxy cast	Muscovite relative near the contact (Wall zone)	32V	0488812	6562743		Axel Müller and Markus Wilhelmsen	04.07-2019
	04071911	Epoxy cast	Muscovite from the center of the pegmatite (Intermediate zone)	32V	0488812	6562743		Axel Müller and Markus Wilhelmsen	04.07-2019
	04071917	Thick section	Medium-grained metagabbro adjacent from the Bratterud pegmatite	32V	0488812	6562743		Axel Müller and Markus Wilhelmsen	04.07-2019
Buvasselva	02071901	Thick section	Black to green, massive and fine-grained amphibolite from Buvasselva (on the way to Svåheii pegmatite)	32V	0482708	6556926		Axel Müller and Markus Wilhelmsen	02.07-2019
Grønliheii	02071915	Epoxy cast	Muscovite near the contact	32V	0482608	6557671		Axel Müller and Markus Wilhelmsen	02.07-2019
Heftetjern 1	15053	Epoxy cast	Bazzite	32V	0485524	6560371			
	17320	Epoxy cast	Crystal fragments of bazzite	32V	0485524	6560371	S161,3	Hans-Jørgen Berg	26.10.1994
	33376	Epoxy cast	Bazzite, garnet, helvite on microcline (var. amazonite) (3.7 kg)	32V	0485524	6560371	S178,6	Geologisk Museums Venner	05.09.1998
	33377	Epoxy cast	Bazzite on microcline (var. amazonite)	32V	0485524	6560371		Geologisk Museums Venner	05.09.1998
	33378	Epoxy cast	Bazzite and fluorite on microcline (var. amazonite) and albite replacement unit	32V	0485524	6560371		Geologisk Museums Venner	05.09.1998
	42326	Epoxy cast	Beryl from intermediate zone of the pegmatite	32V	0485524	6560371	S171,1		2010
Heftetjern 2	05071901	Epoxy cast	Biotite near the south-west contact of the pegmatite (Wall zone)	32V	0485239	6560607		Axel Müller and Markus Wilhelmsen	05.07-2019
	05071902	Thick section	Massive amphibolite	32V	0485239	6560607		Axel Müller and Markus Wilhelmsen	05.07-2019
	02071916	Thick section	Amphibole-biotite-gneiss near the Lislegrønlia pegmatite	32V	0483597	6557818		Axel Müller and Markus Wilhelmsen	02.07-2019

Lislegrønlia	02071917	Epoxy cast	Biotite (c. 3 cm) near the contact (rare)	32V	0483591	6557877		Axel Müller and Markus Wilhelmsen	02.07-2019
Lower Høydalen	23091547	Epoxy cast	Large block (c. 5 kg) with several euhedral gadolinite crystals (up to 2 cm) in wall zone, 5-10 cm from pegmatite contact	32V	0486445	6560532		Axel Müller	23.09.2015
	NHoy01, 31541	Epoxy cast	Morganite from albite replacement unit of the pegmatite	32V	0486445	6560532			
	NHoy02, 03071701	Epoxy cast	Yellowish-green beryl from intermediate zone of the pegmatite	32V	0486445	6560532			
Mjeltedalen 2a	02071918	Thick section	Amphibole-gneiss near the Mjeltedalen 2a pegmatite	32V	0484218	6557306		Axel Müller and Markus Wilhelmsen	02.07-2019
	02071919	Epoxy cast	Biotite on the upper contact between pegmatite and amphibolite (very rare)	32V	0484311	6557191		Axel Müller and Markus Wilhelmsen	02.07-2019
Sjauset	04071918	Epoxy cast	Muscovite from the center of pegmatite (Intermediate zone)	32V	0486505	6562087		Axel Müller and Markus Wilhelmsen	04.07-2019
Skardsfjell	31548	Epoxy cast	Beryl crystals without matrix from intermediate zone of the pegmatite	32V	0483772	6560519	S151,3	Dr. M. Vokes	28.07.1963
Storemyr 1	04071905	Epoxy cast	Biotite close to contact	32V	0485640	6558697		Axel Müller and Markus Wilhelmsen	04.07-2019
Storemyr 2	04071901	Epoxy cast	Biotite near lower contact (rare)	32V	0485437	6558860		Axel Müller and Markus Wilhelmsen	04.07-2019
	04071902	Epoxy cast	Muscovite near lower contact (rare)	32V	0485437	6558860		Axel Müller and Markus Wilhelmsen	04.07-2019
	04071903	Thick section	Massive amphibolite adjacent from the Storemyr 2 pegmatite	32V	0485437	6558860		Axel Müller and Markus Wilhelmsen	04.07-2019
Storemyr 3	04071907	Epoxy cast	Muscovite from the center of the pegmatite	32V	0485627	6558286		Axel Müller and Markus Wilhelmsen	04.07-2019
	04071908	Epoxy cast	Biotite (c. 20 cm) from the center of the pegmatite	32V	0485592	6558281		Axel Müller and Markus Wilhelmsen	04.07-2019
Svåheii 2a	02071911	Epoxy cast	Biotite from wall zone, c. 5 cm from contact	32V	0481593	6556927		Axel Müller and Markus Wilhelmsen	02.07-2019
	02071912	Epoxy cast	Muscovite from intermediate zone inside the pegmatite	32V	0481593	6556927		Axel Müller and Markus Wilhelmsen	02.07-2019
Svåheii 2b	020719099b	Epoxy cast	Biotite and muscovite (in one sample) from middle of wall zone	32V	0481810	6556943		Axel Müller and Markus Wilhelmsen	02.07-2019
	020719099m	Epoxy cast	Biotite and muscovite (in one sample) from middle of wall zone	32V	0481810	6556943		Axel Müller and Markus Wilhelmsen	02.07-2019

	02071910	Epoxy cast	Muscovite on cleavelandite (albite replacement unit) from intermediate zone	32V	0481810	6556943		Axel Müller and Markus Wilhelmsen	02.07-2019
	15061801	Epoxy cast	Beryl from intermediate zone of the pegmatite	32V	0481810	6556943			
Svåheii 3	02071913b	Epoxy cast	Biotite (and muscovite in one sample) from wall zone	32V	0481527	6557009		Axel Müller and Markus Wilhelmsen	02.07-2019
	02071913m	Epoxy cast	Muscovite (and biotite in one sample) from wall zone	32V	0481527	6557009		Axel Müller and Markus Wilhelmsen	02.07-2019
	02071914	Epoxy cast	Muscovite from intermediate zone	32V	0481527	6557009		Axel Müller and Markus Wilhelmsen	02.07-2019
Upper Høydalen	05071903	Thick section	Coarse-grained metagabbro adjacent from the Upper Høydalen pegmatite	32V	0486274	6560473		Axel Müller and Markus Wilhelmsen	05.07-2019
	21341a	Epoxy cast	Large pieces of anhedral crystals in white K-feldspar from wall zone of the pegmatite	32V	0486274	6560473	S93,1	H. Ramberg	1942?
	21341b	Epoxy cast	Large pieces of anhedral crystals in white K-feldspar from wall zone of the pegmatite	32V	0486274	6560473	S93,2	H. Ramberg	1942?
	21345	Epoxy cast	Euhedral crystals in white K-feldspar from wall zone of the pegmatite	32V	0486274	6560473	S93,3	Oftedal	1942
	23091514	Epoxy cast	Muscovite from intermediate zone of the pegmatite	32V	0486274	6560473		Nanna Rossing-Schow (Rosing-Schow et al., 2018)	
	HF441m	Epoxy cast	Morganite from albite replacement unit of the pegmatite	32V	0486274	6560473			
	OHoy01, July2017	Epoxy cast	Clear light green beryl from the intermediate zone of the pegmatite	32V	0486274	6560473			
	OHoy02, 31542	Epoxy cast	Morganite from albite replacement unit of the pegmatite	32V	0486274	6560473			
	OHoy03, 31511	Epoxy cast	Slightly yellowish clear beryl from the intermediate zone of the pegmatite	32V	0486274	6560473			

7.2 Images of studied minerals from Epoxy casts

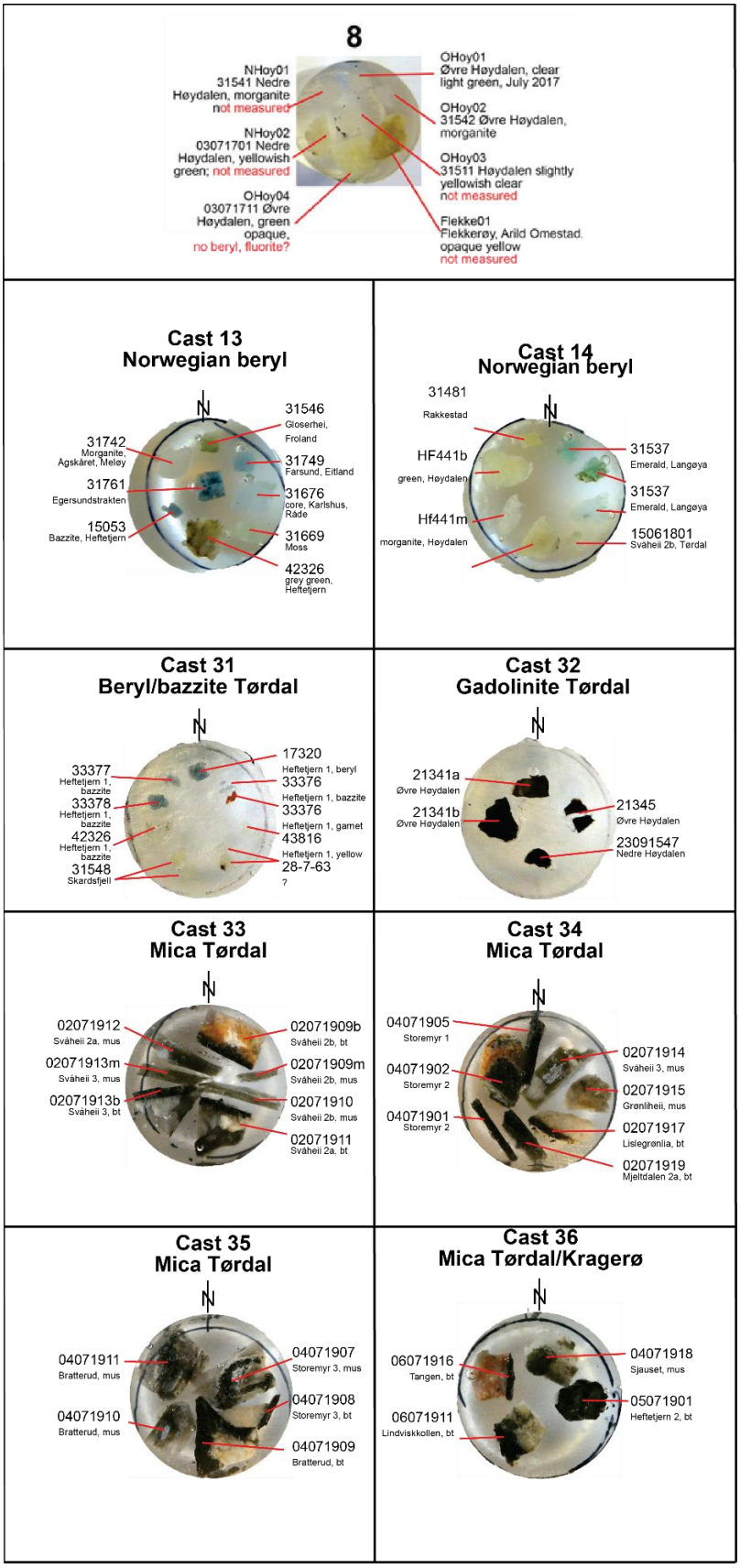

Appendix 7.2. Images of Epoxy casts of studied minerals from Tørdal pegmatites measured by EPMA and LA-ICP-MS. Casts 8), 13), 14), and 31) Beryls and bazzites; Cast 32) Gadolinites; Casts 33-36) Micas.

7.3 Images of studied pegmatite host rocks from thick sections

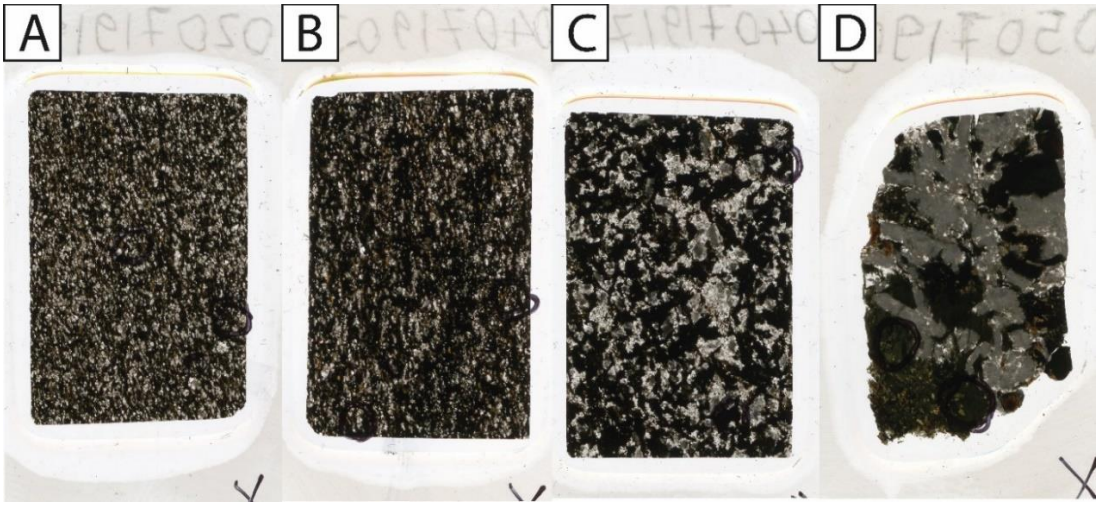

Appendix 7.3. Images of studied pegmatite host rocks measured by EPMA and LA-ICP-MS, from fine-grained to coarse-grained. In addition, host rock samples from Lislegrønlia (sample 02071916) and Heftejtern 2 (sample 05071902) were not created into thick sections. Instead, chemical whole rock analyisis were preformed on this host rocks together with B and C. A – Fine-grained amphibole-biotite gneiss in vicinity of Mjeltedalen 2a pegmatite (sample 02071918). B – Fine-grained massive amphibolite adjacent to Storemyr 2 pegmatite (sample 04071903). C – Medium-grained gabbro adjacent to Bratterud pegmatite (sample 04071917). D – Coarse-grained gabbro adjacent to Upper Høydalen pegmatite (sample 05071903).

7.4 Overview of minerals from studied Tørdal pegmatites according to Mindat (2020g):

Mineral	**Formula**	
Actinolite	$\square Ca_2(Mg_{4.5\text{-}2.5}Fe^{2+}_{0.5\text{-}2.5})Si_8O_{22}(OH)_2$	
Agakhanovite-(Y) (TL)	$YCa\square_2KBe_3Si_{12}O_{30}$	
Albite	$Na(AlSi_3O_8)$	
Var: Cleavelandite	$Na(AlSi_3O_8)$	
Var: Oligoclase-Albite	$Na(AlSi_3O_8)$	
Allanite-(Ce)	$CaCe(Al_2Fe^{2+})[Si_2O_7][SiO_4]O(OH)$	
Anatase	TiO_2	
`Apatite`	$Ca_5(PO_4)_3(Cl/F/OH)$	
`Axinite Group`	Axinite-(Fe)	$Ca_2Fe^{2+}Al_2BSi_4O_{15}OH$
	Axinite-(Mg)	$Ca_2MgAl_2BSi_4O_{15}OH$
	Axinite-(Mn)	$Ca_2Mn^{2+}Al_2BSi_4O_{15}OH$
	Tinzenite	$Ca_2Mn^{2+}{}_4Al_4[B_2Si_8O_{30}](OH)_2$
Bastnäsite-(Ce)	$Ce(CO_3)F$	
Bavenite	$Ca_4Be_{2+x}Al_{2-x}Si_9O_{26-x}(OH)_{2+x}$ (x = 0 to 1)	
Bazzite	$Be_3(Sc,Fe^{3+},Mg)_2Si_6O_{18} \cdot Na_{0.32} \cdot nH_2O$	
Bertrandite	$Be_4Si_2O_7(OH)_2$	
Beryl	$Be_3Al_2Si_6O_{18}$	
Var: Morganite	$Be_3Al_2Si_6O_{18}$	
Beusite	$Mn^{2+}Mn^{2+}{}_2(PO_4)_2$	
`Biotite`	$K(Fe^{2+}/Mg)_2(Al/Fe^{3+}/Mg)([Si/Al]Si_2O_{10})(OH/F)_2$	
Bismoclite	BiOCl	
Bismuth	Bi	
Bismutite	$Bi_2O_2(CO_3)$	
Bohseite	$Ca_4Be_{3+x}Al_{1-x}Si_9O_{25-x}(OH)_{3+x}$, (x = 0 to 1)	
Brookite	TiO_2	

Calcite	$Ca(CO_{3)}$
Cascandite	$CaScSi_3O_8(OH)$
Cassiterite	SnO_2
Cerianite-(Ce)	CeO_2
Cerussite	$Pb(CO_3)$
Clinochlore	$Mg_5Al(AlSi_3O_{10})(OH)_8$
Clinozoisite	$Ca_2Al_3[Si_2O_7][SiO_4]O(OH)$
Epidote	$Ca_2(Al_2Fe^{3+})[Si_2O_7][SiO_4]O(OH)$
Euxenite-(Y)	$(Y,Ca,Ce,U,Th)(Nb,Ta,Ti)_2O_6$
Fergusonite-(Y)	$YNbO_4$
Fluocerite-(Ce)	$CeFe_3$
Fluorite	CaF_2
var: Yttrofluorite	$(Ca_{1-x}Y_x)F_{2+x}$ where $0.05< x <0.3$
Fluor-schorl	$NaFe^{2+}{}_3Al_6(Si_6O_{18})(BO_3)_3(OH)_3F$
`Gadolinite Group`	$A_2MQ_2T_2O_8\varphi_2$ A = Ca, REE, (Y and lanthanoids) M = Fe, □ (vacancy), Al Q = B, Be, Li T = Si φ = O, OH
Gadolinite-(Y)	$Y_2Fe^{2+}Be_2O_2(SiO_4)_2$
Gahnite	$ZnAl_2O_4$
Galena	PbS
Goethite	FeO(OH)
Heftetjernite (TL)	$ScTaO_4$
Hellandite-(Y)	$(Ca,REE)_4Y_2Al□_2(B_4Si_4O_{22})\ (OH)_2$
var: Mn-bearing Hellandite-(Y) (FRL)	$Ca_{1.34}Mn_{1.07}Y_{2.75}Yb_{0.38}Al_{0.92}Fe_{0.08}Si_4B_4O_{21.21}(OH)_{2.79}$
Helvine	$Be_3Mn^{2+}{}_4(SiO_4)_3S$
Hingganite-(Ce)	$BeCe(SiO_4)(OH)$
Hingganite-(Y)	BeY(SiO4)(OH)
Ilmenite	$Fe^{2+}Ti^{4+}O_3$
var: Manganoan Ilmenite	$(Fe,Mn)^{2+}TiO_3$
Ixiolite	$(Ta,Mn,Nb)O_2$
var: Scandian Ixiolite (of Bergstøl & Juve)	$\sim(Sc,Ta,Nb,Sn,Fe,Ti)_4O_8$
Kainosite-(Y)	$Ca_2Y_2(SiO_3)_4(CO_3)\cdot H_2O$
Kamphaugite-(Y)	$CaY(CO_3)_2(OH)\cdot H_2O$
Kristiansenite (TL)	$Ca_2ScSn(Si_2O_7)(Si_2O_6OH)$
Kuliokite-(Y)	$Y_4Al(SiO_4)_2(OH)_2F_5$
Laumontite	$CaAl_2Si_4O_{12}\cdot 4H_2O$
Lepidocrocite	$Fe^{3+}O(OH)$
`Lepidolite`	$KLi_2Al(Si_4O_{10})(F,\ OH)_2$ to $K(Li_{1.5}Al_{1.5})(AlSi_3O_{10})(F,\ OH)_2$
`Limonite`	(Fe,O,OH,H_2O)
Magnetite	$Fe^{2+}Fe^{3+}{}_2O_4$
Microcline	$K(AlSi_3O_8)$
var: Amazonite	$K(AlSi_3O_8)$
`Microlite Group`	$(Ca,Na)_2Ta_2(O,OH,F)_7$
`var: Scandium Microlite (of Bergstøl and Juve)`	Incompletely described Sc-microlite group mineral.
Milarite	$KCa_2(Be_2AlSi_{12})O_{30}\cdot H_2O$
Molybdenite	MoS_2
Monazite-(Ce)	$Ce(PO_4)$
Muscovite	$KAl_2(Si_3Al)O_{10}(OH)_2$
var: Illite	$K_{0.65}Al_{2.0}[Al_{0.65}Si_{3.35}O_{10}](OH)_2$
`Muscovite-2M1`	“Muscovite-polytype”
Nontronite	$Na_{0.3}Fe^{3+}{}_2(Si,Al)_4O_{10}(OH)_2\cdot nH_2O$
Oftedalite (TL)	$KSc_2□_2Be_3Si_{12}O_{30}$
Opal	$SiO_2\cdot nH_2O$

Phenakite	$Be_2(SiO_4)$
Plattnerite	PbO_2
`Plumbomicrolite (of Hogarth 1977)`	Pb-rich microlie, Plumboan member of the microlite-pyrochlore family.
Polycrase-(Y)	$Y(Ti,Nb)_2(O,OH)_6$
Polylithionite	$KLi_2AlSi_4O_{10}F_2$
`Polylithionite-Trilithionite Series`	$KLi_2Al(Si_4O_{10})(F, OH)_2$ to $K(Li_{1.5}Al_{1.5})(AlSi_3O_{10})(F, OH)_2$
Pyrite	FeS_2
`Pyrochlore Group`	$A_2Nb_2(O,OH)_6Z$, where A = Na, Ca, Sn^{2+}, Sr, Pb^{2+}, Sb^{3+}, Y, U^{4+}; H_2O or □. Z = OH, F, O, H_2O or □.
`var: Yttropyrochlore (of Hogarth 1977)`	$A_2Nb_2(O,OH)_6Z$
`Pyrochlore Supergroup`	$A_{2-m}D_2X_{6-w}Z_{1-n}$, where A = Na, Ca, Sr, Pb^{2+}, Sn^{2+}, Sb^{3+}, Y, U, □, or H_2O (less frequently Ag, Mn, Ba, Fe^{2+}, Bi^{3+}, Ce, other REE, Sc or Th). D = Ta, Nb, Ti, Sb^{5+} or W, but also V^{5+}, Sn^{4+}, Zr, Hf, Fe3+, Mg, Al and Si. X = O (also can include OH and F). Z = OH, F, O, □, H_2O, K, Cs, Rb. m, w and n represent parameters that indicate occupancy of the A, X and Z sites.
Quartz	SiO_2
var: Smoky Quartz	SiO_2
Rutile	TiO_2
var: Ilmenorutile	$Fe_x(Nb,Ta)_{2x} \cdot 4Ti_{1-x}O_2$
var: Strüverite	$(Ti,Ta,Fe)O_2$
Rynersonite	$CaTa_2O_6$
Scandiobabingtonite	$(Ca,Na)_2(Fe^{2+},Mn)(Sc,Fe^{3+})Si_5O_{14}(OH)$
Schorl	$NaFe^{2+}{}_3Al_6(Si_6O_{18})(BO_3)_3(OH)_3(OH)$
Siderophyllite	$KFe^{2+}{}_2Al(Si_2Al_2)O_{10}(OH)_2$
var: Magnesian Siderophyllite	$K(Fe^{2+},Mg)_2Al(Si_2Al_2)O_{10}(OH)_2$
`Siderophyllite-Polylithionite Series`	$KFe_2{}^{2+}Al(Al_2Si_2O_{10})(OH)_2$ to $KLi_2Al(Si_4O_{10})(F,OH)_2$
Spessartine	$Mn^{2+}{}_3Al_2(SiO_4)_3$
Sphalerite	ZnS
Stilpnomelane	$(K,Ca,Na)(Fe,Mg,Al)_8(Si,Al)_{12}(O,OH)_{36} \cdot nH_2O$
Synchysite-(Y)	$CaY(CO_3)_2F$
`Tantalite`	$(Mn,Fe)(Ta,Nb)_2O_6$
Tantalite-(Fe)	$Fe^{2+}Ta_2O_6$
Tengerite-(Y)	$Y_2(CO_3)_3 \cdot 2\text{-}3H_2O$
Thalénite-(Y)	$Y_3Si_3O_{10}F$
Thorite	$Th(SiO_4)$
Thortveitite	$Sc_2Si_2O_7$
Titanite	$CaTi(SiO_4)O$
var: Triclinic Titanite	$CaTi(SiO_4)O$
Topaz	$Al_2SiO_4F_2$
`Tourmaline`	$A(D_3)G_6(Si_6O_{18})(BO_3)_3X_3Z$, where A = Ca, Na, K, or is vacant; D = Al, Fe^{2+}, Fe^{3+}, Li, Mg^{2+}, Mn^{2+}; G = Al, Cr^{3+}, Fe^{3+}, V^{3+} Si can sometimes have minor Al and/or B^{3+} substitution. X = O and/or OH; Z = F, O and/or OH.
`Trilithionite`	$KLi_{1.5}Al_{1.5}(Si_3Al)O_{10}F_2$
Tveitite-(Y) (TL)	$(Y,Na)_6(Ca,Na,REE)_{12}(Ca,Na)F_{42}$
Uedaite-(Ce)	$Mn^{2+}CeAl_2Fe^{2+}(Si_2O_7)(SiO_4)O(OH)$
`Unnamed (OH-analogue of Gadolinite-(Y))` (FRL)	$(Y, Ca)_2(Fe, □)Be_2Si_2O_8(OH,O)_2$

Wodginite	$Mn^{2+}Sn^{4+}Ta_2O_8$
Xenotime-(Y)	$Y(PO_4)$
`Yttrobetafite (of Hogarth 1977)`	$A_{2-m}D_2X_{6-w}Z_{1-n}$
Yttrotantalite-(Y)	$(Y,U,Fe^{2+})(Ta,Nb)(O,OH)_4$
`Zinnwaldite`	$KFe^{2+}{}_2Al(Al_2Si_2O_{10})(OH)_2$ to $KLi_2Al(Si_4O_{10})(F,OH)_2$
Zircon	$Zr(SiO_4)$
var: Alvite	$Zr(SiO_4)$

Appendix 7.5-15 are all attached as Excel spreadsheets, while Appendix 7.16 are attached to document from Actlabs. Appendix 7.5. EPMA-acquired data of major and minor element compositions in 9 beryl minerals sampled in epoxy casts from studied Tørdal pegmatites. Appendix 7.6. EPMA-acquired data of major and minor element compositions in 5 bazzite minerals sampled in epoxy casts from studied Tørdal pegmatites. Appendix 7.7. EPMA-acquired data of major and minor element compositions in 4 gadolinite group minerals sampled in epoxy casts from studied Tørdal pegmatites. Appendix 7.8. EPMA-acquired data of major and minor element compositions in 20 mica minerals sampled in epoxy casts from studied Tørdal pegmatites. Appendix 7.9. EPMA-acquired data of major and minor element compositions in 20 biotite mineral crystals sampled in thick sections from studied pegmatite host rocks. Appendix 7.10. EPMA-acquired data of major and minor element compositions in 23 amphibole mineral crystals sampled in thick sections from studied pegmatite host rocks. Appendix 7.11. LA-ICP-MS-acquired data of minor and trace element compositions in 9 beryl minerals sampled in epoxy casts from studied Tørdal pegmatites. Appendix 7.12. LA-ICP-MS-acquired data of minor and trace element compositions in 5 bazzite minerals sampled in epoxy casts from studied Tørdal pegmatites. Appendix 7.13. LA-ICP-MS-acquired data of minor and trace element compositions in 18 mica minerals sampled in epoxy casts from studied Tørdal pegmatites. Two mica minerals from Lislegrønlia (sample 02071917) and Svåheii 2b (sample 02071909b) were not considered for LA-ICP-MS analysis, but only EPMA, since these LA-ICP-MS analysis were contaminated by mineral inclusions in the micas. Appendix 7.14. LA-ICP-MS-acquired data of minor and trace element compositions in 13 biotite mineral crystals sampled in thick sections from studied pegmatite host rocks. To analyze the same biotite minerals from EPMA analysis were considered as relative hard due to the biotite crystals relative small crystal sizes. Appendix 7.15. LA-ICP-MS-acquired data of minor and trace element compositions in 13 amphibole mineral crystals sampled in thick sections from studied pegmatite host rocks. To analyze the same amphibole minerals from EPMA analysis were considered as relative hard due to the amphibole crystals relative small crystal sizes. Appendix 7.16. Data of major, minor and trace element compositions in 4 studied pegmatite host rocks from whole rock analysis.